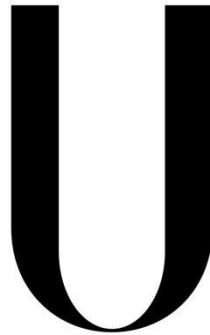


UNIVERSIDADE DE LISBOA
Faculdade de Medicina de Lisboa



LISBOA

UNIVERSIDADE
DE LISBOA

**How early inflammatory events affect bone nano
properties at rheumatoid arthritis onset**

Bruno Miguel Costa Vidal

Orientadores:

Prof. Doutor João Eurico Cortez Cabral da Fonseca

Prof. Doutora Helena Cristina de Matos Santos Canhão

**Tese especialmente elaborada para obtenção do grau de
Doutor em Ciências Biomédicas, especialidade de Ciências
Biopatológicas**

2017

UNIVERSIDADE DE LISBOA
Faculdade de Medicina de Lisboa



**How early inflammatory events affect bone nano properties at rheumatoid
arthritis onset**

Bruno Miguel Costa Vidal

Orientadores:

Prof. Doutor João Eurico Cortez Cabral da Fonseca

Prof. Doutora Helena Cristina de Matos Santos Canhão

**Tese especialmente elaborada para obtenção do grau de Doutor em Ciências
Biomédicas, especialidade de Ciências Biopatológicas**

Jurí:

Presidente:

- Doutor José Luis Bliebernicht Ducla Soares, Professor Catedrático em regime de *tenure* e Vice-Presidente do Conselho Científico da Faculdade de Medicina da Universidade de Lisboa.

Vogais:

- Doutora Maria Manuela Estima Gomes, Investigadora Principal da Universidade do Minho;
- Doutor Fernando Manuel Pimentel dos Santos, Professor Auxiliar Convidado da Faculdade de Ciências Médicas da Universidade Nova de Lisboa;
- Doutora Maria de Fátima Reis Vaz, Professora Associada com Agregação do Instituto Superior Técnico da Universidade de Lisboa;
- Doutor João Eurico Cortez Cabral da Fonseca, Professor Catedrático da Faculdade de Medicina da Universidade de Lisboa; (Orientador)
- Doutor Luís Ricardo Simões da Silva Graça, Professor Associado com Agregação da Faculdade de Medicina da Universidade de Lisboa;
- Doutora Maria José Parreira dos Santos, Professora Auxiliar Convidada da Faculdade de Medicina da Universidade de Lisboa.

Instituições financiadoras:

- FCT – Bolsa de doutoramento SFRH / BD / 81527 / 2011
- Pfizer – ASPIRE 2013 Prize
- ECTS/AMGEN Bone Biology 2014 Prize

2017

As opiniões expressas nesta publicação são da exclusiva responsabilidade do seu autor, não cabendo qualquer responsabilidade à Faculdade de Medicina da Universidade de Lisboa pelos conteúdos nele apresentados.

A impressão desta tese foi aprovada pelo Conselho Científico da Faculdade de Medicina de Lisboa em reunião de 24 de Janeiro de 2017.

**Dissertação apresentada à
Faculdade de Medicina da
Universidade de Lisboa, para
obtenção do grau de Doutor
em Ciências Biomédicas.**

“Porque eu sou do tamanho do que vejo”

“Because I'm the size of what I see”

Fernando Pessoa, 1946

Table of contents

Index of figures	xiii
Index of tables	xv
Acknowledgements	xvii
Abbreviations	xxi
Resumo	xxiii
Summary	xxvii
Chapter I - Introduction	1
• Rheumatoid arthritis and early bone damage	3
• Rheumatoid arthritis	5
○ Definition	5
○ Etiopathogeny	8
• Bone biology	11
○ Bone structure	11
○ Bone matrix	13
○ Collagenous proteins	14
○ Noncollagenous proteins	16
○ Hydroxyapatite crystals	17
• Bone cells	18
○ Osteoclast	18
○ Osteoblast	19
○ Osteocyte	19
• Bone remodeling	20
• Bone mechanics	25
• Rheumatoid arthritis and bone	28
• Treatment options for RA	30
○ Glucocorticoids	30
○ Conventional DMARDs	31

○ Biological DMARDs	31
• Future perspectives	32
Chapter II - Aims	35
Chapter III – Results	39
• I. Arthritis induces early bone high turnover, structural degradation and mechanical weakness.	43
• II. Early arthritis induces disturbances at bone nanostructural level reflected in decreased tissue hardness.	61
• III. Decrease of CD68 Synovial Macrophages in Celestrol Treated Arthritic Rats.	89
• IV. Celestrol preserves bone structure and mechanics in arthritic animals.	123
• V. Effects of tofacitinib in early arthritis bone loss	143
Chapter IV - Discussion	167
Chapter V - Conclusion	175
References	179

Index of Figures

Figure 1 - Representative scheme comparing healthy (A) and arthritic (B) articular joint.	10
Figure 2 - Bone hierarchical structure organization	13
Figure 3 - Collagen type I synthesis process	15
Figure 4 - Structural organization of the BMUs in cortical and trabecular bone.	21
Figure 5 - Physiological phases of the bone remodeling process	22
Figure 6 - RANK–RANKL–OPG signaling pathway scheme	23
Figure 7 - A typical bone specimens loaded in tension stress–strain curve	26
Figure 8 - Immune cells and cytokine networks scheme in rheumatoid arthritis joint	29
Figure 9 - Pathways targets of some currently available biologic agents for RA.	33

Index of Tables

Table 1 – American College of Rheumatology criteria for the classification of RA from 1987	6
Table 2 – American College of Rheumatology / European League Against Rheumatism classification criteria for RA from 2010	7

Acknowledgements

Os agradecimentos não se resumem meramente aos 4 anos...quase 5 de doutoramento, teremos de recuar alguns anos mais!

Primeiramente gostaria de agradecer aos meus pais e irmão que me deram condições familiares para que pudesse estudar e erguer-me social e culturalmente, e que passados todos estes anos continuam ao meu lado a apoiar-me em todas as situações de forma incondicional. Mesmo o meu pai que apesar de partir prematuramente acredito continuar a seguir as minhas pisadas.

Há sensivelmente 8 anos atrás, no final de 2008, entrei pela primeira vez no Edifício Egas Moniz para uma entrevista de trabalho na Unidade de Investigação em Reumatologia. Na verdade não sabia muito bem ao que ia, mas acabei por ficar como “Lab manager” e mais tarde como “Study coordinator”, posições essas que me deram verdadeiro gosto de desempenhar. Esse período permitiu que o meu contacto com a ciência e a clínica fosse cada vez maior, permitindo que adquirisse a ferramenta principal para se trabalhar em ciência, o “espírito crítico”.

Passados 3 anos, iniciei o meu doutoramento...o início foi estranho, tudo muito novo e tão diferente, aquele sentimento de “o que é que é suposto eu fazer?”, “ninguém me dá uma tarefa para realizar?”. No entanto, o processo de adaptação à nova realidade aconteceu, mostrando-me possuir ferramentas que até então desconhecia ter. Senti-me forçado a crescer como profissional e como homem. Desta forma, gostaria de agradecer aos meus orientadores Professor João Eurico Fonseca e Professora Helena Canhão por há 8 anos atrás terem acreditado nas minhas capacidades enquanto recém formado, por há 5 anos atrás me terem aliciado e possibilitado a continuação da minha formação académica e por todos estes anos me terem prestado um apoio incondicional com o intuito de atingir os “meus” objectivos. Apesar de muitas vezes ausentes, sempre estiveram à distância de um email ou telefonema. O meu muito obrigado ao Professor João Eurico por todo o apoio prestado, especialmente nesta recta final. Muitas serão as situações que ficam por agradecer...

Um especial agradecimento à Fundação para a ciência e a tecnologia por me ter concedido uma bolsa de doutoramento, bem como à Pfizer, UCB e ao European Calcified Tissue Society (ECTS)/Amgen por terem financiado este projecto.

Não posso deixar de agradecer ao meu comité de tese, Dr. Jaime Branco, Dr. José Rino e Dr^a Rita Cascão, o meu muito obrigado por todos os “brainstormings” e tempo dispensado em conduzir o meu projecto a um trabalho sólido.

Quero também agradecer aos meus colegas, em especial aos que mais contribuíram para o sucesso desta minha etapa. Um especial agradecimento à Rita Cascão, com a qual trabalhei longas horas, dias, meses, anos e que acabou por ser determinante no meu processo de aprendizagem, revelando ser uma verdadeira co-orientadora. À Ana Lopes que com a qual trabalhei de perto durante vários anos, e sempre se mostrou disponível em ajudar, mesmo que isso lhe custasse atingir as 16h de trabalho por dia. À tão afável Rita Moura, que independentemente da situação tenta sempre dar uma palavra amiga, e que raramente “perde a cabeça”. À Inês Perpétuo que mesmo com o seu feitio rispido sempre me ajudou em todas as minhas dúvidas. À Inês Lopes que apesar de recém chegada tanto trabalhou para este projecto e que permite que nada nos falte no laboratório. À Eunice Paisana que apenas esteve um ano connosco mas que igualmente colaborou de forma activa neste projecto.

Neste percurso tive a oportunidade de me cruzar com inúmeras pessoas que me ensinaram e ajudaram a ultrapassar diversas barreiras científicas, sendo elas, Dr. Pierre Marie, Dr. Simo Saarakala, Dr. Peter Zioupos, Dr. José Rino, Dr^a Fátima Vaz, Dr^a Catarina Vale, António Temudo, Maria João Galvão e Dr. Mikko Finnila, com o qual trabalhei de forma incansável neste último ano e meio, mostrando ser um enorme profissional e pessoa.

Sempre fui pessoa de muitos amigos, no entanto, ao longo da vida, diria eu como fruto de uma lei darwinista, a “selecção natural” acabou por refinar esse meu leque de amizades. Há amizades que preservo desde há muitos anos e que continuarei a regar para que nunca se percam. Amizades de há praticamente 30 anos... Ricardo Frederique (Fred), André Pimenta, 20 anos....Carlos Vieira, João Fernandes, 15 anos...João Carvalho, Miguel Grilo, Marisa Silva, e mais recentemente Inês Rosa, Rudolfo Francisco e Francisco Branco, este que acompanhou de perto este percurso e foi peça essencial em muitas situações do

meu doutoramento, daqueles amigos a preservar! No entanto, todos eles me acompanharam nesta longa caminhada, que entre risadas, confidências e entreaajuda contribuíram para o sucesso desta minha etapa.

Por último, e não menos importante, quero agradecer à minha namorada Andreia Moutinho pelo apoio, compreensão e estabilidade que me proporciona.

Esta etapa seria possível fazer-se sem muitos de vós, mas certamente seria bem mais difícil...muito obrigado!

List of Abbreviations

ACPA Anti-citrullinated protein antibodies
ACR American College of Rheumatology
AIA Adjuvant-induced arthritis
APC Antigen presenting cells
BMD Bone Mineral Density
BMU Bone multientral unit
BRC Bone remodeling compartment
BSAP Bone specific alkaline phosphatase
C-Fms Macrophage colony-stimulating factor receptor
CIA Collagen-induced arthritis
CRF Clinical risk factors
CTSK Cathepsin K
CTX Carboxy-terminal telopeptide of collagen
DMARD Disease-modifying anti-rheumatic drug
DPD Deoxypyridoline
EULAR European League Against Rheumatism
FLS Fibroblasts like-synoviocytes
FTIR Fourier transform infrared
GLA Gamma-carboxylated
Gly Glycine
GM – CSF Granulocyte-macrophage colony-stimulating factor
HLA Human leukocyte antigen
IFN γ Interferon gamma
IGF Insulin-like growth factor
IL Interleukin
ILD Intestinal lung disease
JAK Janus kinase
MCSF Macrophage colony-stimulating factor
Micro-CT Micro computed tomography
MHC Major Histocompatibility Complex

MMP Metalloproteinase
MSCs Mesenchymal stem cells
MTX Methotrexate
NF- κ B Nuclear factor kappa-light-chain-enhancer of activated B-cells
NTX Amino-terminal collagen crosslinks
NSAID Non-steroid anti-inflammatory drug
OA Osteoarthritis
OPG Osteoprogesterine
OPN Osteopontin
P1CP Carboxy terminal propeptides of type I collagen
P1NP Amino terminal propeptides of type I collagen
PL Parallel lamella
PYD Pyridinoline
PTH Parathyroid hormone
RA Rheumatoid arthritis
RANK Receptor activator of nuclear factor
RANKL RANK ligand
RF Rheumatoid factor
Runx 2 Runt-related transcription factor 2
SO Secondary osteons
STAT Signal transducers and activators of transcription
TCR T-cell receptor
TGF- β Tumor growth factor beta
Th T helper
TNF Tumor necrosis factor
TRAP Tartrate resistant acid phosphatase
VEGF Vascular endothelial growth factor
WHO World health organization

Resumo

A artrite reumatóide (AR) é uma doença inflamatória crónica, imuno-mediada, caracterizada pela hiperplasia da membrana sinovial, conduzindo à destruição progressiva da cartilagem e osso, e conseqüente comprometimento funcional e aumento da morbidade e mortalidade.

O diagnóstico precoce aliado a uma estratégia terapêutica adequada são cruciais para prevenir a progressão da artrite reumatóide e a incapacidade funcional.

A AR caracteriza-se pela hiperplasia sinovial, mediada pela interação de várias células do sistema imunitário, tais como, macrófagos, neutrófilos, células T e B, e complexas redes de citocinas (particularmente a interleucina (IL) -1β , IL-6 e o factor de necrose tumoral (TNF)). Esta interacção celular inflamatória conduz à diferenciação e activação de osteoclastos (osteoclastogénese), promovendo alterações na remodelação do tecido ósseo, que causam osteoporose secundária e conseqüente fragilidade óssea.

Existe uma janela de oportunidade terapêutica na fase inicial da AR, na qual é possível prevenir a destruição articular e conseguir a remissão de um maior número de doentes. É expectável que a intervenção terapêutica numa fase inicial da doença interfira sistemicamente com a biologia óssea, evitando alterações das propriedades intrínsecas do osso a um nível nano e micro estrutural.

O desenvolvimento de estratégias terapêuticas capazes de controlar a inflamação e a degradação óssea, com elevada taxa de remissão, baixa incidência de efeitos secundários e baixos custos de produção continua a ser um objectivo por alcançar no tratamento da AR.

A nossa hipótese é de que o impacto da inflamação nas propriedades micro e nano estruturais do osso (propriedades intrínsecas do tecido ósseo, independentes da arquitetura óssea global e directamente dependentes da forma como as células ósseas, o colágeno e os cristais de cálcio interagem) ocorre imediatamente após os primeiros sintomas da AR, e que estes efeitos podem ser prevenidos pela intervenção terapêutica precoce com fármacos capazes de controlar a inflamação e interferir com o metabolismo ósseo.

A presente tese caracteriza as alterações iniciais da degradação óssea na AR e explora o efeito de novas intervenções terapêuticas neste contexto.

Assim, na primeira parte desta tese, demonstrou-se em modelo de rato de artrite induzida por adjuvante (AIA) um aumento da espessura sinovial devido à infiltração de células do sistema imunitário nas camadas íntima e subíntima, conduzindo a erosões ósseas e degradação da superfície da cartilagem articular. Estas alterações estão presentes desde a fase inicial da doença, sendo paralelos a um aumento dos níveis séricos de IL-6. A osteoclastogênese (diferenciação e activação de osteoclastos) é potenciada pelo ambiente inflamatório, causando erosões ósseas articulares e alterações sistémicas na remodelação óssea. De facto, demonstrou-se um aumento da remodelação óssea (aumento da reabsorção e formação), evidenciado pelo aumento do CTX-I (telopectídeo C-terminal do colagénio do tipo I) e do P1NP (propeptídeo amino-terminal do procologénio do tipo I) desde a fase inicial da artrite. A histologia convencional confirmou estes dados. Os animais artríticos apresentaram uma maior frequência de lamelas concêntricas secundárias nos sistemas de havers, como consequência da remodelação óssea intensa. Pelo contrário, os animais saudáveis apresentaram mais estruturas ósseas paralelas. Estas estruturas de osso organizado, característico de estruturas ósseas maduras (remodelação óssea fisiológica), são 10% mais duras que as lamelas de osso concêntricas. O tecido ósseo artrítico é assim composto por um maior número de estruturas imaturas, menos mineralizadas e menos duras, explicando a redução da dureza que observámos através dos testes de nanoindentação. Além disso, observou-se desde uma fase inicial da artrite o aumento da área ocupada pelas lacunas dos osteócitos. Esta aparente alteração da morfologia dos osteócitos pode estar relacionada com necrose óssea, potenciada pelo desenvolvimento da artrite, levando à perda de mineralização óssea, diminuição da dureza e comprometimento da capacidade mecânica.

Na presente tese demonstramos ainda que a artrite induz a perda de mineral e colagénio no osso trabecular desde a fase inicial do desenvolvimento da doença. Resultados de estrutura óssea adquiridos por micro tomografia computadorizada (micro-CT) revelaram que os animais artríticos apresentavam um menor volume de osso cortical e trabecular, com diminuição da espessura trabecular, bem como

um aumento da separação trabecular, em comparação com os animais saudáveis. Os resultados também demonstraram diferenças corticais na capacidade do osso resistir a torção (momento polar de inércia), sugerindo desta forma, alterações da capacidade mecânica nos grupos artríticos desde a fase inicial da artrite. Além disso, registou-se um aumento da porosidade cortical e trabecular nos grupos artríticos em comparação com os controlos saudáveis. Estes dados foram reforçados pelas observações realizadas com histomorfometria clássica, que demonstrou uma diminuição da integridade estrutural em animais artríticos. De forma coerente com estas alterações estruturais ósseas, os nossos resultados também demonstraram uma diminuição das propriedades mecânicas desde uma fase muito inicial da artrite.

Estes resultados revelaram que a inflamação promove alterações estruturais ósseas a nível nano e micro estrutural, conduzindo à fragilidade óssea desde o início da artrite. Além disso, demonstramos que o modelo animal de artrite AIA é adequado para o estudo do impacto da inflamação no osso, bem como para a avaliação e identificação de possíveis compostos para o tratamento da artrite e suas alterações ósseas.

A segunda parte desta tese, procurou contribuir para a pesquisa de novas terapêuticas para a AR, com maior eficácia no controle da inflamação e dano ósseo, mais seguras e menos dispendiosas.

Em estudos anteriores, demonstramos que o celastrol é um candidato terapêutico promissor para a AR por inibição da produção de IL1 β e TNF. Os resultados agora apresentados mostraram que o celastrol foi capaz de reduzir o número de células B e T na membrana sinovial bem como fibroblastos e macrófagos CD68 positivos. O celastrol demonstrou ainda capacidade para a preservação da cartilagem e estrutura óssea, controlando a inflamação focal responsável pela degradação do tecido ósseo. A nível sistémico o celastrol levou à diminuição da remodelação óssea, preservação da estrutura óssea e suas propriedades mecânicas. Além disso, o tratamento com celastrol mostrou efeitos superiores quando administrada numa fase inicial do desenvolvimento da artrite, o que realça a importância do tratamento precoce para prevenir as alterações ósseas induzidas pela inflamação.

O tofacitinib também foi testado no modelo AIA de artrite no rato, a fim de avaliar os efeitos sobre a micro e nano estrutura do osso e as suas propriedades mecânicas.

O tofacitinib é um inibidor selectivo da janus quinase 1 (JAK1) e janus quinase 3 (JAK 3), que interfere com a dimerização do transdutor de sinal e activador de moléculas de transcrição (STAT), bloqueando a activação da transcrição génica que é dependente da via de sinalização JAK -STAT. Os resultados demonstraram uma diminuição das manifestações inflamatórias da artrite, diminuição da inflamação do tecido sinovial e erosões ósseas, acompanhadas por uma redução da taxa de remodelação óssea e uma predominância de estruturas organizadas paralelamente no tecido ósseo. A análise das propriedades intrínsecas do tecido ósseo, através da técnica de nanoindentação, permitiu identificar que o tofacitinib aumentou a dureza cortical e trabecular do osso. No entanto, a micro-CT e os testes de flexão de 3 pontos revelaram que o tofacitinib não reverteu os efeitos da artrite na estrutura óssea cortical e trabecular e nas suas propriedades mecânicas. Este efeito no osso pode estar relacionado com o mecanismo de acção do tofacitinib, que promove interacções moleculares complexas com o osso, podendo estas ter um efeito negativo global, não totalmente compensado pelos benefícios resultantes do controlo da inflamação. Não se pode excluir que o tofacitinib possa necessitar de mais tempo de exposição terapêutica para ter um impacto na qualidade óssea.

De um modo geral, os resultados da presente tese suportam a hipótese de que o impacto da inflamação nas propriedades micro e nano estruturais do osso ocorrem numa fase muito inicial da artrite, após os primeiros sintomas, e que esses efeitos podem ser prevenidos por uma intervenção terapêutica muito precoce com fármacos capazes de controlar a inflamação e as alterações do metabolismo ósseo.

Palavras chave: Artrite reumatóide inicial, Artrite induzida por adjuvante, Inflamação, Osso, Terapêuticas para artrite reumatóide.

Summary

Rheumatoid arthritis (RA) is a chronic, systemic and immune-mediated inflammatory disease that mainly affects the synovial membrane of multiple small joints. As a consequence, RA results in cartilage and bone damage, leading to functional impairment and an increase in morbidity and mortality. Early diagnosis and adequate treatment are critical to prevent RA progression, as joint destruction can occur immediately after its onset.

The most characteristic feature of RA is synovial hyperplasia, which is mediated by several immune cells, such as T-cells, B-cells, neutrophils, macrophages and by a complex cytokine network, especially interleukin (IL)-1 β , tumor necrosis factor (TNF) and IL-6. RA inflammatory environment induces osteoclastogenesis, promoting disturbances in skeletal bone remodeling, which ultimately leads to the development of secondary osteoporosis and consequent bone fragility.

An opportunity for a more effective treatment intervention was identified in early RA, when permanent damage can be prevented and a higher number of patients can achieve remission. Early treatment intervention might also interfere systemically with bone biology preventing bone micro and nano architectural damage. The development of therapeutic strategies able to control both inflammation and bone degradation, with a high rate of disease remission, low incidence of side effects and low production costs is still an unmet medical need in RA.

Our hypothesis is that the impact of inflammation on bone micro and nano properties (intrinsic bone tissue properties, independent of the overall bone architecture and directly dependent on the way bone cells, collagen and calcium crystals interact) occurs almost immediately, upon first symptoms, and that these effects can be prevented by early intervention with drugs able to control inflammation and capable of interfering also with bone metabolism.

This thesis characterizes the early events of bone damage in RA and explores the effect of novel treatment interventions in this context.

Accordingly, in the first part of this thesis, we used an adjuvant induced arthritis (AIA) rat model and observed a synovial sublining layer infiltration, increased lining

layer cells, bone erosions and cartilage surface damage present since the early stages of arthritis, as well as increased levels of IL-6. This inflammatory environment promotes osteoclastogenesis, which is related to the observed local bone erosion and may interfere systemically with bone skeletal remodeling. Indeed, AIA animals showed an increased bone turnover, as depicted by increased CTX-I (Carboxy-terminal telopeptide of type I collagen) and P1NP (amino terminal propeptides of type I collagen) levels since the early stages of arthritis. Bone histology was consistent with this early onset spur of bone remodeling. Arthritic animals showed concentric lamellas in secondary osteons (SO), which are the consequence of intense bone remodeling. On the contrary, healthy animals presented more parallel-lamellae (PL) structures than SO structures and these PL structures are 10% harder than SO structures, representing the mature bone structure (normal bone remodeling). Thus, arthritic bone tissue was composed of a larger number of younger, less mineralized and less hard structures, explaining the reduced hardness that we have observed by nanoindentation. Moreover, an increased area occupied by osteocyte lacunae was detected early on in the arthritis process. This apparent change of osteocyte morphology might be related to bone necrosis, leading to mineral loss, decreased hardness and possibly mechanical weakness. In addition, we have also demonstrated that arthritis induces mineral and collagen loss in trabecular bone since the early phase of arthritis development. At a higher organizational level data, micro computed tomography (micro-CT) revealed in arthritic animals a lower fraction of cortical and trabecular bone volume with reduced trabecular thickness together with a higher trabecular separation, in comparison with controls. Results also demonstrated cortical differences in polar moment of inertia, suggesting mechanical weakness in arthritic groups since the early phase of arthritis. Furthermore, cortical and trabecular porosity were increased in the arthritic groups compared to healthy controls. We also confirmed these observations by classic histomorphometry, which demonstrated a decreased structural integrity in arthritic animals. Coherent with these structural defects, our results also showed that in very early arthritis bone has low mechanical competence. Altogether, these results revealed that inflammation promotes bone nano and micro structural disturbances, leading to bone fragility since the early stages of arthritis. In addition, we also

provided the basis for using the AIA animal model of arthritis as an adequate model for studying the impact of inflammation on bone and for assessing candidate compounds for the control of arthritis and its associated bone damage.

The quest for new RA treatments, more effective at inflammation and bone damage control, safer and less expensive is still a major need. Previously, we had demonstrated that celastrol, acts by downregulating IL1 β and TNF production, was a promising RA therapeutic candidate. Herein we have demonstrated that celastrol was able to reduce the number of synovial B and T-cells as well as fibroblasts and CD68 macrophages. Accordingly, we showed that celastrol protects cartilage and bone from inflammation-induced focal damage. At a systemic level, we observed a reduction in bone turnover together with preservation of bone structural and mechanical properties. Moreover, celastrol therapy showed superior effects if administered in an early phase of arthritis development, which highlights the importance of an early treatment to limit inflammation-induced bone damage.

Tofacitinib was also tested in order to assess the effects on micro and nano structural and mechanical properties of bone in an AIA rat model of arthritis. Tofacitinib is a selective inhibitor of janus kinase 1 (JAK1) and janus kinase 3 (JAK3). Results showed significant reduced arthritis manifestations, synovial tissue inflammation and bone erosions, accompanied by a reduced bone turnover rate and a predominance of parallel structures on bone tissue. At tissue level, measurements performed by nanoindentation showed that tofacitinib increased bone cortical and trabecular hardness. However, micro-CT and 3-point bending tests revealed that tofacitinib did not revert the effects of arthritis on cortical and trabecular bone structure and mechanical properties. This effect on bone might be related to the mechanism of action of tofacitinib which has complex and conflictual molecular interactions with bone. We suggest that these interactions have an overall negative effect not totally compensated by the benefits resulting from the control of inflammation. On the other hand, tofacitinib may require more exposure time to have an impact on bone quality.

Overall, the results of the present thesis support the hypothesis that the impact of inflammation on bone micro and nano properties occurs almost immediately, upon the appearance of first symptoms. Moreover, these observed effects can be

prevented by very early intervention with drugs able to control inflammation and capable of interfering with bone metabolism.

Keywords: Early rheumatoid arthritis, Adjuvant induced arthritis, Inflammation, Bone, Rheumatoid arthritis therapies.

Chapter I

Introduction

Rheumatoid arthritis and early bone damage

The immunological system activation may occur several years before the first clinical signs of rheumatoid arthritis (RA).

Based on our previous studies in a mouse model of chronic arthritis, we have suggested that inflammation promote disturbances in the bone mechanical properties and collagen turnover and organization. Our proposed hypothesis was that the initial steps towards bone fragility are determined by early changes in collagen type I organization and mineralization, capable of interfering with the intrinsic bone tissue properties. These are bone nano level properties, independent of the overall bone architecture and directly dependent on the interaction between bone cells, collagen and calcium crystals.

An opportunity for a more effective treatment intervention was identified in early RA, when permanent damage can be prevented and a higher number of patients can achieve remission. Early treatment interventions might also interfere systemically with bone biology preventing bone nano and micro architectural damage.

This thesis characterizes the early events of bone damage in RA and explores the effect of novel treatment interventions in this context.

Rheumatoid arthritis

Definition

RA is a chronic, systemic progressive and immune-mediated inflammatory disease that mainly affects the synovium of multiple joints, leading to progressive damage of cartilage and bone [1-4]. The inflammatory process typically impacts on small joints, particularly hands and feet joints, usually bilaterally and symmetrically [5].

Systemic inflammation can additionally induce disorders on multiple organs and systems [5] such as interstitial lung disease (ILD) and pleural effusion; secondary renal amyloidosis; and pericardial effusion [6]. RA patients have an increased atherosclerotic burden and consequently a higher cardiovascular risk [7,8]. Hematologic complications of RA are common and may include anemia, Felty's syndrome (characterized by neutropenia), lymphoma and leukemia [6]. Rarely, severe RA patients may present vasculitis, which ranges from mild to very aggressive [9]. RA is also commonly associated to secondary Sjögren's syndrome, which is manifested by mouth and eye dryness, foreign-body sensation in the eye and photophobia [10].

Quality of life is significantly reduced due to pain, fatigue, loss of body function and increased mortality, when compared with the general population [11]. Furthermore, the incidence of RA is higher in individuals between 30 to 50 years of age (75% are women) affecting individuals in the most active period of their personal and professional lives. RA can lead to inability of developing most of the daily tasks [12]. In addition, RA patients have significantly higher expenses in home care, child care, use of medical equipment and devices, and home remodeling in order to adapt their physical condition to the environment [13]. Thus, individual economic burden is often associated with disease progression [14]. RA is a relatively frequent disease (overall world prevalence of 0.5% to 1%) [14] and in Portugal accounts for 0.7% of the population [15], which represents a significant impact on health systems [16].

During the early phase of RA, the disease can be asymptomatic and several months can pass until the final diagnosis is made [17]. Disease progression can range from mild to severe. Clinical, laboratory and radiologic parameters have

determined prognostic factors, such as high joint counts, early disability, high inflammatory markers, positive rheumatoid factor (RF) and anti citrullinated protein antibodies (ACPA), and early joint erosions [18].

Treatment decisions are influenced by these prognostic factors. A rapid diagnosis and an effective therapeutic strategy intervention are crucial to prevent disease progression [19,20].

The RA diagnosis criteria published in 1987 by the American College of Rheumatology (ACR) focused in the identification of patients with established disease [21] (Table 1) .

Table 1 – American College of Rheumatology criteria for the classification of RA from 1987.

Criteria	Definition
1. Morning stiffness	Morning stiffness lasting at least one hour, present for at least six weeks
2. Arthritis of 3 or more joint areas	At least three joint areas simultaneously with soft-tissue swelling or fluid, for at least six weeks
3. Arthritis of hand joints	At least one area swollen in a wrist, metacarpophalangeal, or proximal interphalangeal joint, for at least six weeks
4. Symmetric arthritis	Simultaneously involvement of the same joint areas on both sides of the body, for at least six weeks
5. Rheumatoid nodules	Subcutaneous nodules observed by a physician
6. Positive rheumatoid arthritis	Abnormal amounts of serum rheumatoid factor quantified by any method for which the result has been positive in <5% of healthy individuals
7. Radiographic changes	Radiographic changes on hand and wrist radiographs (erosions or unequivocal bony decalcification)

Patient is diagnosed with RA if meets at least four criteria. Patients with two clinical criteria parameters are not excluded. Adapted from [21]

Consequently, the 1987 criteria failed to identify patients in the initial phase of arthritis. ACR and European League Against Rheumatism (EULAR) developed

new classification criteria to identify patients earlier in the disease process [22] (Table 2).

Table 2 – American College of Rheumatology / European League Against Rheumatism classification criteria for RA from 2010. Adapted from [22].

	Score
Target population (who should be tested) are patients who:	
1. have at least 1 joint with definite clinical synovitis (swelling) ^a	
2. with the synovitis not better explained by another disease ^b	
Classification criteria for rheumatoid arthritis (score-based algorithm):	
Add scores of categories A - D.	
A score of $\geq 6/10$ is needed for classification of a patient as having definite rheumatoid arthritis ^c	
A. <u>Joint involvement</u>^d	
1 large joint ^e	0
2 – 10 large joints	1
1 – 3 small joints (with or without involvement of large joints) ^f	2
4 – 10 small joints (with or without involvement of large joints)	3
>10 joints (at least one small joint)	5
B. <u>Serology (at least one test result is needed for classification)</u>^g	
Negative RF <i>and</i> negative ACPA	0
Low-positive RF <i>or</i> low-positive ACPA	2
High-positive RF <i>or</i> high-positive ACPA	3
C. <u>Acute phase of reactants (at least one test result is needed for classification)</u>^h	
Normal CRP <i>and</i> normal ESR	0
Abnormal CRP <i>or</i> abnormal ESR	1
D. <u>Duration of symptoms</u>ⁱ	
< 6 weeks	0
≥ 6 weeks	1

^a The criteria are aimed at classification of newly presenting patients; ^b Differential diagnoses vary among patients with different presentations. If it is unclear about the relevant differential diagnoses to consider, an expert rheumatologist should be consulted; ^c Although patients with a score of < 6/10 are not classifiable as having rheumatoid arthritis, their status can be reassessed and the criteria might be fulfilled cumulatively over time; ^d Joint involvement refers to any swollen or tender joint on examination, which may be confirmed by imaging evidence of synovitis; ^e Large joints refers to shoulders, elbows, hips, knees, and ankles; ^f Small joints refers to the metacarpophalangeal joints, proximal interphalangeal joints, second through fifth metatarsophalangeal joints, thumb interphalangeal joints and wrists; ^g Negative refers to international unit (IU) values that are less than or equal to the upper limit of normal (ULN) for the laboratory and assay; low-positive refers to IU values that are higher than the ULN but ≤ 3 times the ULN for the laboratory and assay; high-positive refers to IU values that are > 3 times the ULN for the laboratory and assay. Where rheumatoid factor (RF) information is only available as positive or negative, a positive result should be scored as low-positive for RF. ACPA – anti-citrullinated protein antibody; ^h Normal/abnormal is determined by local laboratory standards. CRP – C-reactive protein, ESR – erythrocyte sedimentation rate; ⁱ Duration of symptoms refers to patient self-report of the duration of signs or symptoms of synovitis (e.g. pain, swelling, tenderness) of joints that are clinically involved at the time of assessment, regardless of treatment status. Adapted from [22]

The inflammatory environment that occurs in RA induces bone remodeling disturbances, contributing not only to bone erosions but also to the development of secondary osteoporosis, which increase the risk of bone fracture [23].

The World Health Organization (WHO) developed FRAX, in order to assess, in untreated subjects over 40 years old, the ten year probability of both a major fracture and a hip fracture, with or without the use of Bone Mineral Density (BMD) [24]. FRAX is an algorithm based on a multivariate model, which includes independent clinical risk factors for fracture that allows the determination of the fracture threshold for treatment decision probability [25]. Of interest, RA is one of these independent fracture risk factors.

Etiopathogeny

The exact cause of RA is unknown, however genetic and environmental factors contribute to the etiopathology of this complex disease [26]. The major histocompatibility complex (MHC) is a cell complex that exhibit surface proteins and play an important role for the recognitions of foreign molecules by the immune system, especially T-cells. MHC class II human leukocyte antigen (HLA)-DRB1*0404 and DRB1*0401 alleles, are the strongest genetic factor related to RA [27,28]. In Mediterranean areas, including Portugal, an additional allele was found, DRB1*1001, which is also associated to RA [29]. The specificity of the T-cells are regulated by an association between the T-cell receptor (TCR) and the MHC

molecules that present selected peptides, suggesting that RA results from the presentation of an unidentified, exogenous or endogenous antigen [30,31].

In RA, the production of autoantibodies specific for immunoglobulin or for cyclic citrullinated peptides, precedes the clinically onset [32].

Several studies have reported that smoking is a risk factor for RA in individuals with HLA-DRB1 susceptibility alleles [33], promoting also the development of ACPA [34]. Many other risk factors for RA have been identified, such as breastfeeding, pregnancies, lifestyle, diet, smoking and obesity amongst others [35]. Accordingly, interactions between genes and environmental risk factors are pivotal in the predisposition of individuals to developed RA.

The inflammatory environment present in early and late phases of the disease is responsible for the production of cytokines and consequent perpetuation of inflammation, which maintain inflammatory cells activated in a positive feedback loop [36]. This process involves a complex network between innate and adaptive immune system and their products [1]. The activation of T-cells, mediated by the binding of TCR to (auto)-antigen MHC on antigen presenting cells (APC), leads to the activation of synovial monocytes, macrophages and fibroblasts, through the production of interferon- γ [37,38]. Many of these activated cells express abundant HLA class II and adhesion molecules, which play a role in the inflammatory process by antigen presentation [39-44] and produce pro-inflammatory cytokines, such as interleukin (IL)-1 β , TNF, IL-17 and IL-6 [45] [46]. .

Normal joint (Fig.1 A) is constituted by a thin synovial membrane composed by one to two cell layers, in close contact with the synovial fluid. [47]. RA synovial fluid is enriched predominantly with neutrophils, macrophages, T lymphocytes and dendritic cells (Fig.1 B). Cellularity is increased in synovial membrane and, as a consequence, the lining layer is increased in cells thickness, and is comprised mostly by activated macrophages with an underlying layer of fibroblast-like cells [38].

The deeper layers of RA synovium might have follicles of lymphoid cells around vessels as well as dispersed lymphocytes between them. Neovascularization and activated endothelial cells are increased as well as cellular infiltration in the synovial membrane. In RA synovial membrane, the most abundant cells are

macrophages and T-cells, but plasma cells, dendritic cells, neutrophils and activated fibroblasts are also present [48].

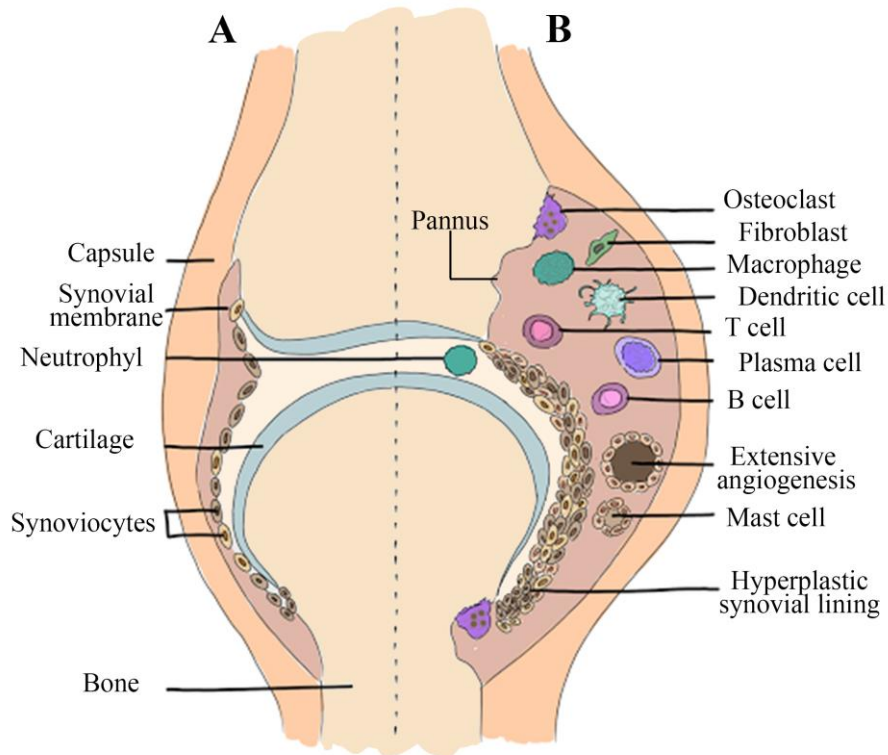


Figure 1 - Representative schemes illustrating and comparing healthy (A) and arthritic (B) articular joint. The joint affected by RA (b) shows increased inflammation and cellular activity. Adapted from [49,50].

Chondrocyte function is affected by several factors produced by RA synovial tissue and fluid, such as the up-regulating products that enhance matrix degradation but also suppress matrix synthesis and repair. Among RA synovial products, IL-1 β and TNF play an important role in cartilage loss [51]. Several studies demonstrated that IL-1 β stimulates metalloproteinases (MMPs) production and other products such as nitric oxide [52-55]. Others studies have also demonstrated that the effects of TNF are similar to, or are synergistic with IL-1 β , thus indicating an additional role for this cytokine in cartilage destruction [55,56]. These cytokines further contribute to the depletion of the cartilage matrix by decreasing the synthesis of cartilage-specific collagens and proteoglycans [57-60]. In addition, the hyperplastic synovium induces cartilage damage, leading to the

loss of normal protective properties [61], inducing changes in the mechanism of protein-binding, promoting the invasion and consequent adhesion by fibroblasts like-synoviocytes (FLS) [62]. FLS synthesize MMPs, which promote collagen type II network disruption, affecting glycosaminoglycan and water content leading to cartilage biomechanical properties dysfunction. These processes ultimately conduct to the destruction of cartilage surface and to radiographic appearance of joint-space narrowing [63].

On the other hand, RA inflammatory environment induces osteoclastogenesis, which is the process of osteoclast formation and maturation, thus promoting bone resorption and focal erosions [64]. In addition, the systemic inflammatory environment promotes disturbances in skeletal bone remodeling, shifting the balance towards bone resorption. This ultimately leads to the development of secondary osteoporosis, which is characterized by bone loss, structural impairment and decreased bone strength, causing an increased fracture risk [65]. In the following sections a detailed description of bone tissue and its mechanical properties and the current knowledge on how these are affected by RA is given.

Bone biology

Bone structure

Bone is a hierarchical structure with mechanical characteristics dependent on the synergistical combination of its organic and inorganic components.

At the nano scale, bone is composed by mineralized collagen fibrils. Collagen fibers are organized in lamellae (Fig. 2A) oriented in the same direction, which are packed in several layers with different angles. Immature bone, present during growing and fracture repair, lack this organization and is known as woven bone [66].

Haversian bone (found in the cortical aspect of bone) is a highly organized structure, arranged in concentric lamellae surrounding the Haversian structures,

which are composed by a vascular channel containing nerves and blood vessels (Fig. 2A). This complex structure is named osteon. Volkmann's canals are transversal to the Haversian canal and provide vascular support to bone [67]. Osteons are the functional units of cortical bone and are in a constant remodeling process. High bone remodeling is associated with the appearance of concentric lamellas in secondary osteons, as previously described [68-70]. Dall'Ara *et al.* suggested that larger numbers of these younger, less mineralized and less hard structures, could be related to reduced hardness of bone tissue. On the contrary, more parallel-lamellae structures are 10% harder than the former, representing a mature bone structure [70].

Between lamellae there are ellipsoidal holes called lacunae, which are occupied by osteocytes. These cells communicate with each other through channels named canaliculi's, occupied by dendritic filaments [71,72].

A cement line is a calcified thin layer of mucopolysaccharides with low collagen and mineral content [73], which is arranged around the new osteon. This cement line represents a weak boundary that plays an important role in the mechanical behavior of bone, responsible for energy dissipation during crack propagation. [73,74].

At the highest hierarchical level, bone is a porous mineralized structure composed by cells, vessels and crystals of calcium compounds (hydroxyapatite).

There are two mature forms of bone, cortical and trabecular, with similar chemical compositions, but different in their structure [66]. Cortical bone represents the external side of skeletal structure and is characterized by a dense and compact structure, which contains 80% of the total bone mass [64]. This skeletal structure organization has a low bone turnover and a higher resistance to torsion and bending. This calcified structure provides mechanical strength, rigidity and protection. In addition, cortical bone can also play an important role in metabolic processes, particularly in the maintenance of calcium levels.

Trabecular bone, located in the medullar part of bones, constitutes 20% of the total skeletal mass [75]. Trabecular bone has a higher turnover rate comparing to cortical bone due to its higher bone surface, representing 80% of the total bone surface. This type of bone is more elastic and less dense, capable of tolerating unusual loads without cracking [76].

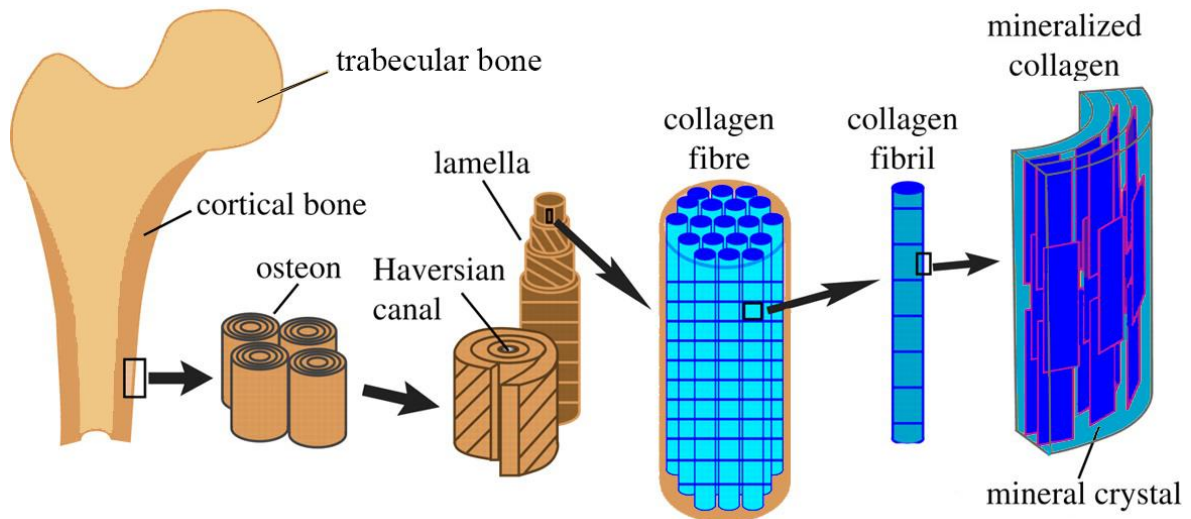


Figure 2 - Bone hierarchical structure organization. Adapted from [77].

Bone matrix

Bone matrix is composed by collagen and noncollagenous proteins, which represent about 90% of the total organic content of the whole bone tissue [78].

Collagen is the most common protein in mammals and represents a family of proteins present in connective tissues. These are ubiquitous proteins, responsible for the maintenance of bone tissue integrity. Structurally, collagen contains a three-polypeptide chain, with a triple-helix structure, which is arranged in fibrils and then assembled into fibers [79].

Collagen type I fibers can be organized in arches, which confer a higher collagen density in bone tissue. Collagen fibers can also be organized parallel to each other or in a concentric conformation in order to surround the Haversian system. The hydroxyapatite crystals $[3\text{Ca}_3(\text{PO}_4)_2 \cdot (\text{OH})_2]$ tend to acquire collagen fibers' organization [64].

Several noncollagenous proteins are present in bone matrix. However, their role is not fully understood. Osteocalcin is one of the major noncollagenous protein present in bone matrix. It plays an important role in calcium binding, hydroxyapatite matrix stabilization and negative regulation of bone formation, inhibiting premature and inappropriate mineralization [80]. Another noncollagenous protein, biglycan, is responsible for the positive regulation of bone formation [81].

Collagenous proteins

Collagen type I is the most common protein in bone matrix. It represents 95% of the total collagen in bone [82]. The remaining 5% of collagen bone composition is composed by other collagenous proteins, such as type III and V, that modulate fiber diameter [83].

Collagen type I is organized in a three dimensional arrays in concentric weaves (Fig. 3A). The collagen structure is composed by three interwoven chains that can vary between homotrimeric or heterotrimeric, according to the collagen type [84,85]. The repeated glycine triplet Gly-X-Y is responsible for the triple helix conformation, where the position X is commonly a proline and the position Y a hydroxyproline [84]. The third position, in the center of the triple helix, is filled by the small amino acid Gly (Fig. 3A).

Fibril structures are constituted by collagen molecules that comprehend short terminal domains, N- and C-propeptides, which subsequently suffer proteolytic cleavage. This process produces tropocollagen, a triple helix collagen structure with short telopeptides (Fig. 3C; D). The final assembly of fibrillary collagen involves the interaction with several proteins that have a role in the organization of the matrix pattern and control the diameter of the fibrils (Fig. 3E) [86,87]. Furthermore, biglycan and decorin, two proteoglycans, interact with the collagen molecules to allow fibril formation and mineral deposition (Fig. 3F) [88-91].

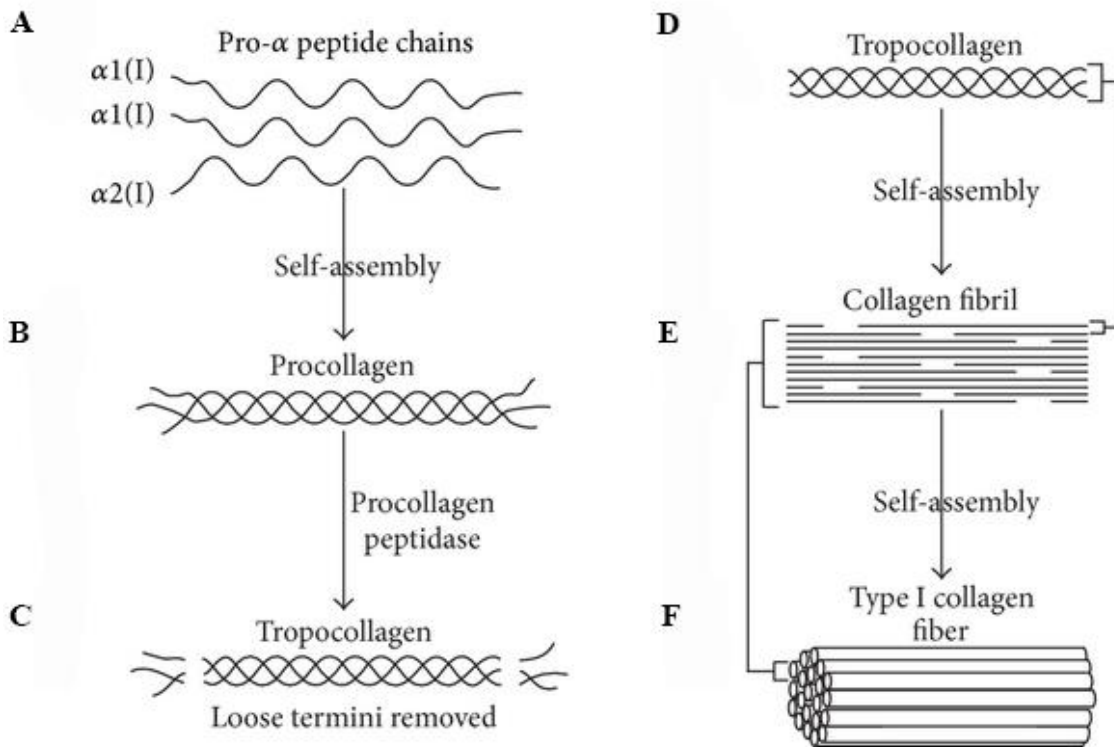


Figure 3 – Collagen type I synthesis process. Two identical $\alpha 1$ and one $\alpha 2$ (A) peptide chains form a procollagen protein (B). Procollagen peptidase (C) removes the chains termini to create a type I tropocollagen molecule (D). Tropocollagen molecules induce the formation of a growing collagen fibril (E). A connected collagen fibrils forms a type I collagen fiber (F). Adapted from [92].

In clinical practice, products of the collagen processing or breakdown, both for formation or degradation, act as markers of collagen turnover and are used to assess bone remodeling [93].

Bone formation can be assessed through the quantification of several serum or plasma markers, such as osteocalcin, bone specific alkaline phosphatase (BSAP) and amino or carboxy-terminal propeptides of collagen type I (P1NP, P1CP) [94]. P1NP is widely used for scientific research, due to the fact that it is a stable soluble marker and has low interindividual variability [95,96]. P1NP results from the posttranslational cleavage of the pro-collagen molecule before its organization into fibrils [97,98]. The propeptides P1NP and P1CP are two small domains, which compose the procollagen molecule that is enzymatically cleaved after secretion into the extracellular space. Quantitative measurements of P1NP correspond to

the amount of newly collagen formation, where serum levels can be correlated with bone formation indices assessed by histomorphometry [99,100].

The majority of bone resorption markers result from the degradation products of collagen type I, with the exception of tartrate resistant acid phosphatase (TRAP5b), which is a bone marker independent from the collagen cleavage [94]. TRAP5b is a bone resorption indicator, which is highly specific for osteoclasts *in vivo*, reflecting the number of osteoclasts [101]. TRAP5b is probably the most reliable resorption marker [95]. Bone resorption markers can be measured in urine through the quantification of pyridinoline (PYD) or deoxypyridinoline (DPD) and in the serum or plasma by dosing carboxy and/or amino-terminal cross-linked telopeptide of type I collagen (NTX I and CTX I, respectively) [95]. The cross-linked telopeptides of collagen type I, carboxy (CTX) and amino-terminal (NTX), are products of the collagen cleavage. Both CTX and NTX are products of cathepsin K (CTSK) action and represent collagen breakdown. However, the circadian variation of CTX represents a major disadvantage and sample acquisition must be collected during morning fasting [102]. In contrast, NTX is easier to be used in the clinical setting as it is not affected by circadian changes and food intake [103].

Noncollagenous proteins

Total bone protein is composed by 10 to 15% of noncollagenous proteins. Osteoblasts are responsible for the major production of noncollagenous proteins. However, 25% of noncollagenous proteins, such as the plasma protein α 2-HS-glycoprotein, are produced in the liver [64]. The noncollagenous proteins albumin and α 2-HS-glycoprotein are able to bind hydroxyapatite, due to their acidic characteristics. Matrix mineralization is partially regulated by resultant products of noncollagenous proteins. In addition, α 2-HS-glycoprotein helps to control cell proliferation of bone [64]. The exogenous noncollagenous proteins are essentially composed of growth factors, which may affect the cellular activity of bone. Several categories divide the noncollagenous proteins in proteoglycans, glycosylated proteins, glycosylated proteins able to cell-binding and γ -carboxylated (gla) proteins. Although their function is not fully understood, roles that include

regulation of bone turnover, mineral bone deposition and bone cellular activity have been suggested [64]. Osteocalcin is produced by osteoblasts and plays an important role in the deposition of calcium in collagen fibrils. However, studies suggest that osteocalcin mainly inhibits bone formation [104]. The highest level of osteocalcin expression is present in osteocytes, which are cells not actively engaged in promoting mineral maturation [105]. Osteocalcin is currently regarded as a bone turnover marker rather than a bone formation marker, considering that serum osteocalcin is a product of osteoclastic activity during bone resorption [64]. The major bone glycosylated protein is alkaline phosphatase, which binds to osteoblast surface through phosphoinositol linkage. However, the specific role of alkaline phosphatase in bone mineralization remains unclear [106]. Osteonectin is another major common noncollagenous protein in bone, playing a role in osteoblast proliferation and bone matrix mineralization [107].

Hydroxyapatite crystals

Bone is composed by 50-70% of minerals, 20- 40% of organic matrix, 5-10% of water, and approximately 3% of lipids [64]. Bone mineral content is mainly hydroxyapatite $[\text{Ca}_{10}(\text{PO}_4)_6(\text{OH})_2]$, with low amounts of carbonate, acid phosphate and magnesium [64]. The mineral deposition is regulated by proteins that bind calcium and phosphate which control the size and amount of the new hydroxyapatite crystals. Mineral content provides structural and mechanical strength and stiffness to bone, while the organic matrix provides elasticity and flexibility, able to absorb loads. [64,108].

Osteoblasts synthesize the extracellular matrix, a protected microenvironment, allowing the increase of calcium and phosphate levels in order to promote precipitation and formation of hydroxyapatite crystals [64].

Vesicles from extracellular matrix are composed by a nucleation core, containing proteins, acidic phospholipids, calcium and inorganic phosphate which precipitate as hydroxyapatite crystals [109]. Bone matrix macromolecules may favor the initial crystal nucleation, which isolate mineral ions in order to increase calcium and phosphorus concentrations or promote heterogeneous nucleation. Macromolecules also control the number, shape and size of newly formed crystals.

Matrix mineralization is regulated by phosphoprotein kinases and alkaline phosphatase. Alkaline phosphatase increase local phosphorus levels by removing phosphate-containing inhibitors of hydroxyapatite crystal growth, or by modifying the ability of phosphoproteins to act as nucleators (mineralization promoters) [110].

Vitamin D indirectly stimulates the mineralization of bone matrix [64]. After vitamin absorption or endogenous skin production, 25-hydroxyvitamin D is synthesized by the liver and subsequently the biologically active form of vitamin D, 1,25-dihydroxyvitamin D [1,25-(OH)₂D], is produced by kidneys. Serum 1,25-(OH)₂D is responsible for the regulation of calcium and phosphorus serum concentrations to permit passive mineralization of bone matrix. Calcium and phosphorus are absorbed by the intestine through serum 1,25-(OH)₂D stimulation [111]. The active form of vitamin D also promotes osteoblast differentiation and stimulate the production of alkaline phosphatase, osteocalcin, osteonectin, osteoprotegerin (OPG) and several other cytokines [112].

Bone cells

Osteoclast

The osteoclast is a giant multinucleated cell, which results from the fusion of mononuclear cells (macrophage / monocyte family) [113]. Osteoclasts are commonly found in close contact with the bone surface, promoting bone resorption and leading to the formation of resorption lacunae (Howship's lacunae).

The osteoclasts attachment to bone commonly occurs through podosomes, dynamic structures that allow their motion throughout bone surface [114]. This process occurs during bone resorption, which involves binding of protein integrins to the bone surface [115], allowing the formation of the sealing zone, where bone resorption occurs.

Osteoclasts have a complex cell organization, with an abundant Golgi apparatus, mitochondria and vesicles for the transport of lysosomal enzymes [116]. These cells present foldings in their plasmatic membrane, named ruffled boarder, which

are in close contact with the sealed zone of the bone matrix [117,118]. TRAP and cathepsin K are two lysosomal enzymes synthesized by osteoclasts that play role in bone resorption [119,120].

Osteoblast

The osteoblast is derived from mesenchymal stem cells and is responsible for bone matrix production [64]. Osteoblasts are arranged in clusters, lining on the layer of bone where they produce new bone matrix [121].

Bone formation occurs in three distinct phases: production, maturation of the osteoid matrix and respective mineralization [122]. Firstly, osteoblasts synthesize osteoid through collagen deposition, which is followed by mineralization proportional to the previous collagen synthesis. Lastly, collagen synthesis decrease, while mineralization still continues, in order to ensure the mineralization of all the new osteoid [122].

Osteoblasts play an important role in the maintenance of bone resorption, through the expression of receptor activator of nuclear factor-kappaB (RANK) ligand (RANKL) that binds to RANK receptor. This receptor lies on the pre-osteoclasts surface, and promotes osteoclast differentiation and fusion. On the other hand, osteoblasts are also able to produce OPG, a RANKL receptor which blocks the RANKL/RANK, preventing the osteoclastogenesis [123,124].

Osteocyte

Osteocytes derive from osteoblasts that have been trapped in the osteoid during bone formation process, are non-proliferative and terminally differentiated cells. Osteocytes constitute the main cellular component of mammalian bone, representing more than 95% of bone cells [125].

It remains unclear if the decision for an osteoblast to become an osteocyte is determined by a specific pattern of gene expression, a cell autonomous response or an event that is controlled by signals received from already embedded osteocytes [126].

Osteocytes locked inside a small lacuna, have numerous microfilaments that are organized during the formation of the matrix and before its calcification. They form a network of thin canaliculi permeating the entire bone matrix [127]. Moreover, osteocytes communicate with each other and with the cells at bone surface through this lacuna-canalicular system [128]. Once embedded within bone matrix, the osteocyte ceases its matrix synthetic activity and initiates the function as strain and stress sensor [129]. Osteocytes react to bone strain by increasing remodeling of bone tissue through osteoclast recruitment [130]. Another function of osteocytes within the bone cell network is the ability to deposit and resorb bone around the lacunae in which they are housed, by a process called osteocytic osteolysis [131]. Both osteocyte functional activity and morphology are dependent on cell age. After osteoblast is trapped into the bone matrix, it starts to lose its osteoblast characteristics, decreasing cell volume and capacity for protein synthesis. During the bone remodeling process, older osteocytes are phagocytosed by osteoclasts [132].

Bone remodeling

Bone is a living organ that retains the ability of regeneration in adult life. Bone remodeling results from bone cellular activity, where matrix is renewed to maintain mechanical strength and mineral homeostasis. The bone remodeling process consists in the resorption of the old bone and formation of the new bone [133,134]. Osteoblasts and osteoclasts closely collaborate in the remodeling process constituting the basic multicellular unit (BMU) [135]. The organization of the BMUs in cortical and trabecular bone differs mainly in morphologic rather than biologic characteristics (Fig. 4).

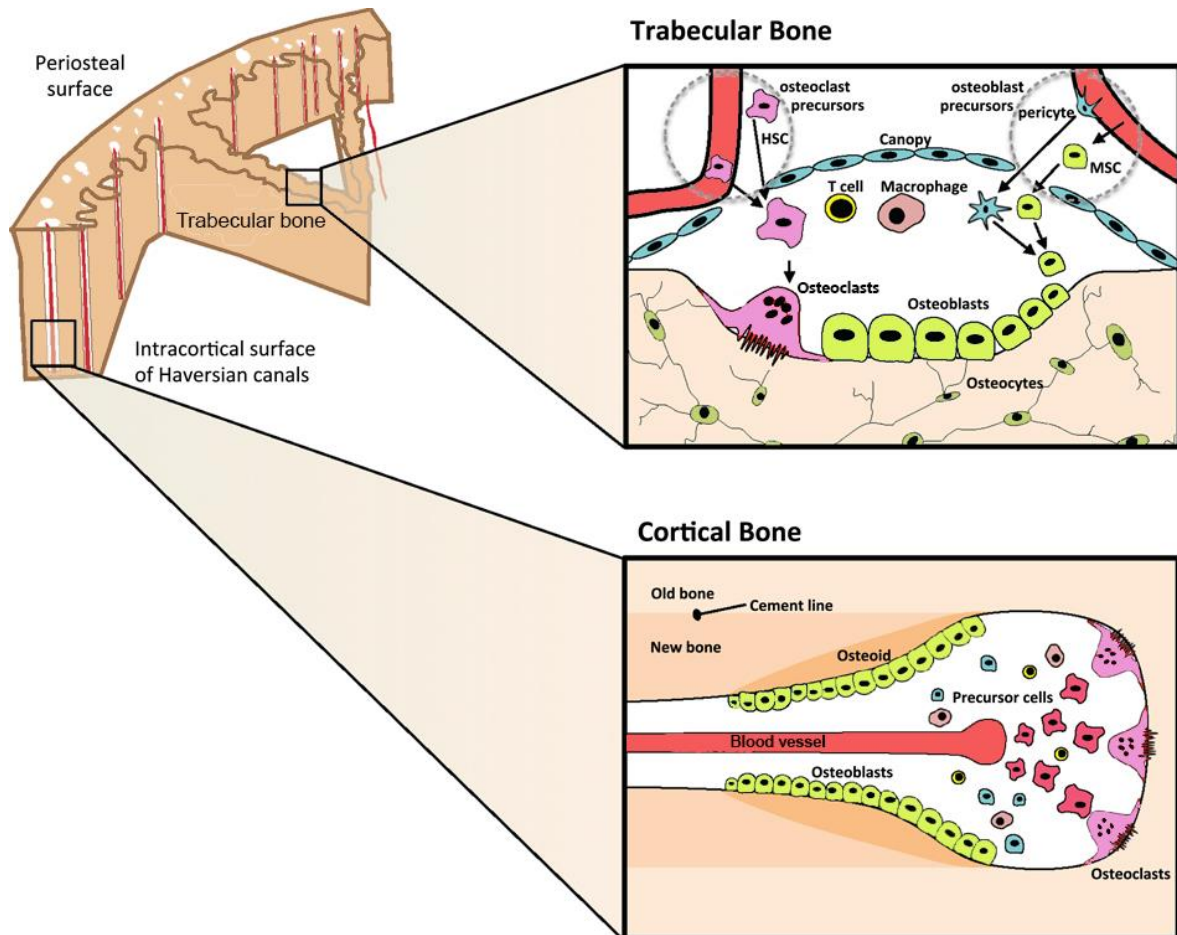


Figure 4 - Structural organization of the basic multicellular units (BMU) in cortical and trabecular bone. Remodeling starts within bone remodeling compartment (BRCs) at trabecular bone (upper panels) and within cortical bone Haversian canals (lower panels). HSCs - hematopoietic precursor cells; MSCs - mesenchymal stem cells. Adapted from [136].

Cortical BMUs are organized in a cylindrical structure that gradually forms a pit within bone tissue [137]. During the remodeling cycle, activated osteoclasts open a circular channel in the load direction. Later, this channel will be occupied by osteoblasts, promoting bone formation [137,138]. Each year, cortical bone is remodeled approximately in 2 - 5% [139]. In contrast, trabecular bone has an annual turnover rate of about 15 -25% [139].

The bone remodeling cycle starts with the activation phase, which involves osteocytes, lining cells and pre-osteoblasts in the bone marrow (Fig. 5). During the resorption phase, pre-osteoclasts begin their migration to the bone surface, where they fuse and differentiate into multinucleated osteoclasts. Then, after osteoclastic

resorption the reversal phase begins with mononuclear cells (reversal cells) on bone surface. Reversal cells are responsible for preparing bone surface for bone formation promoted by osteoblasts. This process will stimulate the differentiation and migration of osteoblasts [140]. After the osteoblastic migration, the formation phase begins, where osteoblasts start to produce new bone matrix. When the formation process is completed, the surface of the new bone is covered by flattened bone-lining cells, beginning a longstanding period where bone rests, before new remodeling cycles begin [64,122].

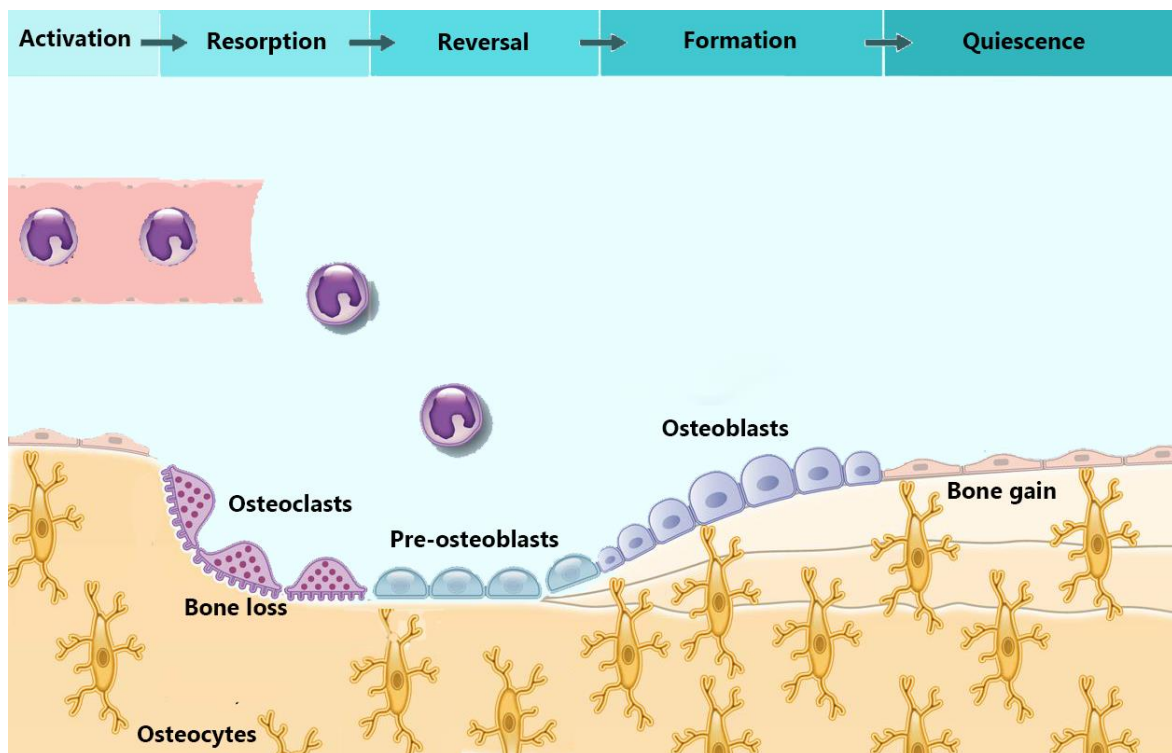


Figure 5 - Physiological phases of the bone remodeling process. The remodeling cycle is composed of six sequential phases: activation, resorption, reversal, formation, termination, and quiescence. Resorption by osteoclasts is the initial stage of bone remodeling, which osteoblasts respond to signals generated by osteocytes or direct endocrine activation signals, recruiting osteoclast precursors to the remodeling site. The following phase, reversal phase, is characterized by disappearance of almost all osteoclasts, conducting to the formation phase by osteoblasts. The termination signals of bone remodeling include the final differentiation of the osteoblast. Adapted from [141].

The bone remodeling maintenance is both systemic and local [122]. Amongst the major systemic regulators of this process, there are several hormones, such as parathyroid hormone (PTH), calcitriol, growth hormone, glucocorticoids, thyroid

hormones and sex hormones [122]. At the level of local regulation of bone remodeling, cytokines and receptors, such as the RANK/RANKL/OPG system (Fig. 6), and growth factors play a role affecting bone cell functions [64]. RANKL/RANK interaction results in activation, differentiation and fusion of hematopoietic cells of the osteoclast lineage, initiating the resorption process [123]. Furthermore, it also prolongs osteoclast survival by suppressing their apoptosis [142]. This signaling indicates that bone resorption and bone formation are coupled processes through RANKL.

OPG, a secretory dimeric glycoprotein, which belongs to the family of TNF receptors, blocks RANKL effects [143]. OPG is a decoy receptor (a soluble receptor acting as antagonist) for RANKL and is mainly synthesized by the osteoblast lineage cells [144,145]. OPG regulates bone resorption through inhibition of the final differentiation and activation of osteoclasts, inducing their apoptosis [122,123] (Fig. 6).

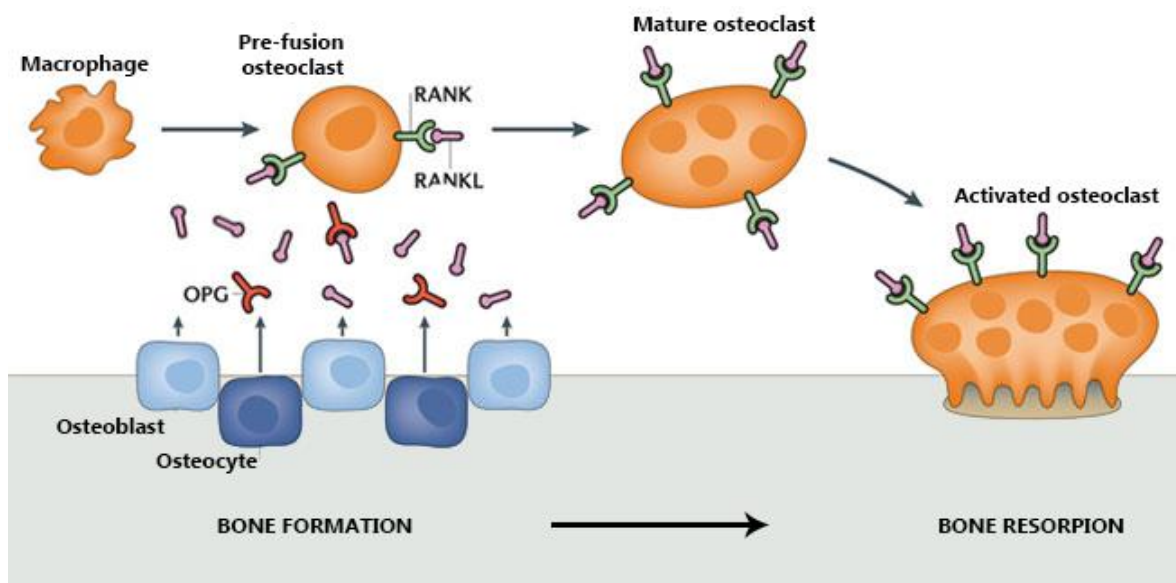


Figure 6 - RANK-RANKL-OPG signaling pathway scheme. Osteoblasts produce receptor activator of nuclear factor kappa-B ligand (RANKL) and osteoprotegerin (OPG). RANKL is inactivated after OPG binds, resulting in the inhibition of differentiation and activation of osteoclasts. In the presence of downregulation of OPG, RANKL activates its receptor, RANK, which is expressed on osteoclasts and preosteoclast. Adapted from [146].

During bone lifetime there are some fluctuations on the balance of bone remodeling. Negative balances may lead to bone loss and increased remodeling rate, compromising bone strength [133]. During growth, the balance between the

volume of resorbed bone and the volume that is formed in BMUs is positive at the level of trabecular surface, thus each remodeling event adds a small fraction of bone [147]. When skeletal size achieves its programmed size, the need for rapid remodeling and a positive balance between the resorbed bone volume and deposited in each BMUs decreases. In adults, one of the first changes in the remodeling machinery that conducts to bone loss is due to the decline in bone formation within BMUs [148]. Some studies demonstrated a reduction in bone formation in midlife [149,150], but this may begin in young adults when the need to build the skeleton declines [151-153]. Bone resorption became a priority, leading to bone loss and structural damage. However, the positive balance in BMUs during growth and the negative balance during aging are small. Thus, the rate of gain in bone growth and loss during aging results more from the high remodeling rate rather than by the magnitude of the positive or negative balance in BMUs [148].

Rapid remodeling is another risk factor for bone fracture, for several reasons. One of them is the contribution for the old bone replacement by younger bone, less densely mineralized with reduced material stiffness [154,155]. As a result, bone may become too flexible, bending excessively and cracking under usual loading conditions. Second, after osteoclast activity bone present concave structures, corresponding to resorption sites which remain temporarily unfilled, because of the delay between resorption and formation, creating stress concentrators that predispose bone to micro damage [156]. Third, increased remodeling impairs isomerization and maturation of collagen, which increases the fragility of bone [157,158], probably by altering the crosslinking between adjacent collagen fibers. Another reason for bone remodeling fluctuations is estrogen deficiency, (e.g., after menopause), which increases the rate of remodeling and the bone-resorbed volume, by prolonging the life span of osteoclasts. It also decreases the bone volume formed by reducing the life span of osteoblasts, conducting to negative bone balance in the BMUs [133,159]. The combination of a rapid rate and imbalanced remodeling in BMUs accelerates bone loss and structural decay after menopause [133,148].

Bone mechanics

Bone has a varied arrangement of material structures that gives bone biological and chemical functions, as well as mechanical competence.

Bone must be ductile and able to absorb energy, allowing deformation during loading. If bone is not sufficiently ductile, the energy applied to tissue will originate bone microcracks because it cannot deform efficiently and absorb energy. Bone must also be light to allow movement [160]. The main determinants of these bone mechanical properties are the amount of mineral, collagen content and fiber's orientation, together with geometric properties that confer structural strength and thus the ability to accumulate microcracks in bone matrix [161]. Bone biomechanics is particularly affected by the volume fraction of mineral crystals, their shape, size and arrangement within the organic collagenous matrix [162].

Bone mechanical tests can be compressive, three- or four-point bending, shear and nanoindentation tests [163]. In biomechanical tests, a load-deflection curve is obtained, which allows the acquisition and determination of different parameters in order to assess several mechanical properties, such as elastic properties, plastic properties, yield point and maximum load among others (Fig. 7).

Bone mechanical properties describe the relationship between applied forces, or loads and bone deformation. The resistance of bone in response to these forces is known as stress and represents the intensity of the local force. The resultant deformation is referred to as strain and is defined as a relative change in size and shape [164]. The mechanical properties of bone can be summed up as the maximum load, deflection and stiffness of the sample, which corresponds to the slope of the linear region of the stress strain curve. The linear section of the stress strain curve represents the elastic phase [157]. Its curve slope represents the Young's modulus, a stiffness indicator of the sample tested. The transition of the linear to the nonlinear curve corresponds to the yield point, where the plastic phase starts. During the elastic phase, the load applied to bone promotes its deformation [157]. However, when the applied load is removed, bone has the capacity to return to its original shape. In contrast, during the plastic phase the applied load promote permanent damage, inducing microcracks in the bone structure which leads to irreversible changes. The total area under the curve which comprises the elastic and plastic phases represents the work that must be done

per unit volume on bone before it fails. Ultimate stress represents the maximum stress sustained by bone without breaking [157]. Another important parameter that can be recorded by stress-strain curve analysis is the toughness, which indicates the energy required for bone fracture [165]. Hardness represents a characteristic that expresses the capacity to resist to permanent deformation. This parameter is closely related to the amount of mineral in bone, which tend to be inverse to toughness [166].

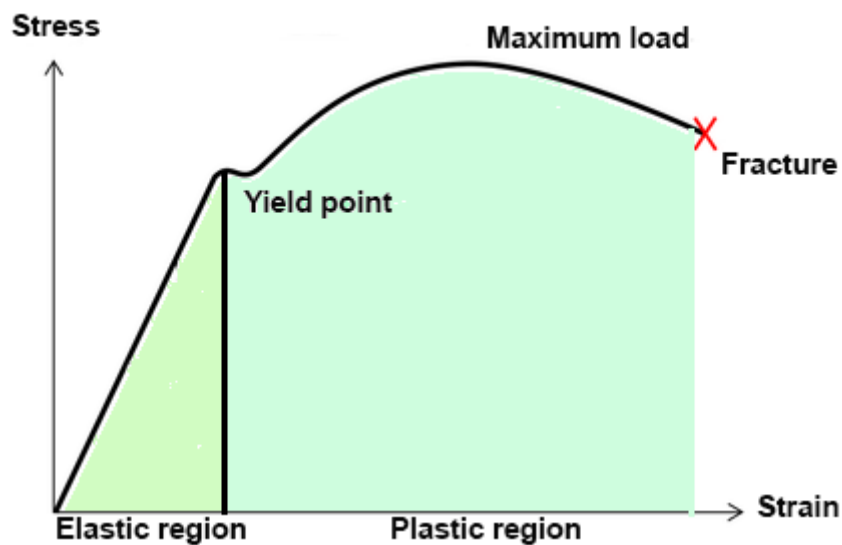


Figure 7 - A typical bone specimen loaded in tension stress–strain curve. Adapted from [167].

Bone is an anisotropic material since its mechanical properties depend on the loading direction. This characteristic reflects bone function and the degree of anisotropy varies with anatomical site and functional loading [168].

The cortical and trabecular types of bone present different biomechanical performances. Cortical bone is stiffer and resist to higher stress but sustains lower strain before failure compared to the trabecular bone. Due to its porous structure, trabecular bone has a large capacity for energy storage. Both cortical and trabecular bone mechanical properties are dependent on bone density [169].

The mineral and organic phases of bone have extremely different mechanical properties. The mineral phase confers strength and stiffness to bone tissue [170]; however, at high levels of mineralization, bone becomes brittle, reducing the energy required for fracture [171]. On the other hand, the organic phase is more

ductile [172]. It is notable that bone gathers the optimal properties of the two phases, the stiffness and the toughness [173,174], by keeping stiffness (mineral phase contribution) and strain to fracture (organic phase contribution). These unusual combined material properties, provides rigidity and resistance against fracture.

Bone quality is a term based on the structural and material properties of bone and their arrangement [175]. These structural properties include geometry (size and shape of the skeleton) and microarchitecture, whereas the material properties include the organization and composition of the mineral and collagens components of extracellular matrix, as well as, the extent of micro damage within the tissue [176,177].

Fractures prevention is not only controlled by specific processes of crack initiation and propagation, but also by the ability of bone tissue to repair micro damages during its remodeling process [178]. During bone remodeling process, old bone is continuously replaced by newly formed material and bone micro damages are removed, causing high heterogeneity in local bone matrix areas [179]. As such, bone is not uniformly mineralized as a consequence of continuous bone remodeling [180]. Discontinuities in bone matrix mineralization might be determinant for crack initiation and propagation in bone and, thus, are essential for its toughness [181].

The optimization of bone mechanical properties is truly dependent on the structural interaction between the organic and mineral components [182]. These properties are a result of a compromise between the need for stiffness and the need for ductility to absorb impacts. Toughness is essential to ensure that microcracks generated during normal life, which are associated with loss of stiffness, do not conduct to bone fracture. If their accumulation is faster than their repairing, microcracks multiply and produce macrocracks, which can culminate in complete fracture [183]. The microcracking increases the compliance of the bone material, and so increasingly larger deformations are produced for a given increase in load. The ability to undergo large strains, and hence large deformations, allows the bone to absorb a considerable amount of energy before fracture [184]. Thus, the ability to microcrack is an important pre-requisite for toughness [182,185].

Many disorders or specific conditions (as part of the normal aging process) can affect bone quality [186]. Progressive loss of bone density occurs with the reduction of bone mass, which occurs earlier and more extensively in trabecular than cortical bone, associated with impaired microarchitecture, increased fragility and risk of fracture [186].

Bone fragility is more prevalent among women than in men mainly because of estrogen deficiency after menopause. In postmenopausal women, high remodeling rate is associated with a bone negative balance that promote structural changes on bone microarchitecture, such as decrease in trabecular and cortical thickness and increased porosity and a consequent reduction in trabecular connectivity. The process of mineralization is not able to follow the accelerated remodeling rate and thus stiffness is reduced [160,187].

Rheumatoid arthritis and Bone

Bone erosions occur rapidly in RA and are detectable in 80% of the patients during the first year after diagnosis [5,188]. Several synovial cytokines, such as RANKL and macrophage colony-stimulating factor (MCSF), promote osteoclastogenesis and their activation [63]. Furthermore, osteoclastogenesis is amplified by TNF, IL-1 β , IL-6 and IL-17 (Fig. 8) [189]. Osteoclast induced joint bone damage promotes resorption pits that are further filled by inflammatory tissue [190]. The consequent cleft in cortical bone allows synovial tissue to access bone marrow, promoting infiltration by B and T-cells, which gradually replace fat bone marrow [191]. However, the origin of these bone inflammatory lesions remains unclear. They can occur as synovium-induced erosions or as a consequence of primary osteitis, which in this case would precede bone erosions [5,192].

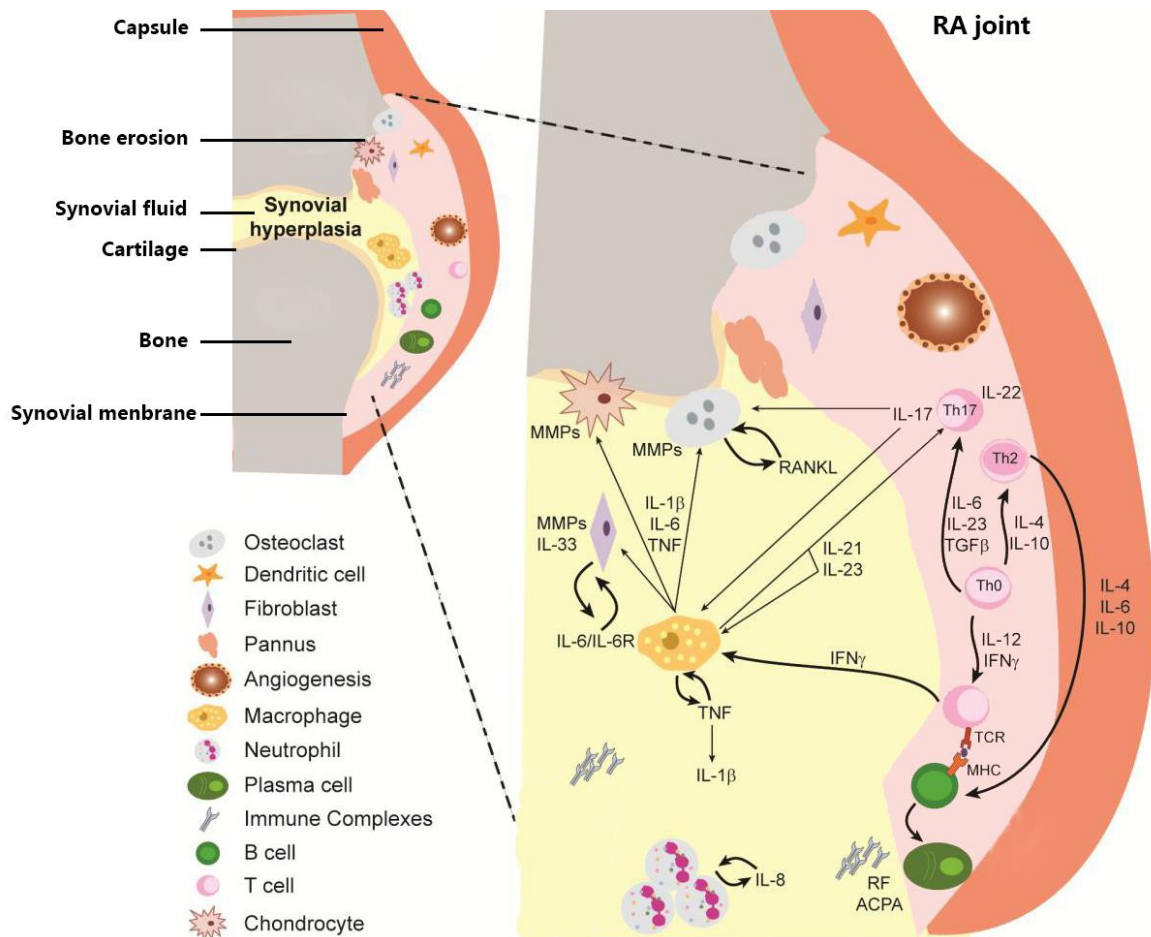


Figure 8—Immune cells and cytokine networks scheme in rheumatoid arthritis joint. RA is characterized by synovial hyperplasia caused by immune cellular infiltration, leading to pannus formation and consequent cartilage and bone destruction. Several cytokines are produced by Immune cells, promoting inflammation and osteoclastogenesis. ACPA – Anti-citrullinated protein antibodies, IFN γ – Interferon gamma, IL – Interleukin, IL-6R – IL-6 receptor, MHC – Major histocompatibility complex, MMP – Metalloproteinase, RANKL - Receptor activator of nuclear factor ligand, RF – Rheumatoid factor, TCR – T-cell receptor, TGF β – Transforming growth factor beta, Th – T helper, TNF – Tumor necrosis factor. Adapted from [193]

The systemic inflammatory process of RA can result in bone loss at several levels: focal joint bone erosion, juxta-articular osteopenia adjacent to inflamed joints and systemic osteoporosis [194,195]. This bone loss results from alterations in the bone remodeling process, leading to changes in bone homeostasis that favor bone resorption over bone formation [196,197].

Osteoclasts express high levels of CTSK and TRAP in their lysosomal compartments. Both enzymes are involved in the degradation of bone matrix in homeostatic and pathologic bone remodeling [198,199].

Synovial tissue comprises activated fibroblasts and T-cells which are the two major cellular sources of RANKL and MCSF, the two major determinants of osteoclast formation [47,200-202]. TNF and IL-1 β upregulate and modulate RANKL expression on osteoclast precursors [203-205]. IL-6 is another cytokine which upregulates RANKL expression, promoting osteoclastogenesis and consequent bone damage [206]. Finally, Th17 can also play a role in osteoclast differentiation via cell-to-cell contact with osteoclast precursors [207,208].

Thus, RA inflammatory environment induces bone remodeling disturbances, leading to bone erosions and also to the development of secondary osteoporosis [133]. This imbalance in bone resorption over bone formation promotes architectural degradation of cortical and trabecular compartments, ultimately leading to bone fragility [209].

Treatment options for RA

RA is chronic disease with major economic and personal costs. The management strategy is based on a prompt diagnosis and treatment intervention, aiming at inducing remission, in order to preserve joint structures and quality of life [210-212]. Drug free remission is the ultimate goal of RA treatment. However, this is an almost impossible goal to be reached by the currently available treatments.

Disease control requires generally a combination of drugs, including non-steroidal anti-inflammatory agents (NSAIDs), low dose glucocorticoids and disease modifying antirheumatic drugs (DMARDs), which slow the disease progression and reduce joint damage [210].

Glucocorticoids

Prednisone, a glucocorticoid, acts rapidly in the control of inflammation and their associated joint pain and swelling [213] and reduce the development of bone erosions [214-218]. Glucocorticoids play an important role during the first weeks of RA diagnosis, due to the fact that DMARDs have a slow onset of action. However, their use is limited, due to adverse effects, especially in high doses [219]

Conventional DMARDs

Conventional DMARDs are the first line treatment of RA. [213,219,220]. Methotrexate (MTX) is the most widely used one as it has the best balance between efficacy and safety, allowing for long-term and sustained responses [221-223]. For patients that have contraindication or develop adverse effects, other DMARDs such as leflunomide, sulfasalazine and hydroxychloroquine can be used. DMARDs have a slow on-set of action (1 up to 6 months) but they are effective and safe at long term [213,224], either as monotherapy or in combination therapy. However, approximately 30% of the patients are either non-responsive to conventional DMARDs or develop serious adverse effects to them [225-227],

Biologic DMARDs

Biological therapies have been developed in the last decades and target individual molecules. Biological therapies are available for patients who have not responded to conventional DMARDs or have presented side-effects from their usage. Usually, biological therapies are given in combination with a conventional DMARD such as MTX, in order to potentiate the effectiveness.

Nine biologic DMARDs are approved by the European Medicines Agency (EMA) for the treatment of RA (Fig. 9). These biologic therapies have demonstrated symptomatic benefit, improvement in functional capacity and prevention of structural damage. [211].

TNF antagonists (etanercept, adalimumab, infliximab, golimumab and certolizumab) are usually the first line biologic DMARDs. The compared effectiveness of TNF antagonists is similar and combination with MTX confers more efficacy than their use as monotherapy [211,228,229].

TNF inhibition downregulates the immune response, which increases the infection risk, particularly tuberculosis reactivation. Patients who fail to respond to a TNF antagonist have a 50% chance to respond to a second one. However, the probability of responding to a third one is much lower [219]. Rituximab (anti CD20 B lymphocyte depleting therapy), tocilizumab (an antibody against the IL-6 receptor) and abatacept (a T-cell co-stimulation blocker), in association to MTX,

are alternatives for RA patients who have failed conventional DMARDs or TNF antagonists [230,231]. They have demonstrated inhibition of bone structural damage [232-236]. Tocilizumab might be more effective in monotherapy than the other DMARDs [237]. Blocking IL-1 β with anakinra was shown to be effective for the treatment of RA (and is approved by EMA), although at a lower efficacy level than TNF antagonists and is now used essentially for other indications [238-241]. There are other biologic agents that target IL-1 β receptor (rilonacept and canakinumab), which are not approved for RA treatment [242].

Switching among biologic DMARDs is often needed in patients with inadequate response to the initial treatment and the selection of the second biologic DMARD depends on individual aspects and on the reason of the first failure [243,244].

Overall, the safety of biologic DMARDs appears to be reasonable, particularly compared with the risks associated with the disease left uncontrolled. However, for all of them an increased risk of infections, injection-site reactions and immune mediated reactions have been observed [245]

Despite all the progresses observed in the treatment of RA, remission is only attained by 30% of the patients and most have a persistent and progressing disease.

Future perspectives

The development of therapeutic strategies able to control both inflammation and bone degradation, with a high rate of disease remission, low incidence of side effects and low production costs is still an unmet medical need in RA. Clinical evidence suggest that RA patients suffer focal and systemic bone damage early in the course of the disease and quite often treatment intervention is not able to truly alter this process.

Our hypothesis is that the impact of inflammation on bone micro and nano properties occurs almost immediately, upon first symptoms, and that these effects can be prevented by early intervention with drugs able to control inflammation and capable of interfering also with bone metabolism.

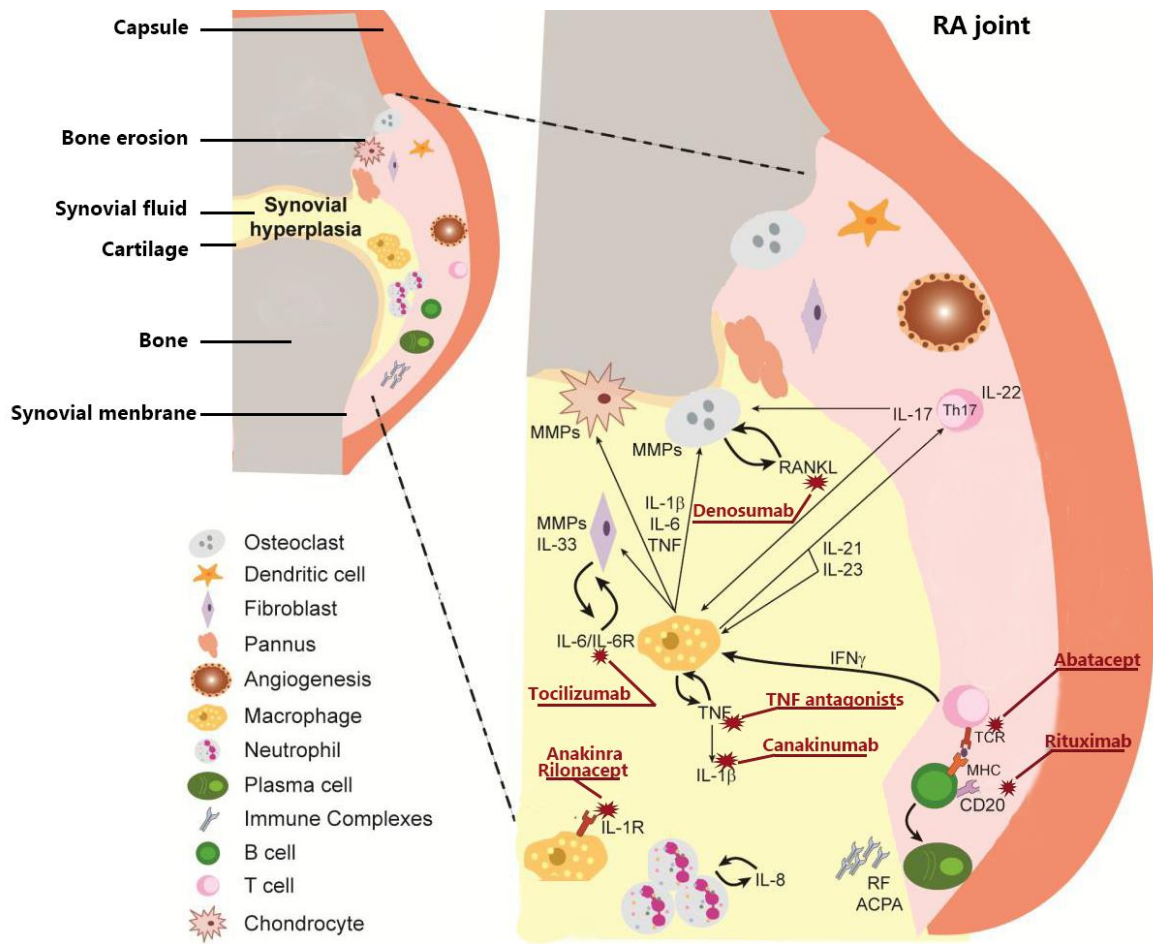


Figure 9 – Pathways targets of some currently available biologic agents for RA.

RA is heterogeneous disease that presents several development pathways. Treatment options for RA have been developed to stop or attenuate disease progression, which targeting some biological pathways. ACPA – Anti-citrullinated protein antibodies, IFN γ – Interferon γ , IL β – Interleukin β , IL-1 β R – IL-1 β receptor, IL-6R – IL-6 receptor, MHC – Major histocompatibility complex, MMP – Metalloproteinase, RANKL - Receptor activator of nuclear factor ligand, RF – Rheumatoid factor, TCR – T-cell receptor, TGF β – Transforming growth factor β , Th – T helper cell, TNF – Tumor necrosis factor. Adapted from [193].

Chapter II

Aims

Aims

The main goal of the present work was to study the impact of early arthritis on bone micro and nano properties and the inhibition of this process through treatment intervention.

- I. Characterization of the early effects of inflammation on bone micro and nano properties in the AIA rat model of arthritis;
 - a. Analysis of the early cytokine and bone turnover markers environment at arthritis onset in the AIA rat model of arthritis;
 - b. Study the influence of arthritis on cortical and trabecular bone micro and nano structure in the AIA rat model of arthritis;
 - c. Address the extent of early arthritis impact on micro and nano biomechanical properties of bone in the AIA rat model of arthritis;
 - d. Study the influence of early inflammation on bone matrix (mineral and collagen) in the AIA rat model of arthritis;
- II. Assess the effects of new compounds on micro and nano structural and mechanical properties of bone.

Chapter III

Results

In agreement with the Decreto-Lei 388/70, art. 8º, parágrafo 2, the results presented and discussed in this thesis were published or submitted for publication in the following scientific peer-reviewed journals:

- I. **Vidal B**, Cascão R, Vale AC, Cavaleiro I, Vaz MF, Brito JA, Canhão H, Fonseca JE. Arthritis induces early bone high turnover, structural degradation and mechanical weakness. PLoS One. 2015; 10(9): e0137372.
- II. **Vidal B**, Rita Cascão, Mikko Finnilä, Inês Lopes, Simo Saarakkala, Peter Zioupos, Helena Canhão, João Fonseca. Early arthritis induces disturbances at bone nanostructural level reflected in decreased tissue hardness. Submitted
- III. Cascão R, **Vidal B**, Lopes IP, Paisana E, Rino J, Moita LF, Fonseca JE. Decrease of CD68 Synovial Macrophages in Celestrol Treated Arthritic Rats. PLoS One. 2015 Dec 11;10(12):e0142448.
- IV. Rita Cascão*, **Vidal B***, Mikko A. J. Finnilä, Inês Pascoal Lopes, Simo Saarakkala, Luis Ferreira Moita, João Eurico Fonseca. Celestrol preserves bone structure and mechanics in arthritic animals. Submitted
- V. **Vidal B**, Rita Cascão, Mikko Finnilä, Inês Lopes, Simo Saarakkala, Peter Zioupos, Helena Canhão, João Fonseca. Effects of tofacitinib in early arthritis bone loss. Submitted

I. Arthritis induces early bone high turnover, structural degradation and mechanical weakness

Bruno Vidal, Rita Cascão, Catarina Vale, Inês Cavaleiro, Maria Fátima Vaz, Joaquim Brito, Helena Canhão, João Eurico Fonseca.

Author Contributions

Vidal and Cascão designed the experiments. Vidal performed all the experiments and wrote the chapter. Vale and Cavaleiro helped to perform 3-point bending tests and energy dispersive X-ray spectroscopy, respectively. Cascão, Vaz, Brito, Canhão and Fonseca supervised the work and revised the text.

Arthritis induces early bone high turnover, structural degradation and mechanical weakness

Bruno Vidal, Rita Cascão, Catarina Vale, Inês Cavaleiro, Maria Fátima Vaz, Joaquim Brito, Helena Canhão, João E. Fonseca.

ABSTRACT

Background – We have previously found in the chronic SKG mouse model of arthritis that long standing (5 and 8 months) inflammation directly leads to high collagen bone turnover, disorganization of the collagen network, disturbed bone microstructure and degradation of bone biomechanical properties. The main goal of the present work was to study the effects of the first days of the inflammatory process on the microarchitecture and mechanical properties of bone.

Methods – Twenty eight Wistar adjuvant-induced arthritis (AIA) rats were monitored during 22 days after disease induction for the inflammatory score, ankle perimeter and body weight. Healthy non-arthritic rats were used as controls for comparison. After 22 days of disease progression rats were sacrificed and bone samples were collected for histomorphometrical, energy dispersive X-ray spectroscopical analysis and 3-point bending. Blood samples were also collected for bone turnover markers.

Results – AIA rats had an increased bone turnover (as inferred from increased P1NP and CTX1, $p = 0.0010$ and $p = 0.0002$, respectively) and this was paralleled by a decreased mineral content (calcium $p = 0.0046$ and phosphorus $p = 0.0046$). Histomorphometry showed a lower trabecular thickness ($p = 0.0002$) and bone volume ($p = 0.0003$) and higher trabecular separation ($p = 0.0009$) in the arthritic group as compared with controls. In addition, bone mechanical tests showed evidence of fragility as depicted by diminished values of yield stress and ultimate fracture point ($p = 0.0061$ and $p = 0.0279$, respectively) in the arthritic group.

Conclusions – We have shown in an AIA rat model that arthritis induces early bone high turnover, structural degradation, mineral loss and mechanical weakness.

INTRODUCTION

Rheumatoid arthritis (RA) is a chronic immune-mediated inflammatory disease, which affects around 1% of the world-population [1]. It causes joint and systemic inflammation that is reflected in local and systemic bone damage [2]. Bone is a dynamic tissue composed mainly of a type I collagen matrix that constitutes the scaffold for calcium hydroxyapatite crystal deposition. Remodeling of bone is a continuous process by which osteoclasts resorb bone tissue and osteoblasts produce new bone matrix that is subsequently mineralized. Biochemical markers of this bone turnover are produced and released into circulation, providing a read-out of kinetics and the balance between bone loss and formation. More specifically, bone-resorbing osteoclasts release carboxy-terminal collagen cross-linking telopeptides (CTX-I), a marker for bone degradation, which is produced by cathepsin K that is involved in systemic bone resorption [3]. During bone formation, collagen is synthesized by osteoblasts in the form of procollagen. This precursor contains a short signal sequence and terminal extension peptides: amino-terminal propeptide (PINP) and carboxy-terminal propeptide. These propeptide extensions are removed by specific proteinases before the collagen molecules form. PINP can be found in the circulation and its concentration reflects the synthesis rate of collagen type I, being thus a marker of bone formation [4]. As RA progresses there is marked articular destruction and decreased joint mobility with radiological evidence of erosion with significant impact on life quality within 2 years of disease onset [5]. In addition, osteoporosis is a common finding in patients with RA [6] and is responsible for increased rates of vertebral and hip fractures in these patients [7,8]. RA is associated with an increased expression of the receptor activator of RANKL (receptor activator of nuclear factor kappa-B ligand, NF-KB ligand) and low levels of its antagonist, osteoprotegerin (OPG) [9]. In addition, very early on in the disease process, RA serum and synovial fluid

present a cytokine profile, including interleukin (IL) 1, IL6, IL17 and tumor necrosis factor (TNF), which further favors osteoclast differentiation and activation [10-12]. Evidence suggests that bone remodeling disturbances in RA contribute not only to local bone erosions but also to the development of systemic osteoporosis [13].

We have previously found in a chronic animal model of arthritis (SKG mouse model) that prolonged inflammation (5 and 8 months) directly leads to the degradation of bone biomechanical properties, namely stiffness, ductility and bone strength, which was paralleled by a high collagen bone turnover and disorganization [4,12,14,15]. Based on the fact that most of the effectors of bone metabolism are engaged in the disease process since the early phase, we now hypothesize that this process starts upon the first inflammatory manifestations [10-12]. To test this we selected the adjuvant-induced arthritis (AIA) model in rats, characterized by a rapid onset polyarticular inflammation and widely used for testing new treatments for arthritis [16-18]. Understanding the systemic inflammatory consequences on bone would expand the use of this model also for testing new drugs with potential bone therapeutic effects.

The main goal of the present work was to study, in a rat model of AIA, the effects of the first days of the systemic inflammatory process on the microarchitecture and mechanical properties of bone.

MATERIALS AND METHODS

Animal experimental design

Twenty-eight Wistar AIA rats were purchased from Charles River Laboratories International (Massachusetts, USA). Eight-week-old females weighing 200 –230 g were maintained under specific pathogen free (SPF) conditions. All experiments were approved by the Animal User and Ethical Committees of the Instituto de Medicina Molecular, Lisbon University, according to the Portuguese law and the European recommendations. Animals were sacrificed when presenting an inflammatory score (0-3) of 3 in 2 paws or when presenting 20% of body weight loss.

Rats were housed per groups (healthy vs arthritic) under standard laboratory conditions (at 22°C under 12-hour light/12-hour dark conditions). The inflammatory score, ankle perimeter and body weight were measured during the study period. Inflammatory signs were evaluated by counting the score of each joint in a scale of 0 – 3 (0 — absence; 1 — erythema; 2 — erythema and swelling; 3 — deformities and functional impairment). The total score of each animal was defined as the sum of the partial scores of each affected joint [19]. Rats were sacrificed by CO₂ narcosis after 22 days of disease evolution and blood as well as bone samples were collected.

Bone remodeling markers quantification

Serum samples were collected at the time of sacrifice and stored at -80°C. Bone remodeling markers CTX I (C-terminal telopeptides of type-I collagen) and P1NP (total procollagen type I N-terminal propeptide) were quantified by Serum Rat-Laps ELISA assay (Immunodiagnostic Systems Ltd, Boldon, UK), according to the provider's instructions.

Bone histomorphometry

The 4th lumbar vertebrae (L4) were collected from each animal at sacrifice for histomorphometric analysis. Samples were fixed immediately in ethanol 70% and then dehydrated with increasing ethanol concentrations (96% and 100%). Samples were next embedded in methylmetacrylate (MMA) solution. Serial transversal sections through L4 were performed with 5- μ m-thick and stained with Aniline Blue in order to distinguish bone and bone marrow, allowing bone structural analysis. Images were acquired using a Leica DM2500 microscope equipped with a color camera Leica CCD Camera (Leica microsystems, Wetzlar, Germany) [20].

All variables were expressed and calculated according to the recommendations of the American Society for Bone and Mineral Research [21], using a morphometric program (Image J 1.46R with plugin Bone J).

Ratio of trabecular bone volume / total tissue volume, trabecular thickness and trabecular separation were evaluated by standard histomorphometric parameters at x12.5 magnification.

Energy dispersive X-ray spectroscopy analysis

Energy dispersive X-ray spectroscopy is a sensitive qualitative and semi-quantitative technique to evaluate the mineral content in bone. The quantitative information is based on the relative elemental abundance.

Using a standard system, semi-quantitative X-ray fluorescence measurements were performed in cortical and trabecular bone powder samples, with the purpose of quantifying calcium and phosphorus concentration.

After excision, fresh femurs were freeze dried for 46 hours, with a multipurpose ice condenser (ModulyoD-230, Thermo Savant, Schwerte, Germany) operated at a nominal temperature of -50 °C, in order to remove excess of water.

The semi-quantitative measurements of bone powder were performed with a 4 kW commercial wavelength dispersive X-ray fluorescence spectrometer (Bruker S4 Pioneer, Karlsruhe, Germany), using a Rh X-ray tube with a 75 mm Be end window and a 34 mm diameter collimator mask. Measurements were performed in helium mode and using high-density polyethylene X-ray fluorescence sample cups with 35.8 mm diameter assembled with a 4 mm prolene film to support the bone sample. The polyethylene cup was placed in steel sample cup holders with an opening diameter of 34 mm.

Bone mechanical testing

Bone mechanical properties were evaluated by a three-point bending method using an electromechanical machine (model 5566, Instron Corporation, Canton, USA) using a load-cell of 500N. The femur was placed on a holding device with a support span distance of 5 mm (L), with the lesser trochanter proximal in contact with the proximal transverse bar. The load was applied at the mid-shaft of the diaphysis with a cross-head speed of 0.005 mm/s until the fracture occurred.

The stress-strain curve can be obtained from the load-displacement representation, with the initial dimensions of the sample, using engineering equations (supplementary figure 1 B).

An example of a stress-strain curve obtained in the three point bending tests is shown in supplementary figure 1 A. The points of the yield stress and ultimate stress are indicated. This stress-strain curve can be broken down into pre-yield and post-yield portions. Pre-yield toughness represents the area under the stress/strain curve up to the yield point, which is where permanent deformation of the bone has occurred while post-yield toughness represents the area under the curve between the yield point and bone fracture. In these bending tests there is a significant amount of displacement between the yield point and the eventual fracture [22].

Statistical analysis

Continuous variables were expressed by mean \pm standard deviation (SD) or median and interquartile range. The normality distribution was assessed by D'Agostino and Pearson test. Statistical differences were determined with parametric t-test or non-parametric Mann Whitney test according variables distribution using GraphPad Prism (GraphPad, California, USA). Differences were considered statistically significant for p values \leq 0.05.

RESULTS

Inflammatory progress

First, we validated the kinetic of disease development of the AIA rat model. Inflammatory signs (fig1. A) and ankle perimeter (fig.1 B) were assessed throughout time, as shown in Fig.1. All animals from the arthritic group (N = 16) presented arthritis signs by the fourth day post disease induction.

The initial acute inflammation was observed around day 4 and progressed during 22 days post disease induction. After 10 days of arthritis induction, the inflammatory manifestations increased sharply as depicted by an increase in ankle perimeter. Maximal swelling occurred at day 19 post disease induction. At day 22 post arthritis induction inflammatory score (fig.1 C) and ankle perimeter (fig.1 D) were significantly increased in the arthritic group ($p=0.0037$ and $p = 0.0085$, respectively) in comparison with healthy control rats.

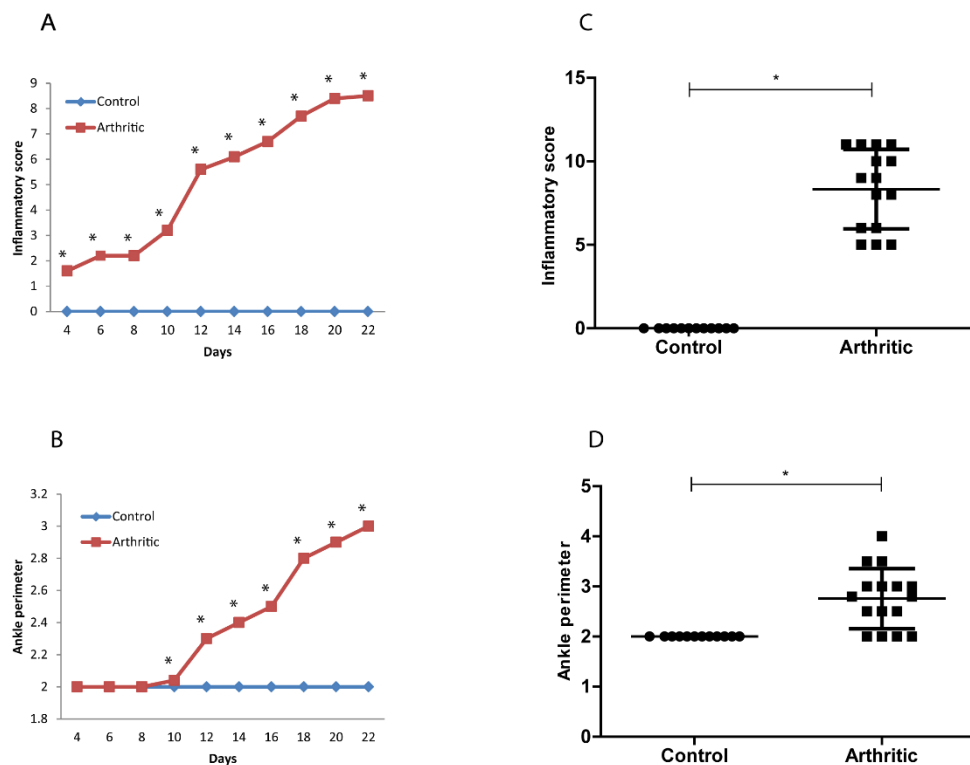


Fig.1 – Inflammatory score (A) and ankle perimeter (B) throughout time.

Inflammatory score (C) ($p=0.0037$) and Ankle perimeter (D) ($p = 0.0085$) in control (N=12) and arthritic groups (N=16) by the time of sacrifice after 22 days post disease induction.

Statistical differences were determined with non-parametric Mann Whitney test using GraphPad Prism (GraphPad, California, USA). Differences were considered statistically significant for p values ≤ 0.05 .

Bone turnover markers

Bone resorption marker CTX I, which reflects osteoclastic activity, is a degradation product of type I collagen, the major structural protein of bone. While the bone formation marker P1NP, a bio product of type I collagen synthesis, is a marker for osteoblastic activity.

We have observed that both CTXI (fig.2 A) and P1NP (fig.2 B) were significantly increased in the arthritic group in comparison with the healthy control animals ($p=0.0002$ and $p=0.0010$, respectively), revealing an increase of bone turnover in the arthritic group.

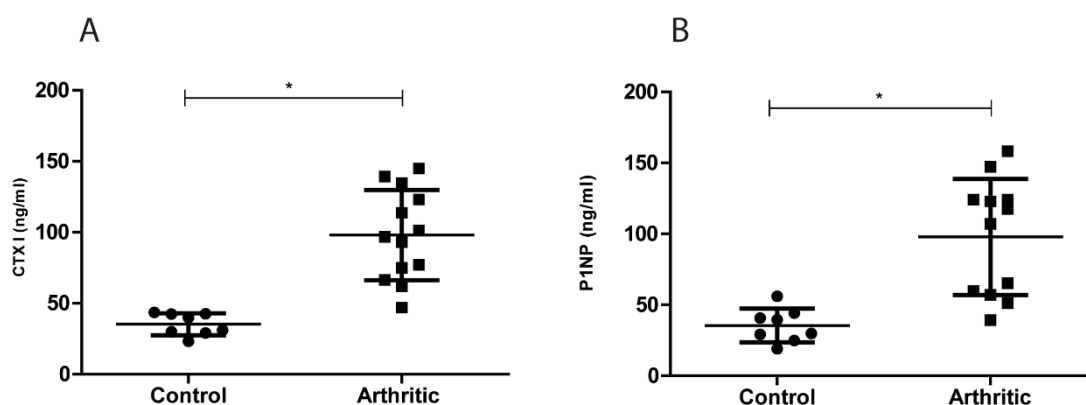


Fig.2 – Bone turnover markers quantification in control (N=9) and arthritic rats (N=13). Serum samples collected at day 22 (sacrificed) were analyzed by ELISA technique. Bone resorption marker, CTX I (A) and bone formation marker, P1NP (B) were increased in arthritic rats ($p=0.0002$ and $p=0.0010$, respectively).

Histomorphometry of bone

Bone histomorphometry was used to measure bone static parameters such as bone trabecular volume, trabecular thickness and trabecular separation in order to determine the effects of inflammation on bone microstructure (fig. 3 A).

Trabecular bone volume ($p = 0.0003$) (fig.3 B) and trabecular thickness ($p = 0.0002$) (fig.3 C) were significantly reduced in arthritic animals comparing with healthy control animals. Moreover, trabecular separation ($p = 0.0009$) (fig. 3 D) was significantly increased in the arthritic group, in comparison with healthy control rats.

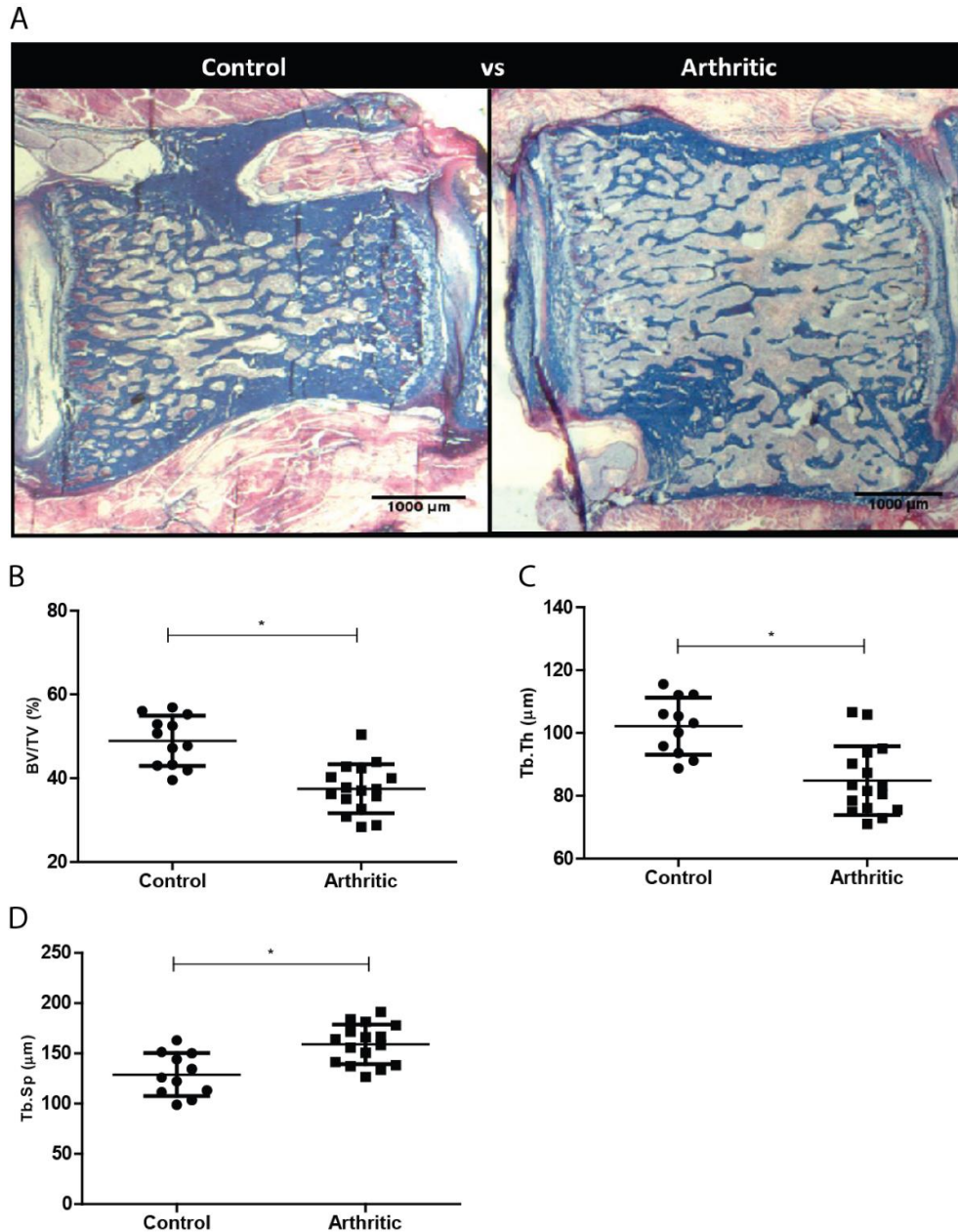


Fig.3 - Bone histomorphometry assessment of the 4th lumbar vertebra (L4). Assessment of L4 in control (N = 12) and arthritic group (N = 16). (A) Illustrative Aniline blue stained sections of L4 vertebra collected at day 22 post disease induction (sacrifice). Bone volume per tissue volume or trabecular bone volume fraction (B) and trabecular thickness (C) were decreased in arthritic rats while trabecular separation (D) was increased. Magnification x12.5.

Energy dispersive X-ray spectroscopy

Calcium (Ca) and Phosphorus (P) are the most abundant elements present in bone mineral matrix. In fact, calcium has been reported as the most important nutrient associated with peak bone mass and may be the only one for which there is epidemiological evidence of a relation to fracture rate[23].

We used energy dispersive X-ray spectroscopy to quantify the calcium and phosphorus content in our samples. We have observed that Ca ($p = 0.0046$) (fig.4 A) and P ($p = 0.0046$) (fig.4 B) content were decreased in the arthritic group as compared to controls.

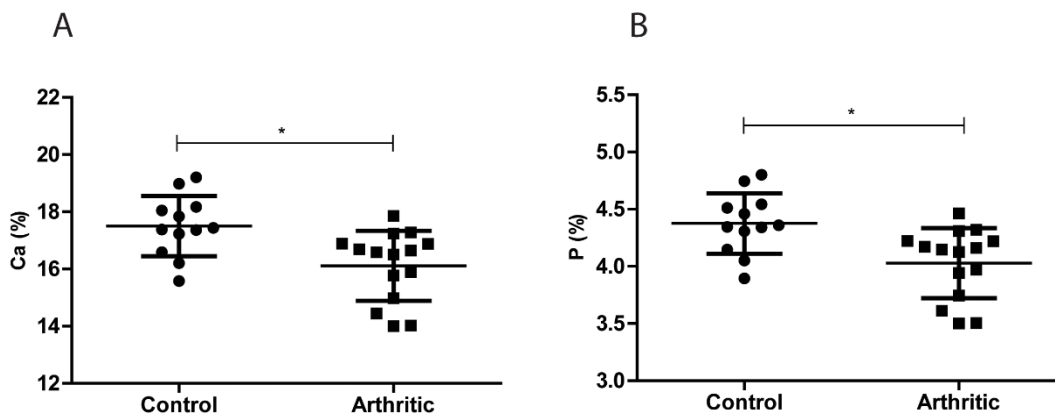


Fig.4 – Calcium and Phosphorus bone content acquired by energy dispersive X-ray spectroscopy. Ca (A) and P (B) bone content were decreased in the arthritic group (N=16) as compared with controls (N=12). Bone powder was acquired from bone samples collected at day 22 post disease induction (sacrifice).

Bone mechanics

The three-point-bending biomechanical tests aimed to explore the bone mechanical competence of both groups 22 days post disease induction. Results showed decreased values of yield stress (moment of occurrence of first micro fractures) ($p = 0.0061$) (fig.5 A) and ultimate stress (moment of occurrence of complete fracture) ($p = 0.0279$) (fig.5 B) in arthritic animals when compared to the control group.

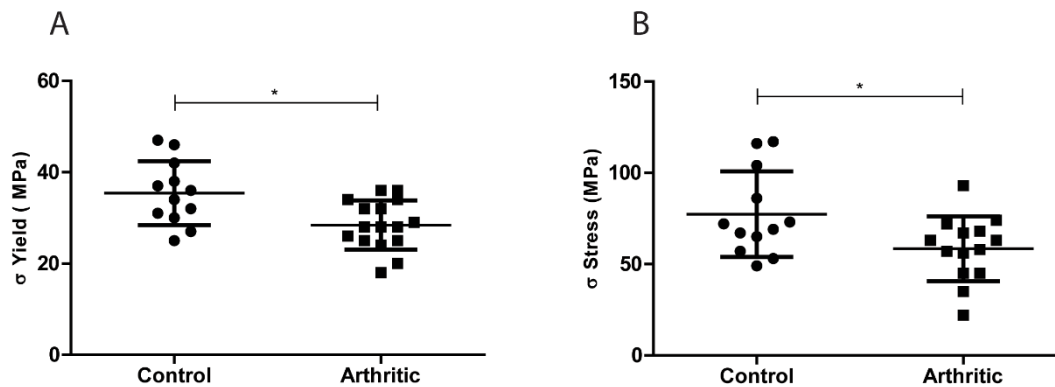


Fig.5 – Mechanical analysis acquired by 3 point bending tests. Yield stress (A) and Ultimate stress (B) were decreased in arthritic rats (N=16) as compared to controls (N=12). Bone samples were collected at day 22 post disease induction (sacrifice).

DISCUSSION

In the present study, we demonstrated in an AIA rat model, that arthritis induces very early high bone turnover, trabecular degradation, mineral loss and mechanical weakness.

Biochemical markers of bone turnover were quantified in order to evaluate the impact of systemic inflammation on bone metabolism. An increased bone turnover activity was shown in arthritic animals, as depicted by increased CTXI and P1NP levels. This observation was consistent with previously published data showing the presence of a large number of osteoclasts in AIA bone [17]. Data already published by our group in another animal model of arthritis (the SKG mice model) have also shown that P1NP levels were increased in arthritic animals and so did CTX-I levels [4], reflecting an overall increase in bone turnover [24]. Studies on RA patients measuring P1NP have produced varying results, whereas measurements in CTX-I mostly show increased levels [25]. In RA patients bone metabolism is more active (increased P1NP) in earlier stages of the disease and a decrease in bone metabolic activity (both P1NP and CTX) occurs with disease progression, both showing correlation with tender and swollen joints [15]. Despite the existing variability, P1NP has been mainly found to be increased in RA patients when compared to controls, together with CTX-I, revealing a compensatory mechanism in bone turnover [26].

Due to increased bone turnover it was therefore of interest to assess the effects of inflammation on bone microstructure. Histomorphometric data revealed, in arthritic animals, a lower fraction of trabecular bone volume and a lower average trabecular thickness as well as a higher average trabecular separation, in comparison with controls. These findings were in line with the described bone volume loss, measured by uCT, in this rat model [17].

In addition, we quantified calcium and phosphorus content, the two major minerals present in bone [27], by energy dispersive X-ray spectroscopy. The arthritic group showed a significant decreased mineral content, when compared to the control group. This result corroborated an overall bone mineral loss, as a result of an unbalanced high bone turnover, which might lead to bone fragility and consequently fracture.

In accordance, mechanical tests revealed that arthritic femurs have a significantly lower yield stress and ultimate stress as compared to control femurs, meaning that bone is more fragile and prone to fracture.

In summary, we have shown, in an AIA rat model, that the systemic inflammation associated with a polyarthritis is able to induce an early high bone turnover, bone microarchitecture degradation, low mineral content and mechanical weakness. In addition, our results have expanded the knowledge on this model. In fact, our findings, suggest that AIA is a fast and adequate model to study the effects of arthritis on bone properties and consequently a potentially accurate model to study anti-arthritic compounds with bone protective effects.

REFERENCES

1. Alamanos Y, Drosos AA (2005) Epidemiology of adult rheumatoid arthritis. *Autoimmun Rev* 4: 130-136.
2. Yelin E, Callahan LF (1995) The economic cost and social and psychological impact of musculoskeletal conditions. National Arthritis Data Work Groups. *Arthritis Rheum* 38: 1351-1362.
3. Gravallesse EM (2002) Bone destruction in arthritis. *Ann Rheum Dis* 61 Suppl 2: ii84-86.
4. Caetano-Lopes J, Nery AM, Canhao H, Duarte J, Cascao R, et al. (2010) Chronic arthritis leads to disturbances in the bone collagen network. *Arthritis Res Ther* 12: R9.
5. Lin YY, Jean YH, Lee HP, Chen WF, Sun YM, et al. (2013) A soft coral-derived compound, 11-epi-sinulariolide acetate suppresses inflammatory response and bone destruction in adjuvant-induced arthritis. *PLoS One* 8: e62926.
6. Haugeberg G, Orstavik RE, Uhlig T, Falch JA, Halse JI, et al. (2002) Bone loss in patients with rheumatoid arthritis: results from a population-based cohort of 366 patients followed up for two years. *Arthritis Rheum* 46: 1720-1728.
7. Eric-Jan J. A. Kroot RFJML (2000) Bone mass in rheumatoid arthritis. *CLINICAL AND EXPERIMENTAL RHEUMATOLOGY*
8. Marshall D, Johnell O, Wedel H (1996) Meta-analysis of how well measures of bone mineral density predict occurrence of osteoporotic fractures. *BMJ* 312: 1254-1259.
9. Fonseca JE, Cortez-Dias N, Francisco A, Sobral M, Canhao H, et al. (2005) Inflammatory cell infiltrate and RANKL/OPG expression in rheumatoid synovium: comparison with other inflammatory arthropathies and correlation with outcome. *Clin Exp Rheumatol* 23: 185-192.
10. Moura RA, Cascao R, Perpetuo I, Canhao H, Vieira-Sousa E, et al. (2011) Cytokine pattern in very early rheumatoid arthritis favors B-cell activation and survival. *Rheumatology (Oxford)* 50: 278-282.
11. Cascao R, Moura RA, Perpetuo I, Canhao H, Vieira-Sousa E, et al. (2010) Identification of a cytokine network sustaining neutrophil and Th17 activation in untreated early rheumatoid arthritis. *Arthritis Res Ther* 12: R196.

12. Caetano-Lopes J, Canhao H, Fonseca JE (2009) Osteoimmunology--the hidden immune regulation of bone. *Autoimmun Rev* 8: 250-255.
13. Caetano-Lopes J, Rodrigues A, Lopes A, Vale AC, Pitts-Kiefer MA, et al. (2014) Rheumatoid Arthritis Bone Fragility Is Associated With Upregulation of IL17 and DKK1 Gene Expression. *Clin Rev Allergy Immunol* 47: 38-45.
14. Caetano-Lopes J, Nery AM, Henriques R, Canhao H, Duarte J, et al. (2009) Chronic arthritis directly induces quantitative and qualitative bone disturbances leading to compromised biomechanical properties. *Clin Exp Rheumatol* 27: 475-482.
15. Wislowska M, Jakubicz D, Stepien K, Cicha M (2009) Serum concentrations of formation (PINP) and resorption (Ctx) bone turnover markers in rheumatoid arthritis. *Rheumatol Int* 29: 1403-1409.
16. Bendele A (2001) Animal models of rheumatoid arthritis. *J Musculoskelet Neuronal Interact* 1: 377-385.
17. Lisa R. Schopf KAaBDJ (2006) Rat models of arthritis: Similarities, differences, advantages, and disadvantages in the identification of novel therapeutics. Cambridge, MA, USA: Millennium Pharmaceuticals.
18. Pearson CM (1956) Development of arthritis, peri-arthritis and periostitis in rats given adjuvants. *Proc Soc Exp Biol Med* 91: 95-101.
19. da Silva JA, Fonseca JE, Graca L, Moita L, Carmo-Fonseca M (1996) Reinnervation of post-arthritic joints in the rat. *Clin Exp Rheumatol* 14: 43-51.
20. Vidal B, Pinto A, Galvao MJ, Santos AR, Rodrigues A, et al. (2012) Bone histomorphometry revisited. *Acta Reumatol Port* 37: 294-300.
21. Parfitt AM, Drezner MK, Glorieux FH, Kanis JA, Malluche H, et al. (1987) Bone histomorphometry: standardization of nomenclature, symbols, and units. Report of the ASBMR Histomorphometry Nomenclature Committee. *J Bone Miner Res* 2: 595-610.
22. Allen MR, Reinwald S, Burr DB (2008) Alendronate reduces bone toughness of ribs without significantly increasing microdamage accumulation in dogs following 3 years of daily treatment. *Calcif Tissue Int* 82: 354-360.
23. Jiang Y, Zhao J, Genant HK, Dequeker J, Geusens P (1997) Long-term changes in bone mineral and biomechanical properties of vertebrae and femur in

aging, dietary calcium restricted, and/or estrogen-deprived/-replaced rats. *J Bone Miner Res* 12: 820-831.

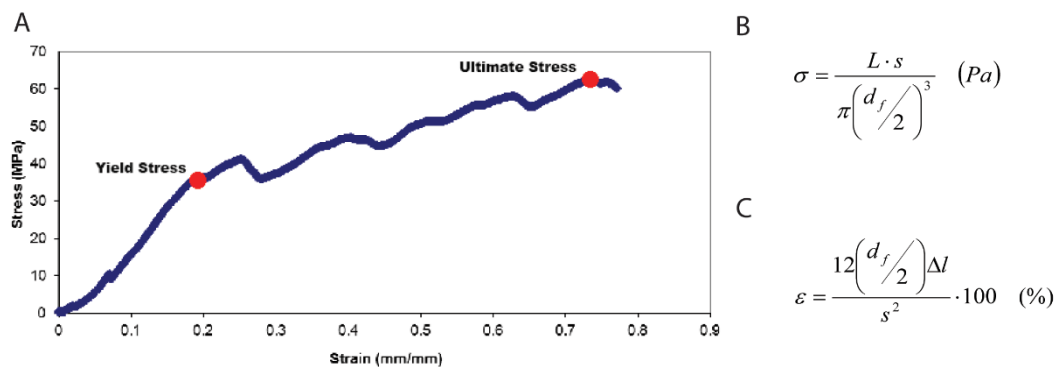
24. Siebuhr AS, Wang J, Karsdal M, Bay-Jensen AC, Y J, et al. (2012) Matrix metalloproteinase-dependent turnover of cartilage, synovial membrane, and connective tissue is elevated in rats with collagen induced arthritis. *J Transl Med* 10: 195.

25. van Schaardenburg D, Nielen MM, Lems WF, Twisk JW, Reesink HW, et al. (2011) Bone metabolism is altered in preclinical rheumatoid arthritis. *Ann Rheum Dis* 70: 1173-1174.

26. Cortet B, Flipo RM, Pigny P, Duquesnoy B, Boersma A, et al. (1998) Is bone turnover a determinant of bone mass in rheumatoid arthritis? *J Rheumatol* 25: 2339-2344.

27. Bonjour JP (2011) Calcium and phosphate: a duet of ions playing for bone health. *J Am Coll Nutr* 30: 438S-448S.

Supplementary figure



Supp Fig.1 – Scheme representative of the yield stress and ultimate stress points in a stress/strain curve. Yield stress and ultimate stress points (A) obtained with bending test with the specific formulas for stress (B) strain (C) calculation, where σ - stress (Pa); L - load (N); s - support span (mm); d_f - femoral outer diameter (mm); ε - strain (%); Δl – displacement (mm).

II. Early arthritis induces disturbances at bone nanostructural level reflected in decreased tissue hardness

Bruno Vidal, Rita Cascão, Mikko Finnilä, Inês Lopes, Simo Saarakkala, Peter Zioupos, Helena Canhão, João Fonseca

Author Contributions

Vidal and Cascão designed the experiments. Vidal performed all the experiments and wrote the chapter. Finnilä, Cascão, Zioupos and Lopes helped to perform some experiments. Cascão, Saarakkala, Zioupos, Canhão and Fonseca supervised the work and revised the text.

Early arthritis induces disturbances at bone nanostructural level reflected in decreased tissue hardness

Bruno Vidal, Rita Cascão, Mikko Finnilä, Inês Lopes, Simo Saarakkala, Peter Zioupos, Helena Canhão, João Fonseca

ABSTRACT

Rheumatoid arthritis (RA) is a chronic immune-mediated inflammatory disease, which causes local and systemic bone damage.

Objectives – The main goal of this work was to analyze the effects of the early phase of systemic inflammatory process at bone tissue level, including nanomechanical properties, microarchitecture and mineral and collagen content.

Methods – Eighty-eight Wistar rats were randomly housed in experimental groups, as follows: an adjuvant induced arthritis (N= 47) and a control healthy group (N= 41). Rats were monitored during 22 days for the inflammatory score, ankle perimeter and body weight and sacrificed at different time points (11 and 22 days post disease induction). Bone samples were collected for histology, micro-CT, 3-point bending test, nanoindentation and Fourier transformed infrared spectroscopy (FTIR) analysis. Blood samples were also collected for bone turnover markers and systemic cytokine quantification.

Results – At bone tissue level, measured by FTIR analysis and nanoindentation, there was a reduction of the mineral and collagen content and of hardness in the arthritic group, associated with an increase of the ratio of bone concentric to parallel lamellae and of the area of the osteocyte lacuna. In addition, increased bone turnover and changes in the microstructure and mechanical properties were observed in arthritic animals since the early phase of arthritis, when compared with healthy controls.

Conclusion – Systemic inflammation induces very early changes at bone tissue level characterized by decreased tissue hardness, associated with changes in

bone lamella organization and osteocyte lacuna surface and with decreased collagen and mineral content. These observations highlight the pertinence of immediate control of inflammation and of bone metabolism variables in the initial stages of arthritis.

INTRODUCTION

Rheumatoid arthritis (RA) is the most common chronic inflammatory joint disease, affecting about 1% of the world population. RA is characterized by synovial hyperplasia caused by a large proliferative cellular infiltrate of leukocytes and high expression levels of proinflammatory cytokines [1]. As RA progresses there is marked articular destruction and decreased joint mobility with radiological evidence of bone erosion within 2 years of disease onset [2]. In addition, osteoporosis is a common finding in patients with RA [3] and is responsible for increased rates of vertebral and hip fractures in these patients [4,5]. RA is associated with an augmented expression of the receptor activator of RANKL (receptor activator of nuclear factor kappa-B ligand, NF-KB ligand) and low levels of its antagonist, osteoprotegerin (OPG) [6]. RANKL is a crucial activator of osteoclastogenesis [7]. In addition, RA serum and synovial fluid present a cytokine profile, including interleukin (IL)1 β , IL6, IL17 and tumor necrosis factor (TNF), which further favors osteoclast differentiation and activation since the early phase of the disease [8-10].

Bone is a dynamic tissue composed mainly of a type I collagen matrix that constitutes the scaffold for calcium hydroxyapatite crystal deposition. Remodeling of bone is a continuous process by which osteoclasts resorb bone tissue and osteoblasts produce new bone matrix that is subsequently mineralized. In this process biochemical markers of bone turnover are produced and released into circulation, providing a read-out of remodeling kinetics. Evidence suggests that bone remodeling disturbances in RA contribute not only to local bone erosions but also to the development of systemic osteoporosis [11].

We have previously found in the adjuvant-induced rat model of arthritis (AIA) that 22 days of sustained and established inflammatory disease progression directly

leads to the degradation of bone biomechanical properties, namely stiffness, ductility and bone strength, which was paralleled by a high collagen bone turnover [12].

The main goal of this work was to analyze the effects of the early phase of systemic inflammatory process at bone tissue level, including nanomechanical properties, microarchitecture and mineral and collagen content.

MATERIALS AND METHODS

Animal experimental design

Eighty-eight, 8 week-old female Wistar rats weighing approximately 230-250gr were housed in European type II standard filter top cages (Tecniplast, Buguggiate, Italy) and transferred into the SPF animal facility at the Instituto de Medicina Molecular, under a 14h light/10h dark light cycle, acclimatized to T= 20-22°C and RH= 50-60%. They were given access to autoclaved rodent breeder chow (Special Diet Service, RM3) and triple filtered water. Rats were purchased from Charles River laboratories international (Barcelona, Spain) and arthritis was induced on their laboratories in 47 animals. The transport service takes 3 days to arrive at Instituto de Medicina Molecular.

Upon arrival, animals were randomly housed in two groups, individually identified and cages were labelled according to the experimental groups, as follows: adjuvant induced arthritis model (N=47) and control healthy group (N=41). The inflammatory score, ankle perimeter and body weight were measured during disease development. Inflammatory signs were evaluated by counting the score of each joint in a scale of 0 – 3 (0 – absence; 1 – erythema; 2 – erythema and swelling; 3 – deformities and functional impairment). The total score of each animal was defined as the sum of the partial scores of each affected joint. Rats were sacrificed at day 11 and 22 post disease induction, and blood, paws and bone samples were collected. All experiments were approved by the Animal User and Ethical Committees at the Instituto de Medicina Molecular (Lisbon University), according to the Portuguese law and the European recommendations.

Histological evaluation of hind paws

Left hind paw samples collected at the time of sacrifice were fixed immediately in 10% neutral buffered formalin solution and then decalcified in 10% formic acid. Samples were then dehydrated and embedded in paraffin, serially sectioned at a thickness of 5µm. Sections were stained with hematoxylin and eosin for histopathological evaluation of structural changes and cellular infiltration. This evaluation was performed in a blind fashion using 5 semi-quantitative scores:

- Sublining layer infiltration score (0-none to diffuse infiltration; 1-lymphoid cell aggregate; 2-lymphoid follicles; 3-lymphoid follicles with germinal center formation);
 - Lining layer cell number score (0-fewer than three layers; 1-three to four layers; 2-five to six layers; 3-more than six layers);
 - Bone erosion score (0-no erosions; 1-minimal; 2-mild; 3-moderate; 4-severe);
 - Cartilage surface (0 –normal; 1 – irregular; 2 – clefts; 3 – clefts to bone);
 - Global severity score (0-no signs of inflammation; 1-mild; 2-moderate; 3-severe)
- [13].

Images were acquired using a Leica DM2500 (Leica Microsystems, Wetzlar, Germany) microscope equipped with a color camera.

Biomarkers quantification

Serum samples were collected at the sacrifice time and stored at -80°C. The proinflammatory cytokine IL-6 (Boster Bio, California, USA) was quantified in serum samples using specific rat ELISA kits. Bone remodeling markers, CTX-I and P1NP, were quantified by Serum Rat Laps ELISA assay (Immunodiagnostic Systems Ltd, Boldon, UK).

For all biomarkers standard curves were generated by using reference biomarker concentrations supplied by the manufacturers. Samples were analyzed using a plate reader Infinite M200 (Tecan, Mannedorf, Switzerland).

Micro-computed tomography (micro-CT) analysis

Structural properties of the trabecular and cortical tibiae were determined with a high-resolution micro-CT system (SkyScan 1272, Bruker microCT, Kontich, Belgium). Moist bones were wrapped in parafilm and covered with dental wax to prevent drying and movement during the scanning. X-ray tube was set to 50kV and beam was filtered with 0.5mm Aluminum filter. Sample position and camera settings were tuned to provide 3.0 μ m isotropic pixel size and projection images were collected every 0.2°. Tissue mineral density values were calibrated against hydroxyapatite phantoms with densities of 250mg/cm³ and 750mg/cm³. Reconstructions were done with NRecon (v 1.6.9.8; Bruker microCT, Kontich, Belgium) where appropriate corrections to reduce beam hardening and ring artefacts were applied. Bone was segmented in slices of 3 μ m thickness. After 200 slices from growth plate, we selected and analyzed 1400 slices of trabecular bone. For cortical bone 300 slices (1800 slices from growth plate) were analyzed.

This evaluation was performed in agreement with guidelines for assessment of bone microstructure in rodents using micro-computed tomography [14]. Trabecular bone morphology was analyzed by applying global threshold and despeckle to provide binary image for 3D analysis. For cortical bone ROI was refined with ROI-shrink wrap operation. This was followed by segmentation of blood vessels using adaptive thresholding. Blood vessels and porosity were analyzed using 3D morphological analyzes.

Bone mechanical tests

The impact of inflammation on bone strength was investigated at the end of the experiment. Femurs were subjected to a 3-point bending test using the universal testing machine (Instron 3366, Instron Corp., Massachusetts, USA). Femurs were placed horizontally anterior side upwards on a support with span length of 5mm. The load was applied with a constant speed of 0.005mm/s until failure occurred. Stiffness was analyzed by fitting first-degree polynomial function to the linear part of recorded load deformation data. A displacement of 0.15 μ m between fitted slope and measured curve was used as criteria for yield point, whereas the breaking

point was defined as set where force reached maximal value. For both yield and breaking points, force, deformation and absorbed energy were defined.

Nanoindentation

Nanoindentation was performed using a CSM-Nano Hardness Tester System (CSM Instruments SA; Switzerland; Indentation v.3.83) equipped with a Berkovich based pyramid diamond indenter. After micro-CT, 0.5mm of top tibia was cut and proximal part was embedded to low viscosity epoxy resin (EpoThin, Buehler, Knorring Oy Ab, Helsinki, Finland). Slow speed diamond saw was used to remove 10% of bone length. The sample surface was polished using silicon carbide sandpaper with a decreasing grid size (800, 1200, 2400 and 4800) and finished with cloth containing 0.05 μ m γ -alumina particles. Indentation protocol was adopted from previous work [15] and an average of 8 indentations were done on both cortical and trabecular bone with quasi-static (so called 'advanced') loading protocol. All indentations were performed under an optical microscope to achieve the precise location of indentations at the center of the targeted area in the tissue [16].

In the 'advanced' protocol, a trapezoidal loading waveform was applied with a loading/unloading rate of 20mN/min, and with an intermediate load-hold-phase lasting 30s hold at a maximum load 10mN. The hardness (HIT), indentation modulus (EIT), indentation creep (CIT) and elastic part of indentation work (η IT) were measured by advanced protocol using the Oliver and Pharr (1992) method [17].

Histological images of rat tibiae from diaphyseal cortical region were acquired during the nanoindentation technique, using a CSM instruments (Switzerland) microscope equipped with a color camera.

A histologic score was applied in order to evaluate the lamellar structures of bone tissue. This evaluation was performed in a blind fashion using a semi-quantitative score:

- Lamellar bone structure: (1- predominantly parallel-lamella; 2 - concentric and parallel-lamellae in the same proportion; 3 – predominantly concentric lamella).

The ratio of osteocyte lacuna area / total tissue area was also evaluated at x200 magnification in order to analyze the percentage of total tissue area occupied by osteocyte lacunae. The method of acquisition and analysis used was the same applied for the evaluation of bone volume / tissue volume in histomorphometry technique [12]. All variables were expressed and calculated according to the recommendations of the American Society for Bone and Mineral Research [18], using a morphometric program (Image J 1.46R with plugin Bone J).

Fourier transformed infrared spectroscopy (FTIR)

Samples used for nanoindentation were also used for FTIR. Chemical composition was measured from bone surfaces separately with the HYPERION 3000 FTIR microscope (Bruker Optics Inc, Billerica, MA, USA) using attenuated total reflection (ATR) objective. The ATR crystal was compressed on the bone with a constant load, and spectral images were recorded with a focal plane array detector (FPA). Spatial and spectral resolutions were set to 1 μ m and 2 cm^{-1} , respectively. Each spectrum between 840–3300 cm^{-1} was averaged 32 times and two spectral maps (32x32 spectra) were collected from the trabecular and cortical bone separately. Data was analyzed using a custom script in the MATLAB environment (MathWorks Inc, Natick, MA, USA). For each spectral map, areas under curves were calculated for amide I, phosphate and carbonate peaks by integrating spectra between 1595–1720 cm^{-1} , 900–1185 cm^{-1} and 850–895 cm^{-1} , respectively. Blood vessels and other porous structures were removed by excluding spectra with maximum phosphate peak height less than 0.5 absorbance units. Average content as well as well-established parameters for bone composition (carbonate:amide I, mineral:matrix and carbonate:phosphate) were finally calculated from the thresholder spectral maps [19].

Statistical analysis

Statistical differences were determined with Mann–Whitney tests using GraphPad Prism (GraphPad, California, USA). Correlation analysis was performed with the Spearman test. Differences were considered statistically significant for $p < 0.05$.

RESULTS

The AIA rat model has a rapid and severe disease progression

Results showed that inflammatory signs (Fig.1) boosted sharply in the arthritic group. The inflammatory score (Fig.1A) increased significantly at day 11 and 22 post disease induction (which correspond to an acute phase and a chronic phase of systemic inflammation, respectively) in arthritic rats when compared to healthy controls ($p = 0.0097$, respectively).

Moreover, arthritic animals at day 11 and 22 post disease induction sharply increased the ankle swelling throughout disease progression (Fig.1B), when compared to healthy rats ($p = 0.0097$, respectively)

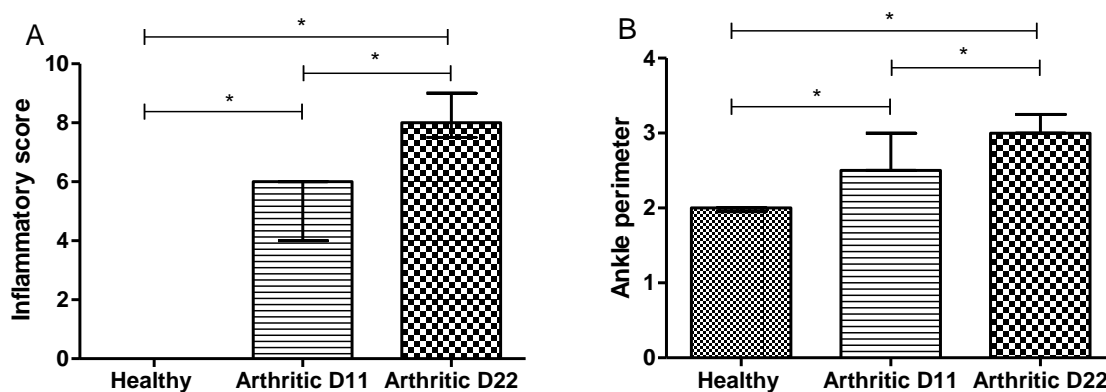


Fig.1 – Inflammatory score and ankle perimeter. Arthritic rats have a rapidly disease progression including ankle swelling, when compared with healthy control rats. Statistical differences were determined with non-parametric Mann Whitney test using GraphPad Prism (GraphPad, California, USA). Differences were considered statistically significant for p values ≤ 0.05 . Healthy D11 $N = 11$, Healthy D22 $N = 30$, Arthritic D11 $N = 16$ and Arthritic D22 $N = 31$.

Inflammation affects local joints and promotes bone damage in AIA rats since the early stage of arthritis

To evaluate the effect of inflammation in local articular joint synovium and bone structures, paw sections stained with hematoxylin and eosin were performed (illustrative images can be observed in Fig 2).

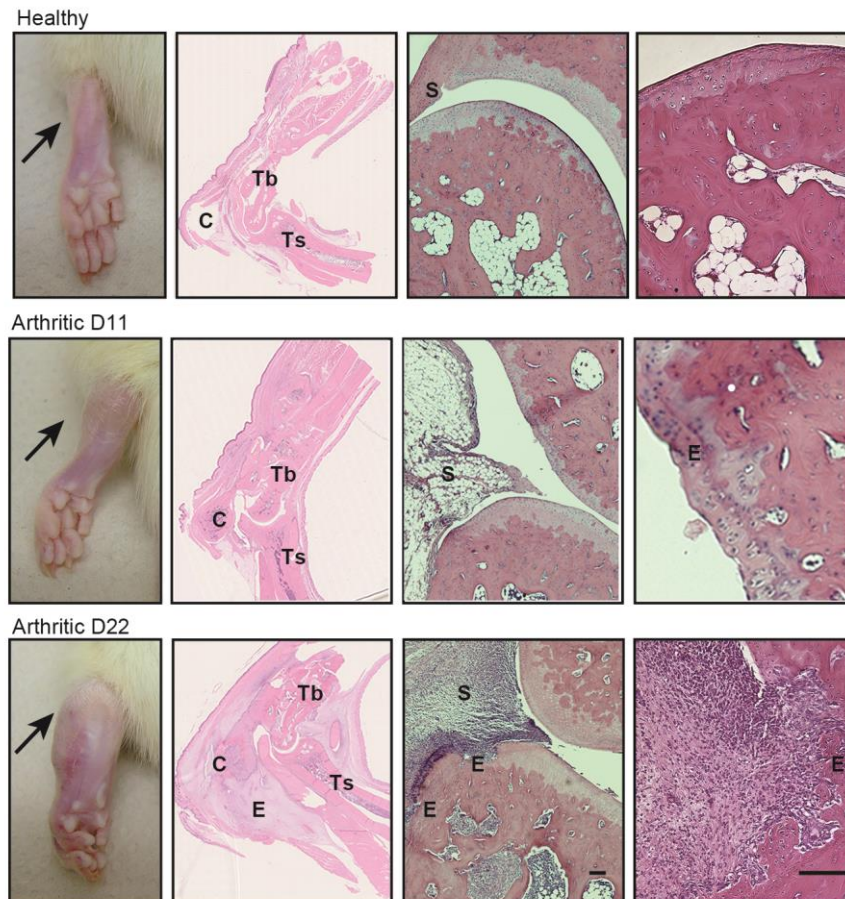


Fig.2 – Histological images of joints after 11 and 22 days of disease induction. These patterns are merely illustrative of the type of histological features observed. Black arrow indicates the absence/presence of ankle swelling in rat hind paws. C–calcaneus, E–edema or erosion, S–synovia, Tb–tibia, Ts–tarso. Magnification of 50X. Bar: 100 μ m.

The histological evaluation using 5 semi-quantitative scores is depicted in Fig 3. Sublining layer infiltration (Fig 3A), number of lining layer cells (Fig 3B) and bone erosion score (Fig 3C) were increased in the arthritic group when compared with healthy controls at day 11 and 22 post disease induction ($p < 0.0001$). Arthritic

samples also showed increased cartilage damage surface (Fig 3D) since the early phase of arthritis at day 11 and 22 ($p=0.0403$ and $p<0.0001$ vs healthy controls, respectively). These data contributed to the increased values of severity score (Fig 3E) in arthritic group ($p<0.0001$ vs healthy controls). Moreover, results also demonstrated a continuous disease progression between day 11 and 22 in arthritic animals, as observed by the increase of the sublining layer infiltration, number of lining layer cells, bone erosion score ($p<0.0001$), cartilage surface score ($p=0.0001$) and global severity score ($p=0.0006$).

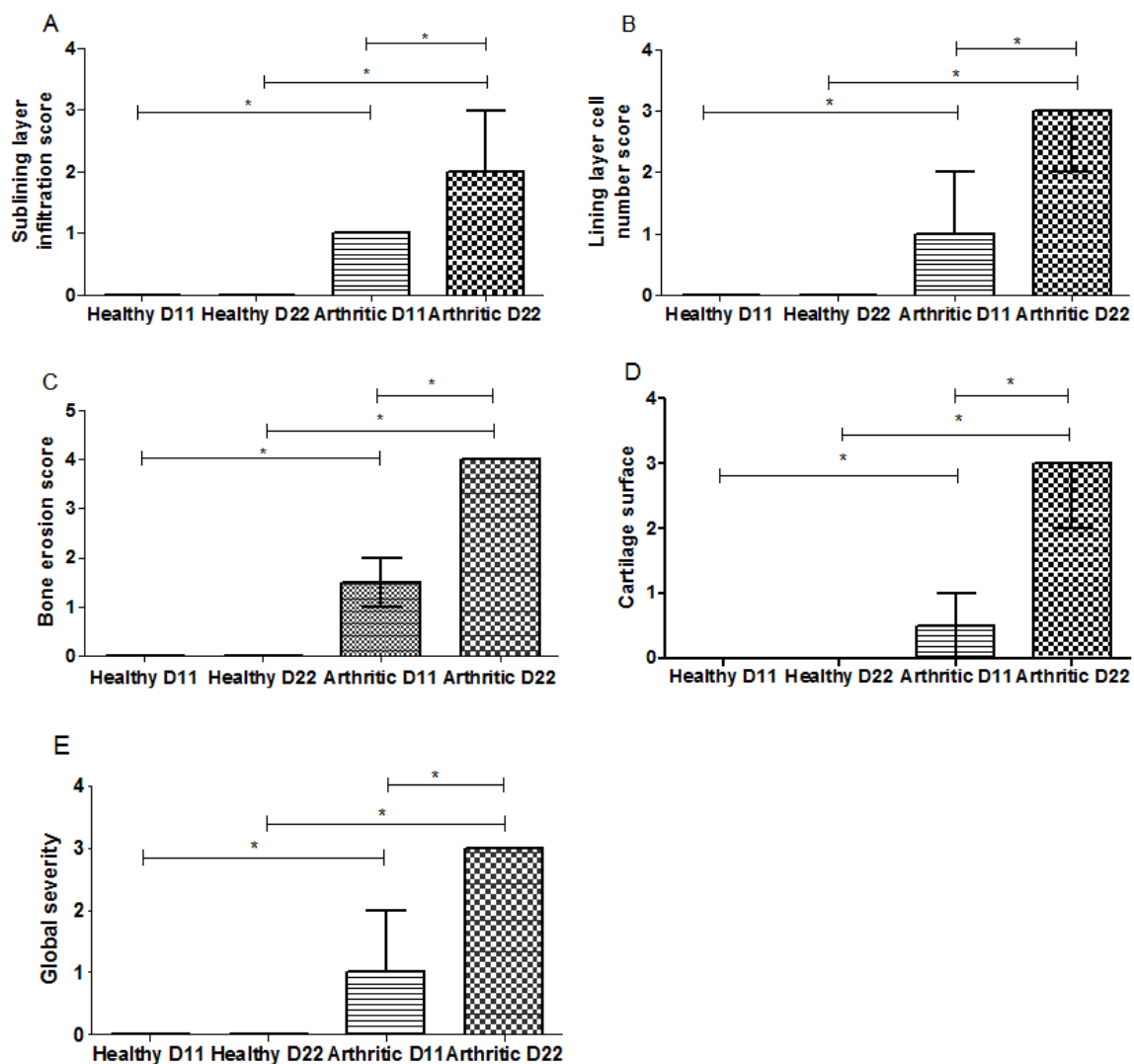


Fig. 3 – Semi-quantitative evaluation of histological sections of inflammation and tissue damage locally in the joints of AIA rats. Notice that results demonstrate that arthritic rats after 11 and 22 days of disease induction increase cellular infiltration (A), number of lining layer cells (B), bone erosions (C) and cartilage surface damage (D). Global disease severity demonstrates this marked

inflammation and progression between day 11 and 22 (E). Data are expressed as median with interquartile range. Differences were considered statistically significant for p -values <0.05 , according to the Mann Whitney test. Healthy D11 N=11, Healthy D22 N=30, Arthritic D11 N=16 and Arthritic D22 N=31.

Systemic inflammation occurs in this model

We observed that IL6 levels were increased in the serum of arthritic rats at day 11 and 22 post disease induction in comparison with healthy controls ($p= 0.0003$ and $p<0.0001$, respectively), as observed in Fig 4. Results also revealed that IL6 levels decreased in arthritic rats at day 22 when compared with day 11 ($p=0.0092$).

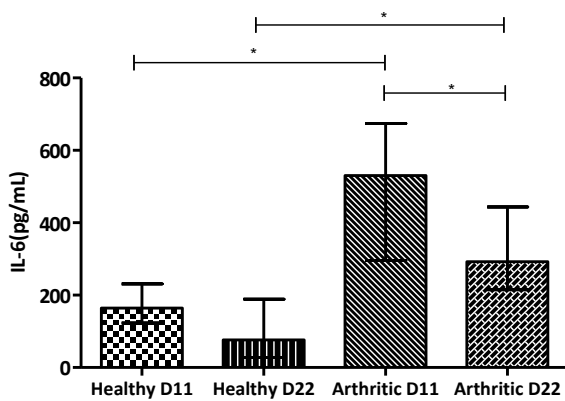


Fig.4 - Serum quantification of IL6. Serum samples collected at day 11 and 22 post disease induction were analyzed by ELISA technique. IL6 was increased in arthritic rats at day 11 and 22 ($p= 0.0003$ and $p<0.0001$ vs healthy controls, respectively). Differences were considered statistically significant for p -values <0.05 , according to the Mann–Whitney tests Healthy D11 N=11, Healthy D22 N=21, Arthritic D11 N=16 and Arthritic D22 N=23.

Systemic inflammation promotes high bone turnover

We have observed that both CTX-I (Fig. 5A) and P1NP (Fig. 5B) were significantly increased in the arthritic group at day 22 in comparison with healthy controls ($p < 0.0001$ and $p = 0.0007$, respectively), revealing an increase of bone turnover in the arthritic group. Moreover, arthritic rats showed already increased values of CTX-I at day 11 post disease induction ($p = 0.0218$ vs healthy rats at day 11) but not of P1NP. These results suggest that systemic inflammation promotes skeletal bone turnover disturbances since the early stages of arthritis.

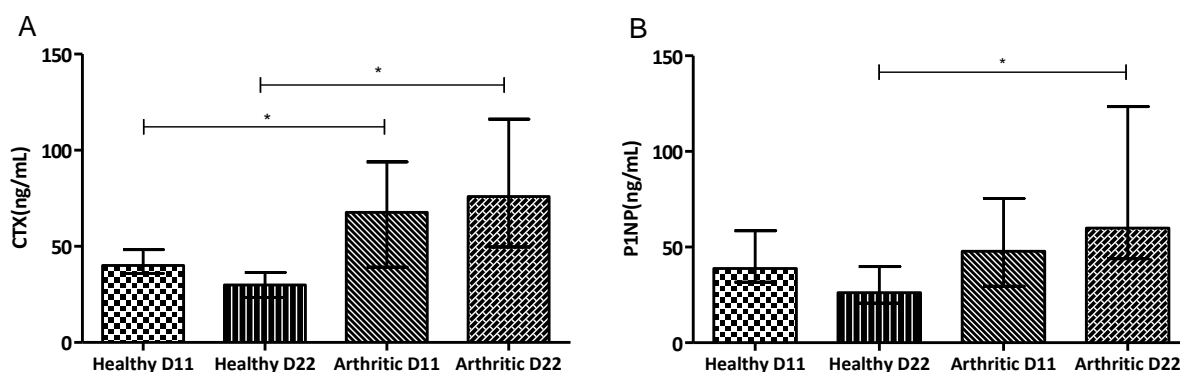


Fig.5 - Bone turnover markers quantification. Serum samples collected at day 11 and 22 post disease induction were analyzed by ELISA technique. Bone resorption marker, CTX-I (A) and bone formation marker, P1NP (B) were increased in arthritic rats at day 22 ($p < 0.0001$ and $p = 0.0007$, respectively). Results also demonstrate increased values of CTX-I in arthritic rats at day 11 when compared with healthy controls ($p = 0.0218$). Differences were considered statistically significant for p -values < 0.05 , according to the Mann–Whitney tests. Healthy D11 N=11, Healthy D22 N=18, Arthritic D11 N=16 and Arthritic D22 N=18.

Micro-CT

The effect of systemic inflammation on cortical and trabecular skeletal bone was assessed by micro-CT in bone tibia.

The arthritic group showed at day 22 a dramatic deterioration of bone tibia integrity associated with a reduction in cortical bone area (Fig. 6A) and crosssectional thickness (Fig. 6B) ($p < 0.0001$ vs healthy controls, respectively) with an evident increased endosteal perimeter (Fig. 6C) ($p = 0.0029$ vs healthy control). However, changes promoted by inflammation on bone structure begin at the early stages of arthritis as we can observe by the results obtained in the arthritic group by day 11 with a decreased cortical bone area (Fig. 6A) ($p = 0.0219$ vs healthy control). Results also demonstrated decreased values of polar moment of inertia in arthritic group at day 11 and 22 post disease induction (Fig. 6D) ($p = 0.0091$ and $p = 0.0024$ vs healthy controls, respectively).

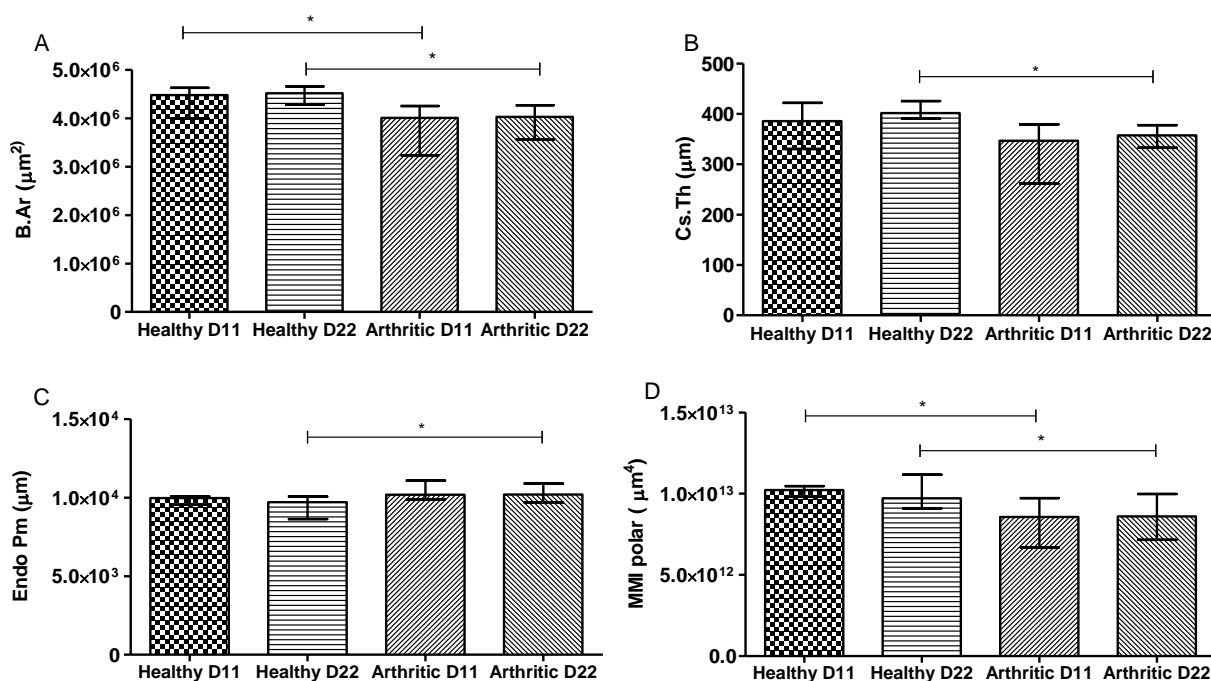


Fig.6 – Micro-computed tomography (micro-CT) - Cortical analysis of tibiae rat sample.

The crosssectional bone area of cortical bone showed decreased values in the arthritic group at day 11 and 22 (A) and polar moment of inertia (D). Arthritic group at day 22 presented a marked deterioration of bone tibia demonstrated by decreased crosssectional thickness of cortical (B) and increased endosteal perimeter (C). Differences were considered statistically significant for p -values < 0.05 , according to the Mann–Whitney tests. Healthy D11 N=11, Healthy D22 N=30, Arthritic D11 N=16 and Arthritic D22 N=31.

Trabecular bone (Fig. 7 and Fig. 8) also showed increased deterioration promoted by inflammation with decreased trabecular bone volume fraction in arthritic rats at day 11 and 22 post disease induction (Fig. 8A) ($p=0.0001$ and $p<0.0001$ vs healthy controls, respectively), thickness (Fig. 8B) ($p<0.0001$ vs healthy controls, respectively), and number (Fig. 8C) ($p=0.0039$ and $p<0.0001$ vs healthy controls, respectively). Results also demonstrated increased values of trabecular separation in the arthritic group at day 11 and 22 (Fig. 8D) ($p=0.0043$ and $p<0.0001$ vs healthy controls) and of porosity (Fig. 8E) ($p=0.0001$ and $p<0.0001$ vs healthy controls, respectively). Furthermore, structure model index (Fig. 8F) showed increased values in arthritic groups at day 11 and 22 ($p=0.0015$ and $p<0.0001$ vs healthy controls, respectively) indicating that the shape of trabeculae is rather rod-like in the arthritic group as compared to plate-like shape in healthy controls. Altogether, these results showed that inflammation promote bone structural disturbances, leading to bone loss and consequent bone fragility in arthritic rats (Fig.7).

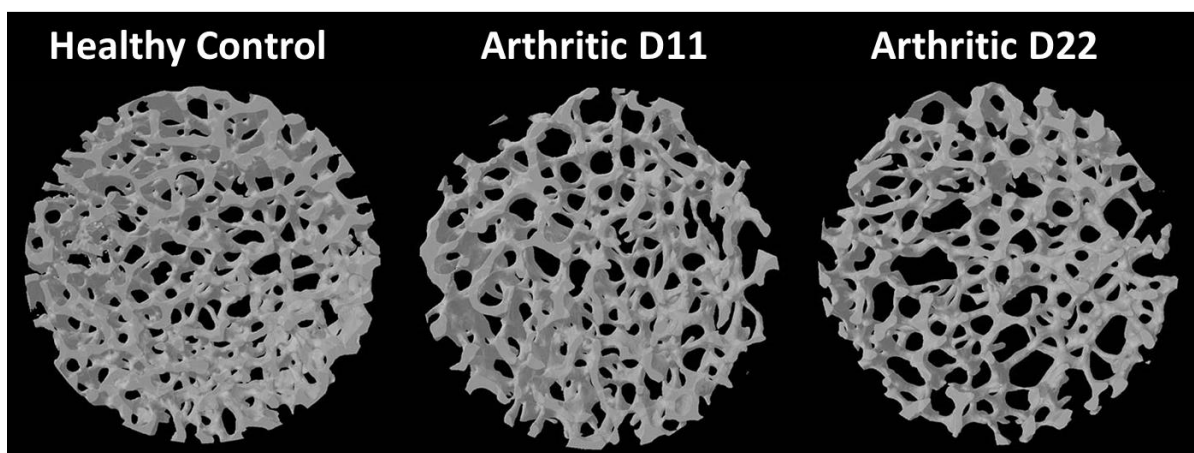


Fig.7 – MicroCT images from healthy and arthritic tibiae rats. Images acquired with SkyScan 1272, Bruker microCT, Kontich, Belgium.

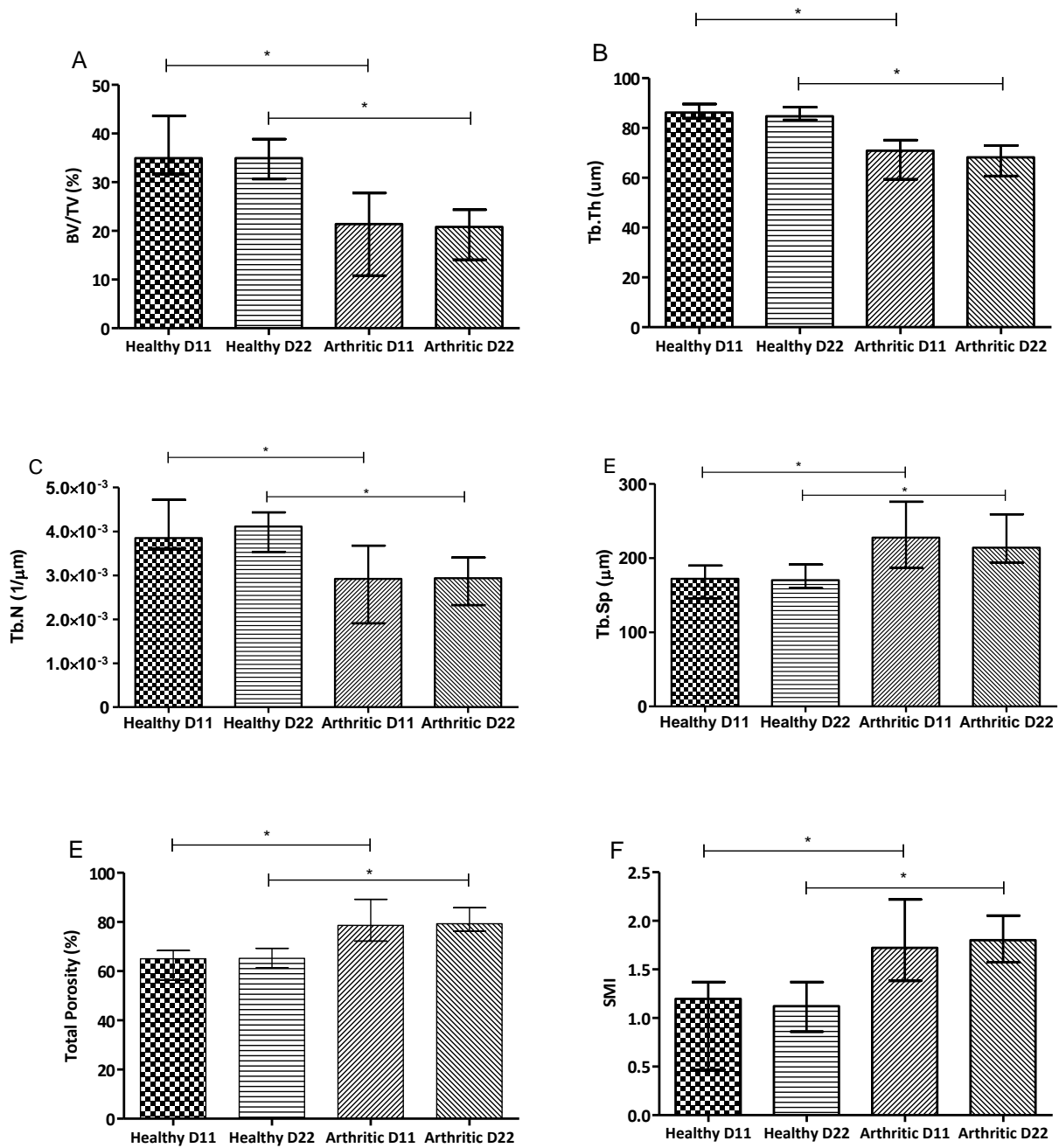


Fig.8 – Micro-computed tomography (micro-CT) –Trabecular analysis of tibiae rat sample.

Results showed decreased values of the ratio bone volume/tissue volume (A), trabecular thickness (B) and number (C) in arthritic group at day 11 and 22 post disease induction. Trabecular bone also showed increased values of trabecular separation (D), porosity (E) and structural model index in both arthritic groups. Differences were considered statistically significant for p-values<0.05, according to the Mann–Whitney tests. Healthy D11 N=11, Healthy D22 N=30, Arthritic D11 N=16 and Arthritic D22 N=31.

Bending

Classical mechanical properties of rat femurs were evaluated using 3-point bending mechanical tests. Yield point occurs when first micro fractures appear in bone. Another interesting point is maximal load at breaking point (where complete fracture occurs) and toughness can be estimated. As shown in Fig. 9, arthritic rats at day 22 revealed biomechanical disturbances with a decrease in mechanical properties at yield point, namely by displacement (Fig. 9A) ($p=0.0192$ vs healthy control), strength (Fig. 9B) ($p=0.0229$ vs healthy control) and pre yield energy (Fig. 9C) (elastic energy) ($p=0.0161$ vs healthy control). These results showed that arthritic bones at day 22 start to accumulate micro fractures with smaller deformations and loads, leading to a decreased energy absorption capability at yield point. Results also demonstrated that arthritic rats at day 22 have decreased maximum load (Fig. 9D) and elastic capabilities at maximum load point (Fig. 9E) ($p= 0.0017$ and $p=0.0134$ vs healthy control, respectively), which indicates increased bone fragility. Finally, arthritic rat groups showed a significant decrease in toughness (Fig. 9F) ($p=0.0143$ vs healthy control), demonstrating that arthritic bone can absorb less energy before fracturing.

Altogether, mechanical data revealed that arthritic groups have significantly lower mechanical properties as compared to healthy controls, meaning that arthritic bones are more fragile and prone to fracture, as highlighted by the significantly lower structural strength and poor biomechanical properties.

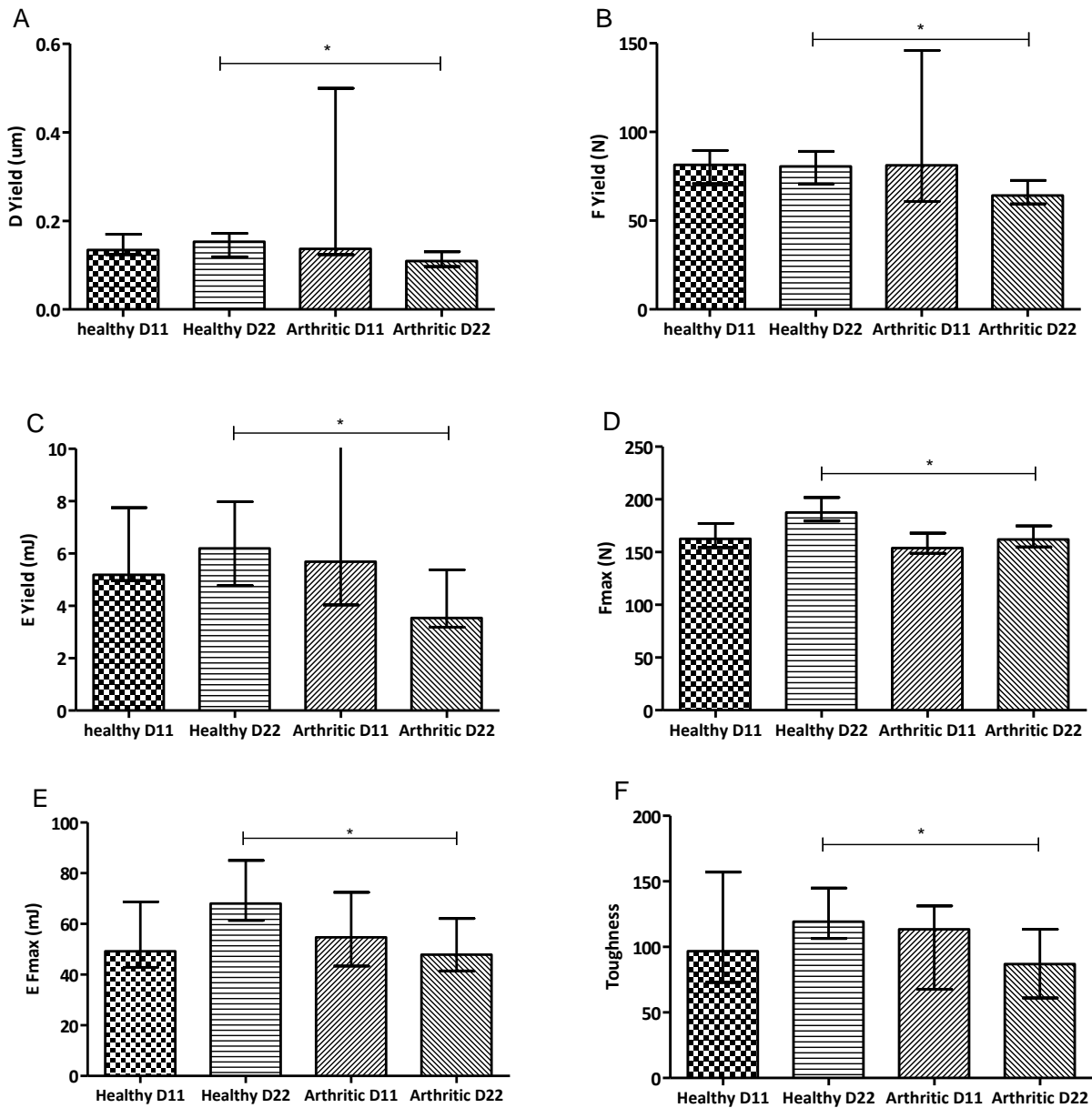


Fig.9 – Bone mechanical properties assessed by three-point bending tests in rat femur.

Results showed that arthritic rats at day 22 have decreased properties at yield point, related to displacement (A), strength (B) and energy (elastic energy) (C). Arthritic bones at day 22 required a lower maximum load (D) to fracture, with a decreased elastic energy at maximum load (E) and toughness (F). Differences were considered statistically significant for p-values < 0.05, according to the Mann–Whitney tests. Healthy D11 N=5, Healthy D22 N=14, Arthritic D11 N=5 and Arthritic D22 N=10.

Decreased hardness in arthritic bone associated with an increase of the ratio of bone concentric to parallel lamellae and of the area of the osteocyte lacuna.

Nanoindentation was performed in order to assess the quality at tissue matrix level as this technique works at the level of a single trabecula or within a confined submicron area of the cortical bone tissue (Fig 10).

Nano-mechanical tests revealed that arthritic rats have decreased hardness in the cortical aspect of bone at day 22 post disease induction (Fig 10A) ($p= 0.0010$ vs healthy control) and at trabecular bone at day 11 and 22 post disease induction (Fig 10B) ($p= 0.0184$ and $p=0.008$ vs healthy controls, respectively). Results also demonstrated the continuous decreasing of cortical hardness (Fig 10A) during arthritis development among arthritic groups ($p=0.0043$). No differences were observed in the other parameters analyzed.

Topographic images gathered during nanoindentation allowed the characterization of histologic features from healthy and arthritic bone at day 11 (Fig 10G) and 22 (Fig 10H) days post disease induction. Concentric lamellas were identified in secondary osteons (SO) and more frequently observed in arthritic animals than in healthy controls ($p= 0.0022$). On the contrary, healthy animals at day 11 (Fig 10E) and 22 (Fig. 10F) presented more parallel-lamellae (PL) structures than SO structures.

Arthritic animals at day 22 post disease induction showed also an increased area occupied by osteocyte lacunae in the total tissue when compared to healthy animals ($p=0.0067$) (Fig 10D). Results also demonstrated a slight tendency towards an increase at day 11 post disease induction (Fig 10D).

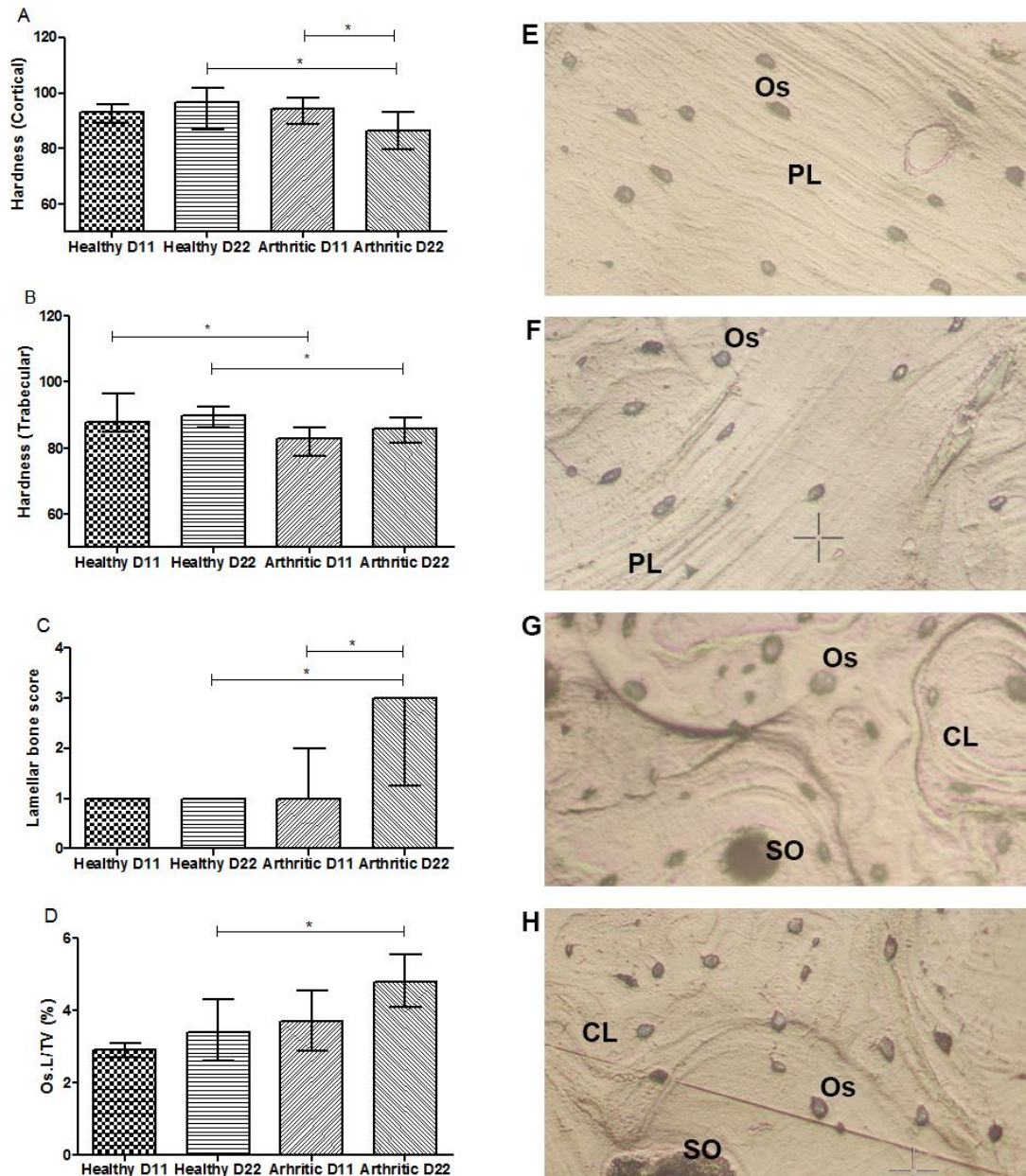


Fig.10 – Bone mechanical properties assessed by nanoindentation in rat femur at 11 and 22 days post disease induction and respective topographic images from the indentation tissue area. Nano-mechanical tests revealed that arthritic rats have decreased cortical hardness at day 22 and of trabecular hardness at day 11 and 22 post disease induction (B). Results demonstrated that concentric lamellae (C) and ratio of area occupied by osteocyte lacunae in the total tissue (D) are increased when compared to healthy animals at day 22.

Images are merely illustrative of the type of histological features observed. Concentric lamellae are identified in secondary osteons (SO), characteristic from arthritic animals at day 11 (G) and 22(H). On the contrary, parallel-lamellae (PL) are identified in healthy at day 11 (E) and 22 (F). Os – Osteocytes, SO – Secondary osteons, PL – Parallel-lamellae, CL – Concentric lamellas. Magnification 20X. Differences were considered statistically significant for p-values<0.05,

according to the Mann–Whitney tests. Healthy D11 N=11, Healthy D22 N=28, Arthritic D11 N=16 and Arthritic D22 N=21.

Decreased collagen and mineral content in the skeletal bone of arthritic animals

FTIR was performed to assess the composition of cortical and trabecular bone. Results demonstrated that the mineral content was decreased in trabecular bone of arthritic animals since the early phase of arthritis when compared to healthy controls. Statistical differences were observed when compared arthritic animals at day 11 and 22 post disease induction with their correspondent healthy controls ($p=0.0457$ and $p=0.0241$, respectively) (Fig.11 A). There was also a significant decrease of mineral content between day 11 and 22 post disease induction ($p=0.0481$) (Fig. 11A). Results also demonstrated decreased collagen matrix in arthritic animals at day 22 post disease induction ($p=0.0229$ vs healthy group at day 22) (Fig. 11B). There was also a significant decrease of collagen content between days 11 and 22 post disease induction ($p=0.0012$) (Fig. 11B).

No statistical significant differences were observed in cortical bone parameters.

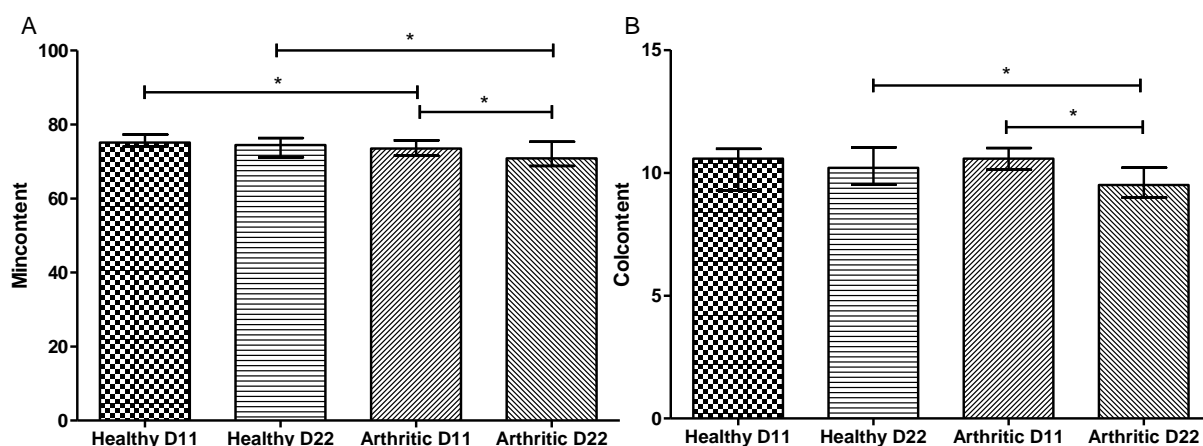


Fig.11 – FTIR measurements from cortical and trabecular bone rat tibia at 11 and 22 days post disease induction. FTIR measurements revealed that arthritic rats had mineral loss in trabecular bone since the early stage of arthritis (A). Collagen was also decreased in arthritic samples at day 22 post disease induction (B). Differences were considered statistically significant for p -values < 0.05 , according to the Mann–Whitney tests. Healthy D11 N=11, Healthy D22 N=28, Arthritic D11 N=15 and Arthritic D22 N=25.

DISCUSSION

Arthritic groups presented inflammatory manifestations with synovial tissue inflammation and local bone erosions, as expected. Increased values of serum IL-6 were observed in arthritic rats since the early stages of arthritis, confirming the systemic inflammatory component of this animal model. This cytokine plays a pivotal role in the pathologic processes of arthritis with a special emphasis on its impact on skeletal bone [20-23]. In accordance with this effect an increased and accelerated bone turnover was shown in arthritic animals, as depicted by increased CTX-I and P1NP levels since the early stages of arthritis. Data already published by our group in the same animal model of arthritis had also shown that P1NP levels were increased at day 22 post disease induction in arthritic animals and so did CTX-I levels [12], reflecting an overall increase in bone turnover [24]. Despite the existing of some variability in human studies, CTX-I and P1NP have been found to be increased in RA patients, revealing the coupled compensatory mechanism of bone turnover [12,25]. Micro-CT data and 3 point bending test confirmed that this interference of inflammation with bone metabolism translates into bone micro architectural and mechanical fragility, as observed in RA patients, further reinforcing our observations that suggested the use of the AIA model as an adequate strategy for a fast insight on the impact of inflammation on bone.

The first part of this study sets the stage for using this model for evaluating the effects of the early phase of systemic inflammatory process at bone tissue level, including nanomechanical properties, microarchitecture and mineral and collagen content.

Nanoindentation was performed in order to assess the quality of bone at tissue matrix level, as this technique can be used at the level of a single trabecula or within a confined submicron area of the cortical bone tissue. Results showed decreased cortical and trabecular hardness in arthritic rats since the early phase of arthritis (days 11 and 22).

We also observed at day 11 and 22 post arthritis induction concentric lamellas in secondary osteons (SO) microstructures, resulting from high bone remodeling, as previously described [12,26,27]. Dall'Ara *et al.* suggested that larger numbers of this younger, less mineralized and less hard structures, could be related to

reduced hardness of bone tissue identified by nanoindentation. On the contrary, healthy animals presented more parallel-lamellae (PL) structures than SO structures and this PL structures are 10% more harder than the former, representing the mature bone structure (and normal bone remodeling) [27]. In addition, arthritic animals had an increased area occupied by osteocyte lacunae in total tissue. Osteocytes are responsible for the maintenance of the bone homeostasis, regulating the behavior of osteoblasts and osteoclasts by communicating through gap junctions [28]. Although no previous data is available in the context of arthritis some studies revealed that osteocytes from osteoarthritis patients have an irregular morphology, with limited ability to reply to mechanical stimuli, leading to significant changes in the structure and mineral density [29]. Despite being still unclear this apparent change of osteocyte morphology in arthritic bone might contribute to the structural and mechanical changes observed in this context.

Finally, FTIR measurements demonstrated that inflammation induces bone mineral and collagen loss since the early phase of arthritis. FTIR imaging have been extensively applied to the analyzes of bone tissue [30-32], providing insights into molecular and chemical changes associated with load and damage of bone and cartilage [33]. Results are in line with our previous data using other techniques in the chronic phase of arthritis, showing a decreased mineral content [12] and also a lower density and organization of collagen fibrils when compared to healthy control bone [34].

CONCLUSION

Systemic inflammation induces very early changes at bone tissue level characterized by decreased tissue hardness, associated with changes in bone lamella organization and osteocyte lacuna surface and with decreased collagen and mineral content.

REFERENCES

1. Yelin E, Callahan LF (1995) The economic cost and social and psychological impact of musculoskeletal conditions. National Arthritis Data Work Groups. *Arthritis Rheum* 38: 1351-1362.
2. Lin YY, Jean YH, Lee HP, Chen WF, Sun YM, et al. (2013) A soft coral-derived compound, 11-epi-sinulariolide acetate suppresses inflammatory response and bone destruction in adjuvant-induced arthritis. *PLoS One* 8: e62926.
3. Haugeberg G, Orstavik RE, Uhlig T, Falch JA, Halse JI, et al. (2002) Bone loss in patients with rheumatoid arthritis: results from a population-based cohort of 366 patients followed up for two years. *Arthritis Rheum* 46: 1720-1728.
4. Marshall D, Johnell O, Wedel H (1996) Meta-analysis of how well measures of bone mineral density predict occurrence of osteoporotic fractures. *BMJ* 312: 1254-1259.
5. Eric-Jan JA K (2000) Bone mass in rheumatoid arthritis. *CLINICAL AND EXPERIMENTAL RHEUMATOLOGY*.
6. Fonseca JE, Cortez-Dias N, Francisco A, Sobral M, Canhao H, et al. (2005) Inflammatory cell infiltrate and RANKL/OPG expression in rheumatoid synovium: comparison with other inflammatory arthropathies and correlation with outcome. *Clin Exp Rheumatol* 23: 185-192.
7. Boyle WJ, Simonet WS, Lacey DL (2003) Osteoclast differentiation and activation. *Nature* 423: 337-342.
8. Moura RA, Cascao R, Perpetuo I, Canhao H, Vieira-Sousa E, et al. (2011) Cytokine pattern in very early rheumatoid arthritis favors B-cell activation and survival. *Rheumatology (Oxford)* 50: 278-282.
9. Cascao R, Moura RA, Perpetuo I, Canhao H, Vieira-Sousa E, et al. (2010) Identification of a cytokine network sustaining neutrophil and Th17 activation in untreated early rheumatoid arthritis. *Arthritis Res Ther* 12: R196.
10. Caetano-Lopes J, Canhao H, Fonseca JE (2009) Osteoimmunology--the hidden immune regulation of bone. *Autoimmun Rev* 8: 250-255.
11. Caetano-Lopes J, Rodrigues A, Lopes A, Vale AC, Pitts-Kiefer MA, et al. (2014) Rheumatoid arthritis bone fragility is associated with upregulation of IL17 and DKK1 gene expression. *Clin Rev Allergy Immunol* 47: 38-45.

12. Vidal B, Cascao R, Vale AC, Cavaleiro I, Vaz MF, et al. (2015) Arthritis induces early bone high turnover, structural degradation and mechanical weakness. *PLoS One* 10: e0117100.
13. Cascao R, Vidal B, Raquel H, Neves-Costa A, Figueiredo N, et al. (2012) Effective treatment of rat adjuvant-induced arthritis by celastrol. *Autoimmun Rev* 11: 856-862.
14. Bouxsein ML, Boyd SK, Christiansen BA, Guldberg RE, Jepsen KJ, et al. (2010) Guidelines for assessment of bone microstructure in rodents using micro-computed tomography. *J Bone Miner Res* 25: 1468-1486.
15. Herlin M, Finnila MA, Zioupos P, Aula A, Risteli J, et al. (2013) New insights to the role of aryl hydrocarbon receptor in bone phenotype and in dioxin-induced modulation of bone microarchitecture and material properties. *Toxicol Appl Pharmacol* 273: 219-226.
16. Zhang R, Gong H, Zhu D, Ma R, Fang J, et al. (2015) Multi-level femoral morphology and mechanical properties of rats of different ages. *Bone* 76: 76-87.
17. W.C. Oliver GMP (1992) An improved technique for determining hardness and elastic modulus using load and displacement sensing indentation experiments.
18. Parfitt AM, Drezner MK, Glorieux FH, Kanis JA, Malluche H, et al. (1987) Bone histomorphometry: standardization of nomenclature, symbols, and units. Report of the ASBMR Histomorphometry Nomenclature Committee. *J Bone Miner Res* 2: 595-610.
19. Isaksson H, Turunen MJ, Rieppo L, Saarakkala S, Tamminen IS, et al. (2010) Infrared spectroscopy indicates altered bone turnover and remodeling activity in renal osteodystrophy. *J Bone Miner Res* 25: 1360-1366.
20. Choy EH, Isenberg DA, Garrood T, Farrow S, Ioannou Y, et al. (2002) Therapeutic benefit of blocking interleukin-6 activity with an anti-interleukin-6 receptor monoclonal antibody in rheumatoid arthritis: a randomized, double-blind, placebo-controlled, dose-escalation trial. *Arthritis Rheum* 46: 3143-3150.
21. Nishimoto N, Yoshizaki K, Miyasaka N, Yamamoto K, Kawai S, et al. (2004) Treatment of rheumatoid arthritis with humanized anti-interleukin-6 receptor antibody: a multicenter, double-blind, placebo-controlled trial. *Arthritis Rheum* 50: 1761-1769.

22. Maeshima K, Yamaoka K, Kubo S, Nakano K, Iwata S, et al. (2012) The JAK inhibitor tofacitinib regulates synovitis through inhibition of interferon-gamma and interleukin-17 production by human CD4+ T cells. *Arthritis Rheum* 64: 1790-1798.
23. Fonseca JE, Santos MJ, Canhao H, Choy E (2009) Interleukin-6 as a key player in systemic inflammation and joint destruction. *Autoimmun Rev* 8: 538-542.
24. Siebuhr AS, Wang J, Karsdal M, Bay-Jensen AC, Y J, et al. (2012) Matrix metalloproteinase-dependent turnover of cartilage, synovial membrane, and connective tissue is elevated in rats with collagen induced arthritis. *J Transl Med* 10: 195.
25. Cortet B, Flipo RM, Pigny P, Duquesnoy B, Boersma A, et al. (1998) Is bone turnover a determinant of bone mass in rheumatoid arthritis? *J Rheumatol* 25: 2339-2344.
26. Bailey AJ, Mansell JP, Sims TJ, Barse X (2004) Biochemical and mechanical properties of subchondral bone in osteoarthritis. *Biorheology* 41: 349-358.
27. Dall'Ara E, Ohman C, Baleani M, Viceconti M (2011) Reduced tissue hardness of trabecular bone is associated with severe osteoarthritis. *J Biomech* 44: 1593-1598.
28. Taylor AF, Saunders MM, Shingle DL, Cimbala JM, Zhou Z, et al. (2007) Mechanically stimulated osteocytes regulate osteoblastic activity via gap junctions. *Am J Physiol Cell Physiol* 292: C545-552.
29. Jaiprakash A, Prasadam I, Feng JQ, Liu Y, Crawford R, et al. (2012) Phenotypic characterization of osteoarthritic osteocytes from the sclerotic zones: a possible pathological role in subchondral bone sclerosis. *Int J Biol Sci* 8: 406-417.
30. Miller LM, Vairavamurthy V, Chance MR, Mendelsohn R, Paschalis EP, et al. (2001) In situ analysis of mineral content and crystallinity in bone using infrared micro-spectroscopy of the nu(4) PO(4)(3-) vibration. *Biochim Biophys Acta* 1527: 11-19.
31. Ou-Yang H, Paschalis EP, Mayo WE, Boskey AL, Mendelsohn R (2001) Infrared microscopic imaging of bone: spatial distribution of CO3(2-). *J Bone Miner Res* 16: 893-900.
32. Paschalis EP, Recker R, DiCarlo E, Doty SB, Atti E, et al. (2003) Distribution of collagen cross-links in normal human trabecular bone. *J Bone Miner Res* 18: 1942-1946.

33. Boskey A, Pleshko Camacho N (2007) FT-IR imaging of native and tissue-engineered bone and cartilage. *Biomaterials* 28: 2465-2478.
34. Caetano-Lopes J, Nery AM, Canhao H, Duarte J, Cascao R, et al. (2010) Chronic arthritis leads to disturbances in the bone collagen network. *Arthritis Res Ther* 12: R9.

III. Decrease of CD68 synovial macrophages in celastrol treated arthritic rats

Rita Cascão, Bruno Vidal, Inês P. Lopes, Eunice Paisana, José Rino, Luis F. Moita, João E. Fonseca.

Author Contributions

Cascão designed the experiments. Cascão and Vidal performed all the experiments and wrote the chapter. Lopes, Paisana and Rino helped to perform some experiments. Moita and Fonseca supervised the work and revised the text.

Decrease of CD68 synovial macrophages in celastrol treated arthritic rats

Rita Cascão, Bruno Vidal, Inês P. Lopes, Eunice Paisana, José Rino, Luis F. Moita, João E. Fonseca

ABSTRACT

Background: Rheumatoid arthritis (RA) is a chronic immune-mediated inflammatory disease characterized by cellular infiltration into the joints, hyperproliferation of synovial cells and bone damage. Available treatments for RA only induce remission in around 30% of the patients, have important adverse effects and its use is limited by their high cost. Therefore, compounds that can control arthritis, with an acceptable safety profile and low production costs are still an unmet need. We have shown, *in vitro*, that celastrol inhibits both IL-1 β and TNF, which play an important role in RA, and, *in vivo*, that celastrol has significant anti-inflammatory properties. Our main goal in this work was to test the effect of celastrol in the number of sublining CD68 macrophages (a biomarker of therapeutic response for novel RA treatments) and on the overall synovial tissue cellularity and joint structure in the adjuvant-induced rat model of arthritis (AIA). **Methods:** Celastrol was administered to AIA rats both in the early (4 days after disease induction) and late (11 days after disease induction) phases of arthritis development. The inflammatory score, ankle perimeter and body weight were evaluated during treatment period. Rats were sacrificed after 22 days of disease progression and blood, internal organs and paw samples were collected for toxicological blood parameters and serum proinflammatory cytokine quantification, as well as histopathological and immunohistochemical evaluation, respectively. **Results:** Here we report that celastrol significantly decreases the number of sublining CD68 macrophages and the overall synovial inflammatory cellularity, and halted joint destruction without side effects. **Conclusions:** Our results validate celastrol as a promising compound for the treatment of arthritis.

INTRODUCTION

Rheumatoid arthritis (RA) is a chronic immune mediated inflammatory disease that is mainly characterized by hyperproliferation of synovial cells, infiltration of mononuclear cells into the synovium and early destruction of articular cartilage and bone, causing progressive damage to the musculoskeletal system and consequently the loss of physical function and life quality [1-3]. The most debilitating feature of RA is joint destruction, which is derived from an uncontrolled inflammatory process. RA joint synovial cellular infiltrate consists of activated macrophages, B and T-cells, which secrete proinflammatory cytokines and other mediators of inflammation [1, 4, 5] that not only perpetuate the inflammatory process but also increase bone resorption [6-10]. In addition, activated synovial fibroblasts, chondrocytes and osteoclasts contribute to the underlying cartilage and bone damage [11]. Despite this clear link between inflammation and increased bone turnover in RA and the existence of several therapeutical options, their efficacy on inflammation and bone treatment seem to be uncoupled, with some drugs suppressing inflammation but failing to protect bone [12, 13] and others halting bone destruction but with no effect on controlling inflammation [14]. Moreover, drugs used to treat RA, ranging from nonsteroidal anti-inflammatory drugs (NSAIDs) to disease-modifying antirheumatic drugs (DMARDs), and biological DMARDs, still cause severe side effects [15, 16] and are only able to induce remission in around 20-30% of the patients, leaving the majority of the individuals affected by RA with a chronic inflammatory process that will lead to damage. In addition to this, the most recent and innovative treatments are highly expensive, representing a burden to national health services and creating a barrier to its use in less affluent areas of the world. Therefore, compounds that can control arthritis, with an acceptable safety profile and low production cost are still an unmet need.

In this context, we have recently identified celastrol, a pentacyclic triterpenoid compound isolated from the roots of the Chinese herb *Tripterygium wilfordii* Hook F, as a potential RA therapeutic candidate [17]. We have shown that celastrol inhibits both interleukin (IL)-1 β and tumor necrosis factor (TNF), which play an important role since the early phase of RA [18], and has significant anti-

inflammatory and anti-proliferative properties in an adjuvant-induced rat model of arthritis (AIA) [17]. Supporting our own results, other studies using celastrol have reported beneficial effects in various models of inflammation, diminishing joint swelling and damage, serum IgG level, TNF and IL-1 β mRNA and preventing disease progression [19]. Importantly, recent studies have also demonstrated that celastrol protects human chondrocytes by down-regulating the expression of metalloproteinases (MMPs) and inducible nitric oxide synthase (iNOS), suppresses several chemokines that mediate cellular joint infiltration [20], impairs B-cell development [21] and also regulates bone remodeling-related immune mediators and proinflammatory cytokines in AIA synovium-infiltrating cells cultured *ex vivo* and in the RAW264.7 macrophagic cell line [22]. Celastrol might thus constitute an attractive candidate to have an early effect not only in controlling inflammation but also in preventing bone structural disturbances that occur in arthritis.

The efficacy of new compounds in the treatment of RA has been associated with a decrease in CD68 positive macrophages in the synovial sublining layer. This effect has been clearly demonstrated for most of the effective treatments for RA, including classic treatments, such as prednisolone [23], gold salts [24], methotrexate [25, 26] and leflunomide [27], and also for biologics such as infliximab [28, 29], anakinra [30, 31] and rituximab [32]. Interestingly, a study of a CCL-2/MCP-1 monoclonal antibody antagonist demonstrated no change in CD68 sublining macrophages and this was associated with no change in disease activity [33]. In accordance, a C5aR antagonist did not affect CD68 sublining macrophages and no clinical effect occurred [34]. Furthermore, a multicenter study on the correlation of the number of sublining CD68 cells and the change in DAS28 demonstrated excellent inter-centre agreement [32] and it has been shown that the number of CD68 macrophages decreases with a reduction in disease activity as measured by Disease Activity Score [35]. Due to these very solid evidences, the number of CD68 sublining macrophages has been proposed as a biomarker of therapeutic response to be used in the test of novel treatments for RA [32]. Of interest, in the preclinical test of new compounds, a number of observations have shown that effective RA treatments such as tofacitinib [36] and methotrexate [37]

also decrease CD68 sublining macrophages in animal models of arthritis. Several experimental compounds have also shown an association between control of arthritis and reduction in the number of CD68 macrophages in animal models of arthritis [38-40].

Our aim in the herein study was to test the effect of celastrol treatment in the number of sublining CD68 macrophages and on the overall synovial tissue cellularity and joint structure in an animal model of arthritis, as a further argument to its possible efficacy in RA treatment.

In this work we report that celastrol significantly decreases the number of sublining CD68 macrophages and the overall synovial inflammatory cellularity, and halted joint destruction without any detectable side effects.

MATERIALS AND METHODS

Animal experimental design

Eight-week-old female wistar AIA rats were purchased from Charles River Laboratories International (Massachusetts, USA). AIA rats were maintained under specific pathogen free (SPF) conditions and housed per groups under standard laboratory conditions (at 22°C under 12-hour light/12-hour dark conditions). Human end-points were established and animals were sacrificed when presenting the maximum inflammatory score in more than 2 paws or when presenting more than 20% of body weight loss. All experiments were approved by the Animal User and Ethical Committees at the Instituto de Medicina Molecular (Lisbon University), according to the Portuguese law and the European recommendations. The dose of celastrol (1µg/g body weight daily) used in this study was based on that used in our previous study [17] and in other studies [22]. The need for daily administrations is also supported by Zhang J. et al who showed that the half-life of pure celastrol is approximately 10 hours [41]. Celastrol (Sigma, Missouri, USA) stock solution of 100mg/ml in DMSO was dissolved in normal saline solution and injected intraperitoneally in AIA rats after 4 days (early treatment group) and after 11 days (late treatment group) of disease induction, when arthritis was already present. A group of healthy non-arthritic and arthritic untreated female age-

matched wistar rats sacrificed at day 4 (baseline for the celastrol early-treated group, at preclinical stage, N=13), day 11 (baseline for the celastrol late-treated group, at acute clinical stage, N=18) and day 22 after disease induction (chronic clinical stage) were used as controls in all experiments for comparison. At the preclinical AIA progression stage evidence of inflammation or bone erosion is still lacking in the contralateral hind paw and fore paws. Hind paw swelling, inflammation and joint erosions are steadily progressing during acute clinical stage and reach a plateau in the chronic stage [42]. The inflammatory score, ankle perimeter and body weight were measured during the period of treatment. Inflammatory score was evaluated by counting the score of each paw joint in a scale of 0–3 (0 — absence; 1 — erythema; 2 — erythema and swelling; 3 — deformities and functional impairment). The total score of each animal was defined as the sum of the partial scores of each affected joint [17, 43]. Rats were sacrificed by CO₂ narcosis and blood, internal organs as well as paw samples were collected.

Toxicological evaluation

For histopathological observation, lung, liver, kidney and spleen samples were collected at the time of sacrifice. Samples were fixed immediately in 10% neutral buffered formalin solution and then dehydrated with increasing ethanol concentrations (70%, 96% and 100%). Samples were next embedded in paraffin, sectioned using a microtome, mounted on microscope slides and stained with hematoxylin and eosin. Tissue histopathological changes were examined by a pathologist blinded to the experimental groups. All images were acquired using a Leica DM 2500 microscope equipped with a color camera Leica MC170 HD (Leica microsystems, Wetzlar, Germany). Moreover, blood toxicological parameters, such as creatine kinase, urea, lactate dehydrogenase and alanine transaminase, were measured in serum samples by enzyme linked immunosorbent assay (ELISA) technique according to the manufacturer's instructions (BioAssay Systems, California, USA). Samples were analyzed using a plate reader Infinite M200 (Tecan, Mannedorf, Switzerland).

Systemic cytokine quantification

Proinflammatory cytokines IL-1 β (Boster Bio, California, USA), IL-6 (Boster Bio, California, USA), IL-17 (Sunred Biological Technology, Shanghai, China) and TNF (RayBiotech, Georgia, USA) were quantified in serum samples using specific rat ELISA kits according to the provider's recommendations. Standard curves for each cytokine were generated by using reference cytokine concentrations supplied by the manufacturer. Samples were analyzed using a plate reader Infinite M200 (Tecan, Mannedorf, Switzerland).

Histological and immunohistochemical evaluation of hind paws

Left hind paw samples collected at the time of sacrifice were fixed immediately in 10% neutral buffered formalin solution and then decalcified in 10% formic acid. Samples were next dehydrated and embedded in paraffin, serially sectioned at a thickness of 5 μ m using a microtome, mounted on microscope slides and stained with hematoxylin and eosin for morphological examination of structural changes and cellular infiltration. Histopathological evaluation of rat joints was performed in a blind fashion using 4 semi-quantitative scores: Sublining layer infiltration score (0 — none to diffuse infiltration; 1 — lymphoid cell aggregate; 2 — lymphoid follicles; 3 — lymphoid follicles with germinal center formation); Lining layer cell number score (0 — fewer than three layers; 1 — three to four layers; 2 — five to six layers; 3 — more than six layers); Bone erosion score (0 — no erosions; 1 — minimal; 2 — mild; 3 — moderate; 4 — marked); Global severity score (0 — no signs of inflammation; 1 — mild; 2 — moderate; 3 — severe) [17, 44, 45]. Paw sections were also used for immunohistochemical staining with CD68 (Abcam, Cambridge, UK), CD163 (Biorbyt, Massachusetts, USA), CD3 (Abcam, Cambridge, UK), CD19 (Biorbyt, Massachusetts, USA) and Ki67 (Abcam, Cambridge, UK) antibodies. Tissue sections were incubated with the primary antibody and with EnVision+ (Dako, Glostrup, Denmark). Color was developed in solution containing diaminobenzadine-tetrahydrochloride (Sigma, Missouri, USA), 0.5% H₂O₂ in phosphate-buffered saline buffer (pH 7.6). Slides were counterstained with

hematoxylin and mounted. Immunohistochemical evaluation of rat joints was performed in a blind fashion using a semi-quantitative score of 0-4 (0 — no staining; 1 — 0-25% staining; 2 — 25-50% staining; 3 — 50-75% staining; 4 — more than 75% staining) [17]. Images were acquired using a Leica DM2500 (Leica Microsystems, Wetzlar, Germany) microscope equipped with a color camera.

For a quantitative analysis of the immunohistochemical staining, we acquired whole-slide color images of single tissue slides using a NanoZoomer SQ slide scanner (Hamamatsu Photonics, Hamamatsu City, Japan) with 20x magnification (0.46 μm resolution). We developed an image analysis software written in MATLAB (Mathworks, Natick, MA) to identify and count the number of positive cells that displayed a specific cytoplasmic staining in representative sections. Briefly, single cell nuclei stained with hematoxylin were identified by color thresholding in the $L^*a^*b^*$ color space with the range of parameters $L^*=[40,72]$, $a^*=[-11,20]$ and $b^*=[-37,12]$ followed by particle analysis. Dilated regions of interest (ROIs) with a radius of 5 pixels were next defined for each detected particle as the cytoplasmic area. The antibody staining was also identified by color thresholding in the $L^*a^*b^*$ color space with the range of parameters $L^*=[40,80]$, $a^*=[-6,20]$ and $b^*=[-0.2,33]$. Each cell ROI was then evaluated for antibody positive staining, defined by the occurrence of at least 20 pixels with a color value included in the cytoplasmic $L^*a^*b^*$ threshold range. We cropped areas of interest from whole-slide color images corresponding to synovial membranes and the software was set to batch process all images and output the total number of cells and the number of cells with positive antibody staining for each section. Then the density of positive cells was calculated by dividing the positive cell count by the area value.

Statistical analysis

Statistical differences were determined with non-parametric Kruskal-Wallis (Dunn's Multiple Comparison tests) and Mann-Whitney tests using GraphPad Prism (GraphPad, California, USA). Correlation analysis was performed with the Spearman test. Differences were considered statistically significant for $p < 0.05$.

RESULTS

Celastrol safely suppresses inflammatory manifestations in rat adjuvant-induced arthritis

To further validate the *in vivo* anti-inflammatory effect of celastrol in the context of arthritis, we have used the AIA rat model. The AIA experimental arthritis shares some characteristics of RA, such as hyperplasia of the synovial membrane, inflammatory infiltration of the joints, deposition of immune complexes in articular cartilage, pannus formation and destruction of bone. This model is also useful to characterize treatment responses by the reduction of inflammation or changes in the synovial tissue [46]. Overall, the AIA model has been extensively used to clarify the mechanisms of human RA pathogenesis and to identify potential targets and new drugs for therapeutic intervention [47], and has thus been our model of choice for our first experimental use of celastrol [17, 48].

Celastrol was intraperitoneally administrated at a dose of 1 μ g/g/daily after 4 days of disease induction (early treatment group) and after 11 days of disease induction (late treatment group) [17]. The inflammatory score and ankle perimeter were evaluated during the treatment period (Fig. 1 and S1 Fig.). As shown in Fig.1A, all animals already presented signs of arthritis by the fourth day of disease induction and after 9 days the untreated arthritic group started to increase the inflammatory manifestations sharply. In contrast, in early celastrol-treated rats there was minimal inflammatory activity or even complete abrogation of arthritis manifestations. In the late treatment group, drug administration was started when animals already presented a mean inflammatory score of 4, but celastrol still caused a significant decrease of arthritis manifestations over time. In fact, the only

remaining sign of swelling was observed in most animals in the local of injection of the adjuvant, for disease induction. This result shows that this drug has a significant anti-inflammatory effect even when administrated at a later phase of arthritis development. Celastrol showed a significant anti-inflammatory effect, as assessed by the evaluation of the inflammatory score ($p < 0.0001$ in early and late treatment groups vs. arthritic animals, shown in Fig. 1B) and also by the measurement of ankle perimeter ($p < 0.0001$ in early and late treatment groups vs. arthritic animals, shown in Fig. 1C). Of note, by the end of the treatment, at day 22, there were no significant differences between the celastrol early and late treatment groups. Importantly, both treated groups showed a significant reduction in the inflammatory score when compared with their baselines ($p = 0.0002$ in celastrol early-treated vs. arthritic rats sacrificed at day 4 and $p < 0.0001$ in celastrol-late treated vs. arthritic rats sacrificed at day 11).

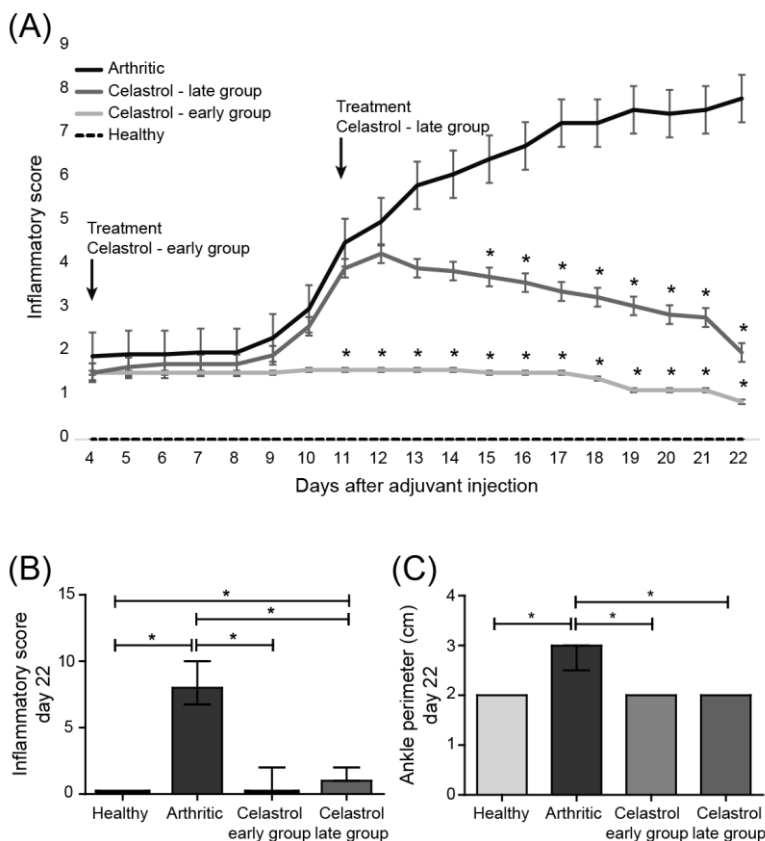


Fig. 1 – (A) Celastrol ameliorates inflammation throughout time. Notice that after 7 days of treatment celastrol early-treated rats presented minimal inflammatory activity, whereas arthritic rats started to increase the inflammatory manifestations sharply. Arrows indicate the beginning of

treatment after 4 and 11 days of disease induction. (B) Celastrol improves the clinical outcome in adjuvant-induced arthritic rats. Inflammatory score in celastrol-treated AIA rats is maintained significantly diminished in comparison with arthritic rats. (C) Celastrol suppresses the progression of swelling in the left hind paw. Left paw edema/swelling is markedly present in arthritic rats in contrast to celastrol-treated animals. Data are expressed as median with interquartile range. Differences were considered statistically significant for p -values <0.05 , according to the Kruskal-Wallis (Dunn's Multiple Comparison tests) and Mann-Whitney tests. Healthy N=19, Arthritic N=23, Celastrol early group N=15 and Celastrol late group N=15.

Up to now significant adverse effects of celastrol administration have not been reported. However the few toxicological analysis of this compound in vivo were based in data from the assessment of animal mortality and some blood parameters in studies using *Tripterygium wilfordii* plant extracts [49]. To investigate the potential side effects of pure celastrol administration in AIA rats, we performed liver and renal function tests, such as the measurement of creatine kinase, urea, lactate dehydrogenase and alanine transaminase in serum samples collected at the time of sacrifice. No significant differences were observed in these parameters when comparing arthritic rats with animals under treatment ($p=0.2$). In addition, a pathologist blinded to experimental groups examined the tissue histological sections and has reported no evidence of drug-induced liver or renal injury, as well as no lung or spleen alterations (S2 Fig.). Of note, body weight variations were recorded throughout treatment duration, and no weight loss was observed due to celastrol administration ($p=0.1265$ and $p=0.6005$ in celastrol early and late treatment groups vs. arthritic rats, respectively). Contrarily, there was an association between disease activity and weigh loss ($p=0.0273$ in arthritic rats vs. healthy animals). In fact, in the late treatment group, animals started to lose weight due to disease activity and after treatment was initiated no more weight loss was observed ($p=0.0436$ in late-treated rats at day 11 vs. day 4, and $p=0.9009$ in late-treated rats at day 22 vs. day 11) (S3 Fig.). Importantly, administration of celastrol has already been tested in healthy animals in a wide range of concentrations [21]. So far, there are no data showing deleterious effects at a dose of 1mg/kg (the concentration used in this work).

Celastrol diminishes systemic proinflammatory cytokine IL-6 in vivo

Proinflammatory cytokines, namely IL-1 β , IL-6, IL-17 and TNF act synergistically to maintain inflammation and bone erosions in animal models of arthritis and in RA patients. These cytokines activate the NF- κ B pathway that in turn leads to the downstream up-regulation of several cytokines, chemokines and MMPs, which are responsible for the inflammatory process and for the destruction of cartilage and bone. We therefore aimed at evaluating the anti-inflammatory effect of celastrol on the peripheral circulating levels of these cytokines. We have observed that IL-6 levels increase in the serum of AIA rats throughout the course of arthritis, although abundant production was seen only after 2 weeks of disease onset. Thus, IL-6, which is produced by monocytes/macrophages, T-cells and synovial fibroblasts [50], seems to be involved in the systemic events underlying arthritis, especially in the transition phase of its development. Fig. 2 shows that celastrol administration significantly reduces the levels of IL-6 detected in peripheral blood, both in early and late treatment groups ($p < 0.0001$ in both groups vs. arthritic rats after 22 days of disease induction), presenting a cytokine concentration similar to healthy controls. Importantly, both treated groups showed a significant reduction in the circulating levels of IL-6 when compared with their baselines ($p = 0.0387$ in celastrol early-treated vs. arthritic rats sacrificed at day 4 and $p < 0.0001$ in celastrol-late treated vs. arthritic rats sacrificed at day 11). This observation is corroborated by data already published which shows that IL-6 mRNA is decreased after celastrol treatment in vitro [51]. We have also quantified the circulating concentration of IL-1 β , IL-17 and TNF, but no differences were found when comparing arthritic rats with animals under celastrol treatment or with healthy controls ($p > 0.05$, S4 Fig.), possibly because these cytokines are not increased in the periphery at this stage of disease development. Previously, we have demonstrated that circulating IL-1 β and IL-17 are only increased in the early phase of RA, in contrast to IL-6, which was found to be increased also in the later phase of the disease [18], arguing that the detection of these cytokines in the periphery is dependent on disease evolution. In addition, literature controversy highlights the likelihood that systemic markers and mediators of arthritis might not fully reflect the underlying local disease progression. AIA rat model have increased levels of IL-1 β (since the

preclinical disease stage), IL-6, IL-17 and TNF (in the acute and chronic stages) locally in the joints [42]. Recently, it has been shown in the same animal model that both Tripterygium and celastrol decrease the levels of these cytokines locally in the arthritic joints [19, 20, 22, 52].

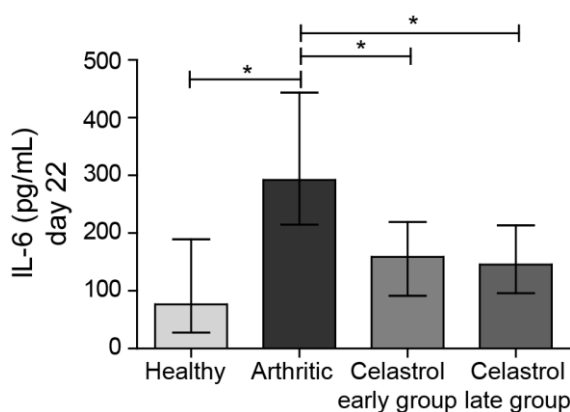


Fig. 2 - Celastrol reduces the serum levels of IL-6 in arthritic rats. Notice that celastrol treatment significantly reduces the systemic concentration of the proinflammatory cytokine IL-6 to levels similar to healthy controls. Data are expressed as median with interquartile range. Differences were considered statistically significant for p -values <0.05 , according to the Kruskal-Wallis (Dunn's Multiple Comparison tests) and Mann-Whitney tests. Healthy $N=21$, Arthritic $N=23$, Celastrol early group $N=15$ and Celastrol late group $N=15$.

Celastrol ameliorates local joint inflammation and bone damage in AIA rats

To evaluate the effect of celastrol in the preservation of local articular joint synovium and bone structures, paw sections stained with hematoxylin and eosin were performed (illustrative images can be observed in Fig. 3). The histological evaluation using 4 semi-quantitative scores is depicted in Fig. 4.

The levels of the sublining layer infiltration (Fig. 4A) and the lining layer cell numbers (Fig. 4B) started to augment immediately after 4 days of disease onset and continued to markedly increase until the end of the study ($p<0.0001$, healthy vs. arthritic rats sacrificed after 22 days of disease induction). The data from Fig. 4D revealed that rats treated with celastrol had a normal joint structure at the end

of the study period, with an abrogation of the inflammatory infiltrate and a reduction of the number of cells present in the lining layer of the synovial membrane ($p < 0.0001$ in early and late treatment groups vs. arthritic animals). Moreover, when comparing the infiltration score of celestrol early-treated group with diseased animals at baseline (day 4), we observed that there was a complete clearance of the cellular infiltrate ($p = 0.0006$ in the early-treated group sacrificed at the end of the treatment period vs. arthritic rats sacrificed at baseline of the treatment period, i.e. after 4 days of disease induction), with a phenotype similar to a healthy control. Regarding the analysis of the lining layer cell number score (Fig. 4B), data showed that both celestrol early and late treatment groups have dramatically reduced scores, in comparison with the animals at the beginning of treatment, corresponding to baseline ($p = 0.0107$ in early-treated arthritic rats sacrificed at the end of the study period vs. arthritic rats sacrificed at baseline, at day 4 and $p < 0.0001$ in late-treated arthritic rats sacrificed at the end of the study period vs. arthritic rats sacrificed at baseline, at day 11, respectively).

Celestrol is also effective in preventing bone articular destruction as shown in Fig. 4C. The development of bone erosions in the AIA rat model occurred immediately after 4 days of disease onset, and markedly increased throughout the development of arthritis ($p < 0.0001$ in healthy vs. arthritic rats sacrificed after 22 days of disease induction), with a strong correlation between erosion and infiltration as well as with proliferation scores ($r^2 = 0.70$, $p = 0.0009$ and $r^2 = 0.97$, $p < 0.0001$, respectively). By the end of the treatment course, celestrol was able to suppress the appearance of bone erosions ($p < 0.0001$ in both celestrol early and late treatment groups vs. arthritic rats), maintaining the phenotype similar to their baselines. These results might suggest that celestrol is able to modulate osteoclast pathways. In fact, a study has demonstrated that celestrol inhibits the formation and activity of mature osteoclasts, induces their apoptosis and reduces osteoblast viability and activity in vitro [53].

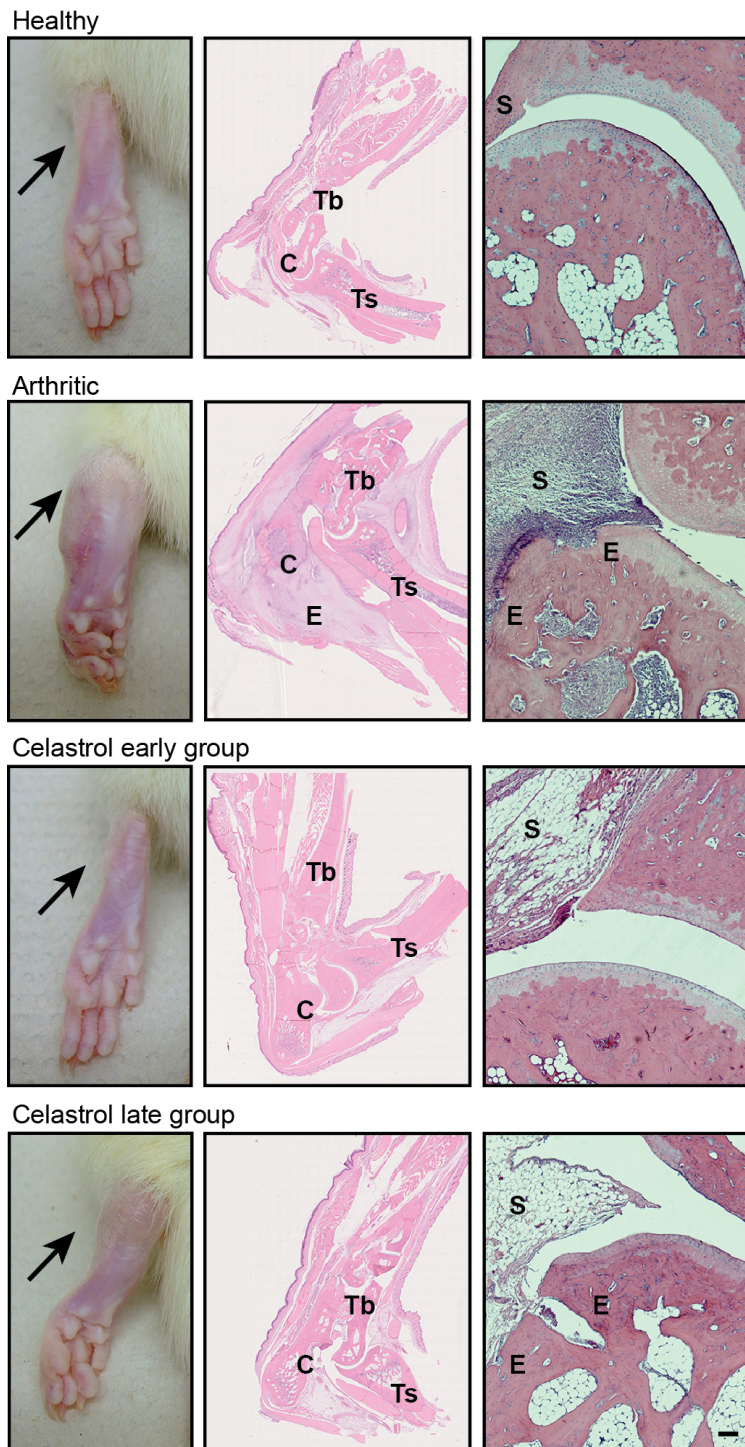


Fig. 3 – Histological images of joints after celastrol treatment. These patterns are merely illustrative of the type of histological features observed. Black arrow indicates the absence/presence of ankle swelling in rat hind paws. C – calcaneus, E – edema or erosion, S – synovia, Tb – tibia, Ts – tarso. Magnification of 50 \times . Bar: 100 μ m.

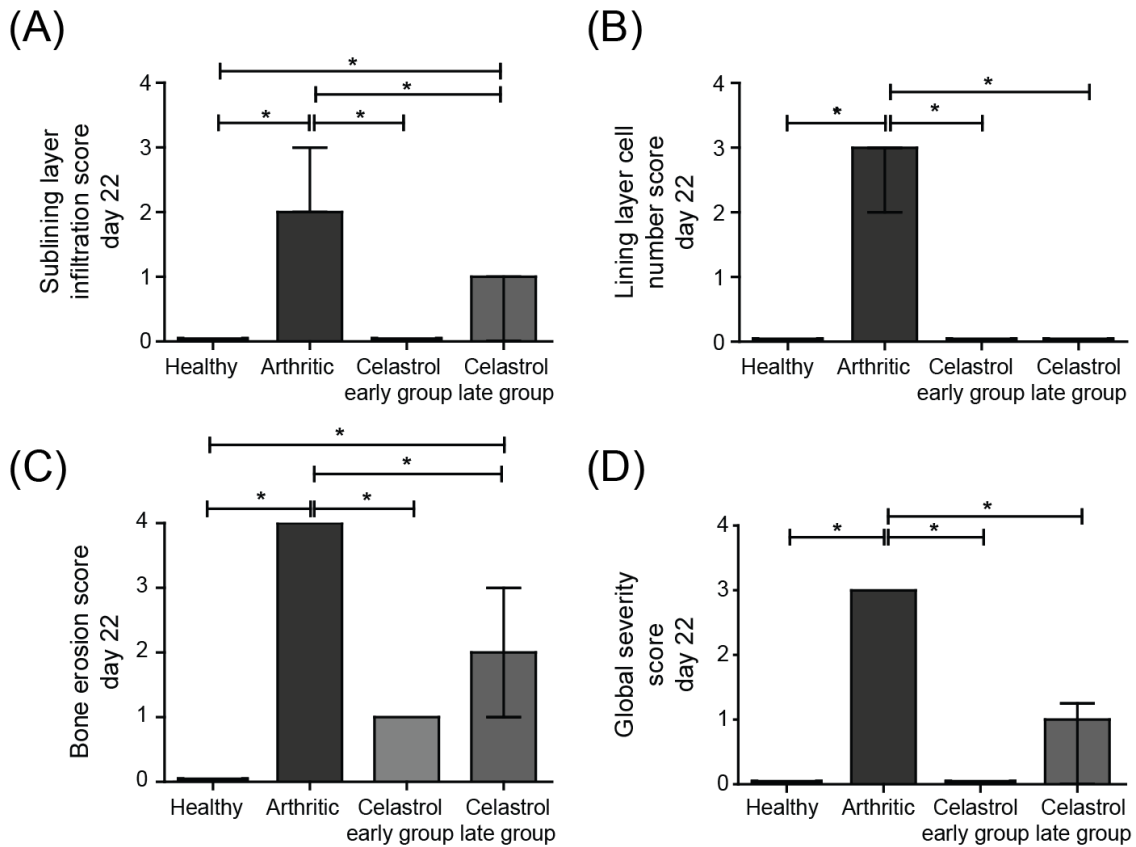


Fig. 4 – Celastrol suppresses arthritic inflammation and tissue damage locally in the joints of AIA rats. A semi-quantitative evaluation of histological sections was performed. Notice that celastrol has inhibited cellular infiltration (A), completely reversed the number of lining layer cells to the normal values (B) and prevented bone erosion occurrence (C), allowing for a normal joint structure comparable to healthy rats in both early and late treatment groups (D). Data are expressed as median with interquartile range. Differences were considered statistically significant for p -values < 0.05 , according to the Kruskal-Wallis (Dunn’s Multiple Comparison tests) and Mann–Whitney tests. Correlation analysis was performed using the Spearman test. Healthy $N=19$, Arthritic $N=23$, Celastrol early group $N=15$ and Celastrol late group $N=15$.

Overall, these data are supported by studies already published in the literature using several plant extracts and different experimental outlines [19, 20, 22, 54, 55]. Thus, there is strong evidence that celastrol is able to significantly diminish inflammation and bone damage, even when administrated in a later phase of arthritis development.

Celastrol inhibits synovial lymphocyte infiltration and cell proliferation in arthritic rat joints

The immunohistochemical analysis revealed that arthritic rats treated with celastrol have reduced levels of lymphocyte infiltration into the joints (Fig. 5 and Fig. 7). As can be observed in Fig. 5B there were significant reductions of CD3+ T-cells ($p < 0.0001$ in early and late treatment groups vs. arthritic rats) and CD19+ B-cells ($p < 0.0001$ in early and late treatment groups vs. arthritic rats). In contrast, the number of these cells markedly increased throughout disease progression in untreated animals ($p < 0.0001$ in healthy vs. arthritic rats, sacrificed at the end of the study period). A study by Venkatesha et al, have shown that celastrol reduces the level of chemokines, which might explain the inhibition of leukocyte migration [20].

In addition, we have also studied cell proliferation by staining joint tissue sections with the Ki67 marker. The immunohistochemical results shown in Fig. 5B revealed that animals treated with celastrol have reduced levels of synovial cell proliferation in both early and late treated rats ($p < 0.0001$ in both groups vs. arthritic animals), with a score similar to the healthy controls.

Results of immunohistochemical quantification also showed that celastrol significantly reduced CD3+ T-cells ($p = 0.0079$ in both early and late treatment groups vs. arthritic rats) and CD19+ B-cells ($p = 0.0317$ in both early and late treatment groups vs. arthritic rats) infiltrated into the joints as well as synovial cell proliferation ($p = 0.0079$ in both early and late treatment groups vs. arthritic rats), as depicted in Fig. 7.

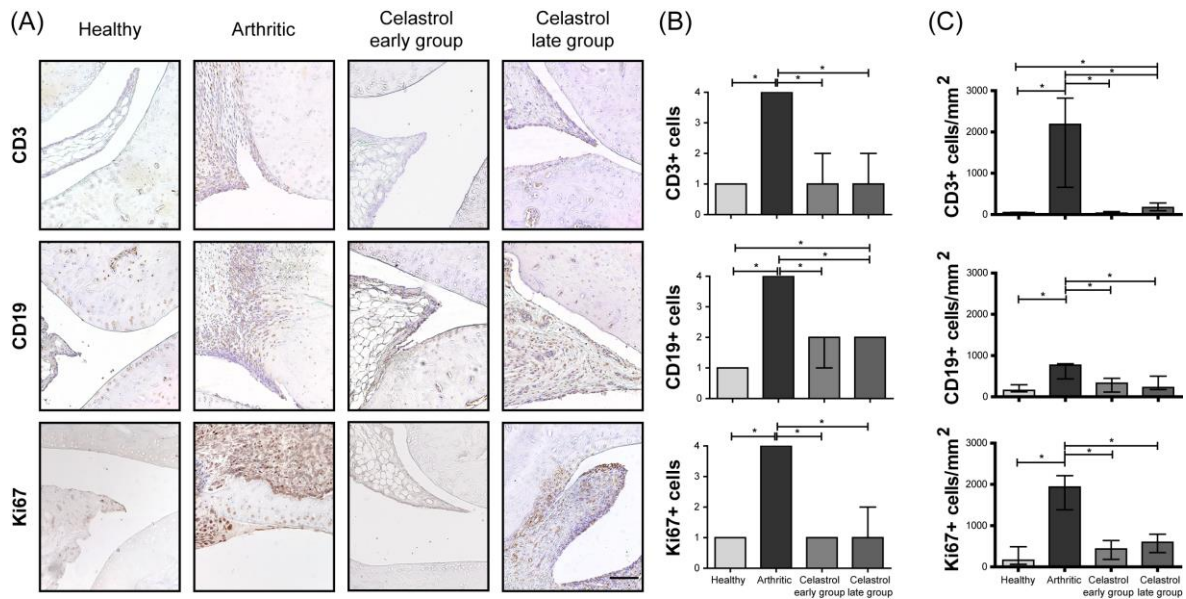


Fig. 5 – Celastrol reduces the number of T-cells and B-cells present in the synovial membrane, and suppresses synovial cell proliferation. (A) Representation of the immunohistochemical evaluation performed in paw sections at day 22 after celastrol treatment. (B) Immunohistochemical analysis was performed using a semi-quantitative score. Notice that both celastrol early and late-treated rats showed a significant reduction in the number of CD3 and CD19 positive cells as well as a reduction in the levels of synovial cell proliferation assessed by Ki67 marker in comparison with arthritic rats at day 22. Magnifications of 200 \times . Bar: 100 μ m. Data are expressed as median with interquartile range. Differences were considered statistically significant for p-values<0.05, according to the Kruskal-Wallis (Dunn’s Multiple Comparison tests) and Mann–Whitney tests. Healthy N=16, Arthritic N=10, Celastrol early group N=15 and Celastrol late group N=15.

Celastrol significantly reduces CD68+ macrophages in the arthritic synovial tissue

The activated macrophages in the synovium are derived from circulating monocytes and secrete various mediators that participate in arthritis induction and tissue injury. Studies of drug efficacy in RA patients have identified, from a large panel of synovial biomarkers, sublining CD68+ macrophages as an optimal marker to evaluate clinical response, with an association between clinical improvement and the reduction of CD68+ macrophage scores. Therefore, CD68+ sublining macrophages have been recognized as a synovial biomarker, with a high sensitivity in discriminating between effective and ineffective therapies or placebo,

useful in an early stage of drug development [34, 56]. We have thus performed the characterization of CD68+ macrophages present in the synovial tissue after treatment with celastrol (Fig. 6 and Fig. 7). Arthritic rats have shown an increase in the number of CD68+ synovial macrophages throughout the development of the disease ($p < 0.0001$ in healthy vs. arthritic rats, as shown in Fig. 6B). Importantly, celastrol significantly decreased the number of CD68+ macrophages infiltrated into the arthritic joint tissue ($p < 0.0001$ in early and late treatment groups vs. arthritic rats). In addition, celastrol administration significantly decreased the levels of CD163+ macrophages ($p < 0.0001$ in early and late treatment groups vs. arthritic rats). CD163 is a useful marker in this context because it is a more selective macrophage marker and helps to discriminate between synovial macrophages and synovial intimal fibroblasts, which also stain positively for CD68 in RA synovium [57]. Previous studies have in fact shown that synovial intimal fibroblasts migration and invasion into the synovium are also reduced by celastrol [55, 58].

Results of immunohistochemical quantification shown in Fig. 7 also revealed that celastrol significantly reduced CD68+ cells ($p = 0.0079$ in both early and late treatment groups vs. arthritic rats) and CD163+ macrophages ($p = 0.0079$ in both early and late treatment groups vs. arthritic rats) infiltrated into the joints.

Because inflammatory synovial tissue macrophages are derived from peripheral blood monocytes, these observations suggest decreased monocyte recruitment into the joints of arthritic rats treated with celastrol, even when treatment was initiated in a later phase of disease development.

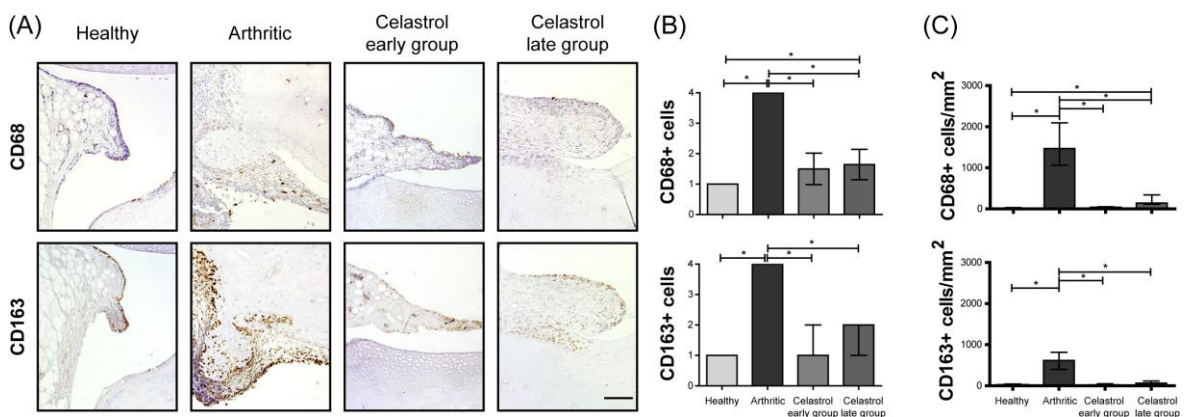


Fig. 6 – Celastrol reduces the number of synovial CD68+ macrophages. (A) Representation of the immunohistochemical evaluation performed in paw sections at day 22 after celastrol treatment. (B) Immunohistochemical analysis was performed using a semi-quantitative score. Notice that both celastrol early and late-treated rats showed a significant reduction in the number of CD68 and CD163 positive cells in comparison with arthritic rats at day 22. Magnifications of 200x. Bar: 100 μ m. Data are expressed as median with interquartile range. Differences were considered statistically significant for p-values<0.05, according to the Kruskal-Wallis (Dunn’s Multiple Comparison tests) and Mann–Whitney tests. Healthy N=16, Arthritic N=10, Celastrol early group N=15 and Celastrol late group N=15.

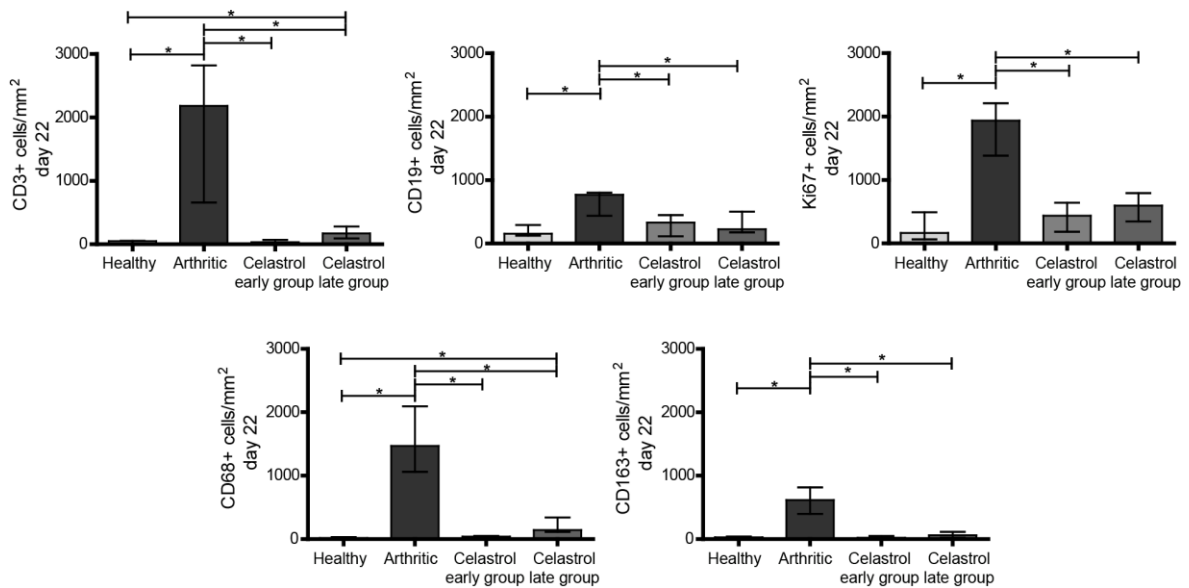


Fig. 7 – Celastrol reduces the number of synovial CD3+, CD19+, Ki67+, CD68+ and CD163+ cells. Immunohistochemical quantification was performed using an image analysis software written in MATLAB to identify and count the number of positive cells for each antibody in representative sections. Notice that both celastrol early and late-treated rats showed a significant reduction in the number of CD3, CD19, Ki67, CD68 and CD163 positive cells in comparison with arthritic rats at day 22. Data are expressed as median with interquartile range. Differences were considered statistically significant for p-values<0.05, according to the Mann–Whitney tests. Healthy N=5, Arthritic N=5, Celastrol early group N=5 and Celastrol late group N=5.

DISCUSSION

In this study, we have shown that celastrol substantially depletes CD68+ sublining synovial cells, considered to be the biomarker with the strongest association with response to treatment in RA. Moreover, celastrol was effective and safe in suppressing synovial inflammation and bone damage in rats with AIA.

We have consistently observed that celastrol treatment reduced serum IL-6 levels in arthritic rats. This observation is relevant because IL-6 is a proinflammatory cytokine that plays a relevant role in the pathogenesis of RA, namely in Th17 polarization and plasma B-cell differentiation, in the production of chemokines, adhesion molecules, and VEGF, and in the secretion of RANKL and MMPs, amplifying inflammatory cell infiltration and inducing osteoclastogenesis [59-61]. Interestingly, it was shown that celastrol can suppress arthritis in part by altering Th17/Treg ratio in inflamed joints [52]. Additionally, celastrol-treated rats showed a significant reduction in the severity of clinical arthritis as well as in pannus formation and leukocyte cell infiltration into the joint synovial tissue. This cell infiltration and proliferation inhibitory effect of celastrol may thus prove to be of interest to prevent and treat the development of the synovial tumor-like pannus tissue characteristic of established RA and responsible for bone damage. Interestingly, histological analysis also revealed that celastrol is effective in suppressing local inflammation-induced bone loss. Of note, celastrol treatment is effective when administered both in the early and established phase of arthritis, which is relevant for the potential clinical implications of our findings. Our report is the first to demonstrate the protective coupled effect of celastrol in vivo on both synovial inflammation and joint bone damage restoring synovial homeostasis, fulfilling this unmet medical need in RA treatment approach. Importantly, CD68+ sublining macrophages, a synovial biomarker with a high sensitivity in selecting effective RA therapies in an early stage of drug development, is significantly reduced in the synovia of celastrol-treated rats.

It has already been reported that celastrol targets NF- κ B, via long-lasting inhibition of IKK β activity [62]. In fact, the inactivation of NF- κ B in animal models has shown the ability to suppress arthritis [63]. NF- κ B participates in the transcription of genes

encoding many proinflammatory cytokines and chemokines, in the regulation of different immune cells and in the expression of adhesion molecules and matrix MMPs [64]. Based on microarray gene expression profile it has been demonstrated that celastrol represses cell proliferation, inflammation and immune responses (targets T and B-cells, antigen processing and presentation), blocks metabolic pathways, has anti-oxidant properties, and targets VEGF, proinflammatory cytokines and chemokines [65]. Indeed, it has been demonstrated that celastrol reduces the levels of chemokines, possibly affecting leukocyte migration [20]. Celastrol has thus a broad spectrum of targets, modulating immune responses rather than inducing immunosuppression [65]. Our results point out that pure celastrol used in the AIA rat model is not associated with increased risk of infections, have no hepatotoxicity or nephrotoxicity, suggesting that at least for short-term RA treatment, celastrol might be a safe drug.

Overall, our results validate celastrol as a promising compound for the treatment of inflammation and inflammation-induced bone damage and provide relevant insights into the usage of celastrol as a future drug for RA. It would be interesting to extend this knowledge by studying the anti-arthritic properties of celastrol in vivo using different animal models of arthritis, namely the collagen induced arthritis (CIA) model, and evaluate differences in efficacy depending on animal gender.

REFERENCES

1. Gorman CL, Cope AP. Immune-mediated pathways in chronic inflammatory arthritis. *Best practice & research Clinical rheumatology*. 2008;22(2):221-38.
2. Hahn B. A pathophysiologic approach to the clinical management of arthritis and pain: current and future implications. *Journal of clinical rheumatology : practical reports on rheumatic & musculoskeletal diseases*. 2004;10(3 Suppl):S3-4.
3. Plasqui G. The role of physical activity in rheumatoid arthritis. *Physiology & behavior*. 2008;94(2):270-5.
4. Steiner G, Tohidast-Akrad M, Witzmann G, Vesely M, Studnicka-Benke A, Gal A, et al. Cytokine production by synovial T cells in rheumatoid arthritis. *Rheumatology*. 1999;38(3):202-13.
5. Astry B, Harberts E, Moudgil KD. A cytokine-centric view of the pathogenesis and treatment of autoimmune arthritis. *Journal of interferon & cytokine research : the official journal of the International Society for Interferon and Cytokine Research*. 2011;31(12):927-40.
6. Boyce BF, Xing L. Functions of RANKL/RANK/OPG in bone modeling and remodeling. *Archives of biochemistry and biophysics*. 2008;473(2):139-46.
7. Karmakar S, Kay J, Gravallesse EM. Bone damage in rheumatoid arthritis: mechanistic insights and approaches to prevention. *Rheumatic diseases clinics of North America*. 2010;36(2):385-404.
8. Kotake S, Udagawa N, Takahashi N, Matsuzaki K, Itoh K, Ishiyama S, et al. IL-17 in synovial fluids from patients with rheumatoid arthritis is a potent stimulator of osteoclastogenesis. *The Journal of clinical investigation*. 1999;103(9):1345-52.
9. Schett G. Rheumatoid arthritis: inflammation and bone loss. *Wiener medizinische Wochenschrift*. 2006;156(1-2):34-41.

10. Xu S, Wang Y, Lu J, Xu J. Osteoprotegerin and RANKL in the pathogenesis of rheumatoid arthritis-induced osteoporosis. *Rheumatology international*. 2012;32(11):3397-403.
11. Gravallesse EM, Manning C, Tsay A, Naito A, Pan C, Amento E, et al. Synovial tissue in rheumatoid arthritis is a source of osteoclast differentiation factor. *Arthritis and rheumatism*. 2000;43(2):250-8.
12. Fonseca JE, Canhao H, Tavares NJ, Cruz M, Branco J, Queiroz MV. Persistent low grade synovitis without erosive progression in magnetic resonance imaging of rheumatoid arthritis patients treated with infliximab over 1 year. *Clinical rheumatology*. 2009;28(10):1213-6.
13. Joosten LA, Helsen MM, Saxne T, van De Loo FA, Heinegard D, van Den Berg WB. IL-1 alpha beta blockade prevents cartilage and bone destruction in murine type II collagen-induced arthritis, whereas TNF-alpha blockade only ameliorates joint inflammation. *Journal of immunology*. 1999;163(9):5049-55.
14. Smolen JS, Han C, Bala M, Maini RN, Kalden JR, van der Heijde D, et al. Evidence of radiographic benefit of treatment with infliximab plus methotrexate in rheumatoid arthritis patients who had no clinical improvement: a detailed subanalysis of data from the anti-tumor necrosis factor trial in rheumatoid arthritis with concomitant therapy study. *Arthritis and rheumatism*. 2005;52(4):1020-30.
15. Singh JA, Furst DE, Bharat A, Curtis JR, Kavanaugh AF, Kremer JM, et al. 2012 update of the 2008 American College of Rheumatology recommendations for the use of disease-modifying antirheumatic drugs and biologic agents in the treatment of rheumatoid arthritis. *Arthritis care & research*. 2012;64(5):625-39.
16. Vivar N, Van Vollenhoven RF. Advances in the treatment of rheumatoid arthritis. *F1000prime reports*. 2014;6:31.
17. Cascao R, Vidal B, Raquel H, Neves-Costa A, Figueiredo N, Gupta V, et al. Effective treatment of rat adjuvant-induced arthritis by celestrol. *Autoimmunity reviews*. 2012;11(12):856-62.

18. Cascao R, Moura RA, Perpetuo I, Canhao H, Vieira-Sousa E, Mourao AF, et al. Identification of a cytokine network sustaining neutrophil and Th17 activation in untreated early rheumatoid arthritis. *Arthritis research & therapy*. 2010;12(5):R196.
19. Li H, Zhang YY, Tan HW, Jia YF, Li D. Therapeutic effect of tripterine on adjuvant arthritis in rats. *Journal of ethnopharmacology*. 2008;118(3):479-84.
20. Venkatesha SH, Astry B, Nanjundaiah SM, Yu H, Moudgil KD. Suppression of autoimmune arthritis by Celastrus-derived Celastrol through modulation of pro-inflammatory chemokines. *Bioorganic & medicinal chemistry*. 2012;20(17):5229-34.
21. Kusy S, Ghosn EE, Herzenberg LA, Contag CH. Development of B cells and erythrocytes is specifically impaired by the drug celastrol in mice. *PloS one*. 2012;7(4):e35733.
22. Nanjundaiah SM, Venkatesha SH, Yu H, Tong L, Stains JP, Moudgil KD. Celastrus and its bioactive celastrol protect against bone damage in autoimmune arthritis by modulating osteoimmune cross-talk. *The Journal of biological chemistry*. 2012;287(26):22216-26.
23. Gerlag DM, Haringman JJ, Smeets TJ, Zwinderman AH, Kraan MC, Laud PJ, et al. Effects of oral prednisolone on biomarkers in synovial tissue and clinical improvement in rheumatoid arthritis. *Arthritis and rheumatism*. 2004;50(12):3783-91.
24. Yanni G, Nabil M, Farahat MR, Poston RN, Panayi GS. Intramuscular gold decreases cytokine expression and macrophage numbers in the rheumatoid synovial membrane. *Annals of the rheumatic diseases*. 1994;53(5):315-22.
25. Smith MD, Kraan MC, Slavotinek J, Au V, Weedon H, Parker A, et al. Treatment-induced remission in rheumatoid arthritis patients is characterized by a reduction in macrophage content of synovial biopsies. *Rheumatology*. 2001;40(4):367-74.

26. Dolhain RJ, Tak PP, Dijkmans BA, De Kuiper P, Breedveld FC, Miltenburg AM. Methotrexate reduces inflammatory cell numbers, expression of monokines and of adhesion molecules in synovial tissue of patients with rheumatoid arthritis. *British journal of rheumatology*. 1998;37(5):502-8.
27. Kraan MC, Reece RJ, Barg EC, Smeets TJ, Farnell J, Rosenberg R, et al. Modulation of inflammation and metalloproteinase expression in synovial tissue by leflunomide and methotrexate in patients with active rheumatoid arthritis. Findings in a prospective, randomized, double-blind, parallel-design clinical trial in thirty-nine patients at two centers. *Arthritis and rheumatism*. 2000;43(8):1820-30.
28. Smeets TJ, Kraan MC, van Loon ME, Tak PP. Tumor necrosis factor alpha blockade reduces the synovial cell infiltrate early after initiation of treatment, but apparently not by induction of apoptosis in synovial tissue. *Arthritis and rheumatism*. 2003;48(8):2155-62.
29. Taylor PC, Peters AM, Paleolog E, Chapman PT, Elliott MJ, McCloskey R, et al. Reduction of chemokine levels and leukocyte traffic to joints by tumor necrosis factor alpha blockade in patients with rheumatoid arthritis. *Arthritis and rheumatism*. 2000;43(1):38-47.
30. Thurlings RM, Vos K, Wijbrandts CA, Zwinderman AH, Gerlag DM, Tak PP. Synovial tissue response to rituximab: mechanism of action and identification of biomarkers of response. *Annals of the rheumatic diseases*. 2008;67(7):917-25.
31. Cunnane G, Madigan A, Murphy E, FitzGerald O, Bresnihan B. The effects of treatment with interleukin-1 receptor antagonist on the inflamed synovial membrane in rheumatoid arthritis. *Rheumatology*. 2001;40(1):62-9.
32. Bresnihan B, Pontifex E, Thurlings RM, Vinkenoog M, El-Gabalawy H, Fearon U, et al. Synovial tissue sublining CD68 expression is a biomarker of therapeutic response in rheumatoid arthritis clinical trials: consistency across centers. *The Journal of rheumatology*. 2009;36(8):1800-2.

33. Haringman JJ, Gerlag DM, Smeets TJ, Baeten D, van den Bosch F, Bresnihan B, et al. A randomized controlled trial with an anti-CCL2 (anti-monocyte chemotactic protein 1) monoclonal antibody in patients with rheumatoid arthritis. *Arthritis and rheumatism*. 2006;54(8):2387-92.
34. Wijbrandts CA, Vergunst CE, Haringman JJ, Gerlag DM, Smeets TJ, Tak PP. Absence of changes in the number of synovial sublining macrophages after ineffective treatment for rheumatoid arthritis: Implications for use of synovial sublining macrophages as a biomarker. *Arthritis and rheumatism*. 2007;56(11):3869-71.
35. Haringman JJ, Gerlag DM, Zwinderman AH, Smeets TJ, Kraan MC, Baeten D, et al. Synovial tissue macrophages: a sensitive biomarker for response to treatment in patients with rheumatoid arthritis. *Annals of the rheumatic diseases*. 2005;64(6):834-8.
36. LaBranche TP, Jesson MI, Radi ZA, Storer CE, Guzova JA, Bonar SL, et al. JAK inhibition with tofacitinib suppresses arthritic joint structural damage through decreased RANKL production. *Arthritis and rheumatism*. 2012;64(11):3531-42.
37. Kim HY, Lee SW, Park SY, Baek SH, Lee CW, Hong KW, et al. Efficacy of concurrent administration of cilostazol and methotrexate in rheumatoid arthritis: pharmacologic and clinical significance. *Life sciences*. 2012;91(7-8):250-7.
38. Ma Y, Wang X, Wu X, Wei X, Ma L, Zheng H, et al. (Z)-5-(4-methoxybenzylidene) thiazolidine-2, 4-dione ameliorates the adjuvant-induced arthritis via inhibiting the migration of macrophage and down-regulating the cytokine mRNA expression. *International immunopharmacology*. 2010;10(11):1456-62.
39. Chen SY, Wu CL, Lai MD, Lin CC, Yo YT, Jou IM, et al. Amelioration of rat collagen-induced arthritis through CD4+ T cells apoptosis and synovial interleukin-17 reduction by indoleamine 2,3-dioxygenase gene therapy. *Human gene therapy*. 2011;22(2):145-54.

40. Le Goff B, Soltner E, Charrier C, Maugars Y, Redini F, Heymann D, et al. A combination of methotrexate and zoledronic acid prevents bone erosions and systemic bone mass loss in collagen induced arthritis. *Arthritis research & therapy*. 2009;11(6):R185.
41. Zhang J, Li CY, Xu MJ, Wu T, Chu JH, Liu SJ, et al. Oral bioavailability and gender-related pharmacokinetics of celastrol following administration of pure celastrol and its related tablets in rats. *Journal of ethnopharmacology*. 2012;144(1):195-200.
42. Stolina M, Bolon B, Middleton S, Dwyer D, Brown H, Duryea D, et al. The evolving systemic and local biomarker milieu at different stages of disease progression in rat adjuvant-induced arthritis. *J Clin Immunol*. 2009;29(2):158-74.
43. da Silva JA, Fonseca JE, Graca L, Moita L, Carmo-Fonseca M. Reinnervation of post-arthritic joints in the rat. *Clinical and experimental rheumatology*. 1996;14(1):43-51.
44. Tsubaki T, Arita N, Kawakami T, Shiratsuchi T, Yamamoto H, Takubo N, et al. Characterization of histopathology and gene-expression profiles of synovitis in early rheumatoid arthritis using targeted biopsy specimens. *Arthritis research & therapy*. 2005;7(4):R825-36.
45. Sims NA, Green JR, Glatt M, Schlicht S, Martin TJ, Gillespie MT, et al. Targeting osteoclasts with zoledronic acid prevents bone destruction in collagen-induced arthritis. *Arthritis and rheumatism*. 2004;50(7):2338-46.
46. Brauer R, Kittlick PD, Thoss K, Henzgen S. Different immunological mechanisms contribute to cartilage destruction in antigen-induced arthritis. *Experimental and toxicologic pathology : official journal of the Gesellschaft fur Toxikologische Pathologie*. 1994;46(4-5):383-8.
47. Bendele AM, Chlipala ES, Scherrer J, Frazier J, Sennello G, Rich WJ, et al. Combination benefit of treatment with the cytokine inhibitors interleukin-1 receptor

antagonist and PEGylated soluble tumor necrosis factor receptor type I in animal models of rheumatoid arthritis. *Arthritis and rheumatism*. 2000;43(12):2648-59.

48. Vidal B, Cascao R, Vale AC, Cavaleiro I, Vaz MF, Brito JA, et al. Arthritis induces early bone high turnover, structural degradation and mechanical weakness. *PloS one*. 2015;10(1):e0117100.

49. Zhu X, Zhang J, Huo R, Lin J, Zhou Z, Sun Y, et al. Evaluation of the efficacy and safety of different Tripterygium preparations on collagen-induced arthritis in rats. *Journal of ethnopharmacology*. 2014;158 Pt A:283-90.

50. Nawroth PP, Bank I, Handley D, Cassimeris J, Chess L, Stern D. Tumor necrosis factor/cachectin interacts with endothelial cell receptors to induce release of interleukin 1. *The Journal of experimental medicine*. 1986;163(6):1363-75.

51. Venkatesha SH, Yu H, Rajaiah R, Tong L, Moudgil KD. Celastrus-derived celastrol suppresses autoimmune arthritis by modulating antigen-induced cellular and humoral effector responses. *The Journal of biological chemistry*. 2011;286(17):15138-46.

52. Astry B, Venkatesha SH, Laurence A, Christensen-Quick A, Garzino-Demo A, Frieman MB, et al. Celastrol, a Chinese herbal compound, controls autoimmune inflammation by altering the balance of pathogenic and regulatory T cells in the target organ. *Clinical immunology*. 2015;157(2):228-38.

53. Idris AI, Krishnan M, Simic P, Landao-Bassonga E, Mollat P, Vukicevic S, et al. Small molecule inhibitors of I κ B kinase signaling inhibit osteoclast formation in vitro and prevent ovariectomy-induced bone loss in vivo. *FASEB journal : official publication of the Federation of American Societies for Experimental Biology*. 2010;24(11):4545-55.

54. Gan K, Xu L, Feng X, Zhang Q, Wang F, Zhang M, et al. Celastrol attenuates bone erosion in collagen-Induced arthritis mice and inhibits osteoclast differentiation and function in RANKL-induced RAW264.7. *International immunopharmacology*. 2015;24(2):239-46.

55. Li G, Liu D, Zhang Y, Qian Y, Zhang H, Guo S, et al. Celastrol inhibits lipopolysaccharide-stimulated rheumatoid fibroblast-like synoviocyte invasion through suppression of TLR4/NF-kappaB-mediated matrix metalloproteinase-9 expression. *PLoS one*. 2013;8(7):e68905.
56. Vieira-Sousa E, Gerlag DM, Tak PP. Synovial tissue response to treatment in rheumatoid arthritis. *The open rheumatology journal*. 2011;5:115-22.
57. Fonseca JE, Edwards JC, Blades S, Goulding NJ. Macrophage subpopulations in rheumatoid synovium: reduced CD163 expression in CD4+ T lymphocyte-rich microenvironments. *Arthritis and rheumatism*. 2002;46(5):1210-6.
58. Li GQ, Zhang Y, Liu D, Qian YY, Zhang H, Guo SY, et al. Celastrol inhibits interleukin-17A-stimulated rheumatoid fibroblast-like synoviocyte migration and invasion through suppression of NF-kappaB-mediated matrix metalloproteinase-9 expression. *International immunopharmacology*. 2012;14(4):422-31.
59. Suzuki M, Hashizume M, Yoshida H, Shiina M, Mihara M. IL-6 and IL-1 synergistically enhanced the production of MMPs from synovial cells by up-regulating IL-6 production and IL-1 receptor I expression. *Cytokine*. 2010;51(2):178-83.
60. Mihara M, Moriya Y, Kishimoto T, Ohsugi Y. Interleukin-6 (IL-6) induces the proliferation of synovial fibroblastic cells in the presence of soluble IL-6 receptor. *British journal of rheumatology*. 1995;34(4):321-5.
61. Romano M, Sironi M, Toniatti C, Polentarutti N, Fruscella P, Ghezzi P, et al. Role of IL-6 and its soluble receptor in induction of chemokines and leukocyte recruitment. *Immunity*. 1997;6(3):315-25.
62. Lee JH, Koo TH, Yoon H, Jung HS, Jin HZ, Lee K, et al. Inhibition of NF-kappa B activation through targeting I kappa B kinase by celastrol, a quinone methide triterpenoid. *Biochemical pharmacology*. 2006;72(10):1311-21.
63. Tas SW, Vervoordeldonk MJ, Hajji N, May MJ, Ghosh S, Tak PP. Local treatment with the selective I kappa B kinase beta inhibitor NEMO-binding domain

peptide ameliorates synovial inflammation. *Arthritis research & therapy*. 2006;8(4):R86.

64. Vincenti MP, Coon CI, Brinckerhoff CE. Nuclear factor kappaB/p50 activates an element in the distal matrix metalloproteinase 1 promoter in interleukin-1beta-stimulated synovial fibroblasts. *Arthritis and rheumatism*. 1998;41(11):1987-94.

65. Yu H, Venkatesha SH, Moudgil KD. Microarray-based gene expression profiling reveals the mediators and pathways involved in the anti-arthritic activity of Celastrus-derived Celastrol. *International immunopharmacology*. 2012;13(4):499-506.

Supporting Information

S1 Fig. Ankle perimeter kinetics. Celastrol was administered to AIA rats both in the early (4 days after disease induction) and late (11 days after disease induction) phases of arthritis development. Notice that after 7 days of treatment celastrol early-treated rats presented an ankle perimeter similar to the healthy control, whereas arthritic rats started to increase left ankle edema/swelling sharply. In the celastrol late-treated group, ankle swelling started to increase in parallel to the augment of the inflammatory score, but after treatment was initiated ankle perimeter started to significantly decrease. Data are expressed as median with interquartile range. Differences were considered statistically significant for p-values<0.05, according to the Kruskal-Wallis (Dunn's Multiple Comparison tests) and Mann-Whitney tests. Healthy N=19, Arthritic N=23, Celastrol early group N=15 and Celastrol late group N=15.

S2 Fig. Administration of pure celastrol induces no hepatic or renal toxicity. At day 22 after disease induction no hepatocellular or renal lesion was observed in any of

the animals. Liver and kidney samples from all animals were analyzed by a pathologist blinded to experimental groups but only representative histological sections are shown. H&E staining; Magnifications of 100×. Bar: 300 μm.

S3 Fig. Celestrol treatment has no effect on body weight. Notice that no weight loss was observed due to celestrol administration. In contrast, there was an association between disease activity and weight loss, which was highlighted in late-treated rats that started to lose weight due to disease activity (day 4 up to day 11) and after treatment was initiated no more weight loss was observed (day 11 up to day 22). Data are expressed as median with interquartile range. Differences were considered statistically significant for p-values<0.05, according to the Mann–Whitney tests.

S4 Fig. Celestrol has no effect in the serum levels of IL-1β, IL-17 and TNF in arthritic rats. Data are expressed as median with interquartile range. Differences were considered statistically significant for p-values<0.05, according to the Kruskal-Wallis (Dunn’s Multiple Comparison tests) and Mann–Whitney tests. Healthy N=19, Arthritic N=23, Celestrol early group N=15 and Celestrol late group N=15.

IV. Celastrol preserves bone structure and mechanics in arthritic rats

Rita Cascão*; Bruno Vidal*; Mikko A. J. Finnilä; Inês P. Lopes; Simo Saarakkala; Luis F. Moita; João E. Fonseca

Author Contributions

Vidal and Cascão designed the experiments. Vidal and Cascão performed all the experiments and wrote the chapter. Finnila performed 3-point bending tests. Lopes helped to perform some techniques. Finnila, Saarakkala, Moita and Fonseca supervised the work and revised the text.

Celastrol preserves bone structure and mechanics in arthritic rats

Rita Cascão*; Bruno Vidal*; Mikko A. J. Finnilä; Inês P. Lopes; Simo Saarakkala; Luis F. Moita; João E. Fonseca

* Contributed equally

ABSTRACT

Objectives – Rheumatoid arthritis (RA) is characterized by chronic inflammation leading to articular bone and cartilage damage. Despite recent progress in RA management, adverse effects, lack of efficacy and economic barriers to treatment access still limit therapeutic success, which means that RA is currently an unremitting and debilitating disease. Therefore, safer and less expensive treatments that control inflammation and bone resorption are needed. We have previously shown that celastrol is a candidate for RA treatment based on its anti-inflammatory properties and ability to decrease synovial CD68 macrophages. Herein our goal was to evaluate the effect of celastrol in local and systemic bone loss. **Methods** – Celastrol was administrated intraperitoneally at a dose of 1µg/g/day to female Wistar adjuvant-induced arthritis (AIA) rats. Rats were sacrificed after 22 days of disease progression and blood, femurs, tibias and paw samples were collected for the quantification of bone remodeling markers, 3-point bending test, micro-computed tomography analysis, and immunohistochemical evaluation. **Results** – We have observed that celastrol preserved articular structures and decreased the number of osteoclasts and osteoblasts present in arthritic joints. Moreover, celastrol reduced TRACP-5b, P1NP and CTX-II levels. Importantly, celastrol prevented bone loss and bone microarchitecture degradation, with an increase in trabecular bone volume fraction and endosteal bone quantity. Animals treated with celastrol also have less fragile bones, as depicted by an increase in maximum load and yield displacement. **Conclusions** –

These results suggest that celastrol reduces both bone resorption and cartilage degradation, and preserves bone structure and mechanics.

INTRODUCTION

Rheumatoid arthritis (RA) is a chronic immune-mediated inflammatory disease with an estimated worldwide prevalence of 1%. This disease has a great impact on both individuals and society. RA patients are ten times more likely to be disabled, have three times more direct healthcare costs and are also two times more likely to require hospitalization than healthy individuals [1, 2]. RA is characterized by chronic edema and inflammation of the synovial tissue that lines joints. As disease progresses, cartilage and bone are damaged leading to articular destruction [3]. This periarticular and systemic bone loss leads to an increased risk of fracture in RA patients [4, 5]. Bone loss in RA results from an imbalance between the osteoblastic synthesis and osteoclastic degradation of bone, with bone resorption dominating over bone formation leading to systemic osteopenia [6].

Over the past 2 decades, more effective therapies for RA have been developed, but they still have issues related with safety and production costs. In addition, only around 30% of the patients reach remission, leaving most of the individuals affected by a chronic unremitting destructive disease, with the need for nonsteroidal anti-inflammatory drugs and corticosteroids for symptoms control [7]. Moreover, current treatment approaches primarily target inflammation with varying success in limiting the progression of bone damage[8]. Therefore, new therapies targeting both inflammatory processes and bone resorption, with a good safety profile and low production costs are still an unmet medical need in the field of RA.

We have previously reported increased levels of IL-1 β in very recent onset arthritis and in the synovial fluid of established RA patients [9]. This may be explained by the activation of caspase-1, responsible for the processing of pro-IL-1 β , which we have also observed to be increased since early RA [10]. Through an *in vitro* drug screening using the THP-1 macrophagic cell line, we have identified compounds that decrease the production of IL-1 β together with a reduction in another central pro-inflammatory cytokine of RA physiopathology, TNF. Among them, celastrol was a promising therapeutic candidate for arthritis, due to its ability to

downregulate the production of IL-1 β and TNF, by inhibiting both the activation of caspase-1 and NF-kB [11]. Celastrol is a pentacyclic-triterpene extracted from a plant used in traditional Chinese medicine, the *Trypterigium wilfordii* Hook. *In vivo*, we have recently described that celastrol has significant anti-inflammatory and anti-proliferative properties, with a decrease in the overall synovial inflammatory cellularity and, most importantly, in the number of sublining CD68 positive macrophages, a biomarker of drug efficacy in RA [11, 12]. In this study we have now hypothesized that celastrol is able to control, not only inflammation, but also focal and systemic bone resorption that occurs in arthritis.

Our aim in the herein study was to evaluate the ability of celastrol to counteract bone loss in the adjuvant-induced arthritis (AIA) rat model. The AIA rat model is the most widely used animal model for the evaluation of experimental compounds for RA treatment [13, 14]. We have recently documented that this is also an adequate model to study the impact of new compounds on bone [15]. In this work, celastrol administration was introduced therapeutically both at the early (preclinical stage) and late (clinical stage peak) phases of arthritis development to more closely model the clinical practice, with a complete analysis of bone quality.

MATERIALS AND METHODS

Animals

Eight-week-old female Wistar AIA rats weighing 230-250gr were purchased from Charles River Laboratories International (Massachusetts, USA). AIA rats were maintained in specific pathogen free (SPF) facilities, randomly housed per groups under standard laboratory conditions (at 20-22°C under 10-hour light/14-hour dark), and given free access to food (RM3, SDS diets, UK) and water (ultrapure). In addition, to minimize animal discomfort it was used paper shavings as bedding material in Double Decker GR1800 cages (Techniplast, UK) with 5 animals each. In accordance with Directive 2010/63/EU, all animal procedures were approved by the institutional animal welfare body (ORBEA-iMM) and licensed by the Portuguese competent authority (DGAV – Direcção Geral de Alimentação e Veterinária). Human end-points were established and animals were sacrificed

when presenting the maximum inflammatory score (0-3) [16] in more than 2 paws or when presenting more than 20% of body weight loss.

Celastrol treatment

The dose of celastrol (1 µg/g/day) used in this study was based on that used in our previous study [11] and in other studies [17]. Also, we have already reported that this dose is effective in suppressing synovial inflammation in the AIA rat model, with no evidence of drug-induced toxicity [12]. Celastrol (Sigma, Missouri, USA) stock solution of 100mg/ml in DMSO was dissolved in normal saline solution and injected intraperitoneally in the early treatment group of AIA rats since the 4th day of disease induction (N=15) and in the late treatment group since the 11th day of disease induction (N=15), and was maintained until day 22. Studies using the AIA model are generally completed at this time point due to a plateau effect of inflammatory manifestations. A group of healthy non-arthritis and arthritis untreated female age-matched Wistar rats sacrificed at day 4 (baseline for the celastrol early-treated group, at preclinical stage, N=5-13), day 11 (baseline for the celastrol late-treated group, at acute clinical stage, N=5-17) and day 22 after disease induction (chronic clinical stage) were used as controls in all experiments. The sample size in each group was calculated using free sample size calculating G*Power version 3.1.9.2 software (Type of power analysis: a priori; α err prob: 0.05; power (1- β err prob): 0.95; Effect size d: 1.526112; Actual power: 0.9576654). At the preclinical AIA progression stage evidence of inflammation or bone erosions is still lacking in the contralateral hind paw and fore paws. Hind paw swelling, inflammation and joint erosions steadily progress during acute clinical stage and reach a plateau in the chronic stage [18]. Rats were sacrificed by CO₂ narcosis and blood, femurs, tibias and paw samples were collected.

Immunohistochemical staining of cathepsin k and osteocalcin positive cells in hind paws

Left hind paw samples collected at the time of sacrifice were fixed immediately in 10% neutral buffered formalin solution and then decalcified in 10% formic acid. Samples were next dehydrated and embedded in paraffin, serially sectioned at a thickness of 5µm using a microtome, and mounted on microscope slides. Immunolocalization of osteoclasts and osteoblasts was performed by staining with cathepsin k (osteoclast marker; mature osteoclast enzyme. Biorbyt, Cambridge, UK) and osteocalcin (osteoblast marker; indicator of osteoblastic activity. Abcam, Cambridge, UK) primary antibodies followed by EnVision+ (Dako, Glostrup, Denmark). Color was developed in solution containing diaminobenzadine-tetrahydrochloride (DAB, Sigma, Missouri, USA), 0.5% H₂O₂ in phosphate-buffered saline buffer (pH 7.6). Slides were counterstained with hematoxylin and mounted. Immunohistochemical evaluation of rat joints was performed in a blinded fashion using a semi-quantitative score of 0-3 (0 — 0-25% staining; 1 — 25-50% staining; 2 — 50-75% staining; 3 — more than 75% staining)[19]. Slides were analyzed using a Leica DM2500 microscope (Leica Microsystems, Wetzlar, Germany).

Serum biochemical measurement of bone and cartilage turnover markers

Bone and cartilage turnover were analyzed by quantifying the levels of TRACP-5b (Tartrate-resistant acid phosphatase 5b), P1NP (procollagen type I amino-terminal propeptide) and CTX-II (C-terminal crosslinked telopeptide of type II collagen) in rat serum using ELISA (Immunodiagnostic System, Boldon, UK). All of the commercial assays were performed according to the manufacturers' instructions and standard curves were generated using supplied reference concentrations. Samples were measured using a plate reader Infinite M200 (Tecan, Mannedorf, Switzerland).

Micro-computed tomography (micro-CT) analysis

Structural properties of the trabecular and cortical tibiae were determined with a high-resolution micro-CT system (SkyScan 1272, Bruker micro-CT, Kontich, Belgium). Moist bones were wrapped in parafilm and covered with dental wax to prevent drying and movement during the scanning. X-ray tube voltage was set to 50kV and the beam was filtered with 0.5mm Aluminum filter. Sample position and camera settings were tuned to provide 3.0 μ m isotropic pixel size and projection images were collected every 0.2°. Density calibration was performed against hydroxyapatite phantoms with densities of 250mg/cm³ and 750mg/cm³. Image reconstruction was done with NRecon software (v1.6.9.8; Bruker micro-CT, Kontich, Belgium) and appropriate corrections were applied to reduce beam hardening and ring artefacts. Trabecular bone was manually segmented from cortical bone, and trabecular bone parameters were analyzed over 1400 slices starting 200 slices distal from growth plate. Cortical bone parameters were analyzed over 300 slices starting 1800 slices distal from growth plate.

Analyzes were performed in agreement with guidelines for assessment of bone microstructure in rodents using micro-CT [20]. Trabecular bone morphology was analyzed by applying global threshold and despeckling to provide binary image for 3D analysis. Cortical bone ROI was refined with ROI-shrink wrap operation, which also provided cortical bone shape for 2D morphological analysis. This was followed by segmentation of blood vessels using adaptive thresholding. Blood vessels (porosity) were analyzed using 3D morphological analyzes.

3-point bending biomechanical test

In order to investigate bone strength after celastrol treatment, femurs were subjected to a 3-point bending test in a universal testing machine (Instron 3366, Instron Corp., Massachusetts, USA) with a load-cell of 500N. Femurs were placed horizontally anterior side upwards on a support with span length of 5mm. The load was applied with a constant speed of 0.005mm/s until a failure occurred. Stiffness was analyzed by fitting first-degree polynomial function to the linear part of recorded load deformation data. The breaking point was defined when force

reached a maximum value and corresponding deformation and absorbed energy were analyzed.

Statistical analysis

Statistical differences were determined with non-parametric Mann–Whitney tests using GraphPad Prism (GraphPad, California, USA). Differences were considered statistically significant for $p < 0.05$. Data are presented as median with interquartile range.

The primary outcome of this study was to prevent the structural and mechanical damage of bone induced by inflammation, and the secondary outcome was to treat the structural and mechanical deterioration of bone in a chronic phase of arthritis development in the AIA rat model.

RESULTS

Celastrol decreases the number of osteoclasts and osteoblasts present in arthritic joints

Previously, we have observed that celastrol administration significantly reduced disease severity and suppressed joint bone erosions in arthritic rats, with no observed adverse effects [12]. At baseline celastrol early-treated group had a mean inflammatory score of 1.5 ± 0.7 and celastrol late-treated group had a mean inflammatory score of 3.9 ± 2.0 , with no differences in body weight comparing to untreated arthritic animals. Arthritic rats showed enhanced numbers of osteoclasts (cathepsin k+ cells) in the hind paw ($p < 0.0001$ vs healthy controls, Fig 1). Importantly, celastrol administration significantly lowered the number of osteoclasts to levels similar to healthy controls ($p < 0.0001$ in both treatment groups vs arthritic rats). Arthritic rats also showed increased numbers of osteoblasts (osteocalcin+ cells) in the hind paw ($p < 0.0001$ vs healthy controls, Fig 1). Notably, celastrol administration significantly reduced the number of osteoblasts ($p < 0.0001$ and $p = 0.0003$ in early and late-treated animals vs arthritic rats, respectively).

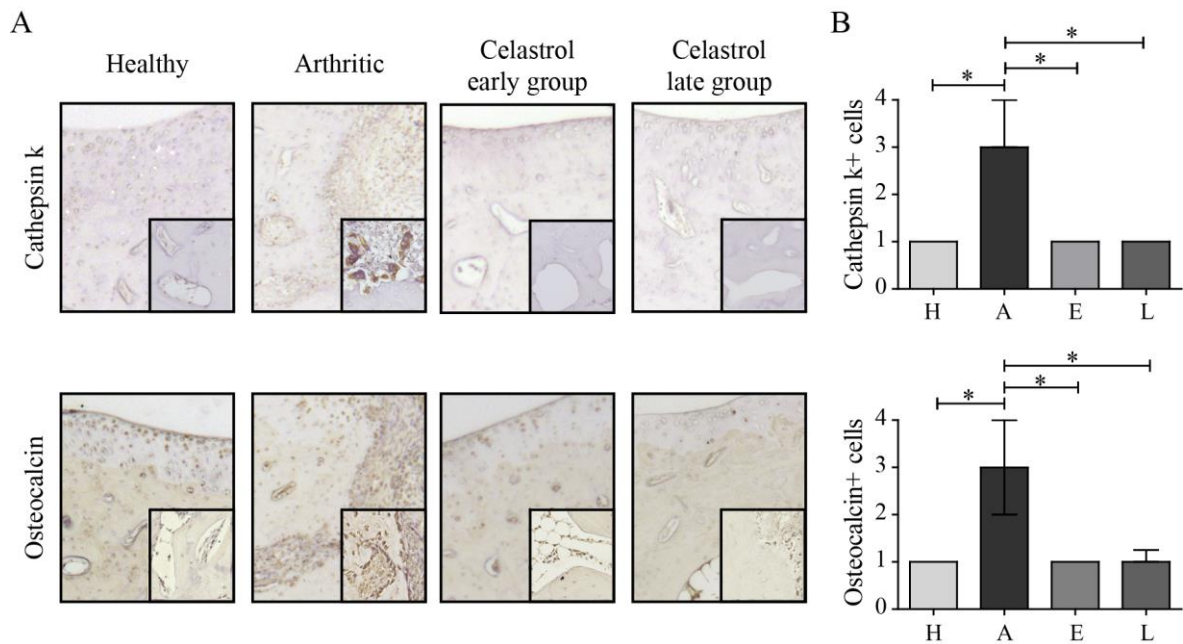


Fig. 1 – Celastrol reduces the number of bone-related cells in arthritic joints. Representation of the immunohistochemical evaluation performed in paw sections at day 22 after celastrol treatment. Magnifications of 200x. Bar: 100 μ m (A). Cathepsin k positive cells and osteocalcin positive cells were identified in arthritic joints by immunohistochemistry of paw sections (B). Immunohistochemical analysis was performed using a semi-quantitative score. Notice that celastrol treatment significantly reduced both types of cells. Paw samples were collected at the time of sacrifice. Data are expressed as median score with interquartile range. Differences were considered statistically significant for p-values<0.05, according to the Mann–Whitney tests. H – Healthy, A – Arthritic, E – Celastrol early-treated, L – Celastrol late-treated. Healthy N=16, Arthritic N=10, Celastrol early-treated N=15 and Celastrol late-treated N=15.

Celastrol reduces arthritis-induced bone resorption and cartilage degradation

To further elucidate the protective effect of celastrol on inflammation-mediated articular joint damage, bone and cartilage turnover markers were quantified in serum samples. The levels of serum TRACP-5b, P1NP and CTX-II of healthy, arthritic and celastrol-treated rats are shown in Fig 2. In the arthritic group, there was a marked increase of TRACP-5b after 4 days of disease induction (p=0.0267 vs healthy controls and p=0.0089 vs arthritic rats after 22 days of disease induction) with a gradual decrease throughout disease progression (Fig 2A), as also previously described by Stolina et al [21, 22]. In addition, there was a

significant increase in serum P1NP ($p=0.0034$, Fig 2B) and CTX-II ($p=0.0082$, Fig 2C), as a consequence of the high bone turnover and cartilage degradation. Importantly, both in celastrol early and late-treated rats there was a significant reduction in TRACP-5b levels comparing with arthritic rats ($p=0.0004$ and $p=0.0001$, respectively) and with treatment baselines ($p=0.0014$ vs arthritic rats at day 4 and $p<0.0001$ vs arthritic rats at day 11, respectively), suggesting a decrease in bone resorption. In addition, both treatment groups showed a significant drop in P1NP levels ($p=0.0069$ in early-treated and $p=0.0135$ in late-treated rats vs arthritic animals). Finally, the decrease in CTX-II ($p=0.0149$ in celastrol early-treated vs arthritic rats) revealed that treatment is also effective in protecting cartilage integrity. Of note, although a strong tendency towards a decrease in CTX-II was observed in celastrol late-treated rats, it did not reach statistical significance. These results suggest that there is a reduction both in bone and cartilage degradation in celastrol treated rats.

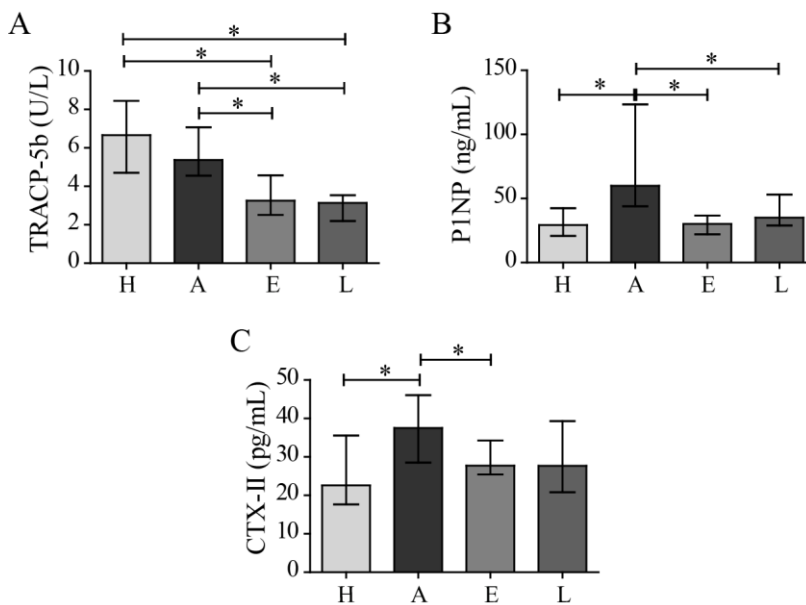


Fig. 2 – Celastrol diminishes bone and cartilage turnover markers. TRACP-5b (A), P1NP (B) and CTX-II (C) levels were quantified in rat serum samples collected at the time of sacrifice. Celastrol is able to significantly reduce the levels of TRACP-5b, P1NP and CTX-II in comparison with untreated arthritic rats. Data are expressed as median with interquartile range. Differences were considered statistically significant for p -values < 0.05 , according to the Mann–Whitney tests. H – Healthy, A – Arthritic, E – Celastrol early-treated, L – Celastrol late-treated. Healthy $N=13$, Arthritic $N=18$, Celastrol early-treated $N=15$ and Celastrol late-treated $N=15$.

Celastrol prevents bone loss and bone microarchitecture degradation in arthritis

The effect of celastrol on inflammation-induced systemic bone loss was assessed by micro-CT analysis of tibial bones (Fig 3). Representative reconstructions of micro-CT analysis of rat tibiae are shown in Fig 3A. Arthritis progression led to significant reductions in trabecular bone mass and in trabecular bone volume fraction and number ($p < 0.0001$ vs healthy controls, Fig 3B), and an increase in trabecular separation and porosity ($p < 0.0001$ vs healthy controls, Fig 3B). Also the structural integrity declines with arthritis, as trabeculae have fewer connections and have rather rod-like appearance, indicated by increased structure model index. A 18-day course of therapy with celastrol, starting 4 days after disease induction, preserved bone mass and integrity, with a significant increase in trabecular bone volume fraction (+16.6%, $p = 0.02$) and number (+20.3%, $p = 0.0047$) as well as with a decrease in trabecular separation (-12.9%, $p = 0.0023$) and porosity (-4.5%, $p = 0.0148$) in comparison to arthritic rats. Importantly, celastrol early-treated rats also showed a significant reduction in trabecular separation even when comparing with their baseline (-22.1%, $p = 0.0101$ vs arthritic rats sacrificed at day 4 after disease induction). Celastrol treatment also preserved structural integrity, as trabeculae have more connections and have less rod-like appearance ($p = 0.0462$ and $p = 0.0047$ in early-treated vs arthritic rats, respectively). Additionally, micro-CT analysis revealed that trabecular thickness is reduced in arthritic rats ($p < 0.0001$ vs healthy controls), but there was no effect after celastrol treatment. As depicted in Fig 3B, no effect in trabecular bone microarchitecture was observed in celastrol late-treated group, except for a significant reduction in trabecular separation (-10.6%, $p = 0.0325$ vs arthritis rats). A similar pattern can be observed for cortical bone. Arthritis decreases cortical bone area (-10.8%, $p < 0.0001$) and thickness (-11%, $p < 0.0001$) in arthritic tibias compared to healthy controls. Although overall cortical porosity is similar between arthritic and healthy controls, blood vessel channels are significantly wider in arthritic bones compared to controls ($p = 0.0146$).

As shown in Fig 3C, both treatment approaches affect cortical bone by inhibiting bone resorption as shown by significantly smaller endosteal volume (-14.5%,

$p=0.0026$ in early-treated and -20.1% , $p=0.0017$ in late-treated celastrol rats vs arthritic animals). Also both groups have decreased cortical porosity (-18.2% , $p=0.0161$ in early-treated and -30.1% , $p=0.0001$ in late-treated) due to a decrease in the number (-17.1% , $p=0.0211$ in early-treated and -29.7% , $p=0.0004$ in late-treated) and thickness (-3.1% , $p=0.0425$ in early-treated and -4.8% , $p=0.0026$ in late-treated) of blood vessel channels and thus increasing their separation ($+7.9\%$, $p=0.180$ in early-treated and $+14.6\%$, $p=0.0037$ in late-treated) compared to arthritic rats. Of note, both treatment groups significantly showed an improvement in these cortical parameters when compared with their respective baselines ($p<0.05$).

These data show that treatment with celastrol significantly prevented the marked inflammation-induced bone loss and microarchitecture degradation of AIA rats as pointed out by the improved trabecular and cortical parameters.

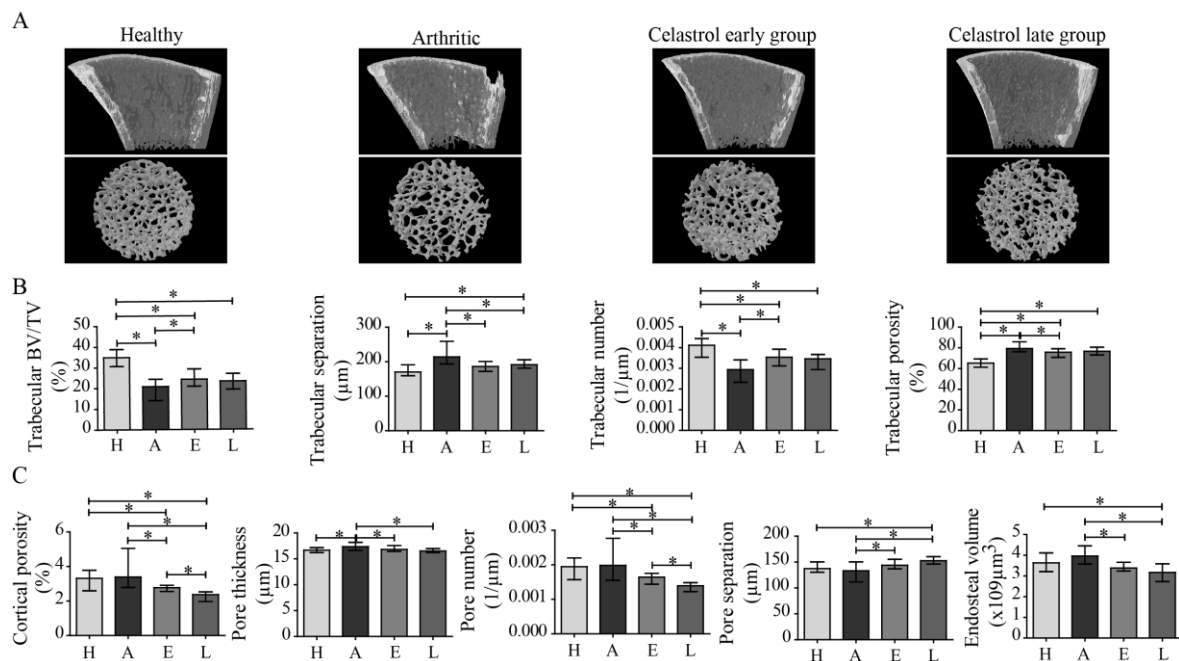


Fig. 3 – Celastrol preserves bone microarchitecture in arthritis. Inflammation-induced bone loss and bone microarchitecture degradation, and the protective effect of celastrol are illustrated in representative micro-CT reconstructions (A). Trabecular (B) and cortical (C) bone indices were quantified from micro-CT reconstructions. Notice that tibiae from the celastrol early-treated group have improved trabecular and cortical parameters comparing with arthritic rats. Tibiae were collected at the time of sacrifice. Data are expressed as median with interquartile range. Differences were considered statistically significant for p -values < 0.05 , according to the Mann–Whitney tests. H – Healthy, A – Arthritic, E – Celastrol early-treated, L – Celastrol late-treated. Healthy $N=30$, Arthritic $N=30$, Celastrol early-treated $N=15$ and Celastrol late-treated $N=15$.

Celastrol improves bone mechanical properties in arthritic rats

Bone strength of rat femurs was evaluated using the 3-point bending test (Fig 4). There was a significant reduction in the maximal load that arthritic femurs were able to resist before breaking as compared to healthy controls (-13.6%, $p=0.0017$). Early administration of celastrol restored bone strength and maximal breaking load was increased by 9.4%, when comparing to arthritic group ($p=0.0434$, Fig 4A). Late celastrol administration was insufficient to correct bone damage and these animals showed decreased maximal deformation and capability to absorb energy, which were significantly reduced by -14.7% ($p=0.0298$, Fig 4B) and -18.8% ($p=0.0377$, Fig 4C), respectively. Additionally, arthritic rats have a reduction in the yield displacement (-28.3%, $p=0.0192$ in arthritic rats vs healthy controls). In contrast, in celastrol early-treated rats there was an increase in the elastic properties of bone with an augment in yield displacement (+20.7%, $p=0.0498$ in celastrol early-treated vs arthritic rats), meaning that a higher elastic deformation of the femur was arising before the first micro fractures occur (Fig 4D). In addition, mechanical results revealed that there was a significant reduction in the load (Fig 4E) and elastic energy at yield point (Fig 4F) in arthritic rats comparing with healthy controls ($p=0.0229$ and $p=0.0161$, respectively), only partially corrected in arthritic rats under celastrol treatment since the early phase of the disease (+7.4% and +34.8% than arthritic rats, respectively). Celastrol early-treated rats also showed a significant reduction in bone stiffness (Fig 4G) in comparison to arthritic rats and celastrol late-treated rats (-7.5%, $p=0.0177$ and -17.8%, $p=0.0016$, respectively). However, no difference was observed between healthy controls and arthritic rats in this mechanical parameter.

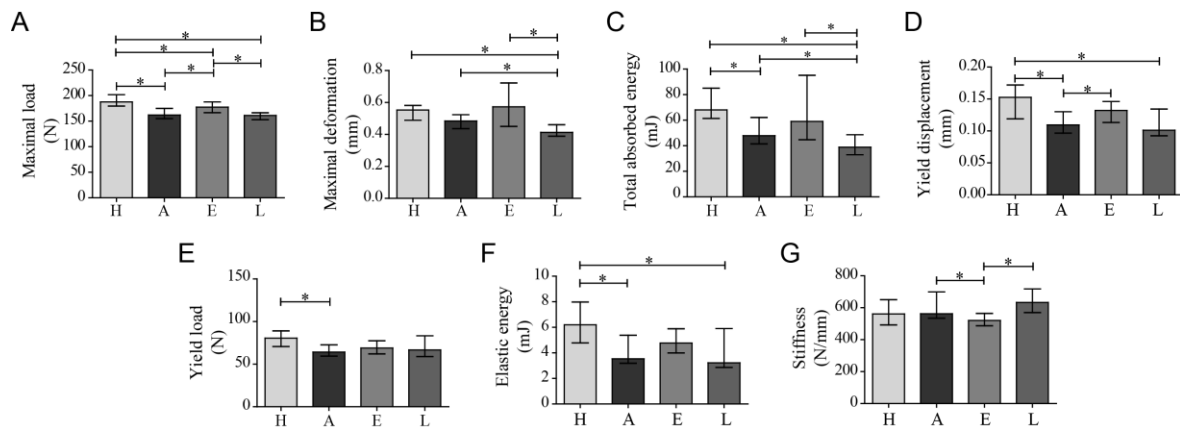


Fig. 4 - Celastrol ameliorates bone mechanical properties in arthritic rats. Maximal load (A), Maximal deformation (B), Total absorbed energy (C), Yield displacement (D), Yield load (E), Elastic energy (F) and Stiffness (G) parameters were obtained by 3-point bending. Celastrol early-treated rats have higher levels of yield point displacement and maximum load comparing with untreated arthritic rats. Femurs were collected after 22 days of disease induction. Data are expressed as median with interquartile range. Differences were considered statistically significant for p-values < 0.05, according to the Mann–Whitney tests. H – Healthy, A – Arthritic, E – Celastrol early-treated, L – Celastrol late-treated. Healthy N=13, Arthritic N=10, Celastrol early-treated N=15 and Celastrol late-treated N=15

DISCUSSION

In this study the AIA rat model was used to assess the bone protective properties of celastrol *in vivo*. Here we demonstrated that celastrol treatment exerts a therapeutic effect on arthritic joint damage, with an efficacy not only limited to anti-inflammatory properties [11, 12], but also with a substantial inhibition of cartilage and focal bone destruction and reduction of systemic bone degradation, translated by the preservation of its structure and strength in arthritic animals early treated with celastrol.

In the present work, we have shown that celastrol decreases the number of joint tissue osteoclasts and osteoblasts. Several cell populations residing in the inflamed synovial membrane provide signals that stimulate osteoclast formation and facilitate bone resorption. We have previously shown that celastrol significantly reduces the number of synovial B and T-cells as well as fibroblasts and macrophages [12]. Macrophages do not only mediate synovial inflammation, but are also critical in osteoclast differentiation [23]. Most importantly, we have

previously shown that celastrol inhibits NF- κ B activation *in vitro* [11]. NF- κ B activation is also crucial for osteoclast formation and function, and is upstream activated by the engagement of RANKL with RANK. Recent *in vitro* findings showed that celastrol inhibits the recruitment of TGF β -activated kinase (TAK)1, an upstream receptor-associated factor of I κ B kinase (IKK), to RANK and TNF receptors[24], inhibiting both RANKL-induced NF- κ B activation and the osteoblast-related ERK signaling [25]. Work from the Moudgil laboratory has shown, *in vitro*, that celastrol reduces other osteoclastic mediators besides RANKL, such as granulocyte-macrophage colony-stimulating factor (GM-CSF), insulin-like growth factor (IGF) and osteopontin (OPN), suggesting a shift in bone remodeling in favor of an anti-osteoclastic activity [17]. Finally, also in line with our data, it has been reported in bone metastasis and ovariectomy-induced bone loss models that celastrol reduces osteoclast numbers and bone loss and preserves its trabecular architecture, together with an inhibitory effect on osteoblasts viability and function [25, 26]. Likewise, the gold standard and first-line drug in RA, methotrexate, also slows down articular damage in RA patients by inhibiting osteoclastogenesis [27] together with a reduction in osteoblasts proliferation [28].

The reduction in osteoclast and osteoblast numbers is consistent with the reduction in serum levels of TRACP-5b and P1NP observed in arthritic rats treated with celastrol, suggesting a reduction in the accelerated bone turnover induced by arthritis.

We have also quantified serum CTX-II. This is a major component of articular cartilage [29] with a significant correlation between serum levels and the severity of cartilage damage [30,31]. Celastrol treatment reduced serum CTX-II concentration, suggesting a chondroprotective effect, which was confirmed by histological observations. This protective effect on cartilage could be explained by the inhibition of heat shock protein 90 β and of NF- κ B activation [32], combined with the control of inflammation.

Trabecular bone microarchitecture is an important feature of bone quality [33]. Micro-CT analysis revealed arthritis-induced reduction of trabecular bone volume fraction and trabecular number as well as increase in trabecular separation and in the occurrence of rod-like shape trabeculae. All these are associated with decreased strength of trabecular bone. Notably, celastrol treatment improved all

these trabecular bone parameters and mitigated bone loss. Consistent with this, our results showed that celastrol administration prevented the loss of bone mechanical compliance of femurs in arthritic rats by increasing maximum load and yield displacement. In addition, celastrol treated arthritic animals also showed positive effects on cortical bone morphology, which is a major factor defining the mechanical properties of bone. In fact, celastrol-treated rats had decreased cortical porosity and increased endosteal bone quantity. Overall, these results suggest that early celastrol treatment could prevent bone fragility in RA patients. Despite celastrol efficacy there are still some differences between treated and healthy phenotypes, therefore it is reasonable to speculate that the extent of bone protection could be even further improved by optimized doses of celastrol or by augmenting treatment duration, which is not possible when using the AIA model. In conclusion, celastrol significantly halted cartilage and bone joint resorption and preserved systemic bone structure and strength, and thus may serve as a useful therapeutic agent for the treatment of inflammation-induced bone damage. Moreover, our study also suggests that an early treatment initiation is crucial to effectively prevent bone destruction in RA patients.

KEY MESSAGES:

1. Celastrol preserves articular joint structures in AIA rats.
2. Celastrol reduces serum TRACP-5b, P1NP and CTX-II in AIA rats.
3. Celastrol prevents inflammation-induced focal and systemic bone damage, counteracting bone loss and fragility.

REFERENCES

1. Birnbaum HG, Barton M, Greenberg PE, et al. Direct and indirect costs of rheumatoid arthritis to an employer. *J Occup Environ Med* 2000;42:588-96.
2. American College of Rheumatology Subcommittee on Rheumatoid Arthritis G. Guidelines for the management of rheumatoid arthritis: 2002 Update. *Arthritis Rheum* 2002;46:328-46.
3. Noss EH, Brenner MB. The role and therapeutic implications of fibroblast-like synoviocytes in inflammation and cartilage erosion in rheumatoid arthritis. *Immunol Rev* 2008;223:252-70.
4. Dequeker J, Geusens P. Osteoporosis and arthritis. *Ann Rheum Dis* 1990;49:276-80.
5. Schett G, Saag KG, Bijlsma JW. From bone biology to clinical outcome: state of the art and future perspectives. *Ann Rheum Dis* 2010;69:1415-9.
6. Schett G, Gravallesse E. Bone erosion in rheumatoid arthritis: mechanisms, diagnosis and treatment. *Nat Rev Rheumatol* 2012;8:656-64.
7. Agarwal SK. Core management principles in rheumatoid arthritis to help guide managed care professionals. *J Manag Care Pharm* 2011;17:S03-8.
8. Dimitroulas T, Nikas SN, Trontzas P, Kitis GD. Biologic therapies and systemic bone loss in rheumatoid arthritis. *Autoimmun Rev* 2013;12:958-66.
9. Cascao R, Moura RA, Perpetuo I, et al. Identification of a cytokine network sustaining neutrophil and Th17 activation in untreated early rheumatoid arthritis. *Arthritis Res Ther* 2010;12:R196.
10. Cascao R, Polido-Pereira J, Canhao H, et al. Caspase-1 is active since the early phase of rheumatoid arthritis. *Clin Exp Rheumatol* 2012;30:144.
11. Cascao R, Vidal B, Raquel H, et al. Effective treatment of rat adjuvant-induced arthritis by celestrol. *Autoimmun Rev* 2012;11:856-62.
12. Cascao R, Vidal B, Lopes IP, et al. Decrease of CD68 Synovial Macrophages in Celestrol Treated Arthritic Rats. *PLoS One* 2015;10:e0142448.
13. Noguchi M, Kimoto A, Kobayashi S, et al. Effect of celecoxib, a cyclooxygenase-2 inhibitor, on the pathophysiology of adjuvant arthritis in rat. *Eur J Pharmacol* 2005;513:229-35.

14. Toh K, Kukita T, Wu Z, et al. Possible involvement of MIP-1 α in the recruitment of osteoclast progenitors to the distal tibia in rats with adjuvant-induced arthritis. *Lab Invest* 2004;84:1092-102.
15. Vidal B, Cascao R, Vale AC, et al. Arthritis induces early bone high turnover, structural degradation and mechanical weakness. *PLoS One* 2015;10:e0117100.
16. da Silva JA, Fonseca JE, Graca L, Moita L, Carmo-Fonseca M. Reinnervation of post-arthritic joints in the rat. *Clin Exp Rheumatol* 1996;14:43-51.
17. Nanjundaiah SM, Venkatesha SH, Yu H, et al. Celastrol and its bioactive celastrol protect against bone damage in autoimmune arthritis by modulating osteoimmune cross-talk. *J Biol Chem* 2012;287:22216-26.
18. Stolina M, Bolon B, Middleton S, et al. The evolving systemic and local biomarker milieu at different stages of disease progression in rat adjuvant-induced arthritis. *J Clin Immunol* 2009;29:158-74.
19. Chen DL, Wang DS, Wu WJ, et al. Overexpression of paxillin induced by miR-137 suppression promotes tumor progression and metastasis in colorectal cancer. *Carcinogenesis* 2013;34:803-11.
20. Bouxsein ML, Boyd SK, Christiansen BA, et al. Guidelines for assessment of bone microstructure in rodents using micro-computed tomography. *J Bone Miner Res* 2010;25:1468-86.
21. Stolina M, Schett G, Dwyer D, et al. RANKL inhibition by osteoprotegerin prevents bone loss without affecting local or systemic inflammation parameters in two rat arthritis models: comparison with anti-TNF α or anti-IL-1 therapies. *Arthritis Res Ther* 2009;11:R187.
22. Stolina M, Adamu S, Ominsky M, et al. RANKL is a marker and mediator of local and systemic bone loss in two rat models of inflammatory arthritis. *J Bone Miner Res* 2005;20:1756-65.
23. Firestein GS. Evolving concepts of rheumatoid arthritis. *Nature* 2003;423:356-61.
24. Sethi G, Ahn KS, Pandey MK, Aggarwal BB. Celastrol, a novel triterpene, potentiates TNF-induced apoptosis and suppresses invasion of tumor cells by inhibiting NF- κ B-regulated gene products and TAK1-mediated NF- κ B activation. *Blood* 2007;109:2727-35.

25. Idris AI, Krishnan M, Simic P, et al. Small molecule inhibitors of I κ B kinase signaling inhibit osteoclast formation in vitro and prevent ovariectomy-induced bone loss in vivo. *FASEB J* 2010;24:4545-55.
26. Idris AI, Libouban H, Nyangoga H, et al. Pharmacologic inhibitors of I κ B kinase suppress growth and migration of mammary carcinosarcoma cells in vitro and prevent osteolytic bone metastasis in vivo. *Mol Cancer Ther* 2009;8:2339-47.
27. Kanagawa H, Masuyama R, Morita M, et al. Methotrexate inhibits osteoclastogenesis by decreasing RANKL-induced calcium influx into osteoclast progenitors. *J Bone Miner Metab* 2015;
28. Annussek T, Kleinheinz J, Thomas S, Joos U, Wermker K. Short time administration of antirheumatic drugs - methotrexate as a strong inhibitor of osteoblast's proliferation in vitro. *Head Face Med* 2012;8:26.
29. Elsaid KA, Chichester CO. Review: Collagen markers in early arthritic diseases. *Clin Chim Acta* 2006;365:68-77.
30. Oestergaard S, Chouinard L, Doyle N, et al. The utility of measuring C-terminal telopeptides of collagen type II (CTX-II) in serum and synovial fluid samples for estimation of articular cartilage status in experimental models of destructive joint diseases. *Osteoarthritis Cartilage* 2006;14:670-9.
31. Oestergaard S, Chouinard L, Doyle N, et al. Early elevation in circulating levels of C-telopeptides of type II collagen predicts structural damage in articular cartilage in the rodent model of collagen-induced arthritis. *Arthritis Rheum* 2006;54:2886-90.
32. Ding QH, Cheng Y, Chen WP, Zhong HM, Wang XH. Celastrol, an inhibitor of heat shock protein 90 β potently suppresses the expression of matrix metalloproteinases, inducible nitric oxide synthase and cyclooxygenase-2 in primary human osteoarthritic chondrocytes. *Eur J Pharmacol* 2013;708:1-7.
33. Dempster DW. The contribution of trabecular architecture to cancellous bone quality. *J Bone Miner Res* 2000;15:20-3.

V. Effects of tofacitinib in early arthritis bone loss

Bruno Vidal, Rita Cascão, Mikko Finnilä, Inês Lopes, Simo Saarakkala, Peter Zioupos , Helena Canhão, João Fonseca

Author Contributions

Vidal and Cascão designed the experiments. Vidal performed all the experiments and wrote the chapter. Cascão, Lopes, Finnila and Zioupos helped to perform some experiments. Cascão, Finnila, Saarakkala, Zioupos and Fonseca supervised the work and revised the text.

Effects of tofacitinib in early arthritis bone loss

Bruno Vidal, Rita Cascão, Mikko Finnilä, Inês Lopes, Simo Saarakkala, Peter Zioupos, Helena Canhão, João Fonseca

ABSTRACT

Rheumatoid arthritis (RA) causes immune mediated local and systemic bone damage. Objectives - The main goal of this work was to analyze, how treatment intervention with tofacitinib prevents the early disturbances on bone structure and mechanics in adjuvant induced arthritis rat model. This is the first study to access the impact of tofacitinib on the systemic bone effects of inflammation. Methods - Fifty Wistar adjuvant-induced arthritis (AIA) rats were randomly housed in experimental groups, as follows: non-arthritic healthy group (N=20), arthritic non-treated (N=20) and 10 animals under tofacitinib treatment. Rats were monitored during 22 days after disease induction for the inflammatory score, ankle perimeter and body weight. Healthy non-arthritic rats were used as controls for comparison. After 22 days of disease progression rats were sacrificed and bone samples were collected for histology, micro-CT, 3-point bending and nanoindentation analysis. Blood samples were also collected for bone turnover markers and systemic cytokine quantification. Results - At tissue level, measured by nanoindentation, tofacitinib increased bone cortical and trabecular hardness. However, micro-CT and 3-point bending tests revealed that tofacitinib did not revert the effects of arthritis on cortical and trabecular bone structure and on mechanical properties. Conclusion - Possible reasons for these observations might be related with the mechanism of action of tofacitinib, which leads to direct interactions with bone metabolism, and/or with kinetics of its bone effects that might need longer exposure.

INTRODUCTION

Rheumatoid arthritis (RA) is a chronic immune-mediated inflammatory disease, which affects around 1% of the world-population [1]. It causes joint and systemic inflammation that is reflected in local and systemic bone damage [2]. In fact, as RA progresses there is marked bone destruction, with radiological evidence of bone erosion within 2 years of disease onset [3]. In addition, osteoporosis is a common finding in patients with RA [4]. This is responsible for increased rates of vertebral and hip fractures in these patients [5, 6]. RA is associated with an increased expression of the receptor activator of nuclear factor kappa-B ligand (RANKL) and low levels of its antagonist, osteoprotegerin (OPG) [7]. RANKL is a crucial activator of osteoclastogenesis [8]. In addition, RA serum and synovial fluid present an inflammatory cytokine profile, including interleukin (IL) 1 β , IL6, IL17 and tumor necrosis factor (TNF), which further favors osteoclast differentiation and activation since the early phase of the disease [9-11]. Evidence suggests that bone remodeling imbalance in RA contribute not only to local bone erosions but also to the development of systemic osteoporosis [12].

We have previously found in the adjuvant-induced arthritis (AIA) rat model that 22 days of inflammatory disease progression directly led to the degradation of bone biomechanical properties, namely stiffness, ductility and bone strength, which was paralleled by a high collagen bone turnover [13].

Tofacitinib is a selective inhibitor of janus kinase 1 (JAK1) and janus kinase 3 (JAK 3), thus interfering with the dimerization of signal transducer and activator of transcription (STAT) molecules, blocking the activation of gene transcription that is dependent on the JAK-STAT signaling pathway [14-16]. The main goal of this work was to analyze, if treatment intervention with tofacitinib in the AIA rat model prevents the early disturbances on bone structure and strength induced by inflammation.

MATERIALS AND METHODS

Animal experimental design

Fifty 8 week-old female Wistar AIA Han rats weighing approximately 200-220gr were housed in European type II standard filter top cages (Tecniplast, Buguggiate, Italy) and transferred into the SPF animal facility at the Instituto de Medicina Molecular, Faculdade de Medicina, Universidade de Lisboa, under a 14h light/10h dark light cycle, acclimatized to T= 20-22°C and RH= 50-60%. They were given access to autoclaved rodent breeder chow (Special Diet Service, RM3) and triple filtered water. AIA rats were purchased from Charles River laboratories international (Barcelona, Spain) and they were delivered at Instituto de Medicina Molecular after three days of disease induction.

Upon arrival, animals were randomly housed in groups, individually identified and cages were labelled according to the experimental groups, as follows: non-arthritic healthy group (N=20), arthritic treated with tofacitinib (10mg/kg/day orally) (N=10) and arthritic non-treated (N=20). Tofacitinib administration was started 4 days after disease induction, when animals already presented clinical signs of arthritis. The inflammatory score, ankle perimeter and body weight were measured during the period of treatment. Inflammatory signs were evaluated by counting the score of each joint in a scale of 0 – 3 (0 – absence; 1 – erythema; 2 – erythema and swelling; 3 – deformities and functional impairment). The total score of each animal was defined as the sum of the partial scores of each affected joint. Rats were sacrificed 22 days post disease induction and blood, paws and bone samples were collected. All experiments were approved by the Animal User and Ethical Committees at the Instituto de Medicina Molecular (Lisbon University), according to the Portuguese law and the European recommendations.

Histological evaluation of hind paws

Left hind paw samples collected at the time of sacrifice were fixed immediately in 10% neutral buffered formalin solution and then decalcified in 10% formic acid. Samples were then dehydrated and embedded in paraffin, serially sectioned at a

thickness of 5 μm . Sections were stained with hematoxylin and eosin for histopathological evaluation of structural changes and cellular infiltration. This evaluation was performed in a blind fashion using 5 semi-quantitative scores:

- Sublining layer infiltration score (0—none to diffuse infiltration; 1—lymphoid cell aggregate; 2—lymphoid follicles; 3—lymphoid follicles with germinal center formation);
- Lining layer cell number score (0—fewer than three layers; 1—three to four layers; 2—five to six layers; 3—more than six layers);
- Bone erosion score (0—no erosions; 1—minimal; 2—mild; 3—moderate; 4—severe);
- Cartilage surface (0—normal; 1—irregular; 2—clefts; 3—clefts to bone);
- Global severity score (0—no signs of inflammation; 1—mild; 2—moderate; 3—severe) [17]

Images were acquired using a Leica DM2500 (Leica Microsystems, Wetzlar, Germany) microscope equipped with a color camera.

Bone remodeling markers quantification

Serum samples were collected at sacrifice and stored at -80°C . Bone remodeling markers, CTX-I and P1NP, were quantified by Serum Rat Laps ELISA assay (Immunodiagnostic Systems Ltd, Boldon, UK).

Proinflammatory cytokines IL-1 β , IL-6 (Boster Bio, California, USA), IL-17, OPG, RANKL (Sunred Biological Technology, Shanghai, China) and TNF (RayBiotech, Georgia, USA) were quantified in serum samples using specific rat ELISA kits. Both kits were used following strictly provider's recommendations.

For all biomarkers standard curves were generated by using reference biomarker concentrations supplied by the manufacturers. Samples were analyzed using a plate reader Infinite M200 (Tecan, Mannedorf, Switzerland).

Micro-computed tomography (micro-CT) analysis

Structural properties of the trabecular and cortical tibiae were determined with a high-resolution micro-CT system (SkyScan 1272, Bruker microCT, Kontich, Belgium). Moist bones were wrapped in parafilm and covered with dental wax to prevent drying and movement during the scanning. X-ray tube was set to 50kV and beam was filtered with 0.5mm Aluminum filter. Sample position and camera settings were tuned to provide 3.0 μ m isotropic pixel size and projection images were collected every 0.2°. Tissue mineral density values were calibrated against hydroxyapatite phantoms with densities of 250mg/cm³ and 750mg/cm³. Reconstructions were done with NRecon (v 1.6.9.8; Bruker microCT, Kontich, Belgium) where appropriate corrections to reduce beam hardening and ring artefacts were applied. Bone was segmented in slices of 3 μ m thickness. After 200 slices from growth plate, we selected and analyzed 1400 slices of trabecular bone. For cortical bone, 300 slices (1800 slices from growth plate) were analyzed.

Analyzes were performed in agreement with guidelines for assessment of bone microstructure in rodents using micro-computed tomography [18]. Trabecular bone morphology was analyzed by applying global threshold and despeckle to provide binary image for 3D analysis. For cortical bone ROI was refined with ROI-shrink wrap operation. This was followed by segmentation of blood vessels using adaptive thresholding. Blood vessels and porosity were analyzed using 3D morphological analyzes.

Bone mechanical tests

Femurs were subjected to a 3-point bending test using a universal materials testing machine (Instron 3366, Instron Corp., Massachusetts, USA). Femurs were placed horizontally anterior side upwards on a support with span length of 5mm. The load was applied with a constant speed of 0.005mm/s until failure occurred. Stiffness was analyzed by fitting first-degree polynomial function to the linear part of recorded load deformation data. A displacement of 0.15 μ m between fitted slope and measured curve was used as criteria for yield point, whereas the breaking

point was defined as set where force reached maximal value. Force, deformation and absorbed energy were defined at both yield and at the breaking point.

Nanoindentation

Nanoindentation was performed using a CSM-Nano Hardness Tester System (CSM Instruments SA; Switzerland; Indentation v.3.83) equipped with a Berkovich based pyramid diamond tip. After micro-CT, 0.5mm of top tibia was cut and proximal part was embedded to low viscosity epoxy resin (EpoThin, Buehler, Knorring Oy Ab, Helsinki, Finland). Slow speed diamond saw was used to remove 10% of bone length. The sample surface was polished using silicon carbide sandpaper with a decreasing grid size (800, 1200, 2400 and 4800) and finished with cloth with containing 0.05 μm γ -alumina particles. Indentation protocol was adopted from previous work and on average 8 indentations were done on both cortical and trabecular bone with a quasi-static (CSM called 'advanced') loading protocol [19]. All indentations were performed under an optical microscope to achieve the precise location of indentations at the center of the targeted area in the tissue [20].

In the 'advanced' protocol, a trapezoidal loading waveform was applied with a loading/unloading rate of 20mN/min and with an intermediate load-hold-phase lasting 30s hold at a maximum load 10 mN. The hardness (HIT), indentation modulus (EIT), indentation creep (CIT) and elastic part of indentation work (η IT) were measured by using the Oliver and Pharr (1992) method [21].

Histological images of rat tibiae from diaphyseal cortical region were acquired during the nanoindentation technique, using a CSM instruments (Switzerland) microscope equipped with a color camera.

A histologic score was applied in order to evaluate the lamellar structures of bone tissue. This evaluation was performed in a blind fashion using a semi-quantitative score:

- Lamellar bone structure: (1- predominantly parallel-lamella; 2 - concentric and parallel-lamellae in the same proportion; 3 – predominantly concentric lamella).

The ratio of osteocyte lacuna area / total tissue area was also evaluated at x200 magnification in order to analyze the percentage of total tissue area occupied by osteocyte lacunae. The method of acquisition and analysis used was the same applied for the evaluation of bone volume / tissue volume in histomorphometry technique [13]. All variables were expressed and calculated according to the recommendations of the American Society for Bone and Mineral Research [22], using a morphometric program (Image J 1.46R with plugin Bone J).

Statistical analysis

Statistical differences were determined with Mann–Whitney tests using GraphPad Prism (GraphPad, California, USA). Correlation analysis was performed with the Spearman test. Differences were considered statistically significant for $p < 0.05$.

RESULTS

Tofacitinib effectively reduced inflammation in the AIA rat model of arthritis. Results showed that 10mg/kg/day of tofacitinib effectively controlled and abrogated disease development in comparison with untreated arthritic rats (fig.1A). Moreover, untreated arthritic animals sharply increased the ankle perimeter throughout disease progression (fig.1B). Rats under tofacitinib treatment presented an ankle perimeter similar to healthy controls.

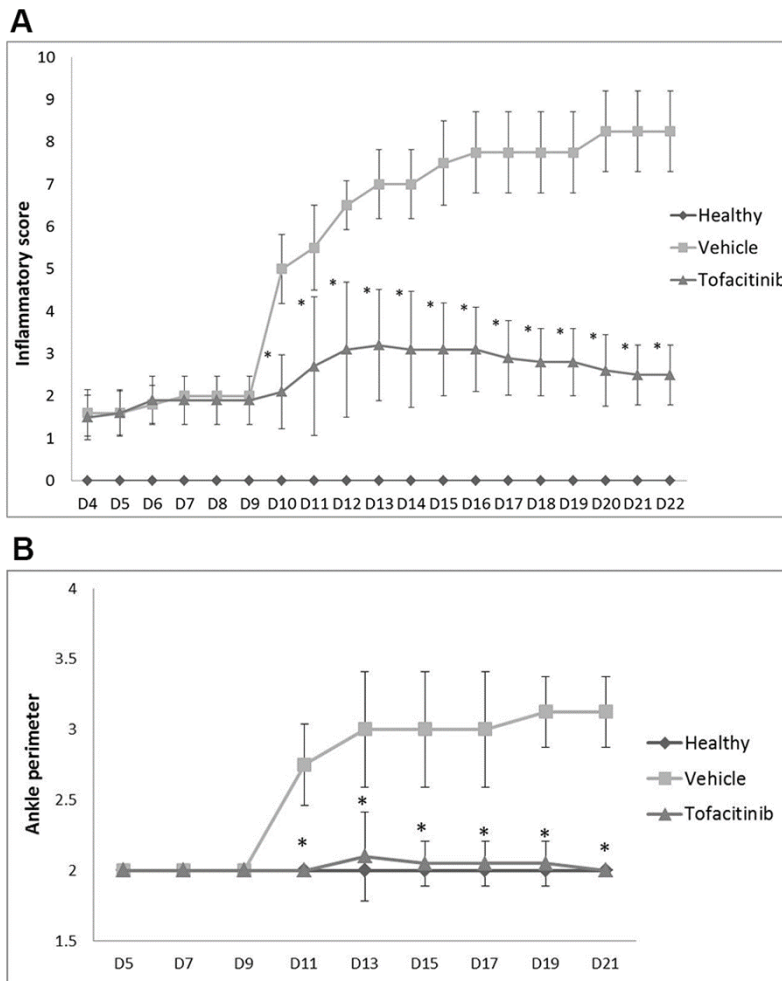


Fig. 1 – Inflammatory score and ankle perimeter. (A) Inflammatory score - Tofacitinib group was compared with the vehicle group (arthritic). Results showed statistical differences throughout time since day 10 $p= 0.0071$ up to day 22 $p= 0.0058$. (B) Ankle perimeter. Tofacitinib group was compared with the vehicle group (arthritic). Results showed statistical differences throughout time since day 11 $p= 0.0057$ up to day 21 $p= 0.0056$. Statistical differences were determined with non-parametric Mann Whitney test using GraphPad Prism (GraphPad, California, USA). Differences were considered statistically significant for p values ≤ 0.05 . Healthy $N=20$, Arthritic $N=20$, Tofacitinib $N=10$.

Tofacitinib abrogated local joint inflammation and local bone and cartilage damage in AIA rats

To evaluate the effect of tofacitinib treatment in the preservation of joint structure and periarticular bone, paw sections stained with haematoxylin and eosin were performed (illustrative images can be observed in Fig 2A). The histological evaluation using 5 semi-quantitative scores is depicted in Fig 2 (B-F).

Sublining layer infiltration (B) and the number of lining layer cells (C) were lower in the tofacitinib group when compared with the untreated arthritic group at the end of the study ($p < 0.0001$). Tofacitinib was also effective in preventing joint bone erosions (D) and cartilage damage (E) ($p < 0.0001$ and $p = 0.0001$ tofacitinib group vs. arthritic rats, respectively).

Thus, these data reveals that tofacitinib was able to significantly diminish inflammation and local bone damage (Fig. 2F, $p < 0.0001$ tofacitinib group vs. arthritic rats).

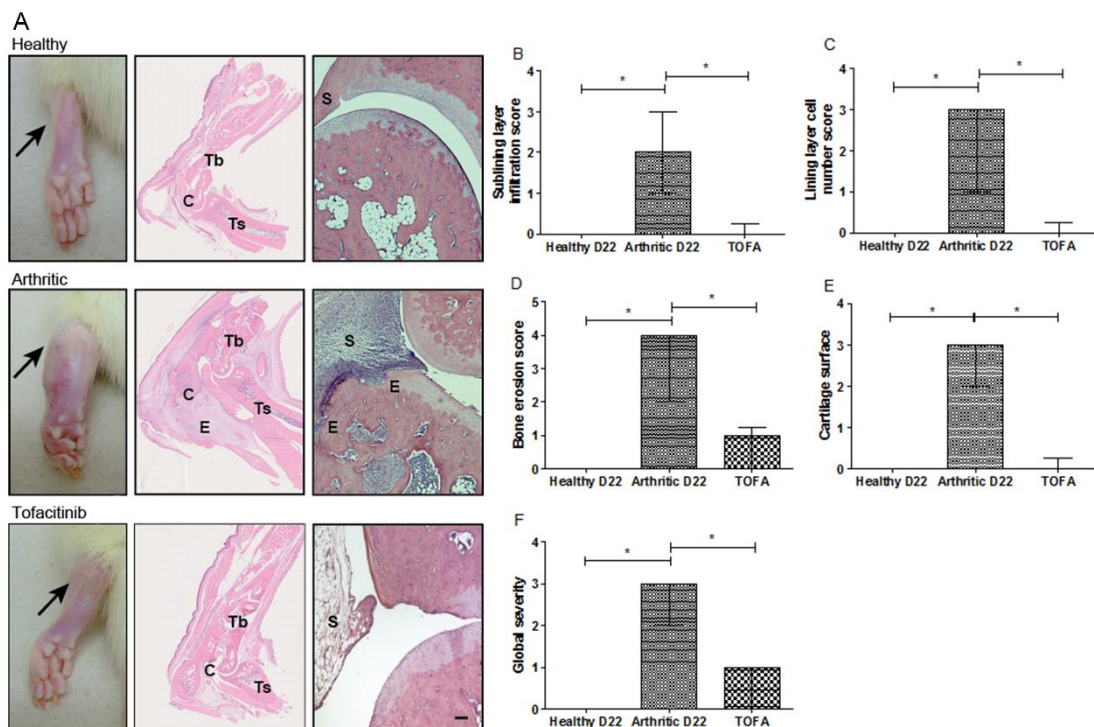


Fig. 2 – (A) Histological images of joints after tofacitinib treatment. These patterns are merely illustrative of the type of histological features observed. Black arrow indicates the absence/presence of ankle swelling in rat hind paws. C–calcaneus, E–edema or erosion, S–synovia, Tb–tibia, Ts–tarso. Magnification of 50X. Bar: 100 μ m. Tofacitinib suppressed inflammation and tissue damage locally in the joints of AIA rats. A semi-quantitative evaluation of histological sections was performed. Notice that tofacitinib inhibited cellular infiltration (B), completely reversed the number of lining layer cells to the normal values (C) and prevented bone erosion occurrence (D), allowing for a normal cartilage (E) and joint structure, comparable to healthy rats (F). Data are expressed as median with interquartile range. Differences were considered statistically significant for p -values < 0.05 , according to Mann Whitney test. Healthy $N=20$, Arthritic $N=20$, Tofacitinib $N=10$.

Tofacitinib reduced bone turnover

We have observed that both CTX-I (Fig. 3A) and P1NP (Fig. 3B) were significantly increased in the arthritic group in comparison with the healthy control animals ($p < 0.0001$ and $p = 0.0015$, respectively), revealing an increase of bone turnover in the arthritic group. The tofacitinib group showed decreased values for CTX-I ($p = 0.0002$) and P1NP ($p = 0.0018$) when compared with the arthritic group, suggesting a decreased bone turnover (Fig.3).

RANKL levels were decreased in the serum of tofacitinib-treated rats in comparison with healthy control and untreated arthritic rats ($p = 0.0083$ and $p = 0.0141$, respectively), as observed in Fig 3C. OPG levels were also reduced in tofacitinib group in comparison with healthy control and untreated arthritic rats ($p = 0.0031$ and $p = 0.0002$, respectively) (Fig. 3D). No differences were observed in RANKL/OPG ratio between tofacitinib and arthritic untreated group. The tofacitinib group showed an increased RANKL/OPG ratio when compared to healthy control group ($p = 0.0370$ Fig. 3E).

We have also quantified the circulating concentration of IL-1 β , IL-6 and TNF, but no differences were found when comparing arthritic rats with animals treated with tofacitinib (Fig. 3F, 3G and 3H). However, there was a slight tendency for IL-6 to be diminished in the tofacitinib group when compared with untreated arthritic animals.

Tofacitinib administration significantly reduced the levels of IL-17 detected in peripheral blood, ($p < 0.0001$, tofacitinib group vs. untreated arthritic rats after 22 days of disease induction) (Fig. 3I).

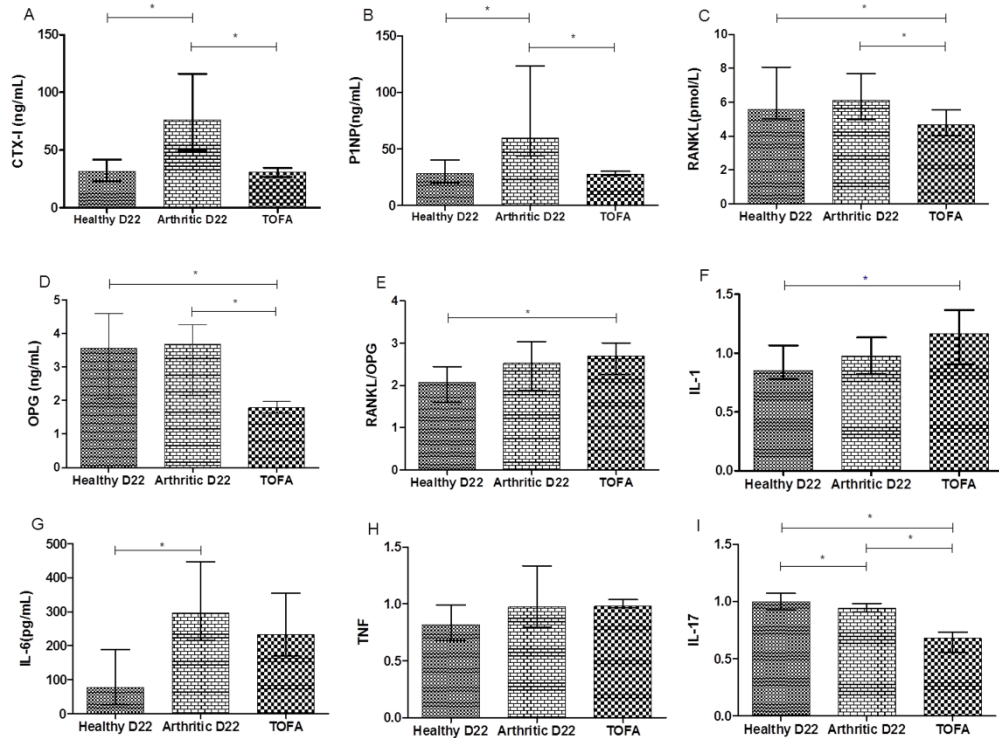


Fig. 3 - Bone turnover markers and systemic cytokines quantifications. Serum samples collected at day 22 (sacrifice) were analyzed by ELISA technique. Bone resorption marker, CTX-I (A) and bone formation marker, P1NP (B) were increased in arthritic rats ($p < 0.0001$ and $p = 0.0015$, respectively). Tofacitinib group showed decreased values for CTX-I ($p = 0.0002$) and P1NP ($p = 0.0018$). RANKL (C) and OPG (D) were diminished in tofacitinib treated rats ($p = 0.0002$ and $p = 0.0141$, respectively). RANKL/OPG ratio (E) showed higher values when compared to healthy group ($p = 0.0370$).

Tofacitinib, in this animal model, did not affect circulating levels of IL-1 β (F) and TNF (H). Results have also demonstrated a significant decrease in the serum quantification of IL-17 (I) ($p < 0.0001$) and a tendency towards a decrease of IL-6 (G). IL-1, TNF and IL-17 were normalized. Differences were considered statistically significant for p -values < 0.05 , according to the Mann Whitney tests. Healthy N=20, Arthritic N=20, Tofacitinib N=10.

Micro-CT

The effect of tofacitinib on inflammation-induced bone loss was assessed by micro-CT of cortical (Fig 4 A-C) and trabecular (Fig 4 D - I) bone tibia. Arthritic rats showed a reduction in cross-sectional area (A) and thickness (B) and tofacitinib

treatment did not restore these cortical changes ($p < 0.0001$ vs healthy controls, respectively). These bone changes affected the ability of bone's torsion as showed by decreased values of polar moment of inertia (C) in arthritic and tofacitinib group ($p = 0.0059$ and $p = 0.0197$ vs healthy controls, respectively). Trabecular bone also presented dramatic deterioration with arthritis as evidenced by a reduced trabecular bone volume fraction (D) ($p = 0.0007$ and $p < 0.0001$ vs healthy controls, respectively), thickness (E) and number (F) ($p < 0.0001$ vs healthy controls) and also by an increased trabecular separation (G) ($p < 0.0001$ in arthritic group and $p = 0.0002$ in tofacitinib group vs healthy controls) and porosity (H) ($p < 0.0001$ vs healthy controls). Furthermore, structure model index (I) showed declined values in arthritic and tofacitinib group ($p < 0.0001$ vs healthy controls, respectively) indicating that trabeculae shape was rather rod-like compared to plate-like shape in healthy controls.

Tofacitinib could not rescue trabecular bone integrity and trabecular bone properties in treated rats (Fig.4J).

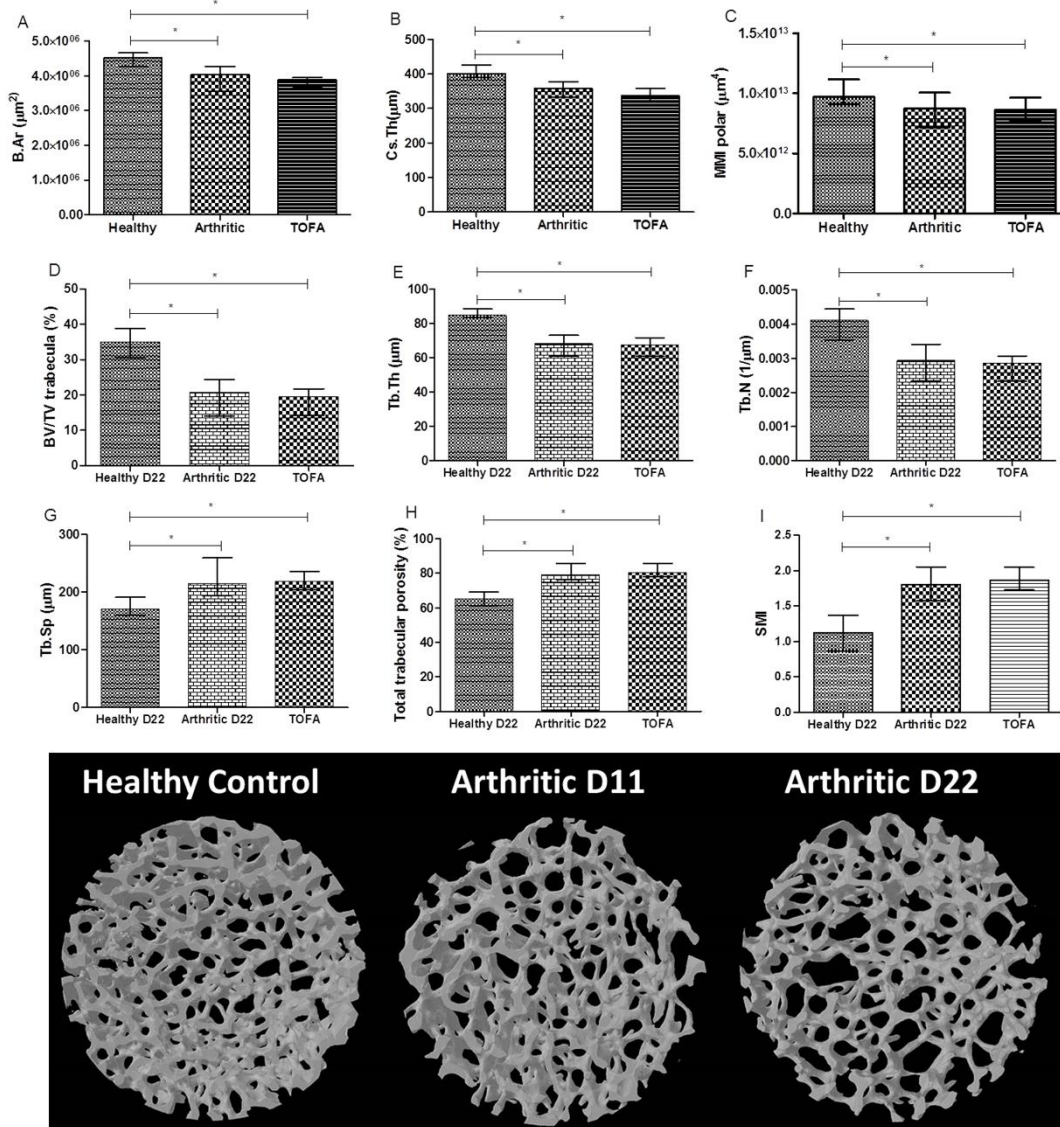


Fig. 4 – Micro-computed tomography (micro-CT) analysis of tibiae rat sample.

The arthritic and tofacitinib groups showed decreased values for cortical cross-sectional bone area (A), thickness (B) and polar moment of inertia (C) when compared to healthy controls. Trabecular bone also showed lower values of ratio bone volume/tissue volume (D), trabecular thickness (E) and number (F) in comparison with healthy controls. Arthritic and tofacitinib rats demonstrated higher values of trabecular separation (G) and porosity (H) when compared to healthy controls. Structural model index showed decreased values in arthritic and tofacitinib rats in comparison to healthy rats. MicroCT images from healthy, arthritic untreated and tofacitinib tibiae rats (J). Images acquired with SkyScan 1272, Bruker microCT, Kontich, Belgium. Differences were considered statistically significant for p -values < 0.05 , according to the Mann–Whitney tests. Healthy $N=20$, Arthritic $N=20$, Tofacitinib $N=10$.

Three-point bending

Tissue-level mechanical properties of rat femurs were evaluated using 3-point bending mechanical test at the end of the experiment. As shown in Fig. 5, arthritic rats revealed decreased mechanical properties at yield point, namely displacement ($p=0.0192$ vs healthy controls, Fig 5A), strength ($p=0.0229$ vs healthy control, Fig 5B) and pre yield energy (elastic energy) ($p=0.0161$ vs healthy controls, Fig 5C). These results showed that arthritic bones started to accumulate micro fractures with smaller deformations and lower loads, leading to a decreased energy absorption capability at yield point. Tofacitinib treated rats showed a significant decreased displacement ($p=0.0039$ vs healthy controls, Fig 5D) and elastic properties ($p=0.0443$ vs healthy controls, Fig 5E) at fracture point, meaning that there was a lower deformation (related to decreased elastic properties) during the plastic phase, before the total fracture of bone. Results also demonstrated that arthritic and tofacitinib rats had decreased maximum load ($p= 0.0017$ vs healthy controls, Fig 5F). Finally, arthritic rats and the tofacitinib treated group showed a significant decrease in toughness ($p=0.0143$ and $p=0.0048$ vs healthy controls, respectively, Fig 5G), demonstrating that arthritic and tofacitinib-treated bone could absorb less energy before fracturing.

Altogether, mechanical data revealed that arthritic and tofacitinib groups had significantly lower mechanical properties as compared to healthy controls, meaning that tofacitinib was unable to abrogate the structural deterioration during the time frame of treatment observed in this animal model.

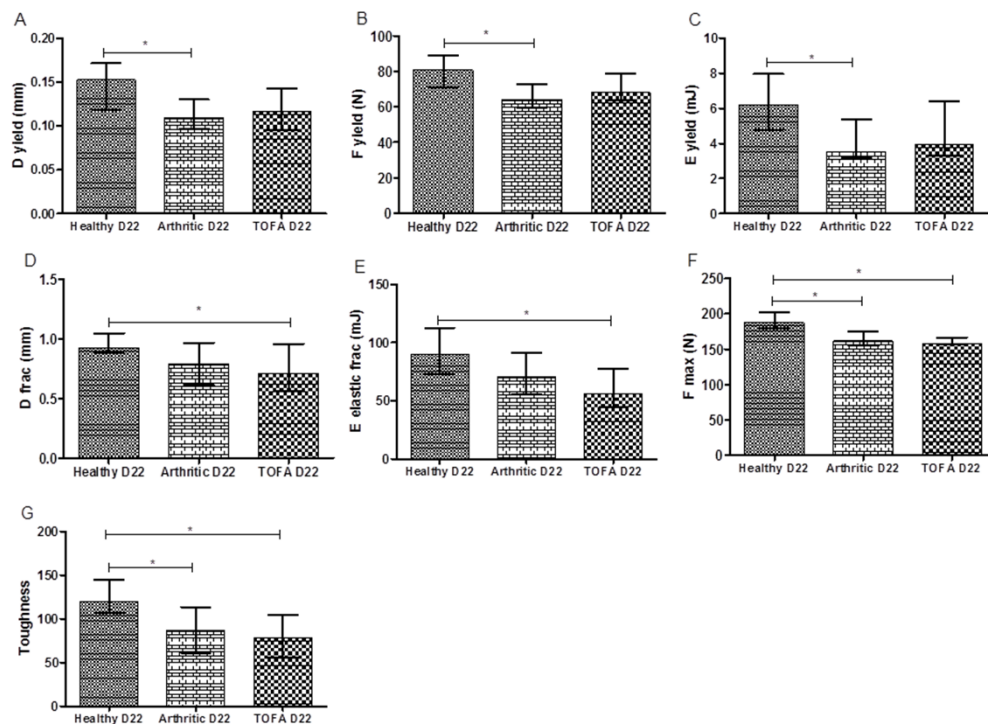


Fig. 5 – Bone mechanical properties assessed by three-point bending tests in rat femur at 22 days post disease induction.

Results showed that arthritic rats have decreased properties at yield point, related to displacement (A), strength (B) and pre yield energy (elastic energy) (C). Tofacitinib treated rats had a significant decrease in displacement (D) and elastic properties (E) at fracture point. Arthritic and tofacitinib treated bones required a lower maximum load (F) to fracture and a decreased toughness (G) was observed. Differences were considered statistically significant for p -values < 0.05 , according to the Mann–Whitney tests. Healthy $N=20$, Arthritic $N=20$, Tofacitinib $N=10$.

Tofacitinib increased bone hardness

Nanoindentation was performed in order to assess the quality at tissue matrix level and this technique can be used at the level of a single trabecula or within a confined submicron area of the cortical bone tissue.

Nano-mechanical tests revealed that arthritic rats had decreased hardness in cortical (Fig. 6A) and trabecular bone (Fig. 6B) ($p= 0.0010$ and $p= 0.0080$ in arthritic rats vs healthy controls, respectively). In contrast, rats treated with tofacitinib showed restored hardness in cortical bone (Fig. 6A) and increased hardness in trabecular (Fig. 6B) bone ($p=0.0003$ and $p=0.0012$ vs untreated

arthritic rats, respectively). No differences were observed in the other parameters analyzed.

Topographic images gathered during nanoindentation allowed the characterization of bone histologic features from healthy animals, arthritic untreated animals and tofacitinib treated animals after 22 days of disease induction.

Concentric lamellas were identified in secondary osteons (SO) and more frequently observed in arthritic animals (Fig.6 F) than in healthy controls ($p=0.0022$) and tofacitinib treated animals ($p=0.0043$) (Fig. 6C). On the contrary, healthy animals (Fig. 6 E) and tofacitinib treated animals (Fig. 6 G) presented more parallel-lamellae (PL) structures than concentric lamellas.

In addition, arthritic animals showed an increased area occupied by osteocyte lacunae in the total tissue when compared to healthy animals and tofacitinib treated animals (Fig. 6D) ($p=0.0067$, $p=0.0011$, respectively).

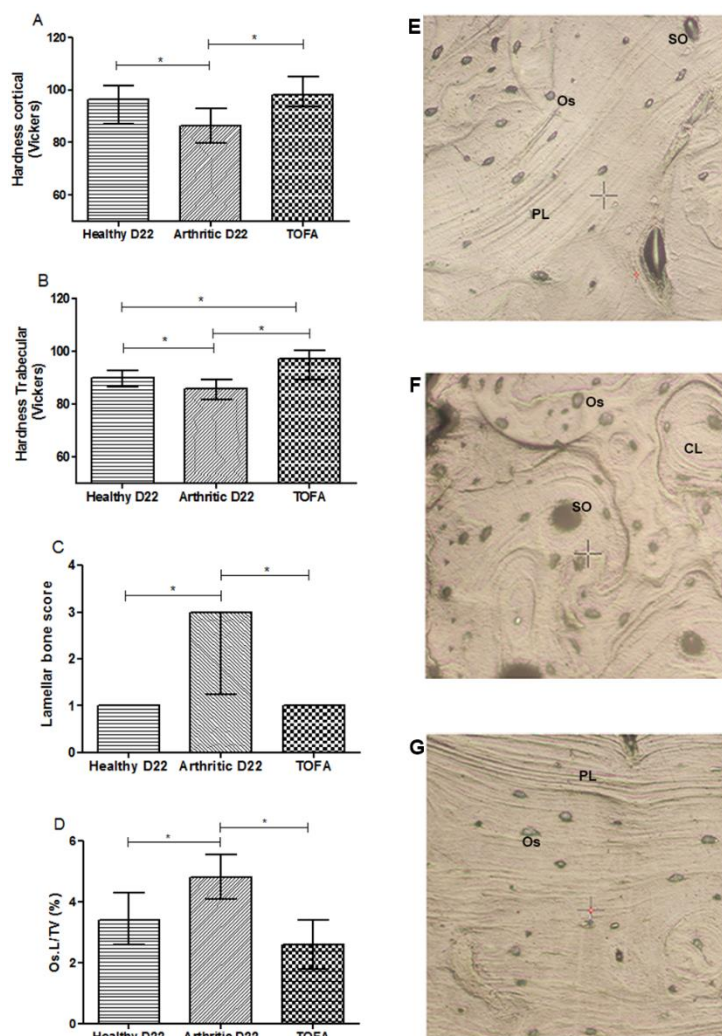


Fig. 6 – Bone mechanical properties assessed by nanoindentation in rat femur at 22 days post disease induction and respective topographic images from the indentation tissue area. Nano-mechanical tests revealed a decreased cortical (A) and trabecular (B) hardness in arthritic group at day 22 when compared to healthy rats. Of notice, rats treated with tofacitinib showed increased hardness in cortical (A) and trabecular (B) bone in comparison with untreated arthritic rats. Results demonstrated that the number of concentric lamellae (C) and ratio of area occupied by osteocyte lacunae in the total tissue (D) were higher when compared to healthy controls and tofacitinib treated groups at day 22.

Images are merely illustrative of the type of histological features observed. Concentric lamellas were identified in secondary osteons (SO), characteristic from arthritic animals (F). On the contrary, parallel-lamellae (PL) were identified in healthy controls (E) and tofacitinib treated groups (G). Os – Osteocytes, SO – Secondary osteons, PL – Parallel-lamellae, CL – Concentric lamellas. Magnification 20X. Differences were considered statistically significant for p-values<0.05, according to the Mann–Whitney tests. Healthy N=20, Arthritic N=20, Tofacitinib N=10.

DISCUSSION

In this study, we used the AIA rat model to evaluate the efficacy of tofacitinib to treat inflammation as well as inflammation-induced bone damage. Tofacitinib showed significantly reduced arthritis manifestations, synovial tissue inflammation and bone erosions, which was associated with lower serum RANKL and OPG levels. These results are in line with previous observations [23].

The effects of tofacitinib on pro-inflammatory cytokines production were assessed through serum quantification of IL-1 β , IL-6, IL-17 and TNF. Our study depicted decreased levels of IL-17 in AIA rats under tofacitinib treatment in comparison with untreated arthritic animals. In addition, we have observed a tendency towards a decrease in serum IL-6 concentration in tofacitinib treated rats. These observations are expected by tofacitinib inhibition of the JAK and STAT3 pathways [15, 24-26]. Tofacitinib did not affect circulating levels of TNF or IL-1 β comparing with untreated arthritic rats, but this might be related to the relatively low circulating levels of these cytokines in this animal model [23].

Biochemical markers of bone turnover were quantified in order to evaluate the impact of tofacitinib on bone metabolism. A reduced bone turnover was shown in tofacitinib treated animals, as depicted by decreased CTX-I and P1NP levels.

At tissue level, measured by nanoindentation, tofacitinib increased bone cortical and trabecular hardness. On the contrary, arthritic animals showed decreased values of hardness after 22 days post disease induction. We also observed at day 11 and 22 post arthritis induction concentric lamellas in secondary osteons (SO) microstructures resulting from high bone remodeling, as previously described [13, 27, 28]. Dall'Ara *et al.* suggested that larger numbers of this younger, less mineralized and less hard structures, could be related to reduced hardness of bone tissue identified by nanoindentation. On the contrary, healthy and tofacitinib treated animals presented more parallel-lamellae (PL) structures than concentric lamellas in SO structures and this PL structures are 10% more harder than the former, representing the mature bone structure (and normal bone remodeling) [28]. In addition, arthritic animals had an increased area occupied by osteocyte lacunae in total tissue. Tofacitinib treated animals, on the contrary, had a normal number of osteocytes lacunae and of the lacunae area per tissue volume. Osteocytes are responsible for the maintenance of the bone homeostasis, regulating the behavior of osteoblasts and osteoclasts by communicating through gap junctions [29]. Although no previous data is available in the context of arthritis some studies revealed that osteocytes from osteoarthritis patients have an irregular morphology, with limited ability to reply to mechanical stimuli, leading to significant changes in the structure and mineral density [30]. Despite being still unclear, this apparent change of osteocyte morphology in arthritic bone might contribute to the nanomechanical changes observed in this context.

Micro-CT and 3-point bending tests revealed that tofacitinib did not revert the effects of arthritis on cortical and trabecular bone structure and mechanical properties. There are several possible explanations for these observations. Using this same animal model we were able to revert the structural and mechanical damage induced by arthritis using an experimental compound [17]. However, the kinetics of the effects of tofacitinib might be different, needing more exposure time to have an impact on bone quality. The effect at a tissue level might be an early sign of its delayed impact on bone. Of interest, an increase in hardness is associated with a decrease in the relative ratio of elastic-to-plastic behavior of the tissue and thus it is unclear if it represents ultimately a true improvement in

mechanical properties. Another explanation might be related with the mechanism of action. Tofacitinib targets JAK1 and 3, downregulating STAT 1 and 3 of the JAK-STAT signaling pathway [15, 16, 23], and these intracellular molecules have complex interactions with bone. JAK1 is expressed in bone cells and is involved in bone formation. The depletion of JAK1 promotes bone growth delays, suggesting that JAK1 is critical for skeletal development. On the other hand, STAT1 inhibits Runx2 transcription in osteoblasts, the master transcription factor of osteoblast differentiation. Thus, STAT1 is an inhibitor of differentiation of osteoblasts and the inactivation of STAT1 leads to an osteopetrotic bone phenotype [31]. Consistent with the higher bone mass in STAT1-deficient mice, inactivation of STAT1 can accelerate fracture repair [32]. These data suggest that STAT1 negatively regulates bone formation in vivo [33]. On the contrary, JAK-STAT3 signal transduction pathway promotes osteoblast differentiation [33]. Inactivation of STAT3 in osteoblasts leads to lower bone mass due to inhibition of bone formation. In humans, STAT3 mutations reduce bone mass and increase incidence of minimal trauma fractures. Clinical studies indicate that STAT3 mutations increase osteoclast number and bone resorption, and are associated with recurrent fractures.

It is conceivable that these types of molecular interactions with bone have an overall effect that might not be totally compensated by the benefits on bone obtained by the control of inflammation. To fully clarify these open questions it will be relevant to test several doses of tofacitinib in longer duration arthritis models and in healthy animals.

KEY MESSAGES

- Tofacitinib was able to control and suppress inflammatory activity in an AIA rat model of arthritis.
- Tofacitinib was not able to revert structural and mechanical bone changes promoted by inflammation.
- JAK-STAT pathway inhibition downregulates several targets which may not be totally beneficial for bone homeostasis.

REFERENCES

1. Alamanos Y, Drosos AA. Epidemiology of adult rheumatoid arthritis. *Autoimmun Rev* 2005; 4: 130-136.
2. Yelin E, Callahan LF. The economic cost and social and psychological impact of musculoskeletal conditions. National Arthritis Data Work Groups. *Arthritis Rheum* 1995; 38: 1351-1362.
3. Lin YY, Jean YH, Lee HP et al. A soft coral-derived compound, 11-epi-sinulariolide acetate suppresses inflammatory response and bone destruction in adjuvant-induced arthritis. *PLoS One* 2013; 8: e62926.
4. Haugeberg G, Orstavik RE, Uhlig T et al. Bone loss in patients with rheumatoid arthritis: results from a population-based cohort of 366 patients followed up for two years. *Arthritis Rheum* 2002; 46: 1720-1728.
5. Marshall D, Johnell O, Wedel H. Meta-analysis of how well measures of bone mineral density predict occurrence of osteoporotic fractures. *BMJ* 1996; 312: 1254-1259.
6. Eric-Jan JA K. Bone mass in rheumatoid arthritis. *CLINICAL AND EXPERIMENTAL RHEUMATOLOGY* 2000.
7. Fonseca JE, Cortez-Dias N, Francisco A et al. Inflammatory cell infiltrate and RANKL/OPG expression in rheumatoid synovium: comparison with other inflammatory arthropathies and correlation with outcome. *Clin Exp Rheumatol* 2005; 23: 185-192.
8. Boyle WJ, Simonet WS, Lacey DL. Osteoclast differentiation and activation. *Nature* 2003; 423: 337-342.
9. Moura RA, Cascao R, Perpetuo I et al. Cytokine pattern in very early rheumatoid arthritis favours B-cell activation and survival. *Rheumatology (Oxford)* 2011; 50: 278-282.
10. Cascao R, Moura RA, Perpetuo I et al. Identification of a cytokine network sustaining neutrophil and Th17 activation in untreated early rheumatoid arthritis. *Arthritis Res Ther* 2010; 12: R196.
11. Caetano-Lopes J, Canhao H, Fonseca JE. Osteoimmunology--the hidden immune regulation of bone. *Autoimmun Rev* 2009; 8: 250-255.

12. Caetano-Lopes J, Rodrigues A, Lopes A et al. Rheumatoid arthritis bone fragility is associated with upregulation of IL17 and DKK1 gene expression. *Clin Rev Allergy Immunol* 2014; 47: 38-45.
13. Vidal B, Cascao R, Vale AC et al. Arthritis induces early bone high turnover, structural degradation and mechanical weakness. *PLoS One* 2015; 10: e0117100.
14. Tofacitinib. *Drugs R D* 2010; 10: 271-284.
15. Meyer DM, Jesson MI, Li X et al. Anti-inflammatory activity and neutrophil reductions mediated by the JAK1/JAK3 inhibitor, CP-690,550, in rat adjuvant-induced arthritis. *J Inflamm (Lond)* 2010; 7: 41.
16. Maeshima K, Yamaoka K, Kubo S et al. The JAK inhibitor tofacitinib regulates synovitis through inhibition of interferon-gamma and interleukin-17 production by human CD4+ T cells. *Arthritis Rheum* 2012; 64: 1790-1798.
17. Cascao R, Vidal B, Raquel H et al. Effective treatment of rat adjuvant-induced arthritis by celestrol. *Autoimmun Rev* 2012; 11: 856-862.
18. Bouxsein ML, Boyd SK, Christiansen BA et al. Guidelines for assessment of bone microstructure in rodents using micro-computed tomography. *J Bone Miner Res* 2010; 25: 1468-1486.
19. Herlin M, Finnila MA, Zioupos P et al. New insights to the role of aryl hydrocarbon receptor in bone phenotype and in dioxin-induced modulation of bone microarchitecture and material properties. *Toxicol Appl Pharmacol* 2013; 273: 219-226.
20. Zhang R, Gong H, Zhu D et al. Multi-level femoral morphology and mechanical properties of rats of different ages. *Bone* 2015; 76: 76-87.
21. W.C. Oliver GMP. An improved technique for determining hardness and elastic modulus using load and displacement sensing indentation experiments. In. 1992.
22. Parfitt AM, Drezner MK, Glorieux FH et al. Bone histomorphometry: standardization of nomenclature, symbols, and units. Report of the ASBMR Histomorphometry Nomenclature Committee. *J Bone Miner Res* 1987; 2: 595-610.
23. LaBranche TP, Jesson MI, Radi ZA et al. JAK inhibition with tofacitinib suppresses arthritic joint structural damage through decreased RANKL production. *Arthritis Rheum* 2012; 64: 3531-3542.

24. Milici AJ, Kudlacz EM, Audoly L et al. Cartilage preservation by inhibition of Janus kinase 3 in two rodent models of rheumatoid arthritis. *Arthritis Res Ther* 2008; 10: R14.
25. Tanaka Y, Maeshima K, Yamaoka K. In vitro and in vivo analysis of a JAK inhibitor in rheumatoid arthritis. *Ann Rheum Dis* 2012; 71 Suppl 2: i70-74.
26. Tanaka Y, Yamaoka K. JAK inhibitor tofacitinib for treating rheumatoid arthritis: from basic to clinical. *Mod Rheumatol* 2013; 23: 415-424.
27. Bailey AJ, Mansell JP, Sims TJ, Banse X. Biochemical and mechanical properties of subchondral bone in osteoarthritis. *Biorheology* 2004; 41: 349-358.
28. Dall'Ara E, Ohman C, Baleani M, Viceconti M. Reduced tissue hardness of trabecular bone is associated with severe osteoarthritis. *J Biomech* 2011; 44: 1593-1598.
29. Taylor AF, Saunders MM, Shingle DL et al. Mechanically stimulated osteocytes regulate osteoblastic activity via gap junctions. *Am J Physiol Cell Physiol* 2007; 292: C545-552.
30. Jaiprakash A, Prasadam I, Feng JQ et al. Phenotypic characterization of osteoarthritic osteocytes from the sclerotic zones: a possible pathological role in subchondral bone sclerosis. *Int J Biol Sci* 2012; 8: 406-417.
31. Kim S, Koga T, Isobe M et al. Stat1 functions as a cytoplasmic attenuator of Runx2 in the transcriptional program of osteoblast differentiation. *Genes Dev* 2003; 17: 1979-1991.
32. Tajima K, Takaishi H, Takito J et al. Inhibition of STAT1 accelerates bone fracture healing. *J Orthop Res* 2010; 28: 937-941.
33. Zhou Y, Tan L, Que Q et al. Study of association between HLA-DR4 and DR53 and autoantibody detection in rheumatoid arthritis. *J Immunoassay Immunochem* 2013; 34: 126-133.

Chapter IV

Discussion

Discussion

In this thesis we have shown that very early in the arthritis course bone tissue changes occur, with implications for nano and micro structural and mechanical properties. We have also demonstrated that early intervention with compounds that control inflammation and interfere with bone metabolism can abrogate arthritic nano and micro bone damage.

All observations were obtained in the most widely used arthritis animal model AIA [246,247] for research and drug development in the field of RA [248-256]. Overall, this arthritic model has been the most widely used by the pharmaceutical industry to test both activity and toxicity of new compounds [254]. Moreover, this arthritic model share key features with human RA [246,247], such as peripheral, symmetrical and destructive joint inflammation with synovial hyperplasia due to inflammatory cell infiltration, homing of macrophages, increased levels of synovial cytokines such as IL-1 β , IL-6 and TNF and marginal erosions. In addition, this model is genetically regulated by MHC and non-MHC genes and is responsive to most therapies that are effective in RA [257]. However, some fundamental aspects of human RA are not replicated in this AIA rat model, such as the presence of RF and synovial lymphoid follicles [257]. The AIA rat model, when compared with other models of arthritis, such as CIA model, clearly exhibits the greatest magnitude of disease, as evaluated by edema, immune cell infiltration, cartilage and bone markers and cytokine levels [258].

In the AIA model the initial acute inflammation is observed around day 3 post disease induction with a swelling of the induced joint and disease progresses up to day 19 [69,258]. We have shown that the sublining layer infiltration, the number of lining layer cells, bone erosions and cartilage surface damage are present at least since day 11 post disease induction. Moreover, we depicted that IL-6 levels, increased around day 11 after disease induction, paralleling what actually happens in RA patients, where IL-6 is also increased in serum since the early stages of arthritis [259]. Of interest, increased levels of IL-6 promote osteoclastogenesis, which may interfere with bone remodeling [260]. Indeed, AIA animals showed an increased bone turnover, as depicted by increased CTX-I and P1NP levels since

the early stages of arthritis. This observation is consistent with previously published data showing the presence of large a number of osteoclasts in the AIA bone [261]. Studies on RA patients measuring P1NP have produced varying results, whereas measurements of CTX-I mostly showed increased levels [262]. In RA patients, bone metabolism is more active (increased P1NP) in earlier stages of the disease and a decrease in bone metabolic activity (both P1NP and CTX) occurs with disease progression [263].

Bone histology was consistent with this early onset spur of bone remodeling. In fact, arthritic animals at day 11 and 22 post disease induction, showed concentric lamellas in secondary osteons (SO), which are the consequence of intense bone remodeling [68-70]. On the contrary, healthy animals presented more parallel-lamellae (PL) structures than SO structures and this PL structures are 10% harder than SO, representing the mature bone structure (associated with normal bone remodeling) [70]. We have shown that arthritic bone tissue is composed of a larger number of younger, less mineralized and less hard structures than healthy bone, contributing to the reduced hardness that we have observed by nanoindentation. Moreover, an increased area occupied by osteocyte lacunae was detected early on in the arthritis process. Osteocytes are responsible for the maintenance of bone homeostasis, regulating the behavior of osteoblasts and osteoclasts [264]. Although no previous data is available in the context of arthritis some studies revealed that osteocytes from osteoarthritis patients have an irregular morphology, with limited ability to reply to mechanical stimuli, leading to significant changes in the structure and mineral density [265]. Despite being still unclear, this apparent change of osteocyte morphology in arthritic bone might contribute to the structural and mechanical changes observed in this context. Also, of interest, these morphological changes can be linked to increased osteocyte apoptosis, which could promote bone necrosis, leading to mineral loss, decreased hardness and possibly mechanical weakness.

Using Fourier transform infrared spectroscopy (FTIR) we demonstrated that arthritis induces mineral and collagen loss in trabecular bone since the early phase of arthritis development. Accordingly, we demonstrated mineral bone loss in arthritic animals using dual X-ray spectroscopy [69].

Bone nano-mechanical properties were assessed by nanoindentation in order to assess the quality of tissue matrix at nano level. This technique allows the analysis at the level of a single trabecula or within a confined submicron area of the cortical bone tissue. Results showed decreased cortical and trabecular hardness in arthritic rats since the early phase of arthritis. At a higher organizational level, micro-CT revealed in arthritic animals a lower fraction of cortical cross-sectional bone area and trabecular bone volume with reduced trabecular thickness as well as a higher trabecular separation, in comparison with controls. Results also demonstrated cortical differences in the polar moment of inertia, suggesting mechanical weakness in the arthritic groups since the early phase of arthritis. Furthermore, cortical and trabecular porosity was increased in the arthritic groups compared to healthy controls. Structure model index also showed increased values in arthritic groups at day 11 and 22 post disease induction indicating that the shape of trabeculae was rod-like rather than plate-like as observed in healthy controls, suggesting a more fragile architecture. We also confirmed these observations by classic histomorphometry, which demonstrated a decreased structural integrity in arthritic animals [69]. We and others have demonstrated this pattern of microarchitectural bone degradation after long standing arthritis [266-269].

Coherent with these structural defects, our results also showed that in very early arthritis bone has low mechanical competence, as can be inferred by the decrease of all mechanical parameters related with yield point, such as elasticity, strength and displacement. Arthritic bones start to accumulate micro fractures with smaller deformations and loads, leading to a decreased capacity to absorb energy at yield point, promoting disturbances in bone behavior through the decrease of maximum load and the absorbed energy before fracture.

Altogether, these results revealed that inflammation promotes bone nano and micro structural disturbances, leading to bone fragility since the early stages of arthritis. In addition, we also provided the basis for using the AIA animal model of arthritis as an adequate model for studying the impact of inflammation on bone and for assessing candidate compounds for the control of arthritis and its associated bone damage.

RA is still a chronic unremitting and progressive disease for most of the affected patients, who suffer the structural burden of this condition at the level of joints and of skeletal bone. The quest for new RA treatments, more effective at inflammation and bone damage control, safer and less expensive continues.

In a previous study from our group we have used a THP-1 macrophage-like cell line to screen 2320 compounds for those that down-regulate both IL-1 β and TNF secretion. Celastrol was one of the most promising therapeutic candidates identified in that study [270]. We demonstrated for the first time that celastrol was able to treat AIA rats, possibly through TNF and IL-1 β inhibition. This compound showed significant anti-inflammatory and anti-proliferative properties, promoting a complete suppression of arthritis development and abrogating joint immune cellular infiltration and proliferation [270].

We have now demonstrated that celastrol was able to reduce the number of synovial B and T-cells as well as fibroblasts and CD68 macrophages [271]. CD68 macrophages are responsible for synovial inflammation and are also critical in osteoclast differentiation [272]. Their numbers are correlated with erosions in RA patients and are an important biomarker for the evaluation of the possible effectiveness of new drugs for RA [273,274]. Additionally, we demonstrated that celastrol decreases the number of osteoclasts and osteoblasts present in joint tissue [271].

We had previously shown that celastrol inhibits NF- κ B activation *in vitro* [270]. NF- κ B activation is crucial for osteoclastogenesis and is upstream activated by the engagement of RANKL with RANK. In addition, it has already been shown *in vitro* that celastrol reduces other osteoclastic mediators besides RANKL, such as granulocyte-macrophage colony-stimulating factor (GM-CSF), insulin-like growth factor (IGF) and osteopontin (OPN), suggesting a shift of bone remodeling in favor of an anti-osteoclastic activity [275]. Finally, also in line with our data, it has been reported that celastrol reduces osteoclast numbers and bone loss in bone metastasis and ovariectomy-induced bone loss models, and preserves trabecular architecture [276,277].

Accordingly, we showed that celastrol protects cartilage and bone from inflammation-induced focal damage. In addition, at a systemic level there was a reduction in serum levels of TRACP-5b, P1NP and OPG observed in arthritic rats

treated with celestrol, suggesting a reduction in bone turnover. In addition, micro-CT analysis showed that celestrol treatment was able to protect bone structure, preventing bone loss and mechanical tests depicted a preservation of bone mechanical properties. These results suggest that early celestrol treatment can prevent bone fragility. Moreover, celestrol therapy showed superior effects if administrated in an early phase of arthritis development, which highlights the importance of early treatment to limit inflammation-induced bone damage.

We have also used the AIA rat model to evaluate the efficacy of tofacitinib to treat inflammation as well as inflammation-induced bone damage. Tofacitinib showed significantly reduced arthritis manifestations, synovial tissue inflammation and bone erosions, which was associated with lower serum RANKL and OPG levels. These results were in line with previous observations, suggesting that the JAK inhibitor tofacitinib suppresses osteoclast-mediated structural damage to arthritic joints and that this effect is secondary to decreased RANKL production [278]. Biochemical markers of bone turnover were also quantified in order to evaluate the impact of tofacitinib on bone metabolism. A reduced bone turnover was shown in tofacitinib treated animals, as depicted by decreased CTX-I and P1NP levels. Accordingly, tofacitinib treated animals presented more parallel-lamellae structures and less area occupied by osteocyte lacunae in total tissue than untreated animals. At tissue level, measured by nanoindentation, tofacitinib increased bone cortical and trabecular hardness. However, micro-CT and 3-point bending tests revealed that tofacitinib did not revert the effects of arthritis on cortical and trabecular bone structure and mechanical properties.

There are several possible explanations for these observations. We were able to revert the structural and mechanical damage induced by arthritis using celestrol [270]. However, the kinetics of the effects of tofacitinib might be different, needing a longer exposure time to have an impact on bone quality. On the other hand, the increase in hardness is associated with a decrease in the relative ratio of elastic-to-plastic behavior of the tissue and thus it is unclear if it represents, per se, a true improvement in mechanical properties. This is why another explanation for the differences between celestrol and tofacitinib micro structural and mechanical results might be related to tofacitinib's mechanism of action. Tofacitinib targets

JAK1 and 3, downregulating STAT 1 and 3 of the JAK-STAT signaling pathway [278-280], and these intracellular molecules have complex interactions with bone. JAK1 is expressed in bone cells and is involved in bone formation. The depletion of JAK1 promotes bone growth delays, suggesting that JAK1 is critical for skeletal development. On the other hand, STAT1 inhibits runt-related transcription factor 2 (Runx2) in osteoblasts, the master transcription factor of osteoblast differentiation. Thus, STAT1 is an inhibitor of differentiation of osteoblasts and the inactivation of STAT1 leads to an osteopetrotic bone phenotype [281]. Consistent with the higher bone mass in STAT1-deficient mice, inactivation of STAT1 can accelerate fracture repair [282]. These data suggest that STAT1 negatively regulates bone formation in vivo [283]. On the contrary, JAK-STAT3 signal transduction pathway promotes osteoblast differentiation and inactivation of STAT3 in osteoblasts leads to lower bone mass due to inhibition of bone formation. In humans, STAT3 mutations reduce bone mass and increase incidence of minimal trauma fractures [283]. Clinical studies indicate that STAT3 mutations increase osteoclast number and bone resorption, and are associated with recurrent fractures. It is conceivable that these types of molecular interactions with bone have an overall effect that might not be totally compensated by the benefits on bone resulting from the control of inflammation. To fully clarify these open questions it will be relevant to test several doses of tofacitinib in longer duration arthritis models and in healthy animals.

Chapter V

Conclusion

Conclusion

We have shown that the impact of inflammation on bone micro and nano properties occurs almost immediately, upon first symptoms, and that these effects can be prevented by early intervention with drugs that control inflammation and interfere with bone metabolism.

In particular, celestrol was able to abrogate the inflammatory signs in the AIA rat model and to significantly preserve bone structure and mechanics, and thus may deserve future clarification of its potential to enter phase I clinical trials for the treatment of RA. Tofacitinib was also able to control inflammation, however it did not revert the effects of arthritis on cortical and trabecular bone structure and mechanical properties. Possible reasons for these observations might be related with the mechanism of action of tofacitinib and/or with kinetics of its bone effects that might need longer treatment exposure. As tofacitinib is already available for clinical use in some countries its possible effects on bone density and quality of RA patients should be clarified.

References

1. McInnes IB, Schett G (2007) Cytokines in the pathogenesis of rheumatoid arthritis. *Nat Rev Immunol* 7: 429-442.
2. Abramson SB, Amin A (2002) Blocking the effects of IL-1 in rheumatoid arthritis protects bone and cartilage. *Rheumatology (Oxford)* 41: 972-980.
3. Alamanos Y, Drosos AA (2005) Epidemiology of adult rheumatoid arthritis. *Autoimmun Rev* 4: 130-136.
4. Michaud K, Wolfe F (2007) Comorbidities in rheumatoid arthritis. *Best Pract Res Clin Rheumatol* 21: 885-906.
5. McInnes IB, Schett G (2011) The pathogenesis of rheumatoid arthritis. *N Engl J Med* 365: 2205-2219.
6. ED H (2001) Clinical features of rheumatoid arthritis. Philadelphia: WB Saunders.
7. Gonzalez-Juanatey C, Llorca J, Testa A, Revuelta J, Garcia-Porrúa C, et al. (2003) Increased prevalence of severe subclinical atherosclerotic findings in long-term treated rheumatoid arthritis patients without clinically evident atherosclerotic disease. *Medicine (Baltimore)* 82: 407-413.
8. Meyer O (2001) Atherosclerosis and connective tissue diseases. *Joint Bone Spine* 68: 564-575.
9. Cojocaru M, Cojocaru IM, Silosi I, Vrabie CD, Tanasescu R (2010) Extra-articular Manifestations in Rheumatoid Arthritis. *Maedica (Buchar)* 5: 286-291.
10. Akpek EK, Klimava A, Thorne JE, Martin D, Lekhanont K, et al. (2009) Evaluation of patients with dry eye for presence of underlying Sjogren syndrome. *Cornea* 28: 493-497.
11. Gonzalez A, Icen M, Kremers HM, Crowson CS, Davis JM, 3rd, et al. (2008) Mortality trends in rheumatoid arthritis: the role of rheumatoid factor. *J Rheumatol* 35: 1009-1014.
12. P E (2011) Pocket Reference to Early Rheumatoid Arthritis. London: Springer Healthcare Ltd.
13. Gabriel SE, Crowson CS, Campion ME, O'Fallon WM (1997) Indirect and nonmedical costs among people with rheumatoid arthritis and osteoarthritis compared with nonarthritic controls. *J Rheumatol* 24: 43-48.
14. Scott DL, Wolfe F, Huizinga TW (2010) Rheumatoid arthritis. *Lancet* 376: 1094-1108.
15. Branco JC, Rodrigues AM, Gouveia N, Eusebio M, Ramiro S, et al. (2016) Prevalence of rheumatic and musculoskeletal diseases and their impact on health-related quality of life, physical function and mental health in Portugal: results from EpiReumaPt- a national health survey. *RMD Open* 2: e000166.
16. Laires PA, Gouveia M, Canhao H, Branco JC (2016) The economic impact of early retirement attributed to rheumatic diseases: results from a nationwide population-based epidemiologic study. *Public Health*.
17. Chantal Simon HE, Françoise van (2014) Oxford Handbook of General Practice: Oxford University Press.
18. Bugatti S, Manzo A, Caporali R, Montecucco C (2012) Assessment of synovitis to predict bone erosions in rheumatoid arthritis. *Ther Adv Musculoskelet Dis* 4: 235-244.
19. McQueen FM, Stewart N, Crabbe J, Robinson E, Yeoman S, et al. (1998) Magnetic resonance imaging of the wrist in early rheumatoid arthritis reveals a high prevalence of erosions at four months after symptom onset. *Ann Rheum Dis* 57: 350-356.
20. McGonagle D, Conaghan PG, O'Connor P, Gibbon W, Green M, et al. (1999) The relationship between synovitis and bone changes in early untreated rheumatoid arthritis: a controlled magnetic resonance imaging study. *Arthritis Rheum* 42: 1706-1711.
21. Arnett FC, Edworthy SM, Bloch DA, McShane DJ, Fries JF, et al. (1988) The American Rheumatism Association 1987 revised criteria for the classification of rheumatoid arthritis. *Arthritis Rheum* 31: 315-324.

22. Aletaha D, Neogi T, Silman AJ, Funovits J, Felson DT, et al. (2010) 2010 Rheumatoid arthritis classification criteria: an American College of Rheumatology/European League Against Rheumatism collaborative initiative. *Arthritis Rheum* 62: 2569-2581.
23. Caetano-Lopes J, Rodrigues A, Lopes A, Vale AC, Pitts-Kiefer MA, et al. (2014) Rheumatoid arthritis bone fragility is associated with upregulation of IL17 and DKK1 gene expression. *Clin Rev Allergy Immunol* 47: 38-45.
24. Unnanuntana A, Gladnick BP, Donnelly E, Lane JM (2010) The assessment of fracture risk. *J Bone Joint Surg Am* 92: 743-753.
25. Kanis JA, McCloskey EV, Johansson H, Oden A, Strom O, et al. (2010) Development and use of FRAX in osteoporosis. *Osteoporos Int* 21 Suppl 2: S407-413.
26. Choy E (2012) Understanding the dynamics: pathways involved in the pathogenesis of rheumatoid arthritis. *Rheumatology (Oxford)* 51 Suppl 5: v3-11.
27. Gough SC, Simmonds MJ (2007) The HLA Region and Autoimmune Disease: Associations and Mechanisms of Action. *Curr Genomics* 8: 453-465.
28. Lanchbury JS (1992) The HLA association with rheumatoid arthritis. *Clin Exp Rheumatol* 10: 301-304.
29. Ligeiro D, Fonseca JE, Abade O, Abreu I, Cruz M, et al. (2007) Influence of human leucocyte antigen-DRB1 on the susceptibility to rheumatoid arthritis and on the production of anti-cyclic citrullinated peptide antibodies in a Portuguese population. *Ann Rheum Dis* 66: 246-248.
30. Gregersen PK, Silver J, Winchester RJ (1987) The shared epitope hypothesis. An approach to understanding the molecular genetics of susceptibility to rheumatoid arthritis. *Arthritis Rheum* 30: 1205-1213.
31. Blass S, Engel JM, Burmester GR (1999) The immunologic homunculus in rheumatoid arthritis. *Arthritis Rheum* 42: 2499-2506.
32. Edwards CJ, Cooper C (2006) Early environmental factors and rheumatoid arthritis. *Clin Exp Immunol* 143: 1-5.
33. Symmons DP, Bankhead CR, Harrison BJ, Brennan P, Barrett EM, et al. (1997) Blood transfusion, smoking, and obesity as risk factors for the development of rheumatoid arthritis: results from a primary care-based incident case-control study in Norfolk, England. *Arthritis Rheum* 40: 1955-1961.
34. Klareskog L, Stolt P, Lundberg K, Kallberg H, Bengtsson C, et al. (2006) A new model for an etiology of rheumatoid arthritis: smoking may trigger HLA-DR (shared epitope)-restricted immune reactions to autoantigens modified by citrullination. *Arthritis Rheum* 54: 38-46.
35. Gerlag DM, Norris JM, Tak PP (2016) Towards prevention of autoantibody-positive rheumatoid arthritis: from lifestyle modification to preventive treatment. *Rheumatology (Oxford)* 55: 607-614.
36. Harris ED, Jr. (1990) Rheumatoid arthritis. Pathophysiology and implications for therapy. *N Engl J Med* 322: 1277-1289.
37. Lundy SK, Sarkar S, Tesmer LA, Fox DA (2007) Cells of the synovium in rheumatoid arthritis. T lymphocytes. *Arthritis Res Ther* 9: 202.
38. Kinne RW, Stuhlmuller B, Burmester GR (2007) Cells of the synovium in rheumatoid arthritis. Macrophages. *Arthritis Res Ther* 9: 224.
39. Janossy G, Panayi G, Duke O, Bofill M, Poulter LW, et al. (1981) Rheumatoid arthritis: a disease of T-lymphocyte/macrophage immunoregulation. *Lancet* 2: 839-842.
40. Klareskog L, Forsum U, Scheynius A, Kabelitz D, Wigzell H (1982) Evidence in support of a self-perpetuating HLA-DR-dependent delayed-type cell reaction in rheumatoid arthritis. *Proc Natl Acad Sci U S A* 79: 3632-3636.

41. Hemler ME, Glass D, Coblyn JS, Jacobson JG (1986) Very late activation antigens on rheumatoid synovial fluid T lymphocytes. Association with stages of T cell activation. *J Clin Invest* 78: 696-702.
42. Cush JJ, Lipsky PE (1988) Phenotypic analysis of synovial tissue and peripheral blood lymphocytes isolated from patients with rheumatoid arthritis. *Arthritis Rheum* 31: 1230-1238.
43. Johnson BA, Haines GK, Harlow LA, Koch AE (1993) Adhesion molecule expression in human synovial tissue. *Arthritis Rheum* 36: 137-146.
44. Morales-Ducret J, Wayner E, Elices MJ, Alvaro-Gracia JM, Zvaifler NJ, et al. (1992) Alpha 4/beta 1 integrin (VLA-4) ligands in arthritis. Vascular cell adhesion molecule-1 expression in synovium and on fibroblast-like synoviocytes. *J Immunol* 149: 1424-1431.
45. Yoshida Y, Tanaka T (2014) Interleukin 6 and rheumatoid arthritis. *Biomed Res Int* 2014: 698313.
46. Cascao R, Moura RA, Perpetuo I, Canhao H, Vieira-Sousa E, et al. (2010) Identification of a cytokine network sustaining neutrophil and Th17 activation in untreated early rheumatoid arthritis. *Arthritis Res Ther* 12: R196.
47. Schett G (2007) Joint remodelling in inflammatory disease. *Ann Rheum Dis* 66 Suppl 3: iii42-44.
48. Feldmann M, Brennan FM, Maini RN (1996) Role of cytokines in rheumatoid arthritis. *Annu Rev Immunol* 14: 397-440.
49. Ademowo OS, Staunton L, FitzGerald O, Pennington SR (2013) Biomarkers of Inflammatory Arthritis and Proteomics.
50. Strand V, Kimberly R, Isaacs JD (2007) Biologic therapies in rheumatology: lessons learned, future directions. *Nat Rev Drug Discov* 6: 75-92.
51. Rannou F, Francois M, Corvol MT, Berenbaum F (2006) Cartilage breakdown in rheumatoid arthritis. *Joint Bone Spine* 73: 29-36.
52. Rediske JJ, Koehne CF, Zhang B, Lotz M (1994) The inducible production of nitric oxide by articular cell types. *Osteoarthritis Cartilage* 2: 199-206.
53. Goldring MB (1999) The role of cytokines as inflammatory mediators in osteoarthritis: lessons from animal models. *Connect Tissue Res* 40: 1-11.
54. Goldring MB, Suen LF, Yamin R, Lai WF (1996) Regulation of Collagen Gene Expression by Prostaglandins and Interleukin-1beta in Cultured Chondrocytes and Fibroblasts. *Am J Ther* 3: 9-16.
55. Saklatvala J (1986) Tumour necrosis factor alpha stimulates resorption and inhibits synthesis of proteoglycan in cartilage. *Nature* 322: 547-549.
56. Henderson B, Pettipher ER (1989) Arthritogenic actions of recombinant IL-1 and tumour necrosis factor alpha in the rabbit: evidence for synergistic interactions between cytokines in vivo. *Clin Exp Immunol* 75: 306-310.
57. Goldring MB, Birkhead J, Sandell LJ, Kimura T, Krane SM (1988) Interleukin 1 suppresses expression of cartilage-specific types II and IX collagens and increases types I and III collagens in human chondrocytes. *J Clin Invest* 82: 2026-2037.
58. Reginato AM, Sanz-Rodriguez C, Diaz A, Dharmavaram RM, Jimenez SA (1993) Transcriptional modulation of cartilage-specific collagen gene expression by interferon gamma and tumour necrosis factor alpha in cultured human chondrocytes. *Biochem J* 294 (Pt 3): 761-769.
59. Seckinger P, Yaron I, Meyer FA, Yaron M, Dayer JM (1990) Modulation of the effects of interleukin-1 on glycosaminoglycan synthesis by the urine-derived interleukin-1 inhibitor, but not by interleukin-6. *Arthritis Rheum* 33: 1807-1814.
60. Goldring SR (2003) Pathogenesis of bone and cartilage destruction in rheumatoid arthritis. *Rheumatology (Oxford)* 42 Suppl 2: ii11-16.

61. Goldring MB (2012) Chondrogenesis, chondrocyte differentiation, and articular cartilage metabolism in health and osteoarthritis. *Ther Adv Musculoskelet Dis* 4: 269-285.
62. Rhee DK, Marcelino J, Baker M, Gong Y, Smits P, et al. (2005) The secreted glycoprotein lubricin protects cartilage surfaces and inhibits synovial cell overgrowth. *J Clin Invest* 115: 622-631.
63. Gravallesse EM, Harada Y, Wang JT, Gorn AH, Thornhill TS, et al. (1998) Identification of cell types responsible for bone resorption in rheumatoid arthritis and juvenile rheumatoid arthritis. *Am J Pathol* 152: 943-951.
64. Clarke B (2008) Normal bone anatomy and physiology. *Clin J Am Soc Nephrol* 3 Suppl 3: S131-139.
65. Nih Consensus Development Panel on Osteoporosis Prevention D, Therapy (2001) Osteoporosis prevention, diagnosis, and therapy. *JAMA* 285: 785-795.
66. ADLER CP (2000) Bones and bone tissue; normal anatomy and histology. *In Bone Diseases*. New York: Springer-Verlag.
67. Robert Marcus DF, Dorothy Nelson, Clifford J. Rosen (1996) *Osteoporosis*: Academic Publisher.
68. Bailey AJ, Mansell JP, Sims TJ, Banse X (2004) Biochemical and mechanical properties of subchondral bone in osteoarthritis. *Biorheology* 41: 349-358.
69. Vidal B, Cascao R, Vale AC, Cavaleiro I, Vaz MF, et al. (2015) Arthritis induces early bone high turnover, structural degradation and mechanical weakness. *PLoS One* 10: e0117100.
70. Dall'Ara E, Ohman C, Baleani M, Viceconti M (2011) Reduced tissue hardness of trabecular bone is associated with severe osteoarthritis. *J Biomech* 44: 1593-1598.
71. Burra S, Nicoletta DP, Francis WL, Freitas CJ, Mueschke NJ, et al. (2010) Dendritic processes of osteocytes are mechanotransducers that induce the opening of hemichannels. *Proc Natl Acad Sci U S A* 107: 13648-13653.
72. Klein-Nulend J, Nijweide PJ, Burger EH (2003) Osteocyte and bone structure. *Curr Osteoporos Rep* 1: 5-10.
73. Burr DB, Schaffler MB, Frederickson RG (1988) Composition of the cement line and its possible mechanical role as a local interface in human compact bone. *J Biomech* 21: 939-945.
74. Lakes R, Saha S (1979) Cement line motion in bone. *Science* 204: 501-503.
75. Eriksen EF, Douglas W. Axelrod, and Flemming Melsen (1994) *Bone histomorphometry*. New York: Raven Press.
76. Joyce NC, Hache LP, Clemens PR (2012) Bone health and associated metabolic complications in neuromuscular diseases. *Phys Med Rehabil Clin N Am* 23: 773-799.
77. Zhang Z, Zhang YW, Gao H (2011) On optimal hierarchy of load-bearing biological materials. *Proc Biol Sci* 278: 519-525.
78. Brodsky B, Persikov AV (2005) Molecular structure of the collagen triple helix. *Adv Protein Chem* 70: 301-339.
79. Depalle B, Qin Z, Shefelbine SJ, Buehler MJ (2015) Influence of cross-link structure, density and mechanical properties in the mesoscale deformation mechanisms of collagen fibrils. *J Mech Behav Biomed Mater* 52: 1-13.
80. Luo G, Ducy P, McKee MD, Pinero GJ, Loyer E, et al. (1997) Spontaneous calcification of arteries and cartilage in mice lacking matrix GLA protein. *Nature* 386: 78-81.
81. Xu T, Bianco P, Fisher LW, Longenecker G, Smith E, et al. (1998) Targeted disruption of the biglycan gene leads to an osteoporosis-like phenotype in mice. *Nat Genet* 20: 78-82.
82. Niyibizi C, Eyre DR (1994) Structural characteristics of cross-linking sites in type V collagen of bone. Chain specificities and heterotypic links to type I collagen. *Eur J Biochem* 224: 943-950.
83. Niyibizi C, Eyre DR (1989) Bone type V collagen: chain composition and location of a trypsin cleavage site. *Connect Tissue Res* 20: 247-250.
84. van der Rest M, Garrone R (1991) Collagen family of proteins. *FASEB J* 5: 2814-2823.

85. Brodsky B, Shah NK (1995) Protein motifs. 8. The triple-helix motif in proteins. *FASEB J* 9: 1537-1546.
86. Kuc IM, Scott PG (1997) Increased diameters of collagen fibrils precipitated in vitro in the presence of decorin from various connective tissues. *Connect Tissue Res* 36: 287-296.
87. Vogel KG, Trotter JA (1987) The effect of proteoglycans on the morphology of collagen fibrils formed in vitro. *Coll Relat Res* 7: 105-114.
88. Myllyharju J, Kivirikko KI (2004) Collagens, modifying enzymes and their mutations in humans, flies and worms. *Trends Genet* 20: 33-43.
89. Dominguez LJ, Barbagallo M, Moro L (2005) Collagen overglycosylation: a biochemical feature that may contribute to bone quality. *Biochem Biophys Res Commun* 330: 1-4.
90. Kuznetsova N, Leikin S (1999) Does the triple helical domain of type I collagen encode molecular recognition and fiber assembly while telopeptides serve as catalytic domains? Effect of proteolytic cleavage on fibrillogenesis and on collagen-collagen interaction in fibers. *J Biol Chem* 274: 36083-36088.
91. Iozzo RV (1999) The biology of the small leucine-rich proteoglycans. Functional network of interactive proteins. *J Biol Chem* 274: 18843-18846.
92. Corporation HP Collagen type I synthesis process. Hindawi Publishing Corporation.
93. Civitelli R, Armamento-Villareal R, Napoli N (2009) Bone turnover markers: understanding their value in clinical trials and clinical practice. *Osteoporos Int* 20: 843-851.
94. Wheeler G, Elshahaly M, Tuck SP, Datta HK, van Laar JM (2013) The clinical utility of bone marker measurements in osteoporosis. *J Transl Med* 11: 201.
95. Vasikaran S, Eastell R, Bruyere O, Foldes AJ, Garnero P, et al. (2011) Markers of bone turnover for the prediction of fracture risk and monitoring of osteoporosis treatment: a need for international reference standards. *Osteoporos Int* 22: 391-420.
96. Stokes FJ, Ivanov P, Bailey LM, Fraser WD (2011) The effects of sampling procedures and storage conditions on short-term stability of blood-based biochemical markers of bone metabolism. *Clin Chem* 57: 138-140.
97. Seibel MJ (2000) Molecular markers of bone turnover: biochemical, technical and analytical aspects. *Osteoporos Int* 11 Suppl 6: S18-29.
98. Melkko J, Hellevik T, Risteli L, Risteli J, Smedsrod B (1994) Clearance of NH₂-terminal propeptides of types I and III procollagen is a physiological function of the scavenger receptor in liver endothelial cells. *J Exp Med* 179: 405-412.
99. Leeming DJ, Alexandersen P, Karsdal MA, Qvist P, Schaller S, et al. (2006) An update on biomarkers of bone turnover and their utility in biomedical research and clinical practice. *Eur J Clin Pharmacol* 62: 781-792.
100. Brandt J, Krogh TN, Jensen CH, Frederiksen JK, Teisner B (1999) Thermal instability of the trimeric structure of the N-terminal propeptide of human procollagen type I in relation to assay technology. *Clin Chem* 45: 47-53.
101. Halleen JM, Tiitinen SL, Ylipahkala H, Fagerlund KM, Vaananen HK (2006) Tartrate-resistant acid phosphatase 5b (TRACP 5b) as a marker of bone resorption. *Clin Lab* 52: 499-509.
102. Bjarnason NH, Henriksen EE, Alexandersen P, Christgau S, Henriksen DB, et al. (2002) Mechanism of circadian variation in bone resorption. *Bone* 30: 307-313.
103. Baxter I, Rogers A, Eastell R, Peel N (2013) Evaluation of urinary N-telopeptide of type I collagen measurements in the management of osteoporosis in clinical practice. *Osteoporos Int* 24: 941-947.
104. Ducy P, Desbois C, Boyce B, Pinero G, Story B, et al. (1996) Increased bone formation in osteocalcin-deficient mice. *Nature* 382: 448-452.
105. Boskey AL, Gadaleta S, Gundberg C, Doty SB, Ducy P, et al. (1998) Fourier transform infrared microspectroscopic analysis of bones of osteocalcin-deficient mice provides insight into the function of osteocalcin. *Bone* 23: 187-196.

106. Whyte MP (1994) Hypophosphatasia and the role of alkaline phosphatase in skeletal mineralization. *Endocr Rev* 15: 439-461.
107. Qian J, Kang Y, Zhang W, Li Z (2008) Fabrication, chemical composition change and phase evolution of biomorphic hydroxyapatite. *J Mater Sci Mater Med* 19: 3373-3383.
108. Landis WJ (1995) The strength of a calcified tissue depends in part on the molecular structure and organization of its constituent mineral crystals in their organic matrix. *Bone* 16: 533-544.
109. Weiner S, Sagi I, Addadi L (2005) Structural biology. Choosing the crystallization path less traveled. *Science* 309: 1027-1028.
110. Zaidi M (2007) Skeletal remodeling in health and disease. *Nat Med* 13: 791-801.
111. Janos Zemleni JWS, Jesse F. Gregory III, Patrick J. Stover (2013) *Handbook of Vitamins: CRC Press*.
112. Bikle DD (2012) Vitamin D and bone. *Curr Osteoporos Rep* 10: 151-159.
113. Teitelbaum SL (2000) Bone resorption by osteoclasts. *Science* 289: 1504-1508.
114. Georgess D, Machuca-Gayet I, Blangy A, Jurdic P (2014) Podosome organization drives osteoclast-mediated bone resorption. *Cell Adh Migr* 8: 191-204.
115. Davies J, Warwick J, Totty N, Philp R, Helfrich M, et al. (1989) The osteoclast functional antigen, implicated in the regulation of bone resorption, is biochemically related to the vitronectin receptor. *J Cell Biol* 109: 1817-1826.
116. Fukushima O, Bekker PJ, Gay CV (1991) Characterization of the functional stages of osteoclasts by enzyme histochemistry and electron microscopy. *Anat Rec* 231: 298-315.
117. Mulari MT, Zhao H, Lakkakorpi PT, Vaananen HK (2003) Osteoclast ruffled border has distinct subdomains for secretion and degraded matrix uptake. *Traffic* 4: 113-125.
118. Blair HC, Teitelbaum SL, Ghiselli R, Gluck S (1989) Osteoclastic bone resorption by a polarized vacuolar proton pump. *Science* 245: 855-857.
119. Vaananen HK, Zhao H, Mulari M, Halleen JM (2000) The cell biology of osteoclast function. *J Cell Sci* 113 (Pt 3): 377-381.
120. Zhao H (2012) Membrane trafficking in osteoblasts and osteoclasts: new avenues for understanding and treating skeletal diseases. *Traffic* 13: 1307-1314.
121. Raggatt LJ, Partridge NC (2010) Cellular and molecular mechanisms of bone remodeling. *J Biol Chem* 285: 25103-25108.
122. Hadjidakis DJ, Androulakis, II (2006) Bone remodeling. *Ann N Y Acad Sci* 1092: 385-396.
123. Boyce BF, Xing L (2008) Functions of RANKL/RANK/OPG in bone modeling and remodeling. *Arch Biochem Biophys* 473: 139-146.
124. Caetano-Lopes J, Canhao H, Fonseca JE (2007) Osteoblasts and bone formation. *Acta Reumatol Port* 32: 103-110.
125. Delgado-Calle J, Anderson J, Cregor MD, Hiasa M, Chirgwin JM, et al. (2016) Bidirectional Notch Signaling and Osteocyte-Derived Factors in the Bone Marrow Microenvironment Promote Tumor Cell Proliferation and Bone Destruction in Multiple Myeloma. *Cancer Res* 76: 1089-1100.
126. Dallas SL, Bonewald LF (2010) Dynamics of the transition from osteoblast to osteocyte. *Ann N Y Acad Sci* 1192: 437-443.
127. Aarden EM, Burger EH, Nijweide PJ (1994) Function of osteocytes in bone. *J Cell Biochem* 55: 287-299.
128. Rochefort GY, Pallu S, Benhamou CL (2010) Osteocyte: the unrecognized side of bone tissue. *Osteoporos Int* 21: 1457-1469.
129. Franz-Odenaal TA, Hall BK, Witten PE (2006) Buried alive: how osteoblasts become osteocytes. *Dev Dyn* 235: 176-190.
130. Lanyon LE (1993) Osteocytes, strain detection, bone modeling and remodeling. *Calcif Tissue Int* 53 Suppl 1: S102-106; discussion S106-107.

131. Matsuo K, Nango N (2012) [Osteocytic osteolysis : measurements of the volume of osteocytic lacunae]. *Clin Calcium* 22: 677-683.
132. Elmardi AS, Katchburian MV, Katchburian E (1990) Electron microscopy of developing calvaria reveals images that suggest that osteoclasts engulf and destroy osteocytes during bone resorption. *Calcif Tissue Int* 46: 239-245.
133. Feng X, McDonald JM (2011) Disorders of bone remodeling. *Annu Rev Pathol* 6: 121-145.
134. Rodan GA (1998) Bone homeostasis. *Proc Natl Acad Sci U S A* 95: 13361-13362.
135. Jilka RL (2003) Biology of the basic multicellular unit and the pathophysiology of osteoporosis. *Med Pediatr Oncol* 41: 182-185.
136. Sims NA, Martin TJ (2014) Coupling the activities of bone formation and resorption: a multitude of signals within the basic multicellular unit. *Bonekey Rep* 3: 481.
137. Petrtyl M, Hert J, Fiala P (1996) Spatial organization of the haversian bone in man. *J Biomech* 29: 161-169.
138. Parfitt AM (1994) Osteonal and hemi-osteonal remodeling: the spatial and temporal framework for signal traffic in adult human bone. *J Cell Biochem* 55: 273-286.
139. Henriksen K, Bollerslev J, Everts V, Karsdal MA (2011) Osteoclast activity and subtypes as a function of physiology and pathology--implications for future treatments of osteoporosis. *Endocr Rev* 32: 31-63.
140. Delaisse JM (2014) The reversal phase of the bone-remodeling cycle: cellular prerequisites for coupling resorption and formation. *Bonekey Rep* 3: 561.
141. Siddiqui JA, Partridge NC (2016) Physiological Bone Remodeling: Systemic Regulation and Growth Factor Involvement. *Physiology (Bethesda)* 31: 233-245.
142. Hsu H, Lacey DL, Dunstan CR, Solovyev I, Colombero A, et al. (1999) Tumor necrosis factor receptor family member RANK mediates osteoclast differentiation and activation induced by osteoprotegerin ligand. *Proc Natl Acad Sci U S A* 96: 3540-3545.
143. Kohli SS, Kohli VS (2011) Role of RANKL-RANK/osteoprotegerin molecular complex in bone remodeling and its immunopathologic implications. *Indian J Endocrinol Metab* 15: 175-181.
144. Hofbauer LC, Schoppet M (2004) Clinical implications of the osteoprotegerin/RANKL/RANK system for bone and vascular diseases. *JAMA* 292: 490-495.
145. Simonet WS, Lacey DL, Dunstan CR, Kelley M, Chang MS, et al. (1997) Osteoprotegerin: a novel secreted protein involved in the regulation of bone density. *Cell* 89: 309-319.
146. Richards JB, Zheng HF, Spector TD (2012) Genetics of osteoporosis from genome-wide association studies: advances and challenges. *Nat Rev Genet* 13: 576-588.
147. Seeman E (2003) Reduced bone formation and increased bone resorption: rational targets for the treatment of osteoporosis. *Osteoporos Int* 14 Suppl 3: S2-8.
148. Seeman E (2008) Structural basis of growth-related gain and age-related loss of bone strength. *Rheumatology (Oxford)* 47 Suppl 4: iv2-8.
149. Lips P, Courpron P, Meunier PJ (1978) Mean wall thickness of trabecular bone packets in the human iliac crest: changes with age. *Calcif Tissue Res* 26: 13-17.
150. Vedi S, Compston JE, Webb A, Tighe JR (1983) Histomorphometric analysis of dynamic parameters of trabecular bone formation in the iliac crest of normal British subjects. *Metab Bone Dis Relat Res* 5: 69-74.
151. Nishida S, Endo N, Yamagiwa H, Tanizawa T, Takahashi HE (1999) Number of osteoprogenitor cells in human bone marrow markedly decreases after skeletal maturation. *J Bone Miner Metab* 17: 171-177.
152. Stenderup K, Justesen J, Eriksen EF, Rattan SI, Kassem M (2001) Number and proliferative capacity of osteogenic stem cells are maintained during aging and in patients with osteoporosis. *J Bone Miner Res* 16: 1120-1129.

153. Oreffo RO, Bord S, Triffitt JT (1998) Skeletal progenitor cells and ageing human populations. *Clin Sci (Lond)* 94: 549-555.
154. Boivin G, Lips P, Ott SM, Harper KD, Sarkar S, et al. (2003) Contribution of raloxifene and calcium and vitamin D3 supplementation to the increase of the degree of mineralization of bone in postmenopausal women. *J Clin Endocrinol Metab* 88: 4199-4205.
155. Boivin G, Meunier PJ (2002) Changes in bone remodeling rate influence the degree of mineralization of bone. *Connect Tissue Res* 43: 535-537.
156. Currey JD (2002) *Bones: structure and mechanics*. Princeton University Press.
157. Vignat-Carrin S, Garnero P, Delmas PD (2006) The role of collagen in bone strength. *Osteoporos Int* 17: 319-336.
158. Garnero P, Cloos P, Sornay-Rendu E, Qvist P, Delmas PD (2002) Type I collagen racemization and isomerization and the risk of fracture in postmenopausal women: the OFELY prospective study. *J Bone Miner Res* 17: 826-833.
159. Manolagas SC (2000) Birth and death of bone cells: basic regulatory mechanisms and implications for the pathogenesis and treatment of osteoporosis. *Endocr Rev* 21: 115-137.
160. Seeman E, Delmas PD (2006) Bone quality--the material and structural basis of bone strength and fragility. *N Engl J Med* 354: 2250-2261.
161. Homminga J, McCreadie BR, Weinans H, Huiskes R (2003) The dependence of the elastic properties of osteoporotic cancellous bone on volume fraction and fabric. *J Biomech* 36: 1461-1467.
162. Doblare M, Garcia JM (2003) On the modelling bone tissue fracture and healing of the bone tissue. *Acta Cient Venez* 54: 58-75.
163. Vashishth D (2008) Small animal bone biomechanics. *Bone* 43: 794-797.
164. John P. Bilezikian LGR, T. John Martin (2008) *Principles of Bone Biology*: Academic Press.
165. Bozzini C, Picasso EO, Champin GM, Alippi RM, Bozzini CE (2012) Biomechanical properties of the mid-shaft femur in middle-aged hypophysectomized rats as assessed by bending test. *Endocrine* 42: 411-418.
166. Herrman K (2011) *Hardness Testing: Principles and Applications*: ASM International.
167. COMMONS W (2008) Typical Stress vs. Strain diagram for a ductile materia.
168. Bennet-Clark H (2011) *The Mechanical Properties of Biological Materials*: Princeton University Press.
169. Kutz M (2003) *Standard Handbook of Biomedical Engineering & Design*: McGRAW-HILL.
170. Boskey AL (2003) Mineral Analysis Provides Insights into the Mechanism of Biomineralization: *Calcified Tissue International*.
171. D. Jaschouz OP, P. Roschger, H.-S. Hwang and P. Fratzl (2003) Pole figure analysis of mineral nanoparticle orientation in individual trabecula of human vertebral bone. *J Appl Cryst*.
172. Wang X, Shen X, Li X, Agrawal CM (2002) Age-related changes in the collagen network and toughness of bone. *Bone* 31: 1-7.
173. John DC (2003) Role of collagen and other organics in the mechanical properties of bone. *Osteoporos Int* 14 Suppl 5: S29-36.
174. Reilly DT, Burstein AH (1975) The elastic and ultimate properties of compact bone tissue. *J Biomech* 8: 393-405.
175. Cole JH, van der Meulen MC (2011) Whole bone mechanics and bone quality. *Clin Orthop Relat Res* 469: 2139-2149.
176. Felsenberg D, Boonen S (2005) The bone quality framework: determinants of bone strength and their interrelationships, and implications for osteoporosis management. *Clin Ther* 27: 1-11.
177. Bouxsein ML (2005) Determinants of skeletal fragility. *Best Pract Res Clin Rheumatol* 19: 897-911.

178. Noble B (2003) Bone microdamage and cell apoptosis. *Eur Cell Mater* 6: 46-55; discussion 55.
179. P. Fratzl HSG, E. P. Paschalisb, P. Roschgerb (2004) Structure and mechanical quality of the collagen–mineral nano-composite in bone. *J Mater Chem*.
180. Meunier PJ, Boivin G (1997) Bone mineral density reflects bone mass but also the degree of mineralization of bone: therapeutic implications. *Bone* 21: 373-377.
181. Donaldson F, Ruffoni D, Schneider P, Levchuk A, Zwahlen A, et al. (2014) Modeling microdamage behavior of cortical bone. *Biomech Model Mechanobiol* 13: 1227-1242.
182. Abdulghani S, Caetano-Lopes J, Canhao H, Fonseca JE (2009) Biomechanical effects of inflammatory diseases on bone-rheumatoid arthritis as a paradigm. *Autoimmun Rev* 8: 668-671.
183. Doblare M GJ, Gomez MJ. (2004) Modelling bone tissue fracture and healing: a review. *Eng Frac Mech* 71: 1809-1840.
184. Reilly GC, Currey JD (1999) The development of microcracking and failure in bone depends on the loading mode to which it is adapted. *J Exp Biol* 202: 543-552.
185. Zioupos P, Currey JD, Sedman AJ (1994) An examination of the micromechanics of failure of bone and antler by acoustic emission tests and Laser Scanning Confocal Microscopy. *Med Eng Phys* 16: 203-212.
186. Unnanuntana A, Rebolledo BJ, Khair MM, DiCarlo EF, Lane JM (2011) Diseases affecting bone quality: beyond osteoporosis. *Clin Orthop Relat Res* 469: 2194-2206.
187. Brandi ML (2009) Microarchitecture, the key to bone quality. *Rheumatology (Oxford)* 48 Suppl 4: iv3-8.
188. van der Heijde DM (1995) Joint erosions and patients with early rheumatoid arthritis. *Br J Rheumatol* 34 Suppl 2: 74-78.
189. Schett G, Teitelbaum SL (2009) Osteoclasts and Arthritis. *J Bone Miner Res* 24: 1142-1146.
190. Schett G (2007) Cells of the synovium in rheumatoid arthritis. *Osteoclasts. Arthritis Res Ther* 9: 203.
191. Jimenez-Boj E, Redlich K, Turk B, Hanslik-Schnabel B, Wanivenhaus A, et al. (2005) Interaction between synovial inflammatory tissue and bone marrow in rheumatoid arthritis. *J Immunol* 175: 2579-2588.
192. Hetland ML, Ejlberg B, Horslev-Petersen K, Jacobsen S, Vestergaard A, et al. (2009) MRI bone oedema is the strongest predictor of subsequent radiographic progression in early rheumatoid arthritis. Results from a 2-year randomised controlled trial (CIMESTRA). *Ann Rheum Dis* 68: 384-390.
193. Rodrigues ARC (2012) The Role of IL-1 β in Rheumatoid Arthritis.
194. Romas E (2005) Bone loss in inflammatory arthritis: mechanisms and therapeutic approaches with bisphosphonates. *Best Pract Res Clin Rheumatol* 19: 1065-1079.
195. Goldring SR, Gravallesse EM (2000) Mechanisms of bone loss in inflammatory arthritis: diagnosis and therapeutic implications. *Arthritis Res* 2: 33-37.
196. Gupta S, Gollapudi S (2006) Molecular mechanisms of TNF-alpha-induced apoptosis in naive and memory T cell subsets. *Autoimmun Rev* 5: 264-268.
197. Caetano-Lopes J, Canhao H, Fonseca JE (2009) Osteoimmunology--the hidden immune regulation of bone. *Autoimmun Rev* 8: 250-255.
198. Costa AG, Cusano NE, Silva BC, Cremers S, Bilezikian JP (2011) Cathepsin K: its skeletal actions and role as a therapeutic target in osteoporosis. *Nat Rev Rheumatol* 7: 447-456.
199. Hayman AR (2008) Tartrate-resistant acid phosphatase (TRAP) and the osteoclast/immune cell dichotomy. *Autoimmunity* 41: 218-223.
200. Seitz M, Loetscher P, Fey MF, Tobler A (1994) Constitutive mRNA and protein production of macrophage colony-stimulating factor but not of other cytokines by synovial fibroblasts from rheumatoid arthritis and osteoarthritis patients. *Br J Rheumatol* 33: 613-619.

201. Gravallesse EM, Manning C, Tsay A, Naito A, Pan C, et al. (2000) Synovial tissue in rheumatoid arthritis is a source of osteoclast differentiation factor. *Arthritis Rheum* 43: 250-258.
202. Shigeyama Y, Pap T, Kunzler P, Simmen BR, Gay RE, et al. (2000) Expression of osteoclast differentiation factor in rheumatoid arthritis. *Arthritis Rheum* 43: 2523-2530.
203. Lam J, Takeshita S, Barker JE, Kanagawa O, Ross FP, et al. (2000) TNF-alpha induces osteoclastogenesis by direct stimulation of macrophages exposed to permissive levels of RANK ligand. *J Clin Invest* 106: 1481-1488.
204. Wei S, Kitaura H, Zhou P, Ross FP, Teitelbaum SL (2005) IL-1 mediates TNF-induced osteoclastogenesis. *J Clin Invest* 115: 282-290.
205. Zwerina J, Redlich K, Polzer K, Joosten L, Kronke G, et al. (2007) TNF-induced structural joint damage is mediated by IL-1. *Proc Natl Acad Sci U S A* 104: 11742-11747.
206. Wei S, Wang MW, Teitelbaum SL, Ross FP (2002) Interleukin-4 reversibly inhibits osteoclastogenesis via inhibition of NF-kappa B and mitogen-activated protein kinase signaling. *J Biol Chem* 277: 6622-6630.
207. Fumoto T, Takeshita S, Ito M, Ikeda K (2014) Physiological functions of osteoblast lineage and T cell-derived RANKL in bone homeostasis. *J Bone Miner Res* 29: 830-842.
208. Won HY, Lee JA, Park ZS, Song JS, Kim HY, et al. (2011) Prominent bone loss mediated by RANKL and IL-17 produced by CD4+ T cells in TallyHo/JngJ mice. *PLoS One* 6: e18168.
209. Carbonell Sala S, Masi L, Marini F, Del Monte F, Falchetti A, et al. (2005) Genetics and pharmacogenetics of osteoporosis. *J Endocrinol Invest* 28: 2-7.
210. American College of Rheumatology Subcommittee on Rheumatoid Arthritis G (2002) Guidelines for the management of rheumatoid arthritis: 2002 Update. *Arthritis Rheum* 46: 328-346.
211. Goekoop-Ruiterman YP, de Vries-Bouwstra JK, Allaart CF, van Zeben D, Kerstens PJ, et al. (2008) Clinical and radiographic outcomes of four different treatment strategies in patients with early rheumatoid arthritis (the BeSt study): A randomized, controlled trial. *Arthritis Rheum* 58: S126-135.
212. Quinn MA, Conaghan PG, O'Connor PJ, Karim Z, Greenstein A, et al. (2005) Very early treatment with infliximab in addition to methotrexate in early, poor-prognosis rheumatoid arthritis reduces magnetic resonance imaging evidence of synovitis and damage, with sustained benefit after infliximab withdrawal: results from a twelve-month randomized, double-blind, placebo-controlled trial. *Arthritis Rheum* 52: 27-35.
213. Gaffo A, Saag KG, Curtis JR (2006) Treatment of rheumatoid arthritis. *Am J Health Syst Pharm* 63: 2451-2465.
214. Kirwan JR, Bijlsma JW, Boers M, Shea BJ (2007) Effects of glucocorticoids on radiological progression in rheumatoid arthritis. *Cochrane Database Syst Rev*: CD006356.
215. Boers M, Verhoeven AC, Markusse HM, van de Laar MA, Westhovens R, et al. (1997) Randomised comparison of combined step-down prednisolone, methotrexate and sulphasalazine with sulphasalazine alone in early rheumatoid arthritis. *Lancet* 350: 309-318.
216. Kirwan JR (1995) The effect of glucocorticoids on joint destruction in rheumatoid arthritis. The Arthritis and Rheumatism Council Low-Dose Glucocorticoid Study Group. *N Engl J Med* 333: 142-146.
217. Landewe RB, Boers M, Verhoeven AC, Westhovens R, van de Laar MA, et al. (2002) COBRA combination therapy in patients with early rheumatoid arthritis: long-term structural benefits of a brief intervention. *Arthritis Rheum* 46: 347-356.
218. van Everdingen AA, Jacobs JW, Siewertsz Van Reesema DR, Bijlsma JW (2002) Low-dose prednisone therapy for patients with early active rheumatoid arthritis: clinical efficacy, disease-modifying properties, and side effects: a randomized, double-blind, placebo-controlled clinical trial. *Ann Intern Med* 136: 1-12.

219. Polido-Pereira J, Vieira-Sousa E, Fonseca JE (2011) Rheumatoid arthritis: what is refractory disease and how to manage it? *Autoimmun Rev* 10: 707-713.
220. Sizova L (2008) Approaches to the treatment of early rheumatoid arthritis with disease-modifying antirheumatic drugs. *Br J Clin Pharmacol* 66: 173-178.
221. Wolfe F, Hawley DJ, Cathey MA (1990) Termination of slow acting antirheumatic therapy in rheumatoid arthritis: a 14-year prospective evaluation of 1017 consecutive starts. *J Rheumatol* 17: 994-1002.
222. Pincus T, Marcum SB, Callahan LF (1992) Longterm drug therapy for rheumatoid arthritis in seven rheumatology private practices: II. Second line drugs and prednisone. *J Rheumatol* 19: 1885-1894.
223. Ortendahl M, Holmes T, Schettler JD, Fries JF (2002) The methotrexate therapeutic response in rheumatoid arthritis. *J Rheumatol* 29: 2084-2091.
224. Cronstein BN (2005) Low-dose methotrexate: a mainstay in the treatment of rheumatoid arthritis. *Pharmacol Rev* 57: 163-172.
225. Cash JM, Klippel JH (1994) Second-line drug therapy for rheumatoid arthritis. *N Engl J Med* 330: 1368-1375.
226. Nagashima M, Matsuoka T, Saitoh K, Koyama T, Kikuchi O, et al. (2006) Treatment continuation rate in relation to efficacy and toxicity in long-term therapy with low-dose methotrexate, sulfasalazine, and bucillamine in 1,358 Japanese patients with rheumatoid arthritis. *Clin Exp Rheumatol* 24: 260-267.
227. Keystone EC (1999) The role of tumor necrosis factor antagonism in clinical practice. *J Rheumatol Suppl* 57: 22-28.
228. Emery P, Breedveld FC, Hall S, Durez P, Chang DJ, et al. (2008) Comparison of methotrexate monotherapy with a combination of methotrexate and etanercept in active, early, moderate to severe rheumatoid arthritis (COMET): a randomised, double-blind, parallel treatment trial. *Lancet* 372: 375-382.
229. Breedveld FC, Weisman MH, Kavanaugh AF, Cohen SB, Pavelka K, et al. (2006) The PREMIER study: A multicenter, randomized, double-blind clinical trial of combination therapy with adalimumab plus methotrexate versus methotrexate alone or adalimumab alone in patients with early, aggressive rheumatoid arthritis who had not had previous methotrexate treatment. *Arthritis Rheum* 54: 26-37.
230. Genovese MC, Becker JC, Schiff M, Luggen M, Sherrer Y, et al. (2005) Abatacept for rheumatoid arthritis refractory to tumor necrosis factor alpha inhibition. *N Engl J Med* 353: 1114-1123.
231. Cohen SB, Emery P, Greenwald MW, Dougados M, Furie RA, et al. (2006) Rituximab for rheumatoid arthritis refractory to anti-tumor necrosis factor therapy: Results of a multicenter, randomized, double-blind, placebo-controlled, phase III trial evaluating primary efficacy and safety at twenty-four weeks. *Arthritis Rheum* 54: 2793-2806.
232. Tak PP, Rigby WF, Rubbert-Roth A, Peterfy CG, van Vollenhoven RF, et al. (2011) Inhibition of joint damage and improved clinical outcomes with rituximab plus methotrexate in early active rheumatoid arthritis: the IMAGE trial. *Ann Rheum Dis* 70: 39-46.
233. Keystone E, Emery P, Peterfy CG, Tak PP, Cohen S, et al. (2009) Rituximab inhibits structural joint damage in patients with rheumatoid arthritis with an inadequate response to tumour necrosis factor inhibitor therapies. *Ann Rheum Dis* 68: 216-221.
234. Genant HK, Peterfy CG, Westhovens R, Becker JC, Aranda R, et al. (2008) Abatacept inhibits progression of structural damage in rheumatoid arthritis: results from the long-term extension of the AIM trial. *Ann Rheum Dis* 67: 1084-1089.
235. Kremer JM, Blanco R, Brzosko M, Burgos-Vargas R, Halland AM, et al. (2011) Tocilizumab inhibits structural joint damage in rheumatoid arthritis patients with inadequate responses to methotrexate: results from the double-blind treatment phase of a

- randomized placebo-controlled trial of tocilizumab safety and prevention of structural joint damage at one year. *Arthritis Rheum* 63: 609-621.
236. Garnero P, Thompson E, Woodworth T, Smolen JS (2010) Rapid and sustained improvement in bone and cartilage turnover markers with the anti-interleukin-6 receptor inhibitor tocilizumab plus methotrexate in rheumatoid arthritis patients with an inadequate response to methotrexate: results from a substudy of the multicenter double-blind, placebo-controlled trial of tocilizumab in inadequate responders to methotrexate alone. *Arthritis Rheum* 62: 33-43.
 237. Nishimoto N, Hashimoto J, Miyasaka N, Yamamoto K, Kawai S, et al. (2007) Study of active controlled monotherapy used for rheumatoid arthritis, an IL-6 inhibitor (SAMURAI): evidence of clinical and radiographic benefit from an x ray reader-blinded randomised controlled trial of tocilizumab. *Ann Rheum Dis* 66: 1162-1167.
 238. Cohen S, Hurd E, Cush J, Schiff M, Weinblatt ME, et al. (2002) Treatment of rheumatoid arthritis with anakinra, a recombinant human interleukin-1 receptor antagonist, in combination with methotrexate: results of a twenty-four-week, multicenter, randomized, double-blind, placebo-controlled trial. *Arthritis Rheum* 46: 614-624.
 239. Bresnihan B, Alvaro-Gracia JM, Cobby M, Doherty M, Domljan Z, et al. (1998) Treatment of rheumatoid arthritis with recombinant human interleukin-1 receptor antagonist. *Arthritis Rheum* 41: 2196-2204.
 240. Alten R, Gomez-Reino J, Durez P, Beaulieu A, Sebba A, et al. (2011) Efficacy and safety of the human anti-IL-1beta monoclonal antibody canakinumab in rheumatoid arthritis: results of a 12-week, Phase II, dose-finding study. *BMC Musculoskelet Disord* 12: 153.
 241. Cavalli G, Dinarello CA (2015) Treating rheumatological diseases and co-morbidities with interleukin-1 blocking therapies. *Rheumatology (Oxford)* 54: 2134-2144.
 242. Molto A, Olive A (2010) Anti-IL-1 molecules: new comers and new indications. *Joint Bone Spine* 77: 102-107.
 243. Vander Cruyssen B, Van Looy S, Wyns B, Westhovens R, Durez P, et al. (2006) Four-year follow-up of infliximab therapy in rheumatoid arthritis patients with long-standing refractory disease: attrition and long-term evolution of disease activity. *Arthritis Res Ther* 8: R112.
 244. Karlsson JA, Kristensen LE, Kapetanovic MC, Gulfe A, Saxne T, et al. (2008) Treatment response to a second or third TNF-inhibitor in RA: results from the South Swedish Arthritis Treatment Group Register. *Rheumatology (Oxford)* 47: 507-513.
 245. Calabrese LH (2003) Molecular differences in anticytokine therapies. *Clin Exp Rheumatol* 21: 241-248.
 246. Philippe L, Gegout-Pottie P, Guingamp C, Bordji K, Terlain B, et al. (1997) Relations between functional, inflammatory, and degenerative parameters during adjuvant arthritis in rats. *Am J Physiol* 273: R1550-1556.
 247. Van Eden W, Waksman BH (2003) Immune regulation in adjuvant-induced arthritis: possible implications for innovative therapeutic strategies in arthritis. *Arthritis Rheum* 48: 1788-1796.
 248. Jaffee BD, Kerr JS, Jones EA, Giannaras JV, McGowan M, et al. (1989) The effect of immunomodulating drugs on adjuvant-induced arthritis in Lewis rats. *Agents Actions* 27: 344-346.
 249. Rovensky J, Svik K, Stancikova M, Istok R (2003) Effect of immunostimulatory ribomunyl on the preventive treatment of rat adjuvant arthritis with cyclosporine and methotrexate. *J Rheumatol* 30: 2027-2032.
 250. Rovensky J, Svik K, Matha V, Istok R, Kamarad V, et al. (2005) Combination treatment of rat adjuvant-induced arthritis with methotrexate, probiotic bacteria *Enterococcus faecium*, and selenium. *Ann N Y Acad Sci* 1051: 570-581.

251. Silva MA, Ishii-Iwamoto EL, Bracht A, Caparroz-Assef SM, Kimura E, et al. (2005) Efficiency of combined methotrexate/chloroquine therapy in adjuvant-induced arthritis. *Fundam Clin Pharmacol* 19: 479-489.
252. Noguchi M, Kimoto A, Kobayashi S, Yoshino T, Miyata K, et al. (2005) Effect of celecoxib, a cyclooxygenase-2 inhibitor, on the pathophysiology of adjuvant arthritis in rat. *Eur J Pharmacol* 513: 229-235.
253. Bendele A, McAbee T, Sennello G, Frazier J, Chlipala E, et al. (1999) Efficacy of sustained blood levels of interleukin-1 receptor antagonist in animal models of arthritis: comparison of efficacy in animal models with human clinical data. *Arthritis Rheum* 42: 498-506.
254. Bendele AM, Chlipala ES, Scherrer J, Frazier J, Sennello G, et al. (2000) Combination benefit of treatment with the cytokine inhibitors interleukin-1 receptor antagonist and PEGylated soluble tumor necrosis factor receptor type I in animal models of rheumatoid arthritis. *Arthritis Rheum* 43: 2648-2659.
255. Miwatashi S, Arikawa Y, Kotani E, Miyamoto M, Naruo K, et al. (2005) Novel inhibitor of p38 MAP kinase as an anti-TNF-alpha drug: discovery of N-[4-[2-ethyl-4-(3-methylphenyl)-1,3-thiazol-5-yl]-2-pyridyl]benzamide (TAK-715) as a potent and orally active anti-rheumatoid arthritis agent. *J Med Chem* 48: 5966-5979.
256. Cole P, Rabasseda X (2004) The soluble tumor necrosis factor receptor etanercept: a new strategy for the treatment of autoimmune rheumatic disease. *Drugs Today (Barc)* 40: 281-324.
257. Joe B WR (1999) Animal models of rheumatoid arthritis. *Mol Med Today* 5: 367-369.
258. Lisa R. Schopf KA, Bruce D. Jaffee (2006) *In Vivo Models of Inflammation*. Basel/Switzerland: Birkhäuser Basel.
259. Madhok R, Crilly A, Watson J, Capell HA (1993) Serum interleukin 6 levels in rheumatoid arthritis: correlations with clinical and laboratory indices of disease activity. *Ann Rheum Dis* 52: 232-234.
260. Roux S, Orcel P (2000) Bone loss. Factors that regulate osteoclast differentiation: an update. *Arthritis Res* 2: 451-456.
261. Cannon GW, McCall S, Cole BC, Griffiths MM, Radov LA, et al. (1990) Effects of indomethacin, cyclosporin, cyclophosphamide, and placebo on collagen-induced arthritis of mice. *Agents Actions* 29: 315-323.
262. van Schaardenburg D, Nielen MM, Lems WF, Twisk JW, Reesink HW, et al. (2011) Bone metabolism is altered in preclinical rheumatoid arthritis. *Ann Rheum Dis* 70: 1173-1174.
263. Wislowska M, Jakubicz D, Stepien K, Cicha M (2009) Serum concentrations of formation (PINP) and resorption (Ctx) bone turnover markers in rheumatoid arthritis. *Rheumatol Int* 29: 1403-1409.
264. Taylor AF, Saunders MM, Shingle DL, Cimbala JM, Zhou Z, et al. (2007) Mechanically stimulated osteocytes regulate osteoblastic activity via gap junctions. *Am J Physiol Cell Physiol* 292: C545-552.
265. Jaiprakash A, Prasadam I, Feng JQ, Liu Y, Crawford R, et al. (2012) Phenotypic characterization of osteoarthritic osteocytes from the sclerotic zones: a possible pathological role in subchondral bone sclerosis. *Int J Biol Sci* 8: 406-417.
266. Noguchi M, Kimoto A, Sasamata M, Miyata K (2008) Micro-CT imaging analysis for the effect of celecoxib, a cyclooxygenase-2 inhibitor, on inflammatory bone destruction in adjuvant arthritis rats. *J Bone Miner Metab* 26: 461-468.
267. Koufany M, Chappard D, Netter P, Bastien C, Weryha G, et al. (2013) The peroxisome proliferator-activated receptor gamma agonist pioglitazone preserves bone microarchitecture in experimental arthritis by reducing the interleukin-17-dependent osteoclastogenic pathway. *Arthritis Rheum* 65: 3084-3095.

268. Caetano-Lopes J, Nery AM, Canhao H, Duarte J, Cascao R, et al. (2010) Chronic arthritis leads to disturbances in the bone collagen network. *Arthritis Res Ther* 12: R9.
269. Caetano-Lopes J, Nery AM, Henriques R, Canhao H, Duarte J, et al. (2009) Chronic arthritis directly induces quantitative and qualitative bone disturbances leading to compromised biomechanical properties. *Clin Exp Rheumatol* 27: 475-482.
270. Cascao R, Vidal B, Raquel H, Neves-Costa A, Figueiredo N, et al. (2012) Effective treatment of rat adjuvant-induced arthritis by celastrol. *Autoimmun Rev* 11: 856-862.
271. Cascao R, Vidal B, Lopes IP, Paisana E, Rino J, et al. (2015) Decrease of CD68 Synovial Macrophages in Celastrol Treated Arthritic Rats. *PLoS One* 10: e0142448.
272. Firestein GS (2003) Evolving concepts of rheumatoid arthritis. *Nature* 423: 356-361.
273. Fonseca JE, Cortez-Dias N, Francisco A, Sobral M, Canhao H, et al. (2005) Inflammatory cell infiltrate and RANKL/OPG expression in rheumatoid synovium: comparison with other inflammatory arthropathies and correlation with outcome. *Clin Exp Rheumatol* 23: 185-192.
274. Bresnihan B, Pontifex E, Thurlings RM, Vinkenoog M, El-Gabalawy H, et al. (2009) Synovial tissue sublining CD68 expression is a biomarker of therapeutic response in rheumatoid arthritis clinical trials: consistency across centers. *J Rheumatol* 36: 1800-1802.
275. Nanjundaiah SM, Venkatesha SH, Yu H, Tong L, Stains JP, et al. (2012) Celastrus and its bioactive celastrol protect against bone damage in autoimmune arthritis by modulating osteoimmune cross-talk. *J Biol Chem* 287: 22216-22226.
276. Idris AI, Krishnan M, Simic P, Landao-Bassonga E, Mollat P, et al. (2010) Small molecule inhibitors of I κ B kinase signaling inhibit osteoclast formation in vitro and prevent ovariectomy-induced bone loss in vivo. *FASEB J* 24: 4545-4555.
277. Idris AI, Libouban H, Nyangoga H, Landao-Bassonga E, Chappard D, et al. (2009) Pharmacologic inhibitors of I κ B kinase suppress growth and migration of mammary carcinosarcoma cells in vitro and prevent osteolytic bone metastasis in vivo. *Mol Cancer Ther* 8: 2339-2347.
278. LaBranche TP, Jesson MI, Radi ZA, Storer CE, Guzova JA, et al. (2012) JAK inhibition with tofacitinib suppresses arthritic joint structural damage through decreased RANKL production. *Arthritis Rheum* 64: 3531-3542.
279. Meyer DM, Jesson MI, Li X, Elrick MM, Funckes-Shippy CL, et al. (2010) Anti-inflammatory activity and neutrophil reductions mediated by the JAK1/JAK3 inhibitor, CP-690,550, in rat adjuvant-induced arthritis. *J Inflamm (Lond)* 7: 41.
280. Maeshima K, Yamaoka K, Kubo S, Nakano K, Iwata S, et al. (2012) The JAK inhibitor tofacitinib regulates synovitis through inhibition of interferon-gamma and interleukin-17 production by human CD4+ T cells. *Arthritis Rheum* 64: 1790-1798.
281. Kim S, Koga T, Isobe M, Kern BE, Yokochi T, et al. (2003) Stat1 functions as a cytoplasmic attenuator of Runx2 in the transcriptional program of osteoblast differentiation. *Genes Dev* 17: 1979-1991.
282. Tajima K, Takaishi H, Takito J, Tohmonda T, Yoda M, et al. (2010) Inhibition of STAT1 accelerates bone fracture healing. *J Orthop Res* 28: 937-941.
283. Li J (2013) JAK-STAT and bone metabolism. *JAKSTAT* 2: e23930.

CURRICULUM VITAE

NAME	POSITION TITLE
Vidal, Bruno	PhD Student

EDUCATION & TRAINING:

START MONTH/YEAR	END MONTH/YEAR	DEGREE (if applicable)	INSTITUTION AND LOCATION	TRAINING MENTOR	SCIENTIFIC DISCIPLINE
01/2012	Present	PhD	Faculdade de Ciências, Universidade de Lisboa	João Eurico Fonseca & Helena Canhão	Ciências Biomédicas
09/2004	08/2008	BSc	Escola Superior de Saúde Egas Moniz	-	Anatomia Patológica, Citológica e Tanatológica

PROFESSIONAL POSITIONS:

START MONTH/YEAR	END MONTH/YEAR	POSITION TITLE	DEPARTMENT	INSTITUTION AND LOCATION
01/2013	Present	ECTS Fellowship	JE Fonseca Lab	Instituto de Medicina Molecular
01/2012	12/2015	FCT PhD Fellowship	JE Fonseca Lab	Instituto de Medicina Molecular
01/2009	12/2011	FCT Research Fellowship	JE Fonseca Lab	Instituto de Medicina Molecular
09/2009	Present	Monitor of Histology	Faculdade de Medicina	Universidade de Lisboa
06/2009	03/2012	Clinical Study Coordinator	Rheumatology department	Centro Hospitalar Lisboa Norte, E.P.E Hospital Santa Maria

SUPERVISION EXPERIENCE

1. September 2015 – October 2016: Supervision of Raquel Maia, Msc student with the thesis entitled “preclinical development of a new compound for the treatment of arthritis”.
 2. September 2015 – October 2016: Supervision of Ânia Sousa, Msc student with the thesis entitled "Efficacy and toxicity evaluation of celastrol in adjuvant-induced arthritis rat model"
 3. September 2014 – October 2015: Supervision of Inês Lopes, Msc student with the thesis entitled “Evaluation of celastrol as a candidate for the treatment of rheumatoid arthritis”
 4. August 2009 – present: Supervision of several Summer/volunteer internships and high school students from “Ciência Viva”.
-

PRIZES

1. ECTS/Amgen Bone Biology Fellowship 2014

PEER-REVIEWED PUBLICATIONS

Research articles

1. Santos MJ, Carmona-Fernandes D, Caetano-Lopes J, Perpétuo IP, **Vidal B**, Capela S, Canas da Silva J, Fonseca JE. TNF promoter -308 G>A and LTA 252 A>G polymorphisms in Portuguese patients with systemic lupus erythematosus. *Rheumatol Int.* 2011
 2. Santos MJ, Fernandes D, Caetano-Lopes J, Perpetuo IP, **Vidal B**, Canhao H, Fonseca JE. Lymphotoxin- α 252 A>G Polymorphism: A Link Between Disease Susceptibility and Dyslipidemia in Rheumatoid Arthritis *J Rheumatol.* 2011
 3. Caetano-Lopes J, Rodrigues A, Lopes A, Vale AC, Pitts-Kiefer MA, **Vidal B**, Perpétuo I, Monjardino T, Monteiro J, Konttinen YT, Vaz MF, Nazarian A, Canhão H, Fonseca JE. (2011) Rheumatoid Arthritis Bone Fragility Is Associated with Increased Dickkopf-1 Expression and Disturbances in the Bone Turnover Regulating genes. *Clin Rev Allergy Immunol.* 2013Apr
 4. Vale AC, Faustino J, Reis L, Lopes A, **Vidal B**, Monteiro J, Fonseca JE, Canhão H, Vaz MF. Effect of the strain rate on the twisting of trabecular bone from women with hip fracture. *J Biomech Eng.* 2013
 5. Rodrigues AM, Caetano-Lopes J, Vale AC, **Vidal B**, Lopes A, Aleixo I, Polido-Pereira J, Sepriano A, Perpétuo IP, Monteiro J, Vaz MF, Fonseca JE, Canhão H. Low osteocalcin/collagen type I bone gene expression ratio is associated with hip fragility fractures. *Bone.* 2012 Dec;
 6. Cascão R, **Vidal B**, Raquel H, Neves-Costa A, Figueiredo N, Gupta V, Fonseca JE, Moita LF. Effective treatment of rat adjuvant-induced arthritis by celastrol. *Autoimmun Rev.* 2012 Oct;
 7. Cascão R, **Vidal B**, Raquel H, Neves-Costa A, Figueiredo N, Gupta V, Fonseca JE, Moita LF. Potent anti-inflammatory and antiproliferative effects of gambogic acid in a rat model of antigen-induced arthritis. *Mediators Inflamm.* 2014
 8. **Vidal B**, Pinto A, Galvão MJ, Santos AR, Rodrigues A, Cascão R, Abdulghani S, Caetano-Lopes J, Ferreira A, Fonseca JE, Canhao H. Bone histomorphometry revisited. *Acta Reumatol Port.* 2012 Oct-Dec
 9. **Vidal B**, Rita Cascão , Ana Catarina Vale, Inês Cavaleiro, Maria Fátima Vaz, José Américo Almeida Brito, Helena Canhão, João Eurico Fonseca. Arthritis induces early bone high turnover, structural degradation and mechanical weakness. *PLOS One*, Dec2014.
 10. Rita Cascão , **Vidal B** , Inês P. Lopes , Eunice Paisana , José Rino , Luis F. Moita , João E. Fonseca. Decrease of CD68 synovial macrophages in celastrol treated arthritic rats. *PLOS One*, Nov2015.
 11. **Vidal B**, Cascão R, Finnilä M, Lopes I, Saarakkala S, Zioupos P, Canhão H, Fonseca JE. Effects of tofacitinib in early arthritis bone loss. (Submitted)
-

12. **Vidal B**, Cascão R, Finnilä M, Lopes I, Saarakkala S, Zioupos P, Canhão H, Fonseca JE. Early arthritis induces disturbances at bone nanostructural level reflected in decreased tissue hardness. (Submitted)
13. Cascão R*, **Vidal B***, Finnilä M, Lopes I, Saarakkala S, Moita L, Fonseca JE. Celastrol preserves bone structure and mechanics in arthritic rats. Vidal B. and Cascão R. *Contributed equally to this work. (Submitted)

SCIENTIFIC COMMUNICATIONS

Oral Presentations

1. **Vidal B**, Canhão H, Fonseca JE “How early inflammatory events affect bone nano - properties at rheumatoid arthritis onset” 12th Medinterna International Meeting, Porto, Portugal
2. **Vidal B**, Cascão R , Vale AC, Cavaleiro I, Vaz MF, Brito JA, Canhão H, Fonseca JE. “How early inflammatory events affect bone nano - properties at rheumatoid arthritis onset” PhD Meeting 2015, Lisboa, Portugal
3. **Vidal B**, Rita Cascão, Mikko Finnilä, Inês Lopes, Simo Saarakkala, Helena Canhão, João Fonseca.”Analyzing the effects of early arthritis in systemic bone loss”. CPR2016. Vilamoura, Portugal

Poster Presentations

1. **Vidal B**, Canhão H, Fonseca JE. “How early inflammatory events affect bone nano - properties at rheumatoid arthritis onset”. PhD Meeting 2012, Lisboa, Portugal
 2. **Vidal B**, Canhão H, Fonseca JE. “How early inflammatory events affect bone nano - properties at rheumatoid arthritis onset”. ECTS 2013, Lisboa, Portugal
 3. **Vidal B**, Cascão R, Canhão H, Fonseca JE. “How early inflammatory events affect bone nano - properties at rheumatoid arthritis onset”. PhD Meeting 2013, Lisboa, Portugal
 4. **Vidal B**, Cascão R, Vale AC, Cavaleiro I, Vaz MF, Brito JA, Canhão H, Fonseca JE. “How early inflammatory events affect bone nano - properties at rheumatoid arthritis onset”. PhD Meeting 2014, Lisboa, Portugal
 5. **Vidal B**, Cascão R , Vale AC, Cavaleiro I, Vaz MF, Brito JA, Canhão H, Fonseca JE. “Arthritis induces early bone high turnover, structural degradation and mechanical weakness”. ewIMID2014 Funchal-Madeira, Portugal
 6. **Vidal B**, Cascão R , Vale AC, Cavaleiro I, Vaz MF, Brito JA, Canhão H, Fonseca JE. “Arthritis induces early bone high turnover, structural degradation and mechanical weakness”. EWRR2015 Budapest, Hungary
-

RESEARCH ARTICLE

Arthritis Induces Early Bone High Turnover, Structural Degradation and Mechanical Weakness

Bruno Vidal^{1*}, Rita Cascão¹, Ana Catarina Vale², Inês Cavaleiro³, Maria Fátima Vaz^{2,4}, José Américo Almeida Brito³, Helena Canhão^{1,5}, João Eurico Fonseca^{1,5}

1 Instituto de Medicina Molecular, Faculdade de Medicina da Universidade de Lisboa, Lisbon, Portugal, **2** Instituto de Ciência e Engenharia de Materiais e Superfícies, Instituto Superior Técnico, University of Lisbon, Lisbon, Portugal, **3** Instituto Superior de Ciências da Saúde Egas Moniz—Campus Universitário, Quinta da Granja, Caparica, Portugal, **4** Departamento de Engenharia Mecânica, Instituto Superior Técnico, UL, Lisbon, Portugal, **5** Rheumatology Department, Lisbon Academic Medical Centre, Lisbon, Portugal

* vidal.bmc@gmail.com



Abstract

Background

We have previously found in the chronic SKG mouse model of arthritis that long standing (5 and 8 months) inflammation directly leads to high collagen bone turnover, disorganization of the collagen network, disturbed bone microstructure and degradation of bone biomechanical properties. The main goal of the present work was to study the effects of the first days of the inflammatory process on the microarchitecture and mechanical properties of bone.

Methods

Twenty eight Wistar adjuvant-induced arthritis (AIA) rats were monitored during 22 days after disease induction for the inflammatory score, ankle perimeter and body weight. Healthy non-arthritic rats were used as controls for comparison. After 22 days of disease progression rats were sacrificed and bone samples were collected for histomorphometrical, energy dispersive X-ray spectroscopical analysis and 3-point bending. Blood samples were also collected for bone turnover markers.

Results

AIA rats had an increased bone turnover (as inferred from increased P1NP and CTX1, $p = 0.0010$ and $p = 0.0002$, respectively) and this was paralleled by a decreased mineral content (calcium $p = 0.0046$ and phos-phorus $p = 0.0046$). Histomorphometry showed a lower trabecular thickness ($p = 0.0002$) and bone volume ($p = 0.0003$) and higher trabecular separation ($p = 0.0009$) in the arthritic group as compared with controls. In addition, bone mechanical tests showed evidence of fragility as depicted by diminished values of yield stress and ultimate fracture point ($p = 0.0061$ and $p = 0.0279$, respectively) in the arthritic group.

OPEN ACCESS

Citation: Vidal B, Cascão R, Vale AC, Cavaleiro I, Vaz MF, Brito JAA, et al. (2015) Arthritis Induces Early Bone High Turnover, Structural Degradation and Mechanical Weakness. PLoS ONE 10(1): e0117100. doi:10.1371/journal.pone.0117100

Academic Editor: Antony Nicodemus Antoniou, University of East London, UNITED KINGDOM

Received: June 17, 2014

Accepted: December 18, 2014

Published: January 24, 2015

Copyright: © 2015 Vidal et al. This is an open access article distributed under the terms of the [Creative Commons Attribution License](https://creativecommons.org/licenses/by/4.0/), which permits unrestricted use, distribution, and reproduction in any medium, provided the original author and source are credited.

Data Availability Statement: All relevant data are within the paper.

Funding: This work was supported by a grant SFRH/BD/81527/2011 from Fundação para a Ciência e a Tecnologia (FCT) and grant ECTS/Amgen Bone Biology Fellowship 2014 from European Calcified Tissue Society. The funders had no role in study design, data collection and analysis, decision to publish, or preparation of the manuscript.

Competing Interests: The authors have declared that no competing interests exist.

Conclusions

We have shown in an AIA rat model that arthritis induces early bone high turnover, structural degradation, mineral loss and mechanical weakness.

Introduction

Rheumatoid arthritis (RA) is a chronic immune-mediated inflammatory disease, which affects around 1% of the world-population[1]. It causes joint and systemic inflammation that is reflected in local and systemic bone damage[2]. Bone is a dynamic tissue composed mainly of a type I collagen matrix that constitutes the scaffold for calcium hydroxyapatite crystal deposition. Remodelling of bone is a continuous process by which osteoclasts resorb bone tissue and osteoblasts produce new bone matrix that is subsequently mineralised. Biochemical markers of this bone turnover are produced and released into circulation, providing a read-out of kinetics and the balance between bone loss and formation. More specifically, bone-resorbing osteoclasts release carboxy-terminal collagen cross-linking telopeptides (CTX-I), a marker for bone degradation, which is produced by cathepsin K that is involved in systemic bone resorption [3]. During bone formation, collagen is synthesized by osteoblasts in the form of procollagen. This precursor contains a short signal sequence and terminal extension peptides: amino-terminal propeptide (PINP) and carboxy-terminal propeptide. These propeptide extensions are removed by specific proteinases before the collagen molecules form. PINP can be found in the circulation and its concentration reflects the synthesis rate of collagen type I, being thus a marker of bone formation [4]. As RA progresses there is marked articular destruction and decreased joint mobility with radiological evidence of erosion with significant impact on life quality within 2 years of disease onset [5]. In addition, osteoporosis is a common finding in patients with RA [6] and is responsible for increased rates of vertebral and hip fractures in these patients [7, 8]. RA is associated with an increased expression of the receptor activator of RANKL (receptor activator of nuclear factor kappa-B ligand, NF-KB ligand) and low levels of its antagonist, osteoprotegerin (OPG) [9]. In addition, very early on in the disease process, RA serum and synovial fluid present a cytokine profile, including interleukin (IL) 1, IL6, IL17 and tumour necrosis factor (TNF), which further favours osteoclast differentiation and activation[10–12]. Evidence suggests that bone remodelling disturbances in RA contribute not only to local bone erosions but also to the development of systemic osteoporosis [13].

We have previously found in a chronic animal model of arthritis (SKG mouse model) that prolonged inflammation (5 and 8 months) directly leads to the degradation of bone biomechanical properties, namely stiffness, ductility and bone strength, which was paralleled by a high collagen bone turnover and disorganization[4, 12, 14, 15]. Based on the fact that most of the effectors of bone metabolism are engaged in the disease process since the early phase, we now hypothesise that this process starts upon the first inflammatory manifestations[10–12]. To test this we selected the adjuvant-induced arthritis (AIA) model in rats, characterized by a rapid onset polyarticular inflammation and widely used for testing new treatments for arthritis [16–18]. Understanding the systemic inflammatory consequences on bone would expand the use of this model also for testing new drugs with potential bone therapeutic effects.

The main goal of the present work was to study, in a rat model of AIA, the effects of the first days of the systemic inflammatory process on the microarchitecture and mechanical properties of bone.

Materials and Methods

Animal experimental design

Twenty-eight Wistar AIA rats were purchased from Charles River Laboratories International (Massachusetts, USA). Eight-week-old females weighing 200–230 g were maintained under specific pathogen free (SPF) conditions. All experiments were approved by the Animal User and Ethical Committees of the Instituto de Medicina Molecular, Lisbon University, according to the Portuguese law and the European recommendations. Animals were sacrificed when presenting an inflammatory score (0–3) of 3 in 2 paws or when presenting 20% of body weight loss.

Rats were housed per groups (healthy *vs* arthritic) under standard laboratory conditions (at 22°C under 12-hour light/12-hour dark conditions). The inflammatory score, ankle perimeter and body weight were measured during the study period. Inflammatory signs were evaluated by counting the score of each joint in a scale of 0–3 (0— absence; 1— erythema; 2— erythema and swelling; 3— deformities and functional impairment). The total score of each animal was defined as the sum of the partial scores of each affected joint [19]. Rats were sacrificed by CO₂ narcosis after 22 days of disease evolution and blood as well as bone samples were collected.

Bone remodelling markers quantification

Serum samples were collected at the time of sacrifice and stored at -80°C. Bone remodelling markers CTX I (C-terminal telopeptides of type-I collagen) and P1NP (total procollagen type I N-terminal propeptide) were quantified by Serum Rat-Laps ELISA assay (Immunodiagnostic Systems Ltd, Boldon, UK), according to the provider's instructions.

Bone histomorphometry

The 4th lumbar vertebrae (L4) were collected from each animal at sacrifice for histomorphometric analysis. Samples were fixed immediately in ethanol 70% and then dehydrated with increasing ethanol concentrations (96% and 100%). Samples were next embedded in methylmethacrylate (MMA) solution. Serial transversal sections through L4 were performed with 5- μ m-thick and stained with Aniline Blue in order to distinguish bone and bone marrow, allowing bone structural analysis. Images were acquired using a Leica DM2500 microscope equipped with a colour camera Leica CCD Camera (Leica microsystems, Wetzlar, Germany)[20].

All variables were expressed and calculated according to the recommendations of the American Society for Bone and Mineral Research [21], using a morphometric program (Image J 1.46R with plugin Bone J).

Ratio of trabecular bone volume / total tissue volume, trabecular thickness and trabecular separation were evaluated by standard histomorphometric parameters at x12.5 magnification.

Energy dispersive X-ray spectroscopy analysis

Energy dispersive X-ray spectroscopy is a sensitive qualitative and semi-quantitative technique to evaluate the mineral content in bone. The quantitative information is based on the relative elemental abundance.

Using a standard system, semi-quantitative X-ray fluorescence measurements were performed in cortical and trabecular bone powder samples, with the purpose of quantifying calcium and phosphorus concentration.

After excision, fresh femurs were freeze dried for 46 hours, with a multipurpose ice condenser (ModulyoD-230, Thermo Savant, Schwerte, Germany) operated at a nominal temperature of -50°C , in order to remove excess of water.

The semi-quantitative measurements of bone powder were performed with a 4 kW commercial wavelength dispersive X-ray fluorescence spectrometer (Bruker S4 Pioneer, Karlsruhe, Germany), using a Rh X-ray tube with a 75 mm Be end window and a 34 mm diameter collimator mask. Measurements were performed in helium mode and using high-density polyethylene X-ray fluorescence sample cups with 35.8 mm diameter assembled with a 4 mm prolene film to support the bone sample. The polyethylene cup was placed in steel sample cup holders with an opening diameter of 34 mm.

Bone mechanical testing

Bone mechanical properties were evaluated by a three-point bending method using a electro-mechanical machine (model 5566, Instron Corporation, Canton, USA) using a load-cell of 500N. The femur was placed on a holding device with a support span distance of 5 mm (L), with the lesser trochanter proximal in contact with the proximal transverse bar. The load was applied at the mid-shaft of the diaphysis with a cross-head speed of 0.005 mm/s until the fracture occurred.

The stress-strain curve can be obtained from the load-displacement representation, with the initial dimensions of the sample, using engineering equations ([S1B Fig.](#)).

An example of a stress-strain curve obtained in the three point bending tests is shown in [S1A Fig.](#) The points of the yield stress and ultimate stress are indicated. This stress-strain curve can be broken down into pre-yield and post-yield portions. Pre-yield toughness represents the area under the stress/strain curve up to the yield point, which is where permanent deformation of the bone has occurred while post-yield toughness represents the area under the curve between the yield point and bone fracture. In these bending tests there is a significant amount of displacement between the yield point and the eventual fracture[[22](#)].

Statistical analysis

Continuous variables were expressed by mean \pm standard deviation (SD) or median and interquartile range. The normality distribution was assessed by D'Agostino and Pearson test. Statistical differences were determined with parametric *t*-test or non-parametric Mann Whitney test according variables distribution using GraphPad Prism (GraphPad, California, USA). Differences were considered statistically significant for *p* values ≤ 0.05 .

Results

Inflammatory progress

First, we validated the kinetic of disease development of the AIA rat model. Inflammatory signs ([Fig. 1A](#)) and ankle perimeter ([Fig. 1B](#)) were assessed throughout time, as shown in [Fig. 1](#). All animals from the arthritic group (N = 16) presented arthritis signs by the fourth day post disease induction.

Statistical differences were determined with non-parametric Mann Whitney test using GraphPad Prism (GraphPad, California, USA). Differences were considered statistically significant for *p* values ≤ 0.05 .

The initial acute inflammation was observed around day 4 and progressed during 22 days post disease induction. After 10 days of arthritis induction, the inflammatory manifestations increased sharply as depicted by an increase in ankle perimeter. Maximal swelling occurred at

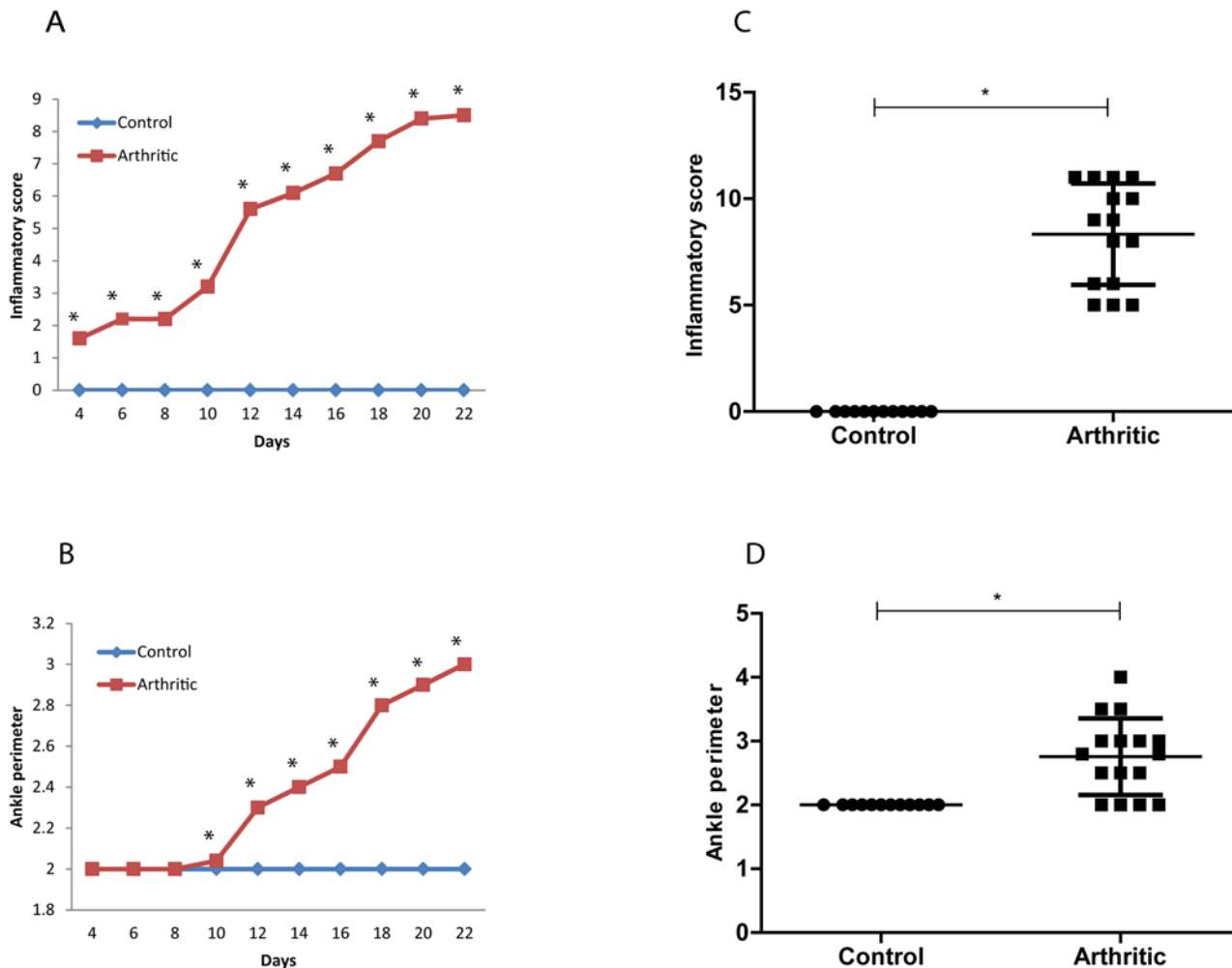


Figure 1. Inflammatory score (A) and ankle perimeter (B) throughout time. Inflammatory score (C) ($p = 0.0037$) and Ankle perimeter (D) ($p = 0.0085$) in control ($N = 12$) and arthritic groups ($N = 16$) by the time of sacrifice after 22 days post disease induction.

doi:10.1371/journal.pone.0117100.g001

day 19 post disease induction. At day 22 post arthritis induction inflammatory score (Fig. 1C) and ankle perimeter (Fig. 1D) were significantly increased in the arthritic group ($p = 0.0037$ and $p = 0.0085$, respectively) in comparison with healthy control rats.

Bone turnover markers

Bone resorption marker CTX I, which reflects osteoclastic activity, is a degradation product of type I collagen, the major structural protein of bone. While the bone formation marker P1NP, a bio product of type I collagen synthesis, is a marker for osteoblastic activity.

We have observed that both CTXI (Fig. 2A) and P1NP (Fig. 2B) were significantly increased in the arthritic group in comparison with the healthy control animals ($p = 0.0002$ and $p = 0.0010$, respectively), revealing an increase of bone turnover in the arthritic group.

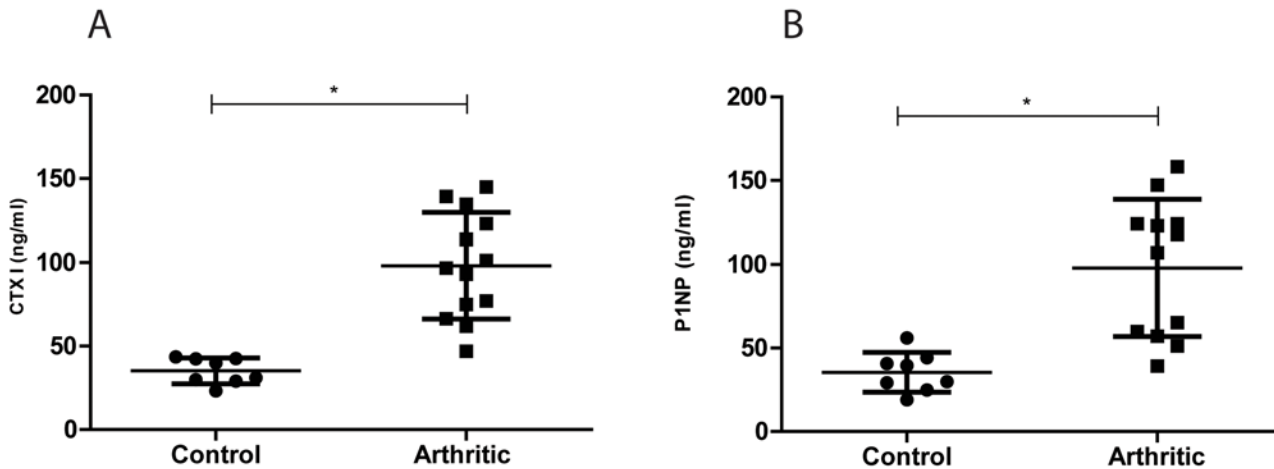


Figure 2. Bone turnover markers quantification in control (N = 9) and arthritic rats (N = 13). Serum samples collected at day 22 (sacrificed) were analysed by ELISA technique. Bone resorption marker, CTX I (A) and bone formation marker, P1NP (B) were increased in arthritic rats ($p = 0.0002$ and $p = 0.0010$, respectively).

doi:10.1371/journal.pone.0117100.g002

Histomorphometry of bone

Bone histomorphometry was used to measure bone static parameters such as bone trabecular volume, trabecular thickness and trabecular separation in order to determine the effects of inflammation on bone microstructure (Fig. 3A).

Trabecular bone volume ($p = 0.0003$) (Fig. 3B) and trabecular thickness ($p = 0.0002$) (Fig. 3C) were significantly reduced in arthritic animals comparing with healthy control animals. Moreover, trabecular separation ($p = 0.0009$) (Fig. 3D) was significantly increased in the arthritic group, in comparison with healthy control rats.

Energy dispersive X-ray spectroscopy

Calcium (Ca) and Phosphorus (P) are the most abundant elements present in bone mineral matrix. In fact, calcium has been reported as the most important nutrient associated with peak bone mass and may be the only one for which there is epidemiological evidence of a relation to fracture rate[23].

We used energy dispersive X-ray spectroscopy to quantify the calcium and phosphorus content in our samples. We have observed that Ca ($p = 0.0046$) (Fig. 4A) and P ($p = 0.0046$) (Fig. 4B) content were decreased in the arthritic group as compared to controls.

Bone mechanics

The three-point-bending biomechanical tests aimed to explore the bone mechanical competence of both groups 22 days post disease induction. Results showed decreased values of yield stress (moment of occurrence of first micro fractures) ($p = 0.0061$) (Fig. 5A) and ultimate stress (moment of occurrence of complete fracture) ($p = 0.0279$) (Fig. 5B) in arthritic animals when compared to the control group.

Discussion

In the present study, we demonstrated in an AIA rat model, that arthritis induces very early high bone turnover, trabecular degradation, mineral loss and mechanical weakness.

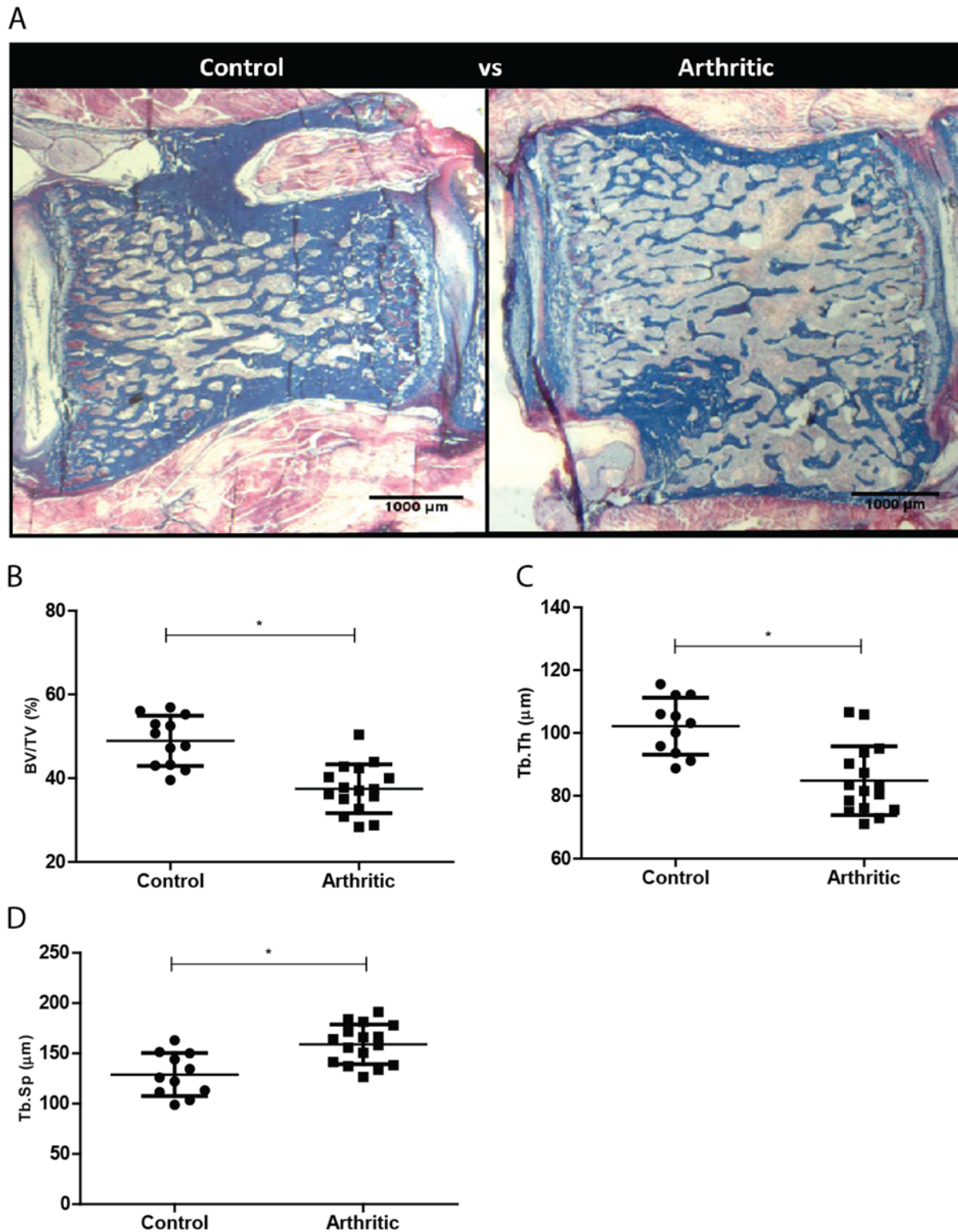


Figure 3. Bone histomorphometry assessment of the 4th lumbar vertebra (L4). Assessment of L4 in control (N = 12) and arthritic group (N = 16). (A) Illustrative Aniline blue stained sections of L4 vertebra collected at day 22 post disease induction (sacrifice). Bone volume per tissue volume or trabecular bone volume fraction (B) and trabecular thickness (C) were decreased in arthritic rats while trabecular separation (D) was increased. Magnification x12.5.

doi:10.1371/journal.pone.0117100.g003

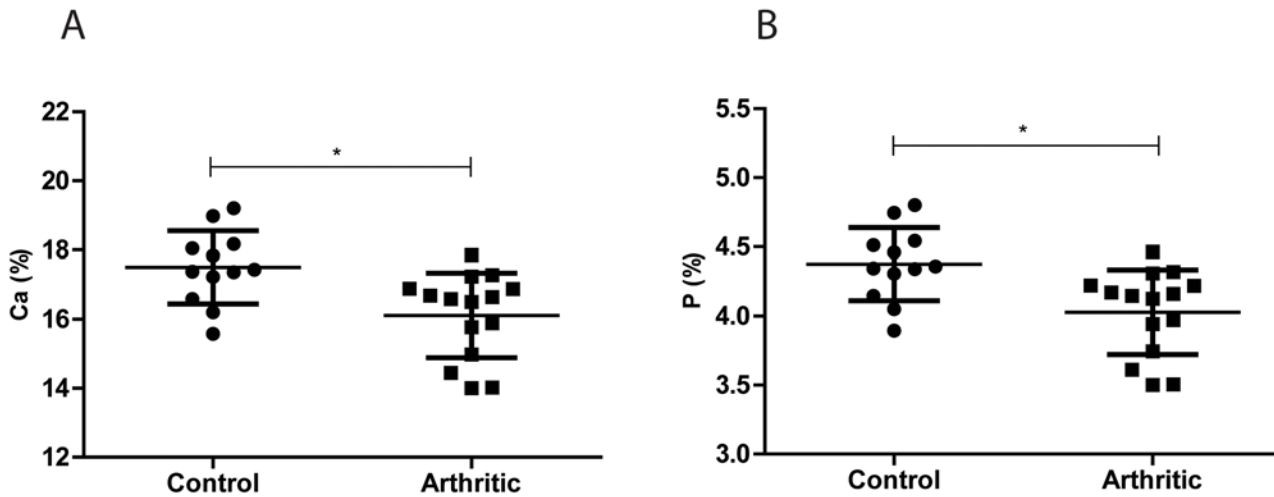


Figure 4. Calcium and Phosphorus bone content acquired by energy dispersive X-ray spectroscopy. Ca (A) and P (B) bone content were decreased in the arthritic group (N = 16) as compared with controls (N = 12). Bone powder was acquired from bone samples collected at day 22 post disease induction (sacrifice).

doi:10.1371/journal.pone.0117100.g004

Biochemical markers of bone turnover were quantified in order to evaluate the impact of systemic inflammation on bone metabolism. An increased bone turnover activity was shown in arthritic animals, as depicted by increased CTXI and P1NP levels. This observation was consistent with previously published data showing the presence of a large number of osteoclasts in AIA bone [17]. Data already published by our group in another animal model of arthritis (the SKG mice model) have also shown that P1NP levels were increased in arthritic animals and so did CTX-I levels [4], reflecting an overall increase in bone turnover [24]. Studies on RA patients measuring P1NP have produced varying results, whereas measurements in CTX-I mostly show increased levels [25]. In RA patients bone metabolism is more active (increased P1NP) in earlier stages of the disease and a decrease in bone metabolic activity (both P1NP and CTX) occurs with disease progression, both showing correlation with tender and swollen joints [15]. Despite the existing variability, P1NP has been mainly found to be increased in RA patients

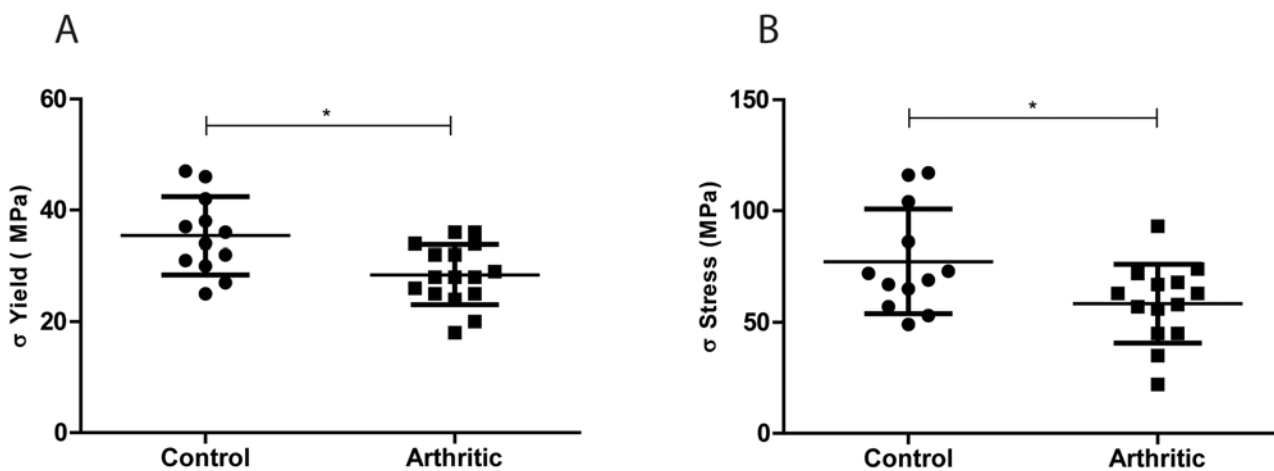


Figure 5. Mechanical analysis acquired by 3 point bending tests. Yield stress (A) and Ultimate stress (B) were decreased in arthritic rats (N = 16) as compared to controls (N = 12). Bone samples were collected at day 22 post disease induction (sacrifice).

doi:10.1371/journal.pone.0117100.g005

when compared to controls, together with CTX-I, revealing a compensatory mechanism in bone turnover [26].

Due to increased bone turnover it was therefore of interest to assess the effects of inflammation on bone microstructure. Histomorphometric data revealed, in arthritic animals, a lower fraction of trabecular bone volume and a lower average trabecular thickness as well as a higher average trabecular separation, in comparison with controls. These findings were in line with the described bone volume loss, measured by uCT, in this rat model [17].

In addition, we quantified calcium and phosphorus content, the two major minerals present in bone [27], by energy dispersive X-ray spectroscopy. The arthritic group showed a significant decreased mineral content, when compared to the control group. This result corroborated an overall bone mineral loss, as a result of an unbalanced high bone turnover, which might lead to bone fragility and consequently fracture.

In accordance, mechanical tests revealed that arthritic femurs have a significantly lower yield stress and ultimate stress as compared to control femurs, meaning that bone is more fragile and prone to fracture.

In summary, we have shown, in an AIA rat model, that the systemic inflammation associated with a polyarthritis is able to induce an early high bone turnover, bone microarchitecture degradation, low mineral content and mechanical weakness. In addition, our results have expanded the knowledge on this model. In fact, our findings, suggest that AIA is a fast and adequate model to study the effects of arthritis on bone properties and consequently a potentially accurate model to study anti-arthritic compounds with bone protective effects.

Supporting Information

S1 Fig. Scheme representative of the yield stress and ultimate stress points in a stress/strain curve. Yield stress and ultimate stress points (A) obtained with bending test with the specific formulas for stress (B) strain (C) calculation, where σ —stress (Pa); L—load (N); s—support span (mm); df—femoral outer diameter (mm); ϵ —strain (%); Δl —displacement (mm). (TIF)

Author Contributions

Conceived and designed the experiments: BV RC HC JF. Performed the experiments: BV ACV IC. Analyzed the data: BV ACV. Contributed reagents/materials/analysis tools: HC JF MV JB. Wrote the paper: BV RC HC JF.

References

1. Alamanos Y, Drosos AA (2005) Epidemiology of adult rheumatoid arthritis. *Autoimmun Rev* 4: 130–136. doi: [10.1016/j.autrev.2004.09.002](https://doi.org/10.1016/j.autrev.2004.09.002) PMID: [15823498](https://pubmed.ncbi.nlm.nih.gov/15823498/)
2. Yelin E, Callahan LF (1995) The economic cost and social and psychological impact of musculoskeletal conditions. *National Arthritis Data Work Groups. Arthritis Rheum* 38: 1351–1362. doi: [10.1002/art.1780381002](https://doi.org/10.1002/art.1780381002) PMID: [7575685](https://pubmed.ncbi.nlm.nih.gov/7575685/)
3. Gravallesse EM (2002) Bone destruction in arthritis. *Ann Rheum Dis* 61 Suppl 2: ii84–86. doi: [10.1136/ard.61.suppl_2.ii84](https://doi.org/10.1136/ard.61.suppl_2.ii84) PMID: [12379632](https://pubmed.ncbi.nlm.nih.gov/12379632/)
4. Caetano-Lopes J, Nery AM, Canhao H, Duarte J, Cascao R, et al. (2010) Chronic arthritis leads to disturbances in the bone collagen network. *Arthritis Res Ther* 12: R9. doi: [10.1186/ar2908](https://doi.org/10.1186/ar2908) PMID: [20078856](https://pubmed.ncbi.nlm.nih.gov/20078856/)
5. Lin YY, Jean YH, Lee HP, Chen WF, Sun YM, et al. (2013) A soft coral-derived compound, 11-episinulariolide acetate suppresses inflammatory response and bone destruction in adjuvant-induced arthritis. *PLoS One* 8: e62926. doi: [10.1371/journal.pone.0062926](https://doi.org/10.1371/journal.pone.0062926) PMID: [23675440](https://pubmed.ncbi.nlm.nih.gov/23675440/)

6. Haugeberg G, Orstavik RE, Uhlig T, Falch JA, Halse JI, et al. (2002) Bone loss in patients with rheumatoid arthritis: results from a population-based cohort of 366 patients followed up for two years. *Arthritis Rheum* 46: 1720–1728. doi: [10.1002/art.10408](https://doi.org/10.1002/art.10408) PMID: [12124854](https://pubmed.ncbi.nlm.nih.gov/12124854/)
7. Eric-Jan JA, Kroot RFJML (2000) Bone mass in rheumatoid arthritis. *CLINICAL AND EXPERIMENTAL RHEUMATOLOGY*.
8. Marshall D, Johnell O, Wedel H (1996) Meta-analysis of how well measures of bone mineral density predict occurrence of osteoporotic fractures. *BMJ* 312: 1254–1259. doi: [10.1136/bmj.312.7041.1254](https://doi.org/10.1136/bmj.312.7041.1254) PMID: [8634613](https://pubmed.ncbi.nlm.nih.gov/8634613/)
9. Fonseca JE, Cortez-Dias N, Francisco A, Sobral M, Canhao H, et al. (2005) Inflammatory cell infiltrate and RANKL/OPG expression in rheumatoid synovium: comparison with other inflammatory arthropathies and correlation with outcome. *Clin Exp Rheumatol* 23: 185–192. PMID: [15895888](https://pubmed.ncbi.nlm.nih.gov/15895888/)
10. Moura RA, Cascao R, Perpetuo I, Canhao H, Vieira-Sousa E, et al. (2011) Cytokine pattern in very early rheumatoid arthritis favours B-cell activation and survival. *Rheumatology (Oxford)* 50: 278–282. doi: [10.1093/rheumatology/keq338](https://doi.org/10.1093/rheumatology/keq338)
11. Cascao R, Moura RA, Perpetuo I, Canhao H, Vieira-Sousa E, et al. (2010) Identification of a cytokine network sustaining neutrophil and Th17 activation in untreated early rheumatoid arthritis. *Arthritis Res Ther* 12: R196. doi: [10.1186/ar3168](https://doi.org/10.1186/ar3168) PMID: [20961415](https://pubmed.ncbi.nlm.nih.gov/20961415/)
12. Caetano-Lopes J, Canhao H, Fonseca JE (2009) Osteoimmunology—the hidden immune regulation of bone. *Autoimmun Rev* 8: 250–255. doi: [10.1016/j.autrev.2008.07.038](https://doi.org/10.1016/j.autrev.2008.07.038) PMID: [18722561](https://pubmed.ncbi.nlm.nih.gov/18722561/)
13. Caetano-Lopes J, Rodrigues A, Lopes A, Vale AC, Pitts-Kiefer MA, et al. (2014) Rheumatoid Arthritis Bone Fragility Is Associated With Upregulation of IL17 and DKK1 Gene Expression. *Clin Rev Allergy Immunol* 47: 38–45. doi: [10.1007/s12016-013-8366-y](https://doi.org/10.1007/s12016-013-8366-y) PMID: [23546988](https://pubmed.ncbi.nlm.nih.gov/23546988/)
14. Caetano-Lopes J, Nery AM, Henriques R, Canhao H, Duarte J, et al. (2009) Chronic arthritis directly induces quantitative and qualitative bone disturbances leading to compromised biomechanical properties. *Clin Exp Rheumatol* 27: 475–482. PMID: [19604441](https://pubmed.ncbi.nlm.nih.gov/19604441/)
15. Wislowska M, Jakubicz D, Stepień K, Cicha M (2009) Serum concentrations of formation (PINP) and resorption (Ctx) bone turnover markers in rheumatoid arthritis. *Rheumatol Int* 29: 1403–1409. doi: [10.1007/s00296-009-0867-x](https://doi.org/10.1007/s00296-009-0867-x) PMID: [19219607](https://pubmed.ncbi.nlm.nih.gov/19219607/)
16. Bendele A (2001) Animal models of rheumatoid arthritis. *J Musculoskelet Neuronal Interact* 1: 377–385. PMID: [15758488](https://pubmed.ncbi.nlm.nih.gov/15758488/)
17. KAaBDJ Lisa R. Schopf (2006) Rat models of arthritis: Similarities, differences, advantages, and disadvantages in the identification of novel therapeutics. Cambridge, MA, USA: Millennium Pharmaceuticals.
18. Pearson CM (1956) Development of arthritis, peri-arthritis and periostitis in rats given adjuvants. *Proc Soc Exp Biol Med* 91: 95–101. doi: [10.3181/00379727-91-22179](https://doi.org/10.3181/00379727-91-22179) PMID: [13297719](https://pubmed.ncbi.nlm.nih.gov/13297719/)
19. da Silva JA, Fonseca JE, Graca L, Moita L, Carmo-Fonseca M (1996) Reinnervation of post-arthritic joints in the rat. *Clin Exp Rheumatol* 14: 43–51. PMID: [8697656](https://pubmed.ncbi.nlm.nih.gov/8697656/)
20. Vidal B, Pinto A, Galvao MJ, Santos AR, Rodrigues A, et al. (2012) Bone histomorphometry revisited. *Acta Reumatol Port* 37: 294–300. PMID: [24126421](https://pubmed.ncbi.nlm.nih.gov/24126421/)
21. Parfitt AM, Drezner MK, Glorieux FH, Kanis JA, Malluche H, et al. (1987) Bone histomorphometry: standardization of nomenclature, symbols, and units. Report of the ASBMR Histomorphometry Nomenclature Committee. *J Bone Miner Res* 2: 595–610. doi: [10.1002/jbmr.5650020617](https://doi.org/10.1002/jbmr.5650020617) PMID: [3455637](https://pubmed.ncbi.nlm.nih.gov/3455637/)
22. Allen MR, Reinwald S, Burr DB (2008) Alendronate reduces bone toughness of ribs without significantly increasing microdamage accumulation in dogs following 3 years of daily treatment. *Calcif Tissue Int* 82: 354–360. doi: [10.1007/s00223-008-9131-8](https://doi.org/10.1007/s00223-008-9131-8) PMID: [18463913](https://pubmed.ncbi.nlm.nih.gov/18463913/)
23. Jiang Y, Zhao J, Genant HK, Dequeker J, Geusens P (1997) Long-term changes in bone mineral and biomechanical properties of vertebrae and femur in aging, dietary calcium restricted, and/or estrogen-deprived/-replaced rats. *J Bone Miner Res* 12: 820–831. doi: [10.1359/jbmr.1997.12.5.820](https://doi.org/10.1359/jbmr.1997.12.5.820) PMID: [9144349](https://pubmed.ncbi.nlm.nih.gov/9144349/)
24. Siebuhr AS, Wang J, Karsdal M, Bay-Jensen AC, YJ, et al. (2012) Matrix metalloproteinase-dependent turnover of cartilage, synovial membrane, and connective tissue is elevated in rats with collagen induced arthritis. *J Transl Med* 10: 195. doi: [10.1186/1479-5876-10-195](https://doi.org/10.1186/1479-5876-10-195) PMID: [22992383](https://pubmed.ncbi.nlm.nih.gov/22992383/)
25. van Schaardenburg D, Nielen MM, Lems WF, Twisk JW, Reesink HW, et al. (2011) Bone metabolism is altered in preclinical rheumatoid arthritis. *Ann Rheum Dis* 70: 1173–1174. doi: [10.1136/ard.2010.135723](https://doi.org/10.1136/ard.2010.135723) PMID: [20956407](https://pubmed.ncbi.nlm.nih.gov/20956407/)
26. Cortet B, Flipo RM, Pigny P, Duquesnoy B, Boersma A, et al. (1998) Is bone turnover a determinant of bone mass in rheumatoid arthritis? *J Rheumatol* 25: 2339–2344. PMID: [9858427](https://pubmed.ncbi.nlm.nih.gov/9858427/)
27. Bonjour JP (2011) Calcium and phosphate: a duet of ions playing for bone health. *J Am Coll Nutr* 30: 438S–448S. doi: [10.1080/07315724.2011.10719988](https://doi.org/10.1080/07315724.2011.10719988) PMID: [22081690](https://pubmed.ncbi.nlm.nih.gov/22081690/)

Manuscript Number: BONE-D-16-00957

Title: Early arthritis induces disturbances at bone nanostructural level reflected in decreased tissue hardness

Article Type: Full length article

Keywords: Rheumatoid arthritis (RA); early arthritis; bone properties; Wistar rats; animal model.

Corresponding Author: Mr. Bruno Vidal,

Corresponding Author's Institution: Instituto de Medicina Molecular, Faculdade de Medicina da Universidade de Lisboa

First Author: Bruno Vidal

Order of Authors: Bruno Vidal; Rita Cascão, PhD; Mikko Finnila, PhD; Inês Lopes, MsC; Simo Saarakkala, PhD; Peter Zioupos, PhD; Helena Canhão, MD, PhD; João Fonseca, MD, PhD

Abstract: Rheumatoid arthritis (RA) is a chronic immune-mediated inflammatory disease, which causes local and systemic bone damage. Objectives - The main goal of this work was to analyze the effects of the early phase of systemic inflammatory process at bone tissue level, including nanomechanical properties, microarchitecture and mineral and collagen content.

Methods - Eighty-eight Wistar rats were randomly housed in experimental groups, as follows: an adjuvant induced arthritis (N= 47) and a control healthy group (N= 41). Rats were monitored during 22 days for the inflammatory score, ankle perimeter and body weight and sacrificed at different time points (11 and 22 days post disease induction). Bone samples were collected for histology, micro-CT, 3-point bending test, nanoindentation and Fourier transformed infrared spectroscopy (FTIR) analysis. Blood samples were also collected for bone turnover markers and systemic cytokine quantification.

Results At bone tissue level, measured by FTIR analysis and nanoindentation, there was a reduction of the mineral and collagen content and of hardness in the arthritic group, associated with an increase of the ratio of bone concentric to parallel lamellae and of the area of the osteocyte lacuna. In addition, increased bone turnover and changes in the microstructure and mechanical properties were observed in arthritic animals since the early phase of arthritis, when compared with healthy controls.

Conclusion - Systemic inflammation induces very early changes at bone tissue level characterized by decreased tissue hardness, associated with changes in bone lamella organization and osteocyte lacuna surface and with decreased collagen and mineral content. These observations highlight the pertinence of immediate control of inflammation and of bone metabolism variables in the initial stages of arthritis.

Suggested Reviewers: Francisco Airton Rocha
arocha@ufc.br

Dominique Baeten
d.l.baeten@amc.uva.nl

Peter Korsten
peter.korsten@med.uni-goettingen.de

Opposed Reviewers:

Early arthritis induces disturbances at bone nanostructural level reflected in decreased tissue hardness

Bruno Vidal¹, Rita Cascão¹, Mikko Finnilä^{2,3}, Inês Lopes¹, Simo Saarakkala^{2,4,5}, Peter Zioupos⁶, Helena Canhão⁷, João Fonseca^{1,8}

1 Instituto de Medicina Molecular, Faculdade de Medicina, Universidade de Lisboa, Lisboa, Portugal; 2 Research Unit of Medical Imaging, Physics and Technology, Faculty of Medicine, University of Oulu, Oulu, Finland; 3 Department of Applied Physics, University of Eastern Finland, Kuopio, Finland; 4 Medical Research Center Oulu, Oulu University, Oulu, Finland; 5 Department of Diagnostic Radiology, Oulu University Hospital, Oulu, Finland; 6 Biomechanics Labs, Cranfield Forensic Institute, Cranfield University, DA of the UK; 7 EpiDoC Unit, CEDOC, NOVA Medical School, NOVA University, Lisbon, Portugal; 8 Rheumatology Department, Centro Hospitalar de Lisboa Norte, EPE, Hospital de Santa Maria, Lisbon Academic Medical Centre, Lisbon, Portugal

Corresponding author:
Full name – Bruno Vidal

1
2 **ABSTRACT**

3 Rheumatoid arthritis (RA) is a chronic immune-mediated inflammatory disease, which
4 causes local and systemic bone damage.
5

6 **Objectives** - The main goal of this work was to analyze the effects of the early phase of
7 systemic inflammatory process at bone tissue level, including nanomechanical properties,
8 microarchitecture and mineral and collagen content.
9

10 **Methods** – Eighty-eight Wistar rats were randomly housed in experimental groups, as
11 follows: an adjuvant induced arthritis (N= 47) and a control healthy group (N= 41). Rats
12 were monitored during 22 days for the inflammatory score, ankle perimeter and body weight
13 and sacrificed at different time points (11 and 22 days post disease induction). Bone
14 samples were collected for histology, micro-CT, 3-point bending test, nanoindentation and
15 Fourier transformed infrared spectroscopy (FTIR) analysis. Blood samples were also
16 collected for bone turnover markers and systemic cytokine quantification.
17

18 **Results** At bone tissue level, measured by FTIR analysis and nanoindentation, there was a
19 reduction of the mineral and collagen content and of hardness in the arthritic group,
20 associated with an increase of the ratio of bone concentric to parallel lamellae and of the
21 area of the osteocyte lacuna. In addition, increased bone turnover and changes in the
22 microstructure and mechanical properties were observed in arthritic animals since the early
23 phase of arthritis, when compared with healthy controls.
24

25 **Conclusion** - Systemic inflammation induces very early changes at bone tissue level
26 characterized by decreased tissue hardness, associated with changes in bone lamella
27 organization and osteocyte lacuna surface and with decreased collagen and mineral
28 content. These observations highlight the pertinence of immediate control of inflammation
29 and of bone metabolism variables in the initial stages of arthritis.
30
31
32
33

34 **KEYWORDS:** Rheumatoid arthritis (RA), early arthritis, bone properties, Wistar rats, animal
35 model
36
37
38
39
40
41
42
43
44

Introduction

Rheumatoid arthritis (RA) is the most common chronic inflammatory joint disease, affecting about 1% of the world population. RA is characterized by synovial hyperplasia caused by a large proliferative cellular infiltrate of leukocytes and high expression levels of proinflammatory cytokines [1]. As RA progresses there is marked articular destruction and decreased joint mobility with radiological evidence of bone erosion within 2 years of disease onset [2]. In addition, osteoporosis is a common finding in patients with RA [3] and is responsible for increased rates of vertebral and hip fractures in these patients [4,5]. RA is associated with an augmented expression of the receptor activator of RANKL (receptor activator of nuclear factor kappa-B ligand, NF-KB ligand) and low levels of its antagonist, osteoprotegerin (OPG) [6]. RANKL is a crucial activator of osteoclastogenesis [7]. In addition, RA serum and synovial fluid present a cytokine profile, including interleukin (IL)1 β , IL6, IL17 and tumor necrosis factor (TNF), which further favors osteoclast differentiation and activation since the early phase of the disease [8-10].

Bone is a dynamic tissue composed mainly of a type I collagen matrix that constitutes the scaffold for calcium hydroxyapatite crystal deposition. Remodeling of bone is a continuous process by which osteoclasts resorb bone tissue and osteoblasts produce new bone matrix that is subsequently mineralized. In this process biochemical markers of bone turnover are produced and released into circulation, providing a read-out of remodeling kinetics. Evidence suggests that bone-remodeling disturbances in RA contribute not only to local bone erosions but also to the development of systemic osteoporosis [11].

We have previously found in the adjuvant-induced rat model of arthritis (AIA) that 22 days of sustained and established inflammatory disease progression directly leads to the degradation of bone biomechanical properties, namely stiffness, ductility and bone strength, which was paralleled by a high collagen bone turnover [12].

The main goal of this work was to analyze the effects of the early phase of systemic inflammatory process at bone tissue level, including nanomechanical properties, microarchitecture and mineral and collagen content.

Methods

Animal experimental design

Eighty-eight, 8 week-old female Wistar rats weighing approximately 230-250gr were housed in European type II standard filter top cages (Tecniplast, Buguggiate, Italy) and transferred into the SPF animal facility at the Instituto de Medicina Molecular, under a 14h light/10h dark light cycle, acclimatized to T= 20-22°C and RH= 50-60%. They were given access to autoclaved rodent breeder chow (Special Diet Service, RM3) and triple filtered water. Rats were purchased from Charles River laboratories international (Barcelona, Spain) and arthritis was induced on their laboratories in 47 animals. The transport service takes 3 days to arrive at Instituto de Medicina Molecular.

Upon arrival, animals were randomly housed in two groups, individually identified and cages were labelled according to the experimental groups, as follows: adjuvant induced arthritis model (N=47) and control healthy group (N=41). The inflammatory score, ankle perimeter and body weight were measured during disease development. Inflammatory signs were evaluated by counting the score of each joint in a scale of 0 – 3 (0 – absence; 1 – erythema; 2 – erythema and swelling; 3 – deformities and functional impairment). The total score of each animal was defined as the sum of the partial scores of each affected joint. Rats were sacrificed at day 11 and 22 post disease induction, and blood, paws and bone samples were collected. All experiments were approved by the Animal User and Ethical Committees at the Instituto de Medicina Molecular (Lisbon University), according to the Portuguese law and the European recommendations, Directive 2010/63/EU revising Directive 86/609/EEC.

Histological evaluation of hind paws

Left hind paw samples collected at the time of sacrifice were fixed immediately in 10% neutral buffered formalin solution and then decalcified in 10% formic acid. Samples were then dehydrated and embedded in paraffin, serially sectioned at a thickness of 5µm. Sections were stained with hematoxylin and eosin for histopathological evaluation of structural changes and cellular infiltration. This evaluation was performed in a blind fashion using 5 semi-quantitative scores:

- Sublining layer infiltration score (0-none to diffuse infiltration; 1-lymphoid cell aggregate; 2-lymphoid follicles; 3-lymphoid follicles with germinal center formation);
- Lining layer cell number score (0-fewer than three layers; 1-three to four layers; 2-five to six layers; 3-more than six layers);
- Bone erosion score (0-no erosions; 1-minimal; 2-mild; 3-moderate; 4-severe);
- Cartilage surface (0 –normal; 1 – irregular; 2 – clefts; 3 – clefts to bone);
- Global severity score (0-no signs of inflammation; 1-mild; 2-moderate; 3-severe) [13].

Images were acquired using a Leica DM2500 (Leica Microsystems, Wetzlar, Germany) microscope equipped with a color camera.

Biomarkers quantification

Serum samples were collected at the sacrifice time and stored at -80°C. The proinflammatory cytokine IL-6 (Boster Bio, California, USA) was quantified in serum samples using specific rat ELISA kits. Bone remodeling markers, CTX-I and P1NP, were quantified by Serum Rat Laps ELISA assay (Immunodiagnostic Systems Ltd, Boldon, UK).

1 For all biomarkers standard curves were generated by using reference biomarker
2 concentrations supplied by the manufacturers. Samples were analyzed using a
3 plate reader Infinite M200 (Tecan, Mannedorf, Switzerland).
4
5

6 7 **Micro-computed tomography (micro-CT) analysis**

8
9 Structural properties of the trabecular and cortical tibiae were determined with a
10 high-resolution micro-CT system (SkyScan 1272, Bruker microCT, Kontich,
11 Belgium). Moist bones were wrapped in parafilm and covered with dental wax to
12 prevent drying and movement during the scanning. X-ray tube was set to 50kV and
13 beam was filtered with 0.5mm Aluminum filter. Sample position and camera settings
14 were tuned to provide 3.0 μ m isotropic pixel size and projection images were
15 collected every 0.2°. Tissue mineral density values were calibrated against
16 hydroxyapatite phantoms with densities of 250mg/cm³ and 750mg/cm³.
17 Reconstructions were done with NRecon (v 1.6.9.8; Bruker microCT, Kontich,
18 Belgium) where appropriate corrections to reduce beam hardening and ring artifacts
19 were applied. Bone was segmented in slices of 3 μ m thickness. After 200 slices from
20 growth plate, we selected and analyzed 1400 slices of trabecular bone. For cortical
21 bone 300 slices (1800 slices from growth plate) were analyzed.
22
23

24 This evaluation was performed in agreement with guidelines for assessment of
25 bone microstructure in rodents using micro-computed tomography [14]. Trabecular
26 bone morphology was analyzed by applying global threshold and despeckle to
27 provide binary image for 3D analyzes. For cortical bone ROI was refined with ROI-
28 shrink wrap operation. This was followed by segmentation of blood vessels using
29 adaptive thresholding. Blood vessels and porosity were analyzed using 3D
30 morphological analyses.
31
32

33 34 **Bone mechanical tests**

35 The impact of inflammation on bone strength was investigated at the end of the
36 experiment. Femurs were subjected to a 3-point bending test using the universal
37 testing machine (Instron 3366, Instron Corp., Massachusetts, USA). Femurs were
38 placed horizontally anterior side upwards on a support with span length of
39 5mm. The load was applied with a constant speed of 0.005mm/s until failure
40 occurred. Stiffness was analyzed by fitting first-degree polynomial function to the
41
42
43
44
45
46
47
48
49
50
51
52
53
54
55
56
57
58
59
60
61
62
63
64
65

1 linear part of recorded load deformation data. A displacement of 0.15 μ m between
2 fitted slope and measured curve was used as criteria for yield point, whereas the
3 breaking point was defined as set where force reached maximal value. For both
4 yield and breaking points, force, deformation and absorbed energy were defined.
5
6
7

8 9 **Nanoindentation**

10 Nanoindentation was performed using a CSM-Nano Hardness Tester System (CSM
11 Instruments SA; Switzerland; Indentation v.3.83) equipped with a Berkovich based
12 pyramid diamond indenter. After micro-CT, 0.5mm of top tibia was cut and proximal
13 part was embedded to low viscosity epoxy resin (EpoThin, Buehler, Knorrung Oy Ab,
14 Helsinki, Finland). Slow speed diamond saw was used to remove 10% of bone
15 length. The sample surface was polished using silicon carbide sandpaper with a
16 decreasing grid size (800, 1200, 2400 and 4800) and finished with cloth containing
17 0.05 μ m γ -alumina particles. Indentation protocol was adopted from previous work
18 [15] and an average of 8 indentations were done on both cortical and trabecular
19 bone with quasi-static (so called 'advanced') loading protocol. All indentations were
20 performed under an optical microscope to achieve the precise location of
21 indentations at the center of the targeted area in the tissue [16].
22
23
24
25
26
27
28
29
30
31
32

33 In the 'advanced' protocol, a trapezoidal loading waveform was applied with a
34 loading/unloading rate of 20mN/min, and with an intermediate load-hold-phase
35 lasting 30s hold at a maximum load 10mN. The hardness (H_{IT}), indentation modulus
36 (E_{IT}), indentation creep (C_{IT}) and elastic part of indentation work (η_{IT}) were
37 measured by advanced protocol using the Oliver and Pharr (1992) method [17].
38
39
40
41
42

43 Histological images of rat tibiae from diaphyseal cortical region were acquired
44 during the nanoindentation technique, using a CSM instruments (Switzerland)
45 microscope equipped with a color camera.
46
47

48 A histologic score was applied in order to evaluate the lamellar structures of bone
49 tissue. This evaluation was performed in a blind fashion using a semi-quantitative
50 score:
51
52
53

- 54 • Lamellar bone structure: (1- predominantly parallel-lamella; 2 - concentric
55 and parallel-lamellae in the same proportion; 3 – predominantly concentric
56 lamella).
57
58
59
60
61
62
63
64
65

1
2
3
4
5
6
7
8
9
10
11
12
13
14
15
16
17
18
19
20
21
22
23
24
25
26
27
28
29
30
31
32
33
34
35
36
37
38
39
40
41
42
43
44
45
46
47
48
49
50
51
52
53
54
55
56
57
58
59
60
61
62
63
64
65

The ratio of osteocyte lacuna area / total tissue area was also evaluated at x200 magnification in order to analyse the percentage of total tissue area occupied by osteocyte lacunae. The method of acquisition and analysis used was the same applied for the evaluation of bone volume / tissue volume in histomorphometry technique [12]. All variables were expressed and calculated according to the recommendations of the American Society for Bone and Mineral Research [18], using a morphometric program (Image J 1.46R with plugin Bone J).

Fourier transformed infrared spectroscopy (FTIR)

Samples used for nanoindentation were also used for FTIR. Chemical composition was measured from bone surfaces separately with the HYPERION 3000 FTIRI microscope (Bruker Optics Inc, Billerica, MA, USA) using attenuated total reflection (ATR) objective. The ATR crystal was compressed on the bone with a constant load, and spectral images were recorded with a focal plane array detector (FPA). Spatial and spectral resolutions were set to 1 μ m and 2 cm^{-1} , respectively. Each spectrum between 840–3300 cm^{-1} was averaged 32 times and two spectral maps (32x32 spectra) were collected from the trabecular and cortical bone separately. Data was analyzed using a custom script in the MATLAB environment (MathWorks Inc, Natick, MA, USA). For each spectral map, areas under curves were calculated for amide I, phosphate and carbonate peaks by integrating spectra between 1595–1720 cm^{-1} , 900–1185 cm^{-1} and 850–895 cm^{-1} , respectively. Blood vessels and other porous structures were removed by excluding spectra with maximum phosphate peak height less than 0.5 absorbance units. Average content as well as well-established parameters for bone composition (carbonate:amide I, mineral:matrix and carbonate:phosphate) were finally calculated from the thresholded spectral maps [19].

Statistical analysis

Statistical differences were determined with Mann–Whitney tests using GraphPad Prism (GraphPad, California, USA). Correlation analysis was performed with the Spearman test. Differences were considered statistically significant for $p < 0.05$.

Results

The AIA rat model has a rapid and severe disease progression

Results showed that inflammatory signs (Fig.1) boosted sharply in the arthritic group. The inflammatory score (Fig.1A) increased significantly at day 11 and 22 post disease induction (which correspond to an acute phase and a chronic phase of systemic inflammation, respectively) in arthritic rats when compared to healthy controls ($p=0.0097$, respectively).

Moreover, arthritic animals at day 11 and 22 post disease induction sharply increased the ankle swelling throughout disease progression (Fig.1B), when compared to healthy rats ($p=0.0097$, respectively)

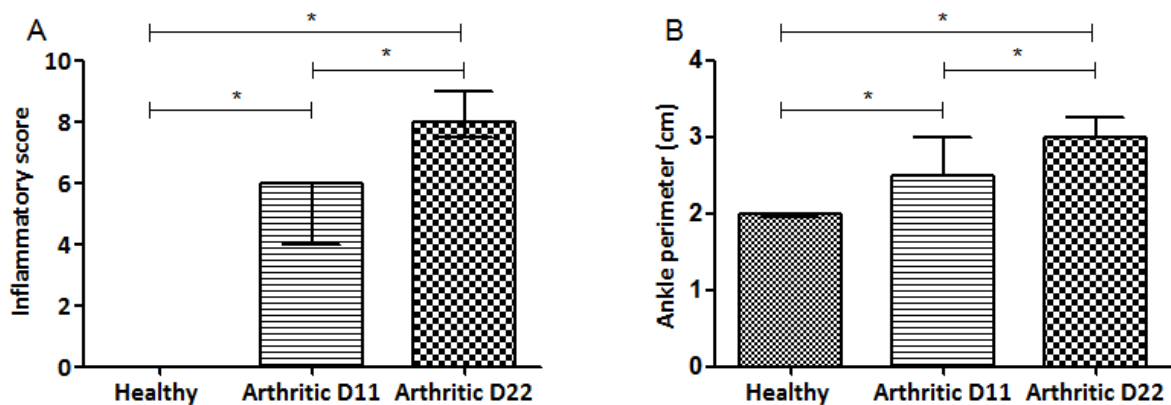
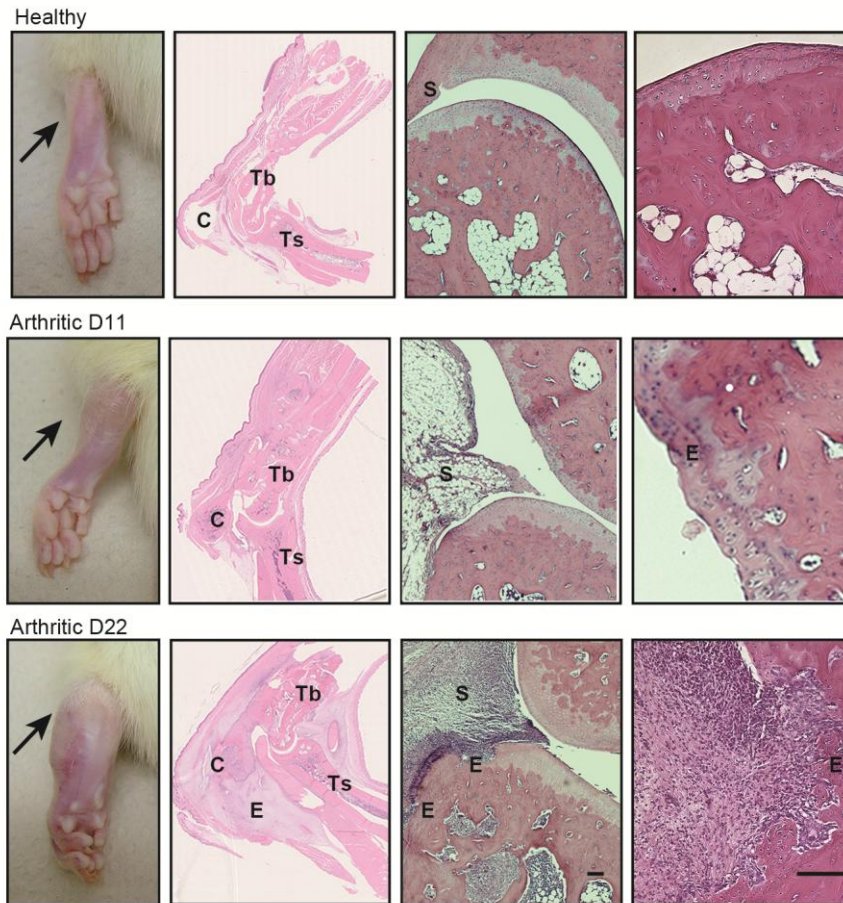


Fig.1 – Inflammatory score and ankle perimeter. Arthritic rats have a rapidly disease progression including ankle swelling, when compared with healthy control rats. Statistical differences were determined with non-parametric Mann Whitney test using GraphPad Prism (GraphPad, California, USA). Differences were considered statistically significant for p values ≤ 0.05 . Healthy D11 N=11, Healthy D22 N=30, Arthritic D11 N=16 and Arthritic D22 N=31.

Inflammation affects local joints and promotes bone damage in AIA rats since the early stage of arthritis

To evaluate the effect of inflammation in local articular joint synovium and bone structures, paw sections stained with hematoxylin and eosin were performed (illustrative images can be observed in Fig 2).



31
32
33
34
35
36
37

Fig.2 – Histological images of joints after 11 and 22 days of disease induction. These patterns are merely illustrative of the type of histological features observed. Black arrow indicates the absence/presence of ankle swelling in rat hind paws. C–calcaneus, E–edema or erosion, S–synovia, Tb–tibia, Ts–tarsus. Magnification of 50X. Bar: 100 μ m.

38
39
40
41
42
43
44
45
46
47
48
49
50
51
52
53
54
55
56
57
58
59
60
61
62
63
64
65

The histological evaluation using 5 semi-quantitative scores is depicted in Fig 3. Sublining layer infiltration (Fig 3A), number of lining layer cells (Fig 3B) and bone erosion score (Fig 3C) were increased in the arthritic group when compared with healthy controls at day 11 and 22 post disease induction ($p < 0.0001$). Arthritic samples also showed increased cartilage damage surface (Fig 3D) since the early phase of arthritis at day 11 and 22 ($p = 0.0403$ and $p < 0.0001$ vs healthy controls, respectively). These data contributed to the increased values of severity score (Fig 3E) in arthritic group ($p < 0.0001$ vs healthy controls). Moreover, results also demonstrated a continuous disease progression between day 11 and 22 in arthritic animals, as observed by the increase of the sublining layer infiltration, number of lining layer cells, bone erosion score ($p < 0.0001$), cartilage surface score ($p = 0.0001$) and global severity score ($p = 0.0006$).

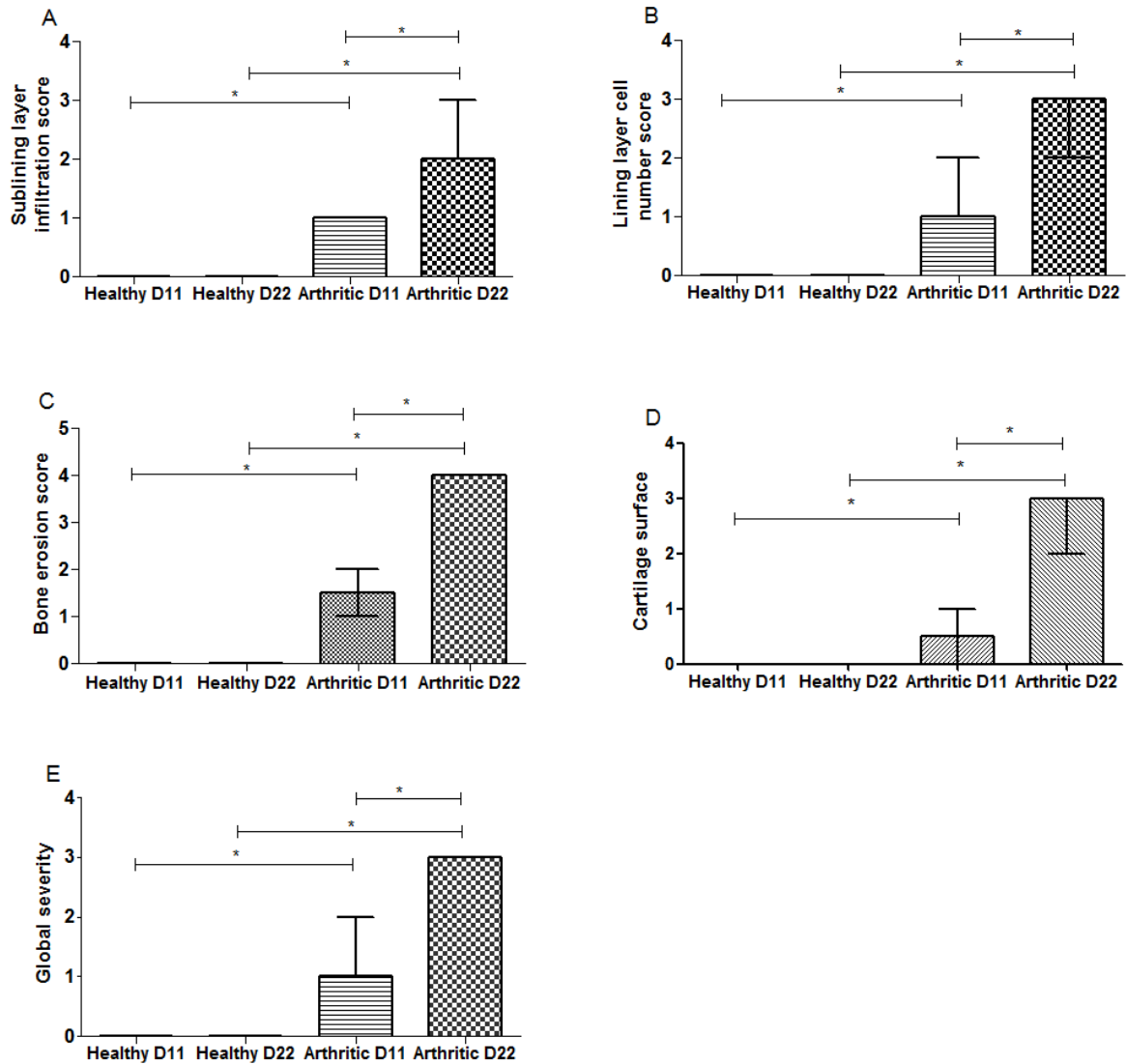


Fig. 3 – Semi-quantitative evaluation of histological sections of inflammation and tissue damage locally in the joints of AIA rats. Notice that results demonstrate that arthritic rats after 11 and 22 days of disease induction increase cellular infiltration (A), number of lining layer cells (B), bone erosions (C) and cartilage surface damage (D). Global disease severity demonstrates this marked inflammation and progression between day 11 and 22 (E). Data are expressed as median with interquartile range. Differences were considered statistically significant for p -values < 0.05 , according to the Mann Whitney test. Healthy D11 N=11, Healthy D22 N=30, Arthritic D11 N=16 and Arthritic D22 N=31.

Systemic inflammation occurs in this model

We observed that IL6 levels were increased in the serum of arthritic rats at day 11 and 22 post disease induction in comparison with healthy controls ($p = 0.0003$ and $p < 0.0001$, respectively), as observed in Fig 4. Results also revealed that IL6 levels decreased in arthritic rats at day 22 when compared with day 11 ($p = 0.0092$).

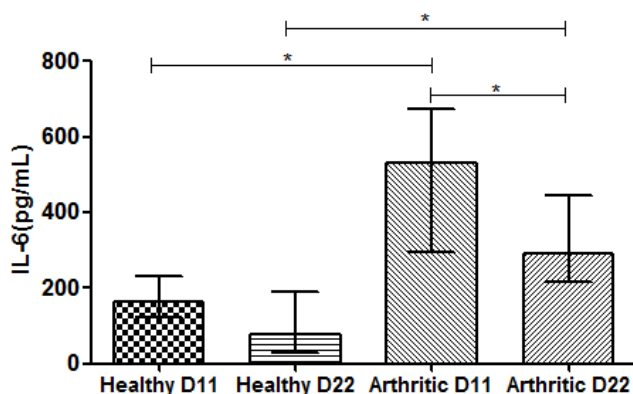


Fig.4 - Serum quantification of IL6. Serum samples collected at day 11 and 22 post disease induction were analyzed by ELISA technique. IL6 was increased in arthritic rats at day 11 and 22 ($p=0.0003$ and $p<0.0001$ vs healthy controls, respectively). Differences were considered statistically significant for p -values <0.05 , according to the Mann–Whitney tests Healthy D11 N=11, Healthy D22 N=21, Arthritic D11 N=16 and Arthritic D22 N=23.

Systemic inflammation promotes high bone turnover

We have observed that both CTX-I (Fig. 5A) and P1NP (Fig. 5B) were significantly increased in the arthritic group at day 22 in comparison with healthy controls ($p<0.0001$ and $p = 0.0007$, respectively), revealing an increase of bone turnover in the arthritic group. Moreover, arthritic rats showed already increased values of CTX-I at day 11 post disease induction ($p=0.0218$ vs healthy rats at day 11) but not of P1NP. These results suggest that systemic inflammation promotes skeletal bone turnover disturbances since the early stages of arthritis.

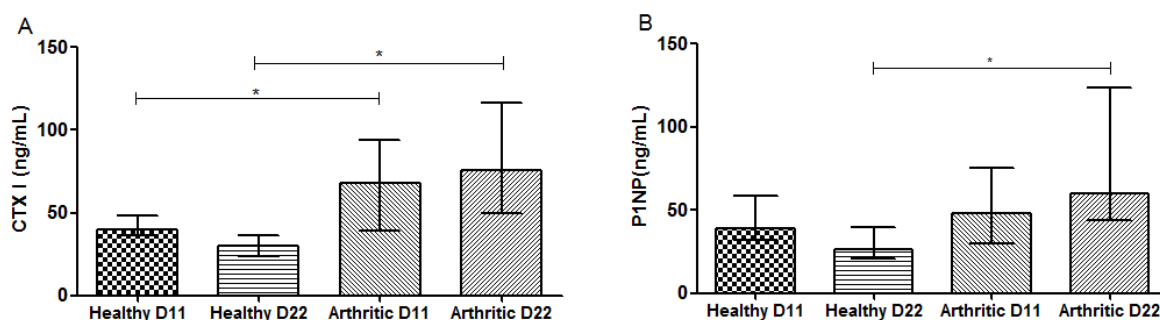


Fig.5 - Bone turnover markers quantification. Serum samples collected at day11 and 22 post disease induction were analyzed by ELISA technique. Bone resorption marker, CTX-I (A) and bone formation marker, P1NP (B) were increased in arthritic rats at day 22 ($p<0.0001$ and $p = 0.0007$, respectively). Results also demonstrate increased values of CTX-I in arthritic rats at day 11 when compared with healthy controls ($p=0.0218$). Differences were considered statistically significant for p -values <0.05 , according to the Mann–Whitney tests. Healthy D11 N=11, Healthy D22 N=18, Arthritic D11 N=16 and Arthritic D22 N=18.

Micro-CT

The effect of systemic inflammation on cortical and trabecular skeletal bone was assessed by micro-CT in bone tibia.

The arthritic group showed at day 22 a dramatic deterioration of bone tibia integrity associated with a reduction in cortical bone area (Fig. 6A) and crosssectional thickness (Fig. 6B) ($p < 0.0001$ vs healthy controls, respectively) with an evident increased endosteal perimeter (Fig. 6C) ($p = 0.0029$ vs healthy control). However, changes promoted by inflammation on bone structure begin at the early stages of arthritis as we can observe by the results obtained in the arthritic group by day 11 with a decreased cortical bone area (Fig. 6A) ($p = 0.0219$ vs healthy control). Results also demonstrated decreased values of polar moment of inertia in arthritic group at day 11 and 22 post disease induction (Fig. 6D) ($p = 0.0091$ and $p = 0.0024$ vs healthy controls,

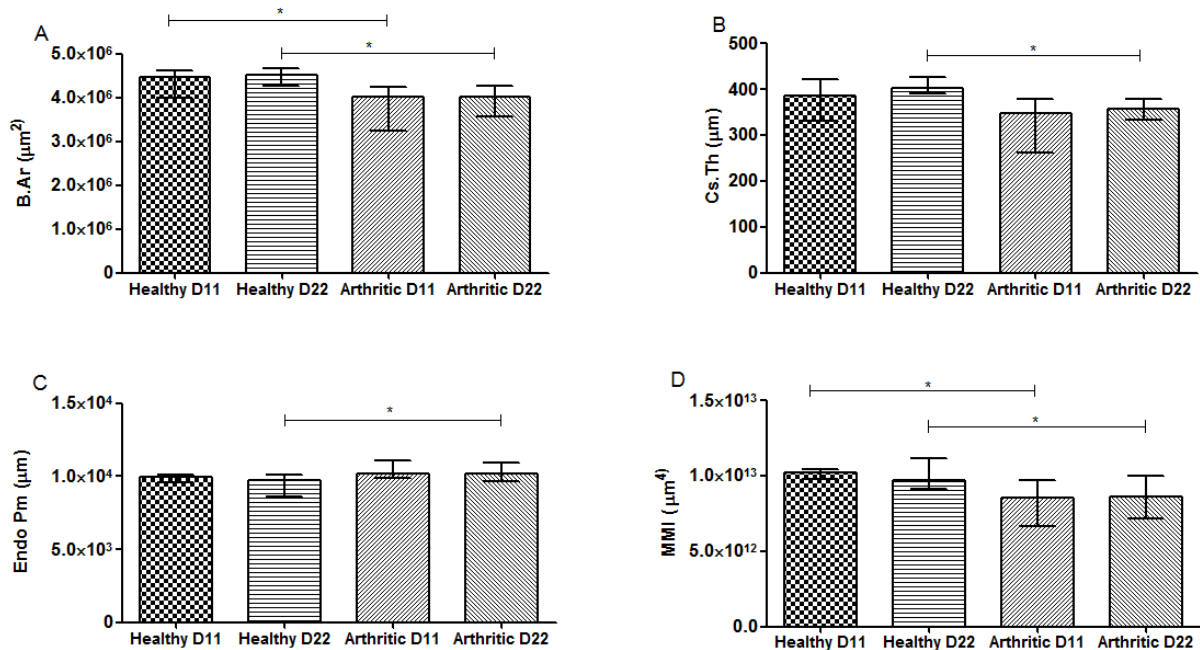


Fig.6 – Micro-computed tomography (micro-CT) - Cortical analysis of tibiae rat sample.

The crosssectional bone area of cortical bone showed decreased values in the arthritic group at day 11 and 22(A) and polar moment of inertia (D). Arthritic group at day 22 presented a marked deterioration of bone tibia demonstrated by decreased crosssectional thickness of cortical (B) and increased endosteal perimeter (C). Differences were considered statistically significant for p -values < 0.05 , according to the Mann–Whitney tests. Healthy D11 N=11, Healthy D22 N=30, Arthritic D11 N=16 and Arthritic D22 N=31.

1
2
3
4
5
6
7
8
9
10
11
12
13
14
15
16
17
18
19
20
21
22
23
24
25
26
27
28
29
30
31
32
33
34
35
36
37
38
39
40
41
42
43
44
45
46
47
48
49
50
51
52
53
54
55
56
57
58
59
60
61
62
63
64
65

Trabecular bone (Fig. 7) also showed increased deterioration promoted by inflammation with decreased trabecular bone volume fraction in arthritic rats at day 11 and 22 post disease induction (Fig. 7B) ($p=0.0001$ and $p<0.0001$ vs healthy controls, respectively), thickness (Fig. 7C) ($p<0.0001$ vs healthy controls, respectively), and number (Fig. 7D) ($p=0.0039$ and $p<0.0001$ vs healthy controls, respectively). Results also demonstrated increased values of trabecular separation in the arthritic group at day 11 and 22 (Fig. 7E) ($p=0.0043$ and $p<0.0001$ vs healthy controls) and of porosity (Fig. 7F) ($p=0.0001$ and $p<0.0001$ vs healthy controls, respectively). Furthermore, structure model index (Fig. 7G) showed increased values in arthritic groups at day 11 and 22 ($p=0.0015$ and $p<0.0001$ vs healthy controls, respectively) indicating that the shape of trabeculae is rather rod-like in the arthritic group as compared to plate-like shape in healthy controls.

Altogether, these results showed that inflammation promote bone structural disturbances, leading to bone loss and consequent bone fragility in arthritic rats (Fig.7A).

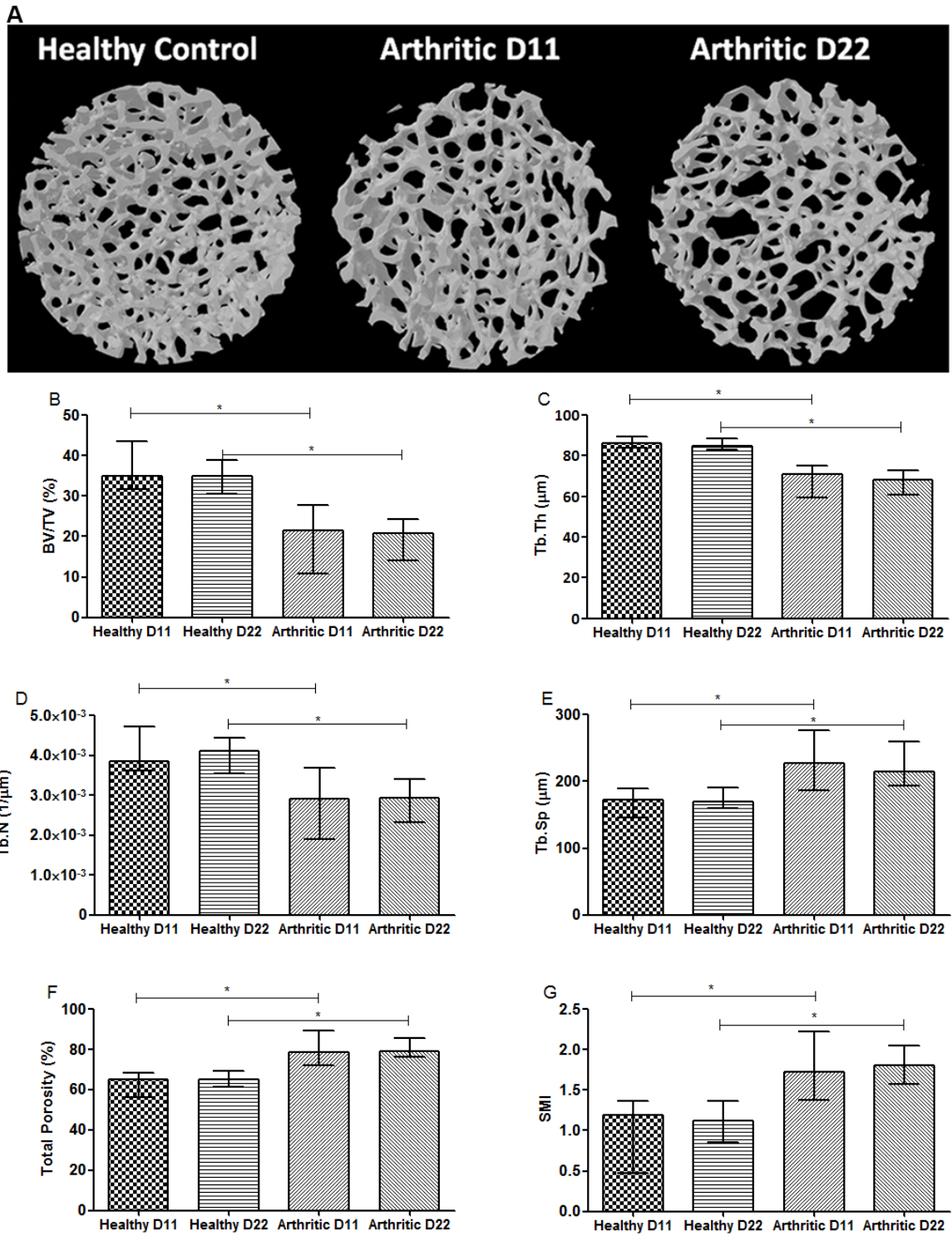


Fig.7 – Micro-computed tomography (micro-CT) –Trabecular analysis of tibiae rat sample.

MicroCT images from healthy and arthritic tibiae rats (A). Images acquired with SkyScan 1272, Bruker microCT, Belgium.

Results showed decreased values of the ratio bone volume/tissue volume (B), trabecular thickness (C) and number (D) in arthritic group at day 11 and 22 post disease induction. Trabecular bone also showed increased values of trabecular separation (E), porosity (F) and structural model index in both arthritic groups (G). Differences were considered statistically significant for p-values<0.05, according to the Mann–Whitney tests. Healthy D11 N=11, Healthy D22 N=30, Arthritic D11 N=16 and Arthritic D22 N=31.

Bending

1
2
3
4
5
6
7
8
9
10
11
12
13
14
15
16
17
18
19
20
21
22
23
24
25
26
27
28
29
30
31
32
33
34
35
36
37
38
39
40
41
42
43
44
45
46
47
48
49
50
51
52
53
54
55
56
57
58
59
60
61
62
63
64
65

Classical mechanical properties of rat femurs were evaluated using 3-point bending mechanical tests. Yield point occurs when first micro fractures appear in bone. Another interesting point is maximal load at breaking point (where complete fracture occurs) and toughness can be estimated. As shown in Fig. 8, arthritic rats at day 22 revealed biomechanical disturbances with a decrease in mechanical properties at yield point, namely by displacement (Fig. 8A) ($p=0.0192$ vs healthy control), strength (Fig. 8B) ($p=0.0229$ vs healthy control) and pre yield energy (Fig. 8C) (elastic energy) ($p=0.0161$ vs healthy control). These results showed that arthritic bones at day 22 start to accumulate micro fractures with smaller deformations and loads, leading to a decreased energy absorption capability at yield point. Results also demonstrated that arthritic rats at day 22 have decreased maximum load (Fig. 8D) and elastic capabilities at maximum load point (Fig. 8E) ($p= 0.0017$ and $p=0.0134$ vs healthy control, respectively), which indicates increased bone fragility. Finally, arthritic rat groups showed a significant decrease in toughness (Fig. 8F) ($p=0.0143$ vs healthy control), demonstrating that arthritic bone can absorb less energy before fracturing.

Altogether, mechanical data revealed that arthritic groups have significantly lower mechanical properties as compared to healthy controls, meaning that arthritic bones are more fragile and prone to fracture, as highlighted by the significantly lower structural strength and poor biomechanical properties.

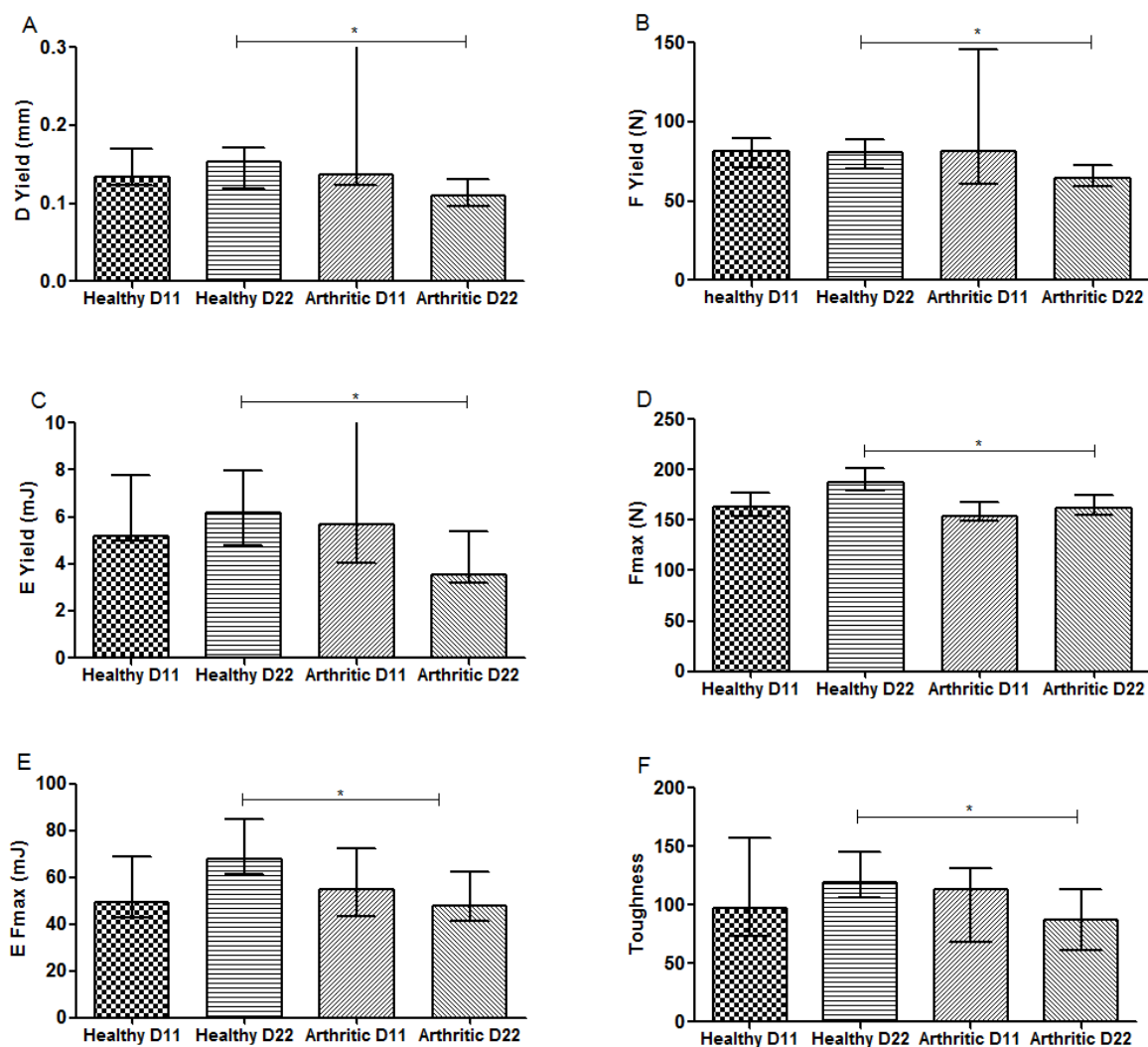


Fig.8 – Bone mechanical properties assessed by three-point bending tests in rat femur.

Results showed that arthritic rats at day 22 have decreased properties at yield point, related to displacement (A), strength (B) and energy (elastic energy) (C). Arthritic bones at day 22 required a lower maximum load (D) to fracture, with a decreased elastic energy at maximum load (E) and toughness (F). Differences were considered statistically significant for p-values < 0.05, according to the Mann–Whitney tests. Healthy D11 N=5, Healthy D22 N=14, Arthritic D11 N=5 and Arthritic D22 N=10.

1
2
3
4
5
6
7
8
9
10
11
12
13
14
15
16
17
18
19
20
21
22
23
24
25
26
27
28
29
30
31
32
33
34
35
36
37
38
39
40
41
42
43
44
45
46
47
48
49
50
51
52
53
54
55
56
57
58
59
60
61
62
63
64
65

Decreased hardness in arthritic bone associated with an increase of the ratio of bone concentric to parallel lamellae and of the area of the osteocyte lacuna.

Nanoindentation was performed in order to assess the quality at tissue matrix level as this technique works at the level of a single trabecula or within a confined submicron area of the cortical bone tissue (Fig 9).

Nano-mechanical tests revealed that arthritic rats have decreased hardness in the cortical aspect of bone at day 22 post disease induction (Fig 9A) ($p= 0.0010$ vs healthy control) and at trabecular bone at day 11 and 22 post disease induction (Fig 9B) ($p= 0.0184$ and $p=0.008$ vs healthy controls, respectively). Results also demonstrated the continuous decreasing of cortical hardness (Fig 9A) during arthritis development among arthritic groups ($p=0.0043$). No differences were observed in the other parameters analysed.

Topographic images gathered during nanoindentation allowed the characterization of histologic features from healthy and arthritic bone at day 11 (Fig 9G) and 22 (Fig 9H) days post disease induction. Concentric lamellas were identified in secondary osteons (SO) and more frequently observed in arthritic animals than in healthy controls ($p= 0.0022$). On the contrary, healthy animals at day 11 (Fig 9E) and 22 (Fig. 9F) presented more parallel-lamellae (PL) structures than SO structures.

Arthritic animals at day 22 post disease induction showed also an increased area occupied by osteocyte lacunae in the total tissue when compared to healthy animals ($p=0.0067$) (Fig 9D). Results also demonstrated a slight tendency towards an increase at day 11 post disease induction (Fig 9D).

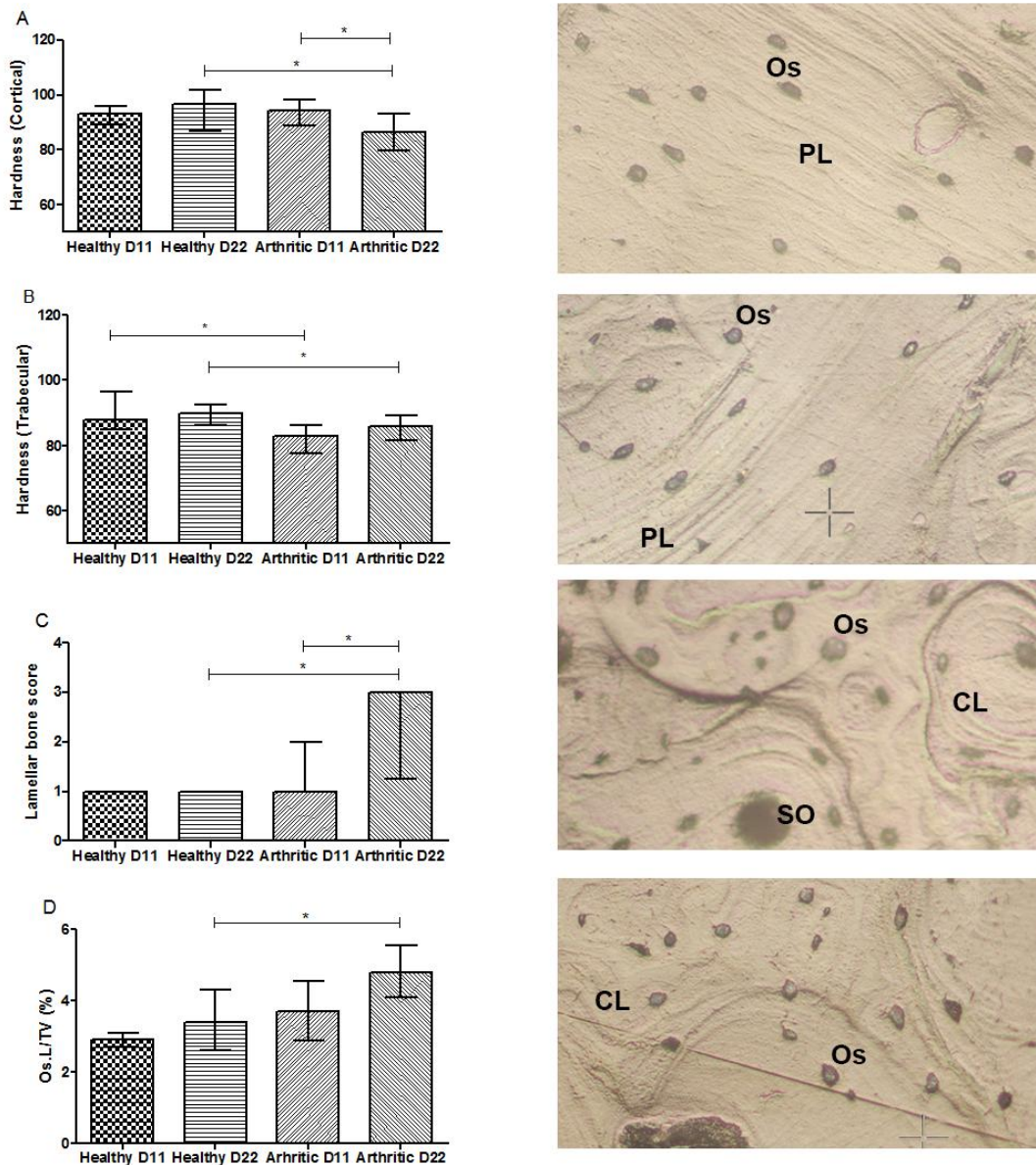


Fig.9 – Bone mechanical properties assessed by nanoindentation in rat femur at 11 and 22 days post disease induction and respective topographic images from the indentation tissue area. Nano-mechanical tests revealed that arthritic rats have decreased cortical hardness at day 22 and of trabecular hardness at day 11 and 22 post disease induction (B). Results demonstrated that concentric lamellae (C) and ratio of area occupied by osteocyte lacunae in the total tissue (D) are increased when compared to healthy animals at day 22.

Images are merely illustrative of the type of histological features observed. Concentric lamellae are identified in secondary osteons (SO), characteristic from arthritic animals at day 11 (G) and 22(H). On the contrary, parallel-lamellae (PL) are identified in healthy at day 11 (E) and 22 (F). Os – Osteocytes, SO – Secondary osteons, PL – Parallel-lamellae, CL – Concentric lamellas. Magnification 20X. Differences were considered statistically significant for p-values<0.05, according to the Mann–Whitney tests. Healthy D11 N=11, Healthy D22 N=28, Arthritic D11 N=16 and Arthritic D22 N=21.

Decreased collagen and mineral content in the skeletal bone of arthritic animals

FTIR was performed to assess the composition of cortical and trabecular bone. Results demonstrated that the mineral content was decreased in trabecular bone of arthritic animals since the early phase of arthritis when compared to healthy controls. Statistical differences were observed when compared arthritic animals at day 11 and 22 post disease induction with their correspondent healthy controls ($p=0.0457$ and $p=0.0241$, respectively) (Fig.10 A). There was also a significant decrease of mineral content between day 11 and 22 post disease induction ($p=0.0481$) (Fig. 10A). Results also demonstrated decreased collagen matrix in arthritic animals at day 22 post disease induction ($p=0.0229$ vs healthy group at day 22) (Fig. 10B). There was also a significant decrease of collagen content between days 11 and 22 post disease induction ($p=0.0012$) (Fig. 10B).

No statistical significant differences were observed in cortical bone parameters.

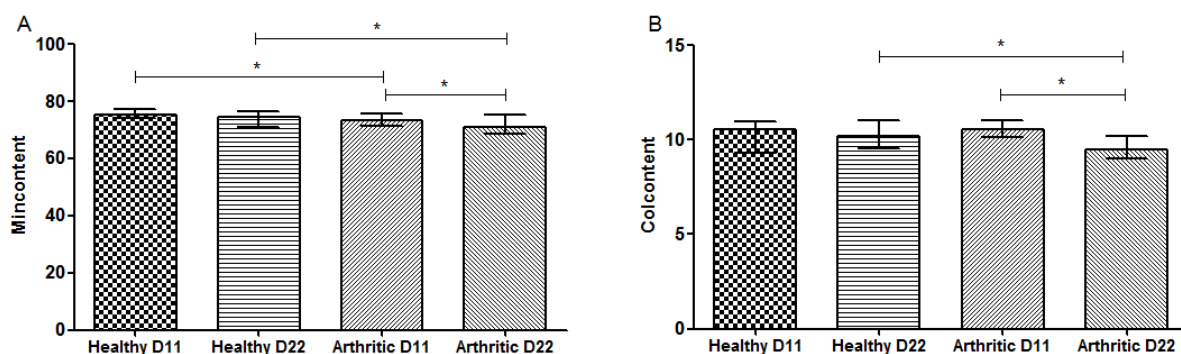


Fig.10 – FTIR measurements from cortical and trabecular bone rat tibia at 11 and 22 days post disease induction . FTIR measurements revealed that arthritic rats had mineral loss in trabecular bone since the early stage of arthritis (A). Collagen was also decreased in arthritic samples at day 22 post disease induction (B). Differences were considered statistically significant for p -values <0.05 , according to the Mann–Whitney tests. Healthy D11 N=11, Healthy D22 N=28, Arthritic D11 N=15 and Arthritic D22 N=25.

Discussion

Arthritic groups presented inflammatory manifestations with synovial tissue inflammation and local bone erosions, as expected. Increased values of serum IL-6 were observed in arthritic rats since the early stages of arthritis, confirming the systemic inflammatory component of this animal model. This cytokine plays a pivotal role in the pathologic processes of arthritis with a special emphasis on its impact on skeletal bone [20-23]. In accordance with this effect an increased and accelerated bone turnover was shown in arthritic animals, as depicted by increased CTX-I and P1NP levels since the early stages of arthritis. Data already published by our group in the same animal model of arthritis had also shown that P1NP levels were increased at day 22 post disease induction in arthritic animals and so did CTX-I levels[12], reflecting an overall increase in bone turnover [24]. Despite the existing of some variability in human studies, CTX-I and P1NP have been found to be increased in RA patients, revealing the coupled compensatory mechanism of bone turnover [12,25]. Micro-CT data and 3 point bending test confirmed that this interference of inflammation with bone metabolism translates into bone micro architectural and mechanical fragility, as observed in RA patients, further reinforcing our observations that suggested the use of the AIA model as an adequate strategy for a fast insight on the impact of inflammation on bone.

The first part of this study sets the stage for using this model for evaluating the effects of the early phase of systemic inflammatory process at bone tissue level, including nanomechanical properties, microarchitecture and mineral and collagen content.

Nanoindentation was performed in order to assess the quality of bone at tissue matrix level, as this technique can be used at the level of a single trabecula or within a confined submicron area of the cortical bone tissue. Results showed decreased cortical and trabecular hardness in arthritic rats since the early phase of arthritis (days 11 and 22).

We also observed at day 11 and 22 post arthritis induction concentric lamellas in secondary osteons (SO) microstructures, resulting from high bone remodelling, as previously described [12,26,27]. Dall'Ara et al. suggested that larger numbers of this younger, less mineralised and less hard structures, could be related to reduced hardness of bone tissue identified by nanoindentation. On the contrary, healthy

1 animals presented more parallel-lamellae (PL) structures than SO structures and
2 this PL structures are 10% more harder than the former, representing the mature
3 bone structure (and normal bone remodelling)[27]. In addition, arthritic animals had
4 an increased area occupied by osteocyte lacunae in total tissue. Osteocytes are
5 responsible for the maintenance of the bone homeostasis, regulating the behaviour
6 of osteoblasts and osteoclasts by communicating through gap junctions [28].
7 Although no previous data is available in the context of arthritis some studies
8 revealed that osteocytes from osteoarthritis patients have an irregular morphology,
9 with limited ability to reply to mechanical stimuli, leading to significant changes in
10 the structure and mineral density [29]. Despite being still unclear this apparent
11 change of osteocyte morphology in arthritic bone might contribute to the structural
12 and mechanical changes observed in this context.
13
14
15
16
17
18
19
20

21 Finally, FTIR measurements demonstrated that inflammation induces bone mineral
22 and collagen loss since the early phase of arthritis. FTIR imaging have been
23 extensively applied to the analyses of bone tissue [30-32], providing insights into
24 molecular and chemical changes associated with load and damage of bone and
25 cartilage [33]. Results are in line with our previous data using other techniques in
26 the chronic phase of arthritis, showing a decreased mineral content [12] and also a
27 lower density and organization of collagen fibrils when compared to healthy control
28 bone [34].
29
30
31
32
33
34
35
36
37
38
39

40 **Conclusion**

41 Systemic inflammation induces very early changes at bone tissue level
42 characterized by decreased tissue hardness, associated with changes in bone
43 lamella organization and osteocyte lacuna surface and with decreased collagen and
44 mineral content.
45
46
47
48
49
50
51
52
53
54
55
56
57
58
59
60
61
62
63
64
65

Competing interests

The authors have declared that no competing interests exist.

Acknowledgments

The authors would like to acknowledge ECTS/AMGEN BONE BIOLOGY for funding this project.

Funding

This work was supported by ECTS/AMGEN BONE BIOLOGY FELLOWSHIP. The funders had no role in study design, data collection and analysis, decision to publish, or preparation of the manuscript.

1
2
3
4
5
6
7
8
9
10
11
12
13
14
15
16
17
18
19
20
21
22
23
24
25
26
27
28
29
30
31
32
33
34
35
36
37
38
39
40
41
42
43
44
45
46
47
48
49
50
51
52
53
54
55
56
57
58
59
60
61
62
63
64
65

Bibliography

1. Yelin E, Callahan LF (1995) The economic cost and social and psychological impact of musculoskeletal conditions. National Arthritis Data Work Groups. *Arthritis Rheum* 38: 1351-1362.
2. Lin YY, Jean YH, Lee HP, Chen WF, Sun YM, et al. (2013) A soft coral-derived compound, 11-episinulariolide acetate suppresses inflammatory response and bone destruction in adjuvant-induced arthritis. *PLoS One* 8: e62926.
3. Haugeberg G, Orstavik RE, Uhlig T, Falch JA, Halse JI, et al. (2002) Bone loss in patients with rheumatoid arthritis: results from a population-based cohort of 366 patients followed up for two years. *Arthritis Rheum* 46: 1720-1728.
4. Marshall D, Johnell O, Wedel H (1996) Meta-analysis of how well measures of bone mineral density predict occurrence of osteoporotic fractures. *BMJ* 312: 1254-1259.
5. Eric-Jan JA K (2000) Bone mass in rheumatoid arthritis. *CLINICAL AND EXPERIMENTAL RHEUMATOLOGY*.
6. Fonseca JE, Cortez-Dias N, Francisco A, Sobral M, Canhao H, et al. (2005) Inflammatory cell infiltrate and RANKL/OPG expression in rheumatoid synovium: comparison with other inflammatory arthropathies and correlation with outcome. *Clin Exp Rheumatol* 23: 185-192.
7. Boyle WJ, Simonet WS, Lacey DL (2003) Osteoclast differentiation and activation. *Nature* 423: 337-342.
8. Moura RA, Cascao R, Perpetuo I, Canhao H, Vieira-Sousa E, et al. (2011) Cytokine pattern in very early rheumatoid arthritis favours B-cell activation and survival. *Rheumatology (Oxford)* 50: 278-282.
9. Cascao R, Moura RA, Perpetuo I, Canhao H, Vieira-Sousa E, et al. (2010) Identification of a cytokine network sustaining neutrophil and Th17 activation in untreated early rheumatoid arthritis. *Arthritis Res Ther* 12: R196.
10. Caetano-Lopes J, Canhao H, Fonseca JE (2009) Osteoimmunology--the hidden immune regulation of bone. *Autoimmun Rev* 8: 250-255.
11. Caetano-Lopes J, Rodrigues A, Lopes A, Vale AC, Pitts-Kiefer MA, et al. (2014) Rheumatoid arthritis bone fragility is associated with upregulation of IL17 and DKK1 gene expression. *Clin Rev Allergy Immunol* 47: 38-45.
12. Vidal B, Cascao R, Vale AC, Cavaleiro I, Vaz MF, et al. (2015) Arthritis induces early bone high turnover, structural degradation and mechanical weakness. *PLoS One* 10: e0117100.
13. Cascao R, Vidal B, Raquel H, Neves-Costa A, Figueiredo N, et al. (2012) Effective treatment of rat adjuvant-induced arthritis by celestrol. *Autoimmun Rev* 11: 856-862.
14. Bouxsein ML, Boyd SK, Christiansen BA, Guldberg RE, Jepsen KJ, et al. (2010) Guidelines for assessment of bone microstructure in rodents using micro-computed tomography. *J Bone Miner Res* 25: 1468-1486.
15. Herlin M, Finnila MA, Zioupos P, Aula A, Risteli J, et al. (2013) New insights to the role of aryl hydrocarbon receptor in bone phenotype and in dioxin-induced modulation of bone microarchitecture and material properties. *Toxicol Appl Pharmacol* 273: 219-226.
16. Zhang R, Gong H, Zhu D, Ma R, Fang J, et al. (2015) Multi-level femoral morphology and mechanical properties of rats of different ages. *Bone* 76: 76-87.
17. W.C. Oliver GMP (1992) An improved technique for determining hardness and elastic modulus using load and displacement sensing indentation experiments.
18. Parfitt AM, Drezner MK, Glorieux FH, Kanis JA, Malluche H, et al. (1987) Bone histomorphometry: standardization of nomenclature, symbols, and units. Report of the ASBMR Histomorphometry Nomenclature Committee. *J Bone Miner Res* 2: 595-610.
19. Isaksson H, Turunen MJ, Rieppo L, Saarakkala S, Tamminen IS, et al. (2010) Infrared spectroscopy indicates altered bone turnover and remodeling activity in renal osteodystrophy. *J Bone Miner Res* 25: 1360-1366.

20. Choy EH, Isenberg DA, Garrood T, Farrow S, Ioannou Y, et al. (2002) Therapeutic benefit of blocking interleukin-6 activity with an anti-interleukin-6 receptor monoclonal antibody in rheumatoid arthritis: a randomized, double-blind, placebo-controlled, dose-escalation trial. *Arthritis Rheum* 46: 3143-3150.
21. Nishimoto N, Yoshizaki K, Miyasaka N, Yamamoto K, Kawai S, et al. (2004) Treatment of rheumatoid arthritis with humanized anti-interleukin-6 receptor antibody: a multicenter, double-blind, placebo-controlled trial. *Arthritis Rheum* 50: 1761-1769.
22. Maeshima K, Yamaoka K, Kubo S, Nakano K, Iwata S, et al. (2012) The JAK inhibitor tofacitinib regulates synovitis through inhibition of interferon-gamma and interleukin-17 production by human CD4+ T cells. *Arthritis Rheum* 64: 1790-1798.
23. Fonseca JE, Santos MJ, Canhao H, Choy E (2009) Interleukin-6 as a key player in systemic inflammation and joint destruction. *Autoimmun Rev* 8: 538-542.
24. Siebuhr AS, Wang J, Karsdal M, Bay-Jensen AC, Y J, et al. (2012) Matrix metalloproteinase-dependent turnover of cartilage, synovial membrane, and connective tissue is elevated in rats with collagen induced arthritis. *J Transl Med* 10: 195.
25. Cortet B, Flipo RM, Pigny P, Duquesnoy B, Boersma A, et al. (1998) Is bone turnover a determinant of bone mass in rheumatoid arthritis? *J Rheumatol* 25: 2339-2344.
26. Bailey AJ, Mansell JP, Sims TJ, Banse X (2004) Biochemical and mechanical properties of subchondral bone in osteoarthritis. *Biorheology* 41: 349-358.
27. Dall'Ara E, Ohman C, Baleani M, Viceconti M (2011) Reduced tissue hardness of trabecular bone is associated with severe osteoarthritis. *J Biomech* 44: 1593-1598.
28. Taylor AF, Saunders MM, Shingle DL, Cimbala JM, Zhou Z, et al. (2007) Mechanically stimulated osteocytes regulate osteoblastic activity via gap junctions. *Am J Physiol Cell Physiol* 292: C545-552.
29. Jaiprakash A, Prasadam I, Feng JQ, Liu Y, Crawford R, et al. (2012) Phenotypic characterization of osteoarthritic osteocytes from the sclerotic zones: a possible pathological role in subchondral bone sclerosis. *Int J Biol Sci* 8: 406-417.
30. Miller LM, Vairavamurthy V, Chance MR, Mendelsohn R, Paschalis EP, et al. (2001) In situ analysis of mineral content and crystallinity in bone using infrared micro-spectroscopy of the nu(4) PO(4)(3-) vibration. *Biochim Biophys Acta* 1527: 11-19.
31. Ou-Yang H, Paschalis EP, Mayo WE, Boskey AL, Mendelsohn R (2001) Infrared microscopic imaging of bone: spatial distribution of CO3(2-). *J Bone Miner Res* 16: 893-900.
32. Paschalis EP, Recker R, DiCarlo E, Doty SB, Atti E, et al. (2003) Distribution of collagen cross-links in normal human trabecular bone. *J Bone Miner Res* 18: 1942-1946.
33. Boskey A, Pleshko Camacho N (2007) FT-IR imaging of native and tissue-engineered bone and cartilage. *Biomaterials* 28: 2465-2478.
34. Caetano-Lopes J, Nery AM, Canhao H, Duarte J, Cascao R, et al. (2010) Chronic arthritis leads to disturbances in the bone collagen network. *Arthritis Res Ther* 12: R9.

RESEARCH ARTICLE

Decrease of CD68 Synovial Macrophages in Celastrol Treated Arthritic Rats

Rita Cascão^{1*}, Bruno Vidal¹, Inês P. Lopes¹, Eunice Paisana¹, José Rino¹, Luis F. Moita^{2‡}, João E. Fonseca^{1,3‡}

1 Instituto de Medicina Molecular, Faculdade de Medicina da Universidade de Lisboa, Lisbon, Portugal, **2** Instituto Gulbenkian de Ciência, Oeiras, Portugal, **3** Rheumatology Department, Centro Hospitalar de Lisboa Norte, EPE, Hospital de Santa Maria, Lisbon Academic Medical Centre, Lisbon, Portugal

‡ LFM and JEF are joint senior authors on this work.

* ritacascão@medicina.ulisboa.pt



Abstract

Background

Rheumatoid arthritis (RA) is a chronic immune-mediated inflammatory disease characterized by cellular infiltration into the joints, hyperproliferation of synovial cells and bone damage. Available treatments for RA only induce remission in around 30% of the patients, have important adverse effects and its use is limited by their high cost. Therefore, compounds that can control arthritis, with an acceptable safety profile and low production costs are still an unmet need. We have shown, *in vitro*, that celastrol inhibits both IL-1 β and TNF, which play an important role in RA, and, *in vivo*, that celastrol has significant anti-inflammatory properties. Our main goal in this work was to test the effect of celastrol in the number of sublining CD68 macrophages (a biomarker of therapeutic response for novel RA treatments) and on the overall synovial tissue cellularity and joint structure in the adjuvant-induced rat model of arthritis (AIA).

Methods

Celastrol was administered to AIA rats both in the early (4 days after disease induction) and late (11 days after disease induction) phases of arthritis development. The inflammatory score, ankle perimeter and body weight were evaluated during treatment period. Rats were sacrificed after 22 days of disease progression and blood, internal organs and paw samples were collected for toxicological blood parameters and serum proinflammatory cytokine quantification, as well as histopathological and immunohistochemical evaluation, respectively.

Results

Here we report that celastrol significantly decreases the number of sublining CD68 macrophages and the overall synovial inflammatory cellularity, and halted joint destruction without side effects.

OPEN ACCESS

Citation: Cascão R, Vidal B, Lopes IP, Paisana E, Rino J, Moita LF, et al. (2015) Decrease of CD68 Synovial Macrophages in Celastrol Treated Arthritic Rats. PLoS ONE 10(12): e0142448. doi:10.1371/journal.pone.0142448

Editor: Lisa F.P. Ng, Singapore Immunology Network, Agency for Science, Technology and Research (A*STAR), SINGAPORE

Received: July 30, 2015

Accepted: October 21, 2015

Published: December 11, 2015

Copyright: © 2015 Cascão et al. This is an open access article distributed under the terms of the [Creative Commons Attribution License](https://creativecommons.org/licenses/by/4.0/), which permits unrestricted use, distribution, and reproduction in any medium, provided the original author and source are credited.

Data Availability Statement: All relevant data are within the paper and its Supporting Information files.

Funding: RC was supported with a fellowship from Fundação para a Ciência e a Tecnologia (FCT, SFRH/BPD/92860/2013). The funders had no role in study design, data collection and analysis, decision to publish, or preparation of the manuscript.

Competing Interests: The authors have declared that no competing interests exist.

Conclusions

Our results validate celastrol as a promising compound for the treatment of arthritis.

Introduction

Rheumatoid arthritis (RA) is a chronic immune mediated inflammatory disease that is mainly characterized by hyperproliferation of synovial cells, infiltration of mononuclear cells into the synovium and early destruction of articular cartilage and bone, causing progressive damage to the musculoskeletal system and consequently the loss of physical function and life quality [1–3]. The most debilitating feature of RA is joint destruction, which is derived from an uncontrolled inflammatory process. RA joint synovial cellular infiltrate consists of activated macrophages, B and T cells, which secrete proinflammatory cytokines and other mediators of inflammation [1, 4, 5] that not only perpetuate the inflammatory process but also increase bone resorption [6–10]. In addition, activated synovial fibroblasts, chondrocytes and osteoclasts contribute to the underlying cartilage and bone damage [11]. Despite this clear link between inflammation and increased bone turnover in RA and the existence of several therapeutic options, their efficacy on inflammation and bone treatment seem to be uncoupled, with some drugs suppressing inflammation but failing to protect bone [12, 13] and others halting bone destruction but with no effect on controlling inflammation [14]. Moreover, drugs used to treat RA, ranging from nonsteroidal anti-inflammatory drugs (NSAIDs) to disease-modifying antirheumatic drugs (DMARDs), and biological DMARDs, still cause severe side effects [15, 16] and are only able to induce remission in around 20–30% of the patients, leaving the majority of the individuals affected by RA with a chronic inflammatory process that will lead to damage. In addition to this, the most recent and innovative treatments are highly expensive, representing a burden to national health services and creating a barrier to its use in less affluent areas of the world. Therefore, compounds that can control arthritis, with an acceptable safety profile and low production cost are still an unmet need.

In this context, we have recently identified celastrol, a pentacyclic triterpenoid compound isolated from the roots of the Chinese herb *Tripterygium wilfordii* Hook F, as a potential RA therapeutic candidate [17]. We have shown that celastrol inhibits both interleukin (IL)-1 β and tumour necrosis factor (TNF), which play an important role since the early phase of RA [18], and has significant anti-inflammatory and anti-proliferative properties in an adjuvant-induced rat model of arthritis (AIA) [17]. Supporting our own results, other studies using celastrol have reported beneficial effects in various models of inflammation, diminishing joint swelling and damage, serum IgG level, TNF and IL-1 β mRNA and preventing disease progression [19]. Importantly, recent studies have also demonstrated that celastrol protects human chondrocytes by down-regulating the expression of metalloproteinases (MMPs) and inducible nitric oxide synthase (iNOS), suppresses several chemokines that mediate cellular joint infiltration [20], impairs B cell development [21] and also regulates bone remodelling-related immune mediators and proinflammatory cytokines in AIA synovium-infiltrating cells cultured *ex vivo* and in the RAW264.7 macrophagic cell line [22]. Celastrol might thus constitute an attractive candidate to have an early effect not only in controlling inflammation but also in preventing bone structural disturbances that occur in arthritis.

The efficacy of new compounds in the treatment of RA has been associated with a decrease in CD68 positive macrophages in the synovial sublining layer. This effect has been clearly demonstrated for most of the effective treatments for RA, including classic treatments, such as

prednisolone [23], gold salts [24], methotrexate [25, 26] and leflunomide [27], and also for biologics such as infliximab [28, 29], anakinra [30, 31] and rituximab [32]. Interestingly, a study of a CCL-2/MCP-1 monoclonal antibody antagonist demonstrated no change in CD68 sublining macrophages and this was associated with no change in disease activity [33]. In accordance, a C5aR antagonist did not affect CD68 sublining macrophages and no clinical effect occurred [34]. Furthermore, a multicenter study on the correlation of the number of sublining CD68 cells and the change in DAS28 demonstrated excellent inter-centre agreement [32] and it has been shown that the number of CD68 macrophages decreases with a reduction in disease activity as measured by Disease Activity Score [35]. Due to these very solid evidences, the number of CD68 sublining macrophages has been proposed as a biomarker of therapeutic response to be used in the test of novel treatments for RA [32]. Of interest, in the preclinical test of new compounds, a number of observations have shown that effective RA treatments such as tofacitinib [36] and methotrexate [37] also decrease CD68 sublining macrophages in animal models of arthritis. Several experimental compounds have also shown an association between control of arthritis and reduction in the number of CD68 macrophages in animal models of arthritis [38–40].

Our aim in the herein study was to test the effect of celastrol treatment in the number of sublining CD68 macrophages and on the overall synovial tissue cellularity and joint structure in an animal model of arthritis, as a further argument to its possible efficacy in RA treatment.

In this work we report that celastrol significantly decreases the number of sublining CD68 macrophages and the overall synovial inflammatory cellularity, and halted joint destruction without any detectable side effects.

Materials and Methods

Animal experimental design

Eight-week-old female wistar AIA rats were purchased from Charles River Laboratories International (Massachusetts, USA). AIA rats were maintained under specific pathogen free (SPF) conditions and housed per groups under standard laboratory conditions (at 22°C under 12-hour light/12-hour dark conditions). Humane end-points were established and animals were sacrificed when presenting the maximum inflammatory score in more than 2 paws or when presenting more than 20% of body weight loss. All experiments were approved by the Animal User and Ethical Committees at the Instituto de Medicina Molecular (Lisbon University), according to the Portuguese law and the European recommendations. The dose of celastrol (1µg/g body weight daily) used in this study was based on that used in our previous study [17] and in other studies [22]. The need for daily administrations is also supported by Zhang J. et al who showed that the half-life of pure celastrol is approximately 10 hours [41]. Celastrol (Sigma, Missouri, USA) stock solution of 100mg/ml in DMSO was dissolved in normal saline solution and injected intraperitoneally in AIA rats after 4 days (early treatment group) and after 11 days (late treatment group) of disease induction, when arthritis was already present. A group of healthy non-arthritic and arthritic untreated female age-matched wistar rats sacrificed at day 4 (baseline for the celastrol early-treated group, at preclinical stage, N = 13), day 11 (baseline for the celastrol late-treated group, at acute clinical stage, N = 18) and day 22 after disease induction (chronic clinical stage) were used as controls in all experiments for comparison. At the preclinical AIA progression stage evidence of inflammation or bone erosion is still lacking in the contralateral hind paw and fore paws. Hind paw swelling, inflammation and joint erosions are steadily progressing during acute clinical stage and reach a plateau in the chronic stage [42]. The inflammatory score, ankle perimeter and body weight were measured during the period of treatment. Inflammatory score was evaluated by counting the score of

each paw joint in a scale of 0–3 (0—absence; 1—erythema; 2—erythema and swelling; 3—deformities and functional impairment). The total score of each animal was defined as the sum of the partial scores of each affected joint [17, 43]. Rats were sacrificed by CO₂ narcosis and blood, internal organs as well as paw samples were collected.

Toxicological evaluation

For histopathological observation, lung, liver, kidney and spleen samples were collected at the time of sacrifice. Samples were fixed immediately in 10% neutral buffered formalin solution and then dehydrated with increasing ethanol concentrations (70%, 96% and 100%). Samples were next embedded in paraffin, sectioned using a microtome, mounted on microscope slides and stained with hematoxylin and eosin. Tissue histopathological changes were examined by a pathologist blinded to the experimental groups. All images were acquired using a Leica DM 2500 microscope equipped with a color camera Leica MC170 HD (Leica microsystems, Wetzlar, Germany). Moreover, blood toxicological parameters, such as creatine kinase, urea, lactate dehydrogenase and alanine transaminase, were measured in serum samples by enzyme linked immunosorbent assay (ELISA) technique according to the manufacturer's instructions (BioAssay Systems, California, USA). Samples were analyzed using a plate reader Infinite M200 (Tecan, Mannedorf, Switzerland).

Systemic cytokine quantification

Proinflammatory cytokines IL-1 β (Boster Bio, California, USA), IL-6 (Boster Bio, California, USA), IL-17 (Sunred Biological Technology, Shanghai, China) and TNF (RayBiotech, Georgia, USA) were quantified in serum samples using specific rat ELISA kits according to the provider's recommendations. Standard curves for each cytokine were generated by using reference cytokine concentrations supplied by the manufacturer. Samples were analyzed using a plate reader Infinite M200 (Tecan, Mannedorf, Switzerland).

Histological and immunohistochemical evaluation of hind paws

Left hind paw samples collected at the time of sacrifice were fixed immediately in 10% neutral buffered formalin solution and then decalcified in 10% formic acid. Samples were next dehydrated and embedded in paraffin, serially sectioned at a thickness of 5 μ m using a microtome, mounted on microscope slides and stained with hematoxylin and eosin for morphological examination of structural changes and cellular infiltration. Histopathological evaluation of rat joints was performed in a blind fashion using 4 semi-quantitative scores: Sublining layer infiltration score (0—none to diffuse infiltration; 1—lymphoid cell aggregate; 2—lymphoid follicles; 3—lymphoid follicles with germinal center formation); Lining layer cell number score (0—fewer than three layers; 1—three to four layers; 2—five to six layers; 3—more than six layers); Bone erosion score (0—no erosions; 1—minimal; 2—mild; 3—moderate; 4—marked); Global severity score (0—no signs of inflammation; 1—mild; 2—moderate; 3—severe) [17, 44, 45]. Paw sections were also used for immunohistochemical staining with CD68 (Abcam, Cambridge, UK), CD163 (Biorbyt, Massachusetts, USA), CD3 (Abcam, Cambridge, UK), CD19 (Biorbyt, Massachusetts, USA) and Ki67 (Abcam, Cambridge, UK) antibodies. Tissue sections were incubated with the primary antibody and with EnVision+ (Dako, Glostrup, Denmark). Color was developed in solution containing diaminobenzadine-tetrahydrochloride (Sigma, Missouri, USA), 0.5% H₂O₂ in phosphate-buffered saline buffer (pH 7.6). Slides were counter-stained with hematoxylin and mounted. Immunohistochemical evaluation of rat joints was performed in a blind fashion using a semi-quantitative score of 0–4 (0—no staining; 1–0–25% staining; 2–25–50% staining; 3–50–75% staining; 4—more than 75% staining) [17]. Images

were acquired using a Leica DM2500 (Leica Microsystems, Wetzlar, Germany) microscope equipped with a color camera.

For a quantitative analysis of the immunohistochemical staining, we acquired whole-slide color images of single tissue slides using a NanoZoomer SQ slide scanner (Hamamatsu Photonics, Hamamatsu City, Japan) with 20x magnification (0.46 μm resolution). We developed an image analysis software written in MATLAB (Mathworks, Natick, MA) to identify and count the number of positive cells that displayed a specific cytoplasmic staining in representative sections. Briefly, single cell nuclei stained with hematoxylin were identified by color thresholding in the $L^*a^*b^*$ color space with the range of parameters $L^* = [40,72]$, $a^* = [-11,20]$ and $b^* = [-37,12]$ followed by particle analysis. Dilated regions of interest (ROIs) with a radius of 5 pixels were next defined for each detected particle as the cytoplasmic area. The antibody staining was also identified by color thresholding in the $L^*a^*b^*$ color space with the range of parameters $L^* = [40,80]$, $a^* = [-6,20]$ and $b^* = [-0.2,33]$. Each cell ROI was then evaluated for antibody positive staining, defined by the occurrence of at least 20 pixels with a color value included in the cytoplasmic $L^*a^*b^*$ threshold range. We cropped areas of interest from whole-slide color images corresponding to synovial membranes and the software was set to batch process all images and output the total number of cells and the number of cells with positive antibody staining for each section. Then the density of positive cells was calculated by dividing the positive cell count by the area value.

Statistical analysis

Statistical differences were determined with non-parametric Kruskal-Wallis (Dunn's Multiple Comparison tests) and Mann-Whitney tests using GraphPad Prism (GraphPad, California, USA). Correlation analysis was performed with the Spearman test. Differences were considered statistically significant for $p < 0.05$.

Results

Celastrol safely suppresses inflammatory manifestations in rat adjuvant-induced arthritis

To further validate the *in vivo* anti-inflammatory effect of celastrol in the context of arthritis, we have used the AIA rat model. The AIA experimental arthritis shares some characteristics of RA, such as hyperplasia of the synovial membrane, inflammatory infiltration of the joints, deposition of immune complexes in articular cartilage, pannus formation and destruction of bone. This model is also useful to characterize treatment responses by the reduction of inflammation or changes in the synovial tissue [46]. Overall, the AIA model has been extensively used to clarify the mechanisms of human RA pathogenesis and to identify potential targets and new drugs for therapeutic intervention [47], and has thus been our model of choice for our first experimental use of celastrol [17, 48].

Celastrol was intraperitoneally administrated at a dose of 1 $\mu\text{g/g}$ /daily after 4 days of disease induction (early treatment group) and after 11 days of disease induction (late treatment group) [17]. The inflammatory score and ankle perimeter were evaluated during the treatment period (Fig 1 and S1 Fig). As shown in Fig 1A, all animals already presented signs of arthritis by the fourth day of disease induction and after 9 days the untreated arthritic group started to increase the inflammatory manifestations sharply. In contrast, in early celastrol-treated rats there was minimal inflammatory activity or even complete abrogation of arthritis manifestations. In the late treatment group, drug administration was started when animals already presented a mean inflammatory score of 4, but celastrol still caused a significant decrease of arthritis manifestations

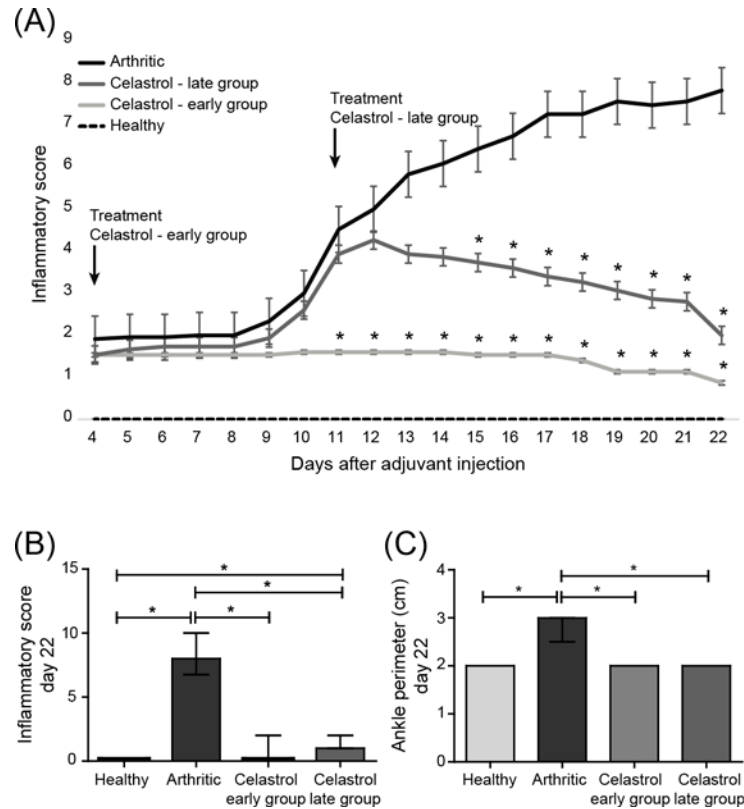


Fig 1. (A) Celastrol ameliorates inflammation throughout time. Notice that after 7 days of treatment celastrol early-treated rats presented minimal inflammatory activity, whereas arthritic rats started to increase the inflammatory manifestations sharply. Arrows indicate the beginning of treatment after 4 and 11 days of disease induction. (B) Celastrol improves the clinical outcome in adjuvant-induced arthritic rats. Inflammatory score in celastrol-treated AIA rats is maintained significantly diminished in comparison with arthritic rats. (C) Celastrol suppresses the progression of swelling in the left hind paw. Left paw edema/swelling is markedly present in arthritic rats in contrast to celastrol-treated animals. Data are expressed as median with interquartile range. Differences were considered statistically significant for p-values < 0.05, according to the Kruskal-Wallis (Dunn's Multiple Comparison tests) and Mann-Whitney tests. Healthy N = 19, Arthritic N = 23, Celastrol early group N = 15 and Celastrol late group N = 15.

doi:10.1371/journal.pone.0142448.g001

over time. In fact, the only remaining sign of swelling was observed in most animals in the local of injection of the adjuvant, for disease induction. This result shows that this drug has a significant anti-inflammatory effect even when administrated at a later phase of arthritis development. Celastrol showed a significant anti-inflammatory effect, as assessed by the evaluation of the inflammatory score ($p < 0.0001$ in early and late treatment groups vs. arthritic animals, shown in Fig 1B) and also by the measurement of ankle perimeter ($p < 0.0001$ in early and late treatment groups vs. arthritic animals, shown in Fig 1C). Of note, by the end of the treatment, at day 22, there were no significant differences between the celastrol early and late treatment groups. Importantly, both treated groups showed a significant reduction in the inflammatory score when compared with their baselines ($p = 0.0002$ in celastrol early-treated vs. arthritic rats sacrificed at day 4 and $p < 0.0001$ in celastrol-late treated vs. arthritic rats sacrificed at day 11).

Up to now significant adverse effects of celastrol administration have not been reported. However the few toxicological analysis of this compound *in vivo* were based in data from the assessment of animal mortality and some blood parameters in studies using *Tripterygium wilfordii* plant extracts [49]. To investigate the potential side effects of pure celastrol

administration in AIA rats, we performed liver and renal function tests, such as the measurement of creatine kinase, urea, lactate dehydrogenase and alanine transaminase in serum samples collected at the time of sacrifice. No significant differences were observed in these parameters when comparing arthritic rats with animals under treatment ($p = 0.2$). In addition, a pathologist blinded to experimental groups examined the tissue histological sections and has reported no evidence of drug-induced liver or renal injury, as well as no lung or spleen alterations (S2 Fig). Of note, body weight variations were recorded throughout treatment duration, and no weight loss was observed due to celastrol administration ($p = 0.1265$ and $p = 0.6005$ in celastrol early and late treatment groups vs. arthritic rats, respectively). Contrarily, there was an association between disease activity and weight loss ($p = 0.0273$ in arthritic rats vs. healthy animals). In fact, in the late treatment group, animals started to lose weight due to disease activity and after treatment was initiated no more weight loss was observed ($p = 0.0436$ in late-treated rats at day 11 vs. day 4, and $p = 0.9009$ in late-treated rats at day 22 vs. day 11) (S3 Fig). Importantly, administration of celastrol has already been tested in healthy animals in a wide range of concentrations [21]. So far, there are no data showing deleterious effects at a dose of 1mg/kg (the concentration used in this work).

Celastrol diminishes systemic proinflammatory cytokine IL-6 *in vivo*

Proinflammatory cytokines, namely IL-1 β , IL-6, IL-17 and TNF act synergistically to maintain inflammation and bone erosions in animal models of arthritis and in RA patients. These cytokines activate the NF- κ B pathway that in turn leads to the downstream up-regulation of several cytokines, chemokines and MMPs, which are responsible for the inflammatory process and for the destruction of cartilage and bone. We therefore aimed at evaluating the anti-inflammatory effect of celastrol on the peripheral circulating levels of these cytokines. We have observed that IL-6 levels increase in the serum of AIA rats throughout the course of arthritis, although abundant production was seen only after 2 weeks of disease onset. Thus, IL-6, which is produced by monocytes/macrophages, T cells and synovial fibroblasts [50], seems to be involved in the systemic events underlying arthritis, especially in the transition phase of its development. Fig 2 shows that celastrol administration significantly reduces the levels of IL-6 detected in peripheral blood, both in early and late treatment groups ($p < 0.0001$ in both groups vs. arthritic rats

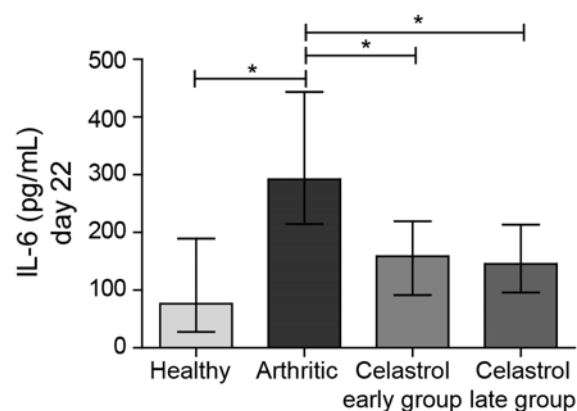


Fig 2. Celastrol reduces the serum levels of IL-6 in arthritic rats. Notice that celastrol treatment significantly reduces the systemic concentration of the proinflammatory cytokine IL-6 to levels similar to healthy controls. Data are expressed as median with interquartile range. Differences were considered statistically significant for p -values < 0.05 , according to the Kruskal-Wallis (Dunn's Multiple Comparison tests) and Mann-Whitney tests. Healthy $N = 21$, Arthritic $N = 23$, Celastrol early group $N = 15$ and Celastrol late group $N = 15$.

doi:10.1371/journal.pone.0142448.g002

after 22 days of disease induction), presenting a cytokine concentration similar to healthy controls. Importantly, both treated groups showed a significant reduction in the circulating levels of IL-6 when compared with their baselines ($p = 0.0387$ in celastrol early-treated vs. arthritic rats sacrificed at day 4 and $p < 0.0001$ in celastrol-late treated vs. arthritic rats sacrificed at day 11). This observation is corroborated by data already published which shows that IL-6 mRNA is decreased after celastrol treatment *in vitro* [51]. We have also quantified the circulating concentration of IL-1 β , IL-17 and TNF, but no differences were found when comparing arthritic rats with animals under celastrol treatment or with healthy controls ($p > 0.05$, S4 Fig), possibly because these cytokines are not increased in the periphery at this stage of disease development. Previously, we have demonstrated that circulating IL-1 β and IL-17 are only increased in the early phase of RA, in contrast to IL-6, which was found to be increased also in the later phase of the disease [18], arguing that the detection of these cytokines in the periphery is dependent on disease evolution. In addition, literature controversy highlights the likelihood that systemic markers and mediators of arthritis might not fully reflect the underlying local disease progression. AIA rat model have increased levels of IL-1 β (since the preclinical disease stage), IL-6, IL-17 and TNF (in the acute and chronic stages) locally in the joints [42]. Recently, it has been shown in the same animal model that both Tripterygium and celastrol decrease the levels of these cytokines locally in the arthritic joints [19, 20, 22, 52].

Celastrol ameliorates local joint inflammation and bone damage in AIA rats

To evaluate the effect of celastrol in the preservation of local articular joint synovium and bone structures, paw sections stained with hematoxylin and eosin were performed (illustrative images can be observed in Fig 3). The histological evaluation using 4 semi-quantitative scores is depicted in Fig 4.

The levels of the sublining layer infiltration (Fig 4A) and the lining layer cell numbers (Fig 4B) started to augment immediately after 4 days of disease onset and continued to markedly increase until the end of the study ($p < 0.0001$, healthy vs. arthritic rats sacrificed after 22 days of disease induction). The data from Fig 4D revealed that rats treated with celastrol had a normal joint structure at the end of the study period, with an abrogation of the inflammatory infiltrate and a reduction of the number of cells present in the lining layer of the synovial membrane ($p < 0.0001$ in early and late treatment groups vs. arthritic animals). Moreover, when comparing the infiltration score of celastrol early-treated group with diseased animals at baseline (day 4), we observed that there was a complete clearance of the cellular infiltrate ($p = 0.0006$ in the early-treated group sacrificed at the end of the treatment period vs. arthritic rats sacrificed at baseline of the treatment period, i.e. after 4 days of disease induction), with a phenotype similar to a healthy control. Regarding the analysis of the lining layer cell number score (Fig 4B), data showed that both celastrol early and late treatment groups have dramatically reduced scores, in comparison with the animals at the beginning of treatment, corresponding to baseline ($p = 0.0107$ in early-treated arthritic rats sacrificed at the end of the study period vs. arthritic rats sacrificed at baseline, at day 4 and $p < 0.0001$ in late-treated arthritic rats sacrificed at the end of the study period vs. arthritic rats sacrificed at baseline, at day 11, respectively).

Celastrol is also effective in preventing bone articular destruction as shown in Fig 4C. The development of bone erosions in the AIA rat model occurred immediately after 4 days of disease onset, and markedly increased throughout the development of arthritis ($p < 0.0001$ in healthy vs. arthritic rats sacrificed after 22 days of disease induction), with a strong correlation between erosion and infiltration as well as with proliferation scores ($r^2 = 0.70$, $p = 0.0009$ and

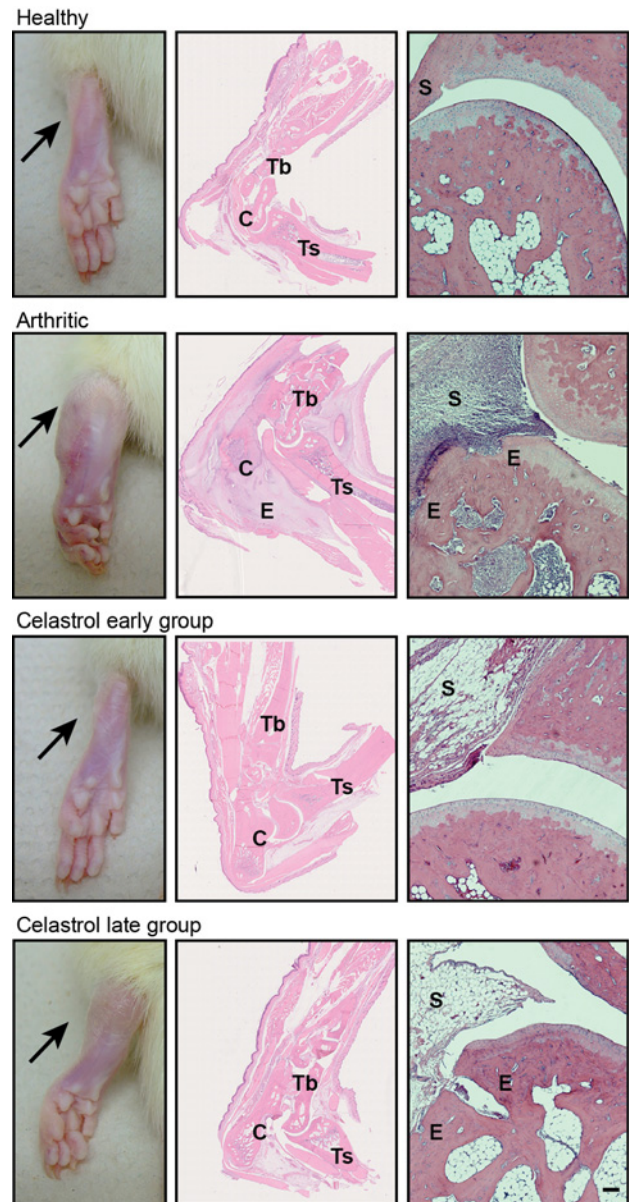


Fig 3. Histological images of joints after celastrol treatment. These patterns are merely illustrative of the type of histological features observed. Black arrow indicates the absence/presence of ankle swelling in rat hind paws. C—calcaneus, E—edema or erosion, S—synovia, Tb—tibia, Ts—tarso. Magnification of 50x. Bar: 100 μ m.

doi:10.1371/journal.pone.0142448.g003

$r^2 = 0.97$, $p < 0.0001$, respectively). By the end of the treatment course, celastrol was able to suppress the appearance of bone erosions ($p < 0.0001$ in both celastrol early and late treatment groups vs. arthritic rats), maintaining the phenotype similar to their baselines. These results might suggest that celastrol is able to modulate osteoclast pathways. In fact, a study has demonstrated that celastrol inhibits the formation and activity of mature osteoclasts, induces their apoptosis and reduces osteoblast viability and activity *in vitro* [53].

Overall, these data are supported by studies already published in the literature using several plant extracts and different experimental outlines [19, 20, 22, 54, 55]. Thus, there is strong

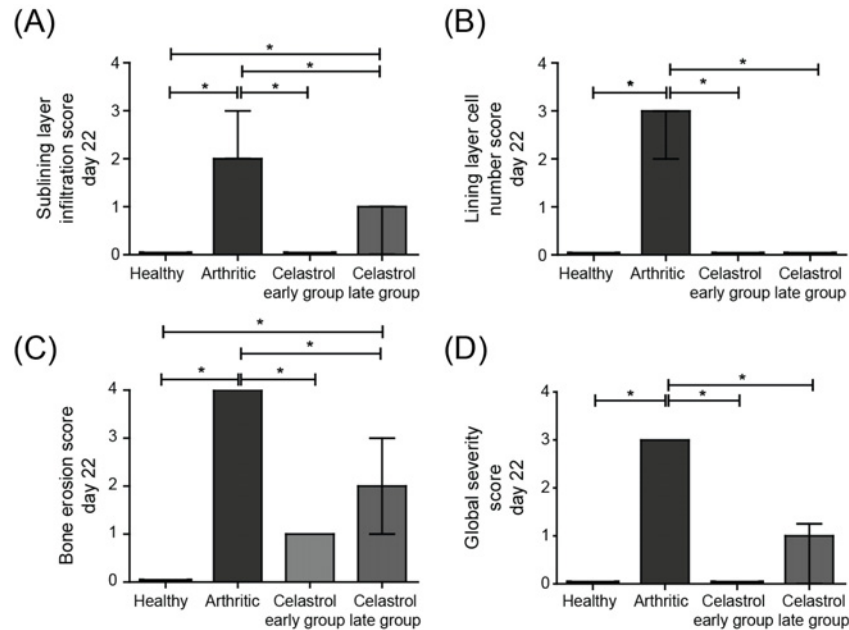


Fig 4. Celastrol suppresses arthritic inflammation and tissue damage locally in the joints of AIA rats. A semi-quantitative evaluation of histological sections was performed. Notice that celastrol has inhibited cellular infiltration (A), completely reversed the number of lining layer cells to the normal values (B) and prevented bone erosion occurrence (C), allowing for a normal joint structure comparable to healthy rats in both early and late treatment groups (D). Data are expressed as median with interquartile range. Differences were considered statistically significant for p -values < 0.05 , according to the Kruskal-Wallis (Dunn's Multiple Comparison tests) and Mann-Whitney tests. Correlation analysis was performed using the Spearman test. Healthy $N = 19$, Arthritic $N = 23$, Celastrol early group $N = 15$ and Celastrol late group $N = 15$.

doi:10.1371/journal.pone.0142448.g004

evidence that celastrol is able to significantly diminish inflammation and bone damage, even when administrated in a later phase of arthritis development.

Celastrol inhibits synovial lymphocyte infiltration and cell proliferation in arthritic rat joints

The immunohistochemical analysis revealed that arthritic rats treated with celastrol have reduced levels of lymphocyte infiltration into the joints (Fig 5). As can be observed in Fig 5B there were significant reductions of CD3+ T cells ($p < 0.0001$ in early and late treatment groups vs. arthritic rats) and CD19+ B cells ($p < 0.0001$ in early and late treatment groups vs. arthritic rats). In contrast, the number of these cells markedly increased throughout disease progression in untreated animals ($p < 0.0001$ in healthy vs. arthritic rats, sacrificed at the end of the study period). A study by Venkatesha et al, have shown that celastrol reduces the level of chemokines, which might explain the inhibition of leukocyte migration [20].

In addition, we have also studied cell proliferation by staining joint tissue sections with the Ki67 marker. The immunohistochemical results shown in Fig 5B revealed that animals treated with celastrol have reduced levels of synovial cell proliferation in both early and late treated rats ($p < 0.0001$ in both groups vs. arthritic animals), with a score similar to the healthy controls.

Results of immunohistochemical quantification also showed that celastrol significantly reduced CD3+ T cells ($p = 0.0079$ in both early and late treatment groups vs. arthritic rats) and CD19+ B cells ($p = 0.0317$ in both early and late treatment groups vs. arthritic rats) infiltrated into the joints as well as synovial cell proliferation ($p = 0.0079$ in both early and late treatment groups vs. arthritic rats), as depicted in Fig 5C.

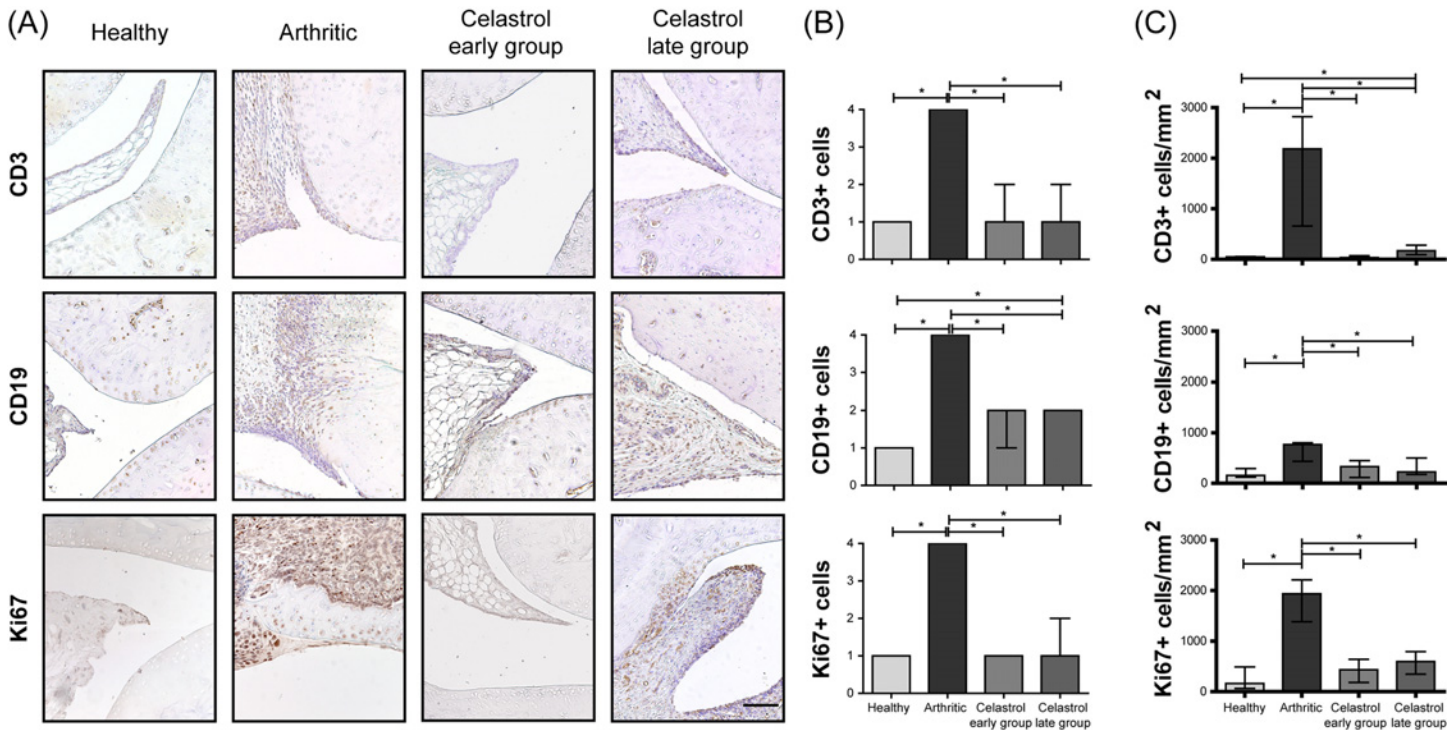


Fig 5. Celastrol reduces the number of T cells and B cells present in the synovial membrane, and suppresses synovial cell proliferation. (A) Representation of the immunohistochemical evaluation performed in paw sections at day 22 after celastrol treatment. Magnifications of 200x. Bar: 100 μ m. (B) Immunohistochemical analysis was performed using a semi-quantitative score. Notice that both celastrol early and late-treated rats showed a significant reduction in the number of CD3 and CD19 positive cells as well as a reduction in the levels of synovial cell proliferation assessed by Ki67 marker in comparison with arthritic rats at day 22. Healthy N = 16, Arthritic N = 10, Celastrol early group N = 15 and Celastrol late group N = 15. (C) Immunohistochemical quantification was performed using an image analysis software written in MATLAB to identify and count the number of positive cells for each antibody in representative sections. Notice that both celastrol early and late-treated rats showed a significant reduction in the number of CD3, CD19 and Ki67 positive cells in comparison with arthritic rats at day 22. Healthy N = 5, Arthritic N = 5, Celastrol early group N = 5 and Celastrol late group N = 5. Data are expressed as median with interquartile range. Differences were considered statistically significant for p-values < 0.05, according to the Kruskal-Wallis (Dunn's Multiple Comparison tests) and Mann-Whitney tests.

doi:10.1371/journal.pone.0142448.g005

Celastrol significantly reduces CD68+ macrophages in the arthritic synovial tissue

The activated macrophages in the synovium are derived from circulating monocytes and secrete various mediators that participate in arthritis induction and tissue injury. Studies of drug efficacy in RA patients have identified, from a large panel of synovial biomarkers, sublining CD68+ macrophages as an optimal marker to evaluate clinical response, with an association between clinical improvement and the reduction of CD68+ macrophage scores. Therefore, CD68+ sublining macrophages have been recognized as a synovial biomarker, with a high sensitivity in discriminating between effective and ineffective therapies or placebo, useful in an early stage of drug development [34, 56]. We have thus performed the characterization of CD68+ macrophages present in the synovial tissue after treatment with celastrol (Fig 6). Arthritic rats have shown an increase in the number of CD68+ synovial macrophages throughout the development of the disease ($p < 0.0001$ in healthy vs. arthritic rats, as shown in Fig 6B). Importantly, celastrol significantly decreased the number of CD68+ macrophages infiltrated into the arthritic joint tissue ($p < 0.0001$ in early and late treatment groups vs. arthritic rats). In addition, celastrol administration significantly decreased the levels of CD163+ macrophages ($p < 0.0001$ in early and late treatment groups vs. arthritic rats). CD163 is a useful marker in

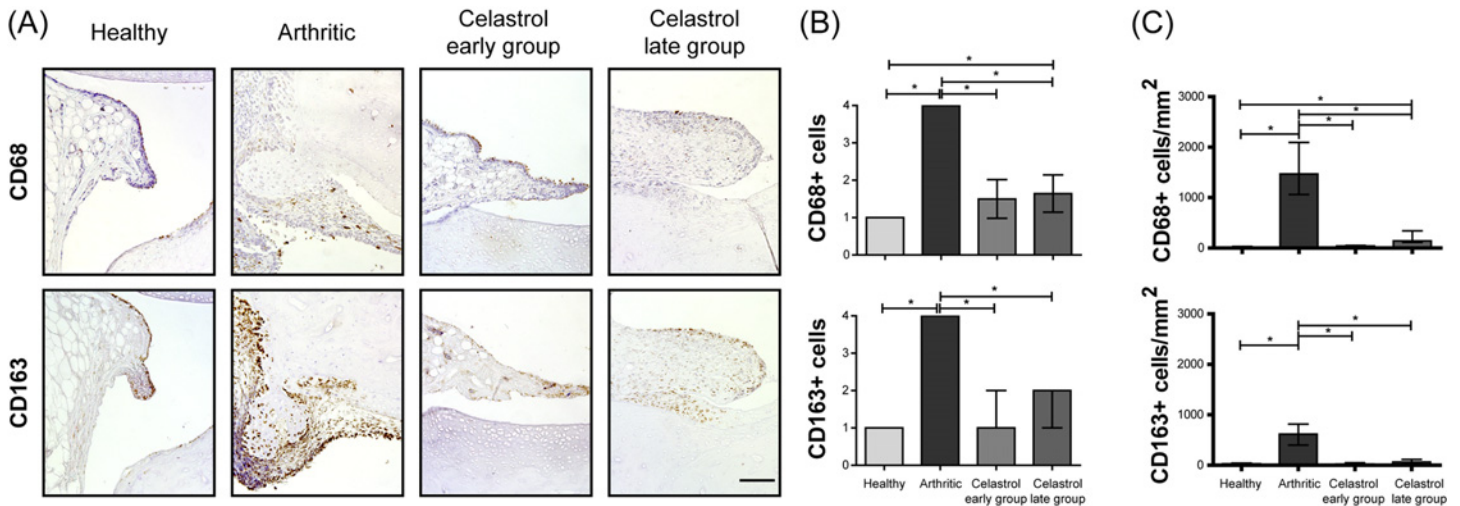


Fig 6. Celastrol reduces the number of synovial CD68+ macrophages. (A) Representation of the immunohistochemical evaluation performed in paw sections at day 22 after celastrol treatment. Magnifications of 200x. Bar: 100 μ m. (B) Immunohistochemical analysis was performed using a semi-quantitative score. Notice that both celastrol early and late-treated rats showed a significant reduction in the number of CD68 and CD163 positive cells in comparison with arthritic rats at day 22. Healthy N = 16, Arthritic N = 10, Celastrol early group N = 15 and Celastrol late group N = 15. (C) Immunohistochemical quantification was performed using an image analysis software written in MATLAB to identify and count the number of positive cells for each antibody in representative sections. Notice that both celastrol early and late-treated rats showed a significant reduction in the number of CD68 and CD163 positive cells in comparison with arthritic rats at day 22. Healthy N = 5, Arthritic N = 5, Celastrol early group N = 5 and Celastrol late group N = 5. Data are expressed as median with interquartile range. Differences were considered statistically significant for p-values < 0.05, according to the Kruskal-Wallis (Dunn's Multiple Comparison tests) and Mann-Whitney tests.

doi:10.1371/journal.pone.0142448.g006

this context because it is a more selective macrophage marker and helps to discriminate between synovial macrophages and synovial intimal fibroblasts, which also stain positively for CD68 in RA synovium [57]. Previous studies have in fact shown that synovial intimal fibroblasts migration and invasion into the synovium are also reduced by celastrol [55, 58].

Results of immunohistochemical quantification shown in Fig 6C also revealed that celastrol significantly reduced CD68+ cells ($p = 0.0079$ in both early and late treatment groups vs. arthritic rats) and CD163+ macrophages ($p = 0.0079$ in both early and late treatment groups vs. arthritic rats) infiltrated into the joints.

Because inflammatory synovial tissue macrophages are derived from peripheral blood monocytes, these observations suggest decreased monocyte recruitment into the joints of arthritic rats treated with celastrol, even when treatment was initiated in a later phase of disease development.

Discussion

In this study, we have shown that celastrol substantially depletes CD68+ sublining synovial cells, considered to be the biomarker with the strongest association with response to treatment in RA. Moreover, celastrol was effective and safe in suppressing synovial inflammation and bone damage in rats with AIA.

We have consistently observed that celastrol treatment reduced serum IL-6 levels in arthritic rats. This observation is relevant because IL-6 is a proinflammatory cytokine that plays a relevant role in the pathogenesis of RA, namely in Th17 polarization and plasma B cell differentiation, in the production of chemokines, adhesion molecules, and VEGF, and in the secretion of RANKL and MMPs, amplifying inflammatory cell infiltration and inducing osteoclastogenesis [59–61]. Interestingly, it was shown that celastrol can suppress arthritis in part by altering Th17/Treg ratio in inflamed joints [52]. Additionally, celastrol-treated rats showed a significant

reduction in the severity of clinical arthritis as well as in pannus formation and leukocyte cell infiltration into the joint synovial tissue. This cell infiltration and proliferation inhibitory effect of celastrol may thus prove to be of interest to prevent and treat the development of the synovial tumor-like pannus tissue characteristic of established RA and responsible for bone damage. Interestingly, histological analysis also revealed that celastrol is effective in suppressing local inflammation-induced bone loss. Of note, celastrol treatment is effective when administered both in the early and established phase of arthritis, which is relevant for the potential clinical implications of our findings. Our report is the first to demonstrate the protective coupled effect of celastrol *in vivo* on both synovial inflammation and joint bone damage restoring synovial homeostasis, fulfilling this unmet medical need in RA treatment approach. Importantly, CD68 + sublining macrophages, a synovial biomarker with a high sensitivity in selecting effective RA therapies in an early stage of drug development, is significantly reduced in the synovia of celastrol-treated rats.

It has already been reported that celastrol targets NF- κ B, via long-lasting inhibition of IKK β activity [62]. In fact, the inactivation of NF- κ B in animal models has shown the ability to suppress arthritis [63]. NF- κ B participates in the transcription of genes encoding many proinflammatory cytokines and chemokines, in the regulation of different immune cells and in the expression of adhesion molecules and matrix MMPs [64]. Based on microarray gene expression profile it has been demonstrated that celastrol represses cell proliferation, inflammation and immune responses (targets T and B cells, antigen processing and presentation), blocks metabolic pathways, has anti-oxidant properties, and targets VEGF, proinflammatory cytokines and chemokines [65]. Indeed, it has been demonstrated that celastrol reduces the levels of chemokines, possibly affecting leukocyte migration [20]. Celastrol has thus a broad spectrum of targets, modulating immune responses rather than inducing immunosuppression [65]. Our results point out that pure celastrol used in the AIA rat model is not associated with increased risk of infections, have no hepatotoxicity or nephrotoxicity, suggesting that at least for short-term RA treatment, celastrol might be a safe drug.

Overall, our results validate celastrol as a promising compound for the treatment of inflammation and inflammation-induced bone damage and provide relevant insights into the usage of celastrol as a future drug for RA. It would be interesting to extend this knowledge by studying the anti-arthritic properties of celastrol *in vivo* using different animal models of arthritis, namely the CIA model, and evaluate differences in efficacy depending on animal gender.

Supporting Information

S1 Fig. Ankle perimeter kinetics. Celastrol was administered to AIA rats both in the early (4 days after disease induction) and late (11 days after disease induction) phases of arthritis development. Notice that after 7 days of treatment celastrol early-treated rats presented an ankle perimeter similar to the healthy control, whereas arthritic rats started to increase left ankle edema/swelling sharply. In the celastrol late-treated group, ankle swelling started to increase in parallel to the augment of the inflammatory score, but after treatment was initiated ankle perimeter started to significantly decrease. Data are expressed as median with interquartile range. Differences were considered statistically significant for p-values < 0.05, according to the Kruskal-Wallis (Dunn's Multiple Comparison tests) and Mann-Whitney tests. Healthy N = 19, Arthritic N = 23, Celastrol early group N = 15 and Celastrol late group N = 15. (TIF)

S2 Fig. Administration of pure celastrol induces no hepatic or renal toxicity. At day 22 after disease induction no hepatocellular or renal lesion was observed in any of the animals. Liver and kidney samples from all animals were analyzed by a pathologist blinded to experimental

groups but only representative histological sections are shown. H&E staining; Magnifications of 100×. Bar: 300 μm.

(TIF)

S3 Fig. Celestrol treatment has no effect on body weight. Notice that no weight loss was observed due to celestrol administration. In contrast, there was an association between disease activity and weight loss, which was highlighted in late-treated rats that started to lose weight due to disease activity (day 4 up to day 11) and after treatment was initiated no more weight loss was observed (day 11 up to day 22). Data are expressed as median with interquartile range. Differences were considered statistically significant for p-values < 0.05, according to the Mann-Whitney tests.

(TIF)

S4 Fig. Celestrol has no effect in the serum levels of IL-1β, IL-17 and TNF in arthritic rats. Data are expressed as median with interquartile range. Differences were considered statistically significant for p-values < 0.05, according to the Kruskal-Wallis (Dunn's Multiple Comparison tests) and Mann-Whitney tests. Healthy N = 19, Arthritic N = 23, Celestrol early group N = 15 and Celestrol late group N = 15.

(TIF)

Acknowledgments

The authors would like to acknowledge Ana Lopes, the Histology and Comparative Pathology Laboratory and the Bioimaging Facility from Instituto de Medicina Molecular for technical assistance.

Author Contributions

Conceived and designed the experiments: RC LFM JEF. Performed the experiments: RC BV IPL EP JR. Analyzed the data: RC BV IPL EP. Contributed reagents/materials/analysis tools: JR JEF. Wrote the paper: RC LFM JEF.

References

1. Gorman CL, Cope AP. Immune-mediated pathways in chronic inflammatory arthritis. *Best practice & research Clinical rheumatology*. 2008; 22(2):221–38.
2. Hahn B. A pathophysiologic approach to the clinical management of arthritis and pain: current and future implications. *Journal of clinical rheumatology: practical reports on rheumatic & musculoskeletal diseases*. 2004; 10(3 Suppl):S3–4.
3. Plasqui G. The role of physical activity in rheumatoid arthritis. *Physiology & behavior*. 2008; 94(2):270–5.
4. Steiner G, Tohidast-Akrad M, Witzmann G, Vesely M, Studnicka-Benke A, Gal A, et al. Cytokine production by synovial T cells in rheumatoid arthritis. *Rheumatology*. 1999; 38(3):202–13. PMID: [10325658](#)
5. Astry B, Harberts E, Moudgil KD. A cytokine-centric view of the pathogenesis and treatment of autoimmune arthritis. *Journal of interferon & cytokine research: the official journal of the International Society for Interferon and Cytokine Research*. 2011; 31(12):927–40.
6. Boyce BF, Xing L. Functions of RANKL/RANK/OPG in bone modeling and remodeling. *Archives of biochemistry and biophysics*. 2008; 473(2):139–46. doi: [10.1016/j.abb.2008.03.018](#) PMID: [18395508](#)
7. Karmakar S, Kay J, Gravallese EM. Bone damage in rheumatoid arthritis: mechanistic insights and approaches to prevention. *Rheumatic diseases clinics of North America*. 2010; 36(2):385–404. doi: [10.1016/j.rdc.2010.03.003](#) PMID: [20510240](#)
8. Kotake S, Udagawa N, Takahashi N, Matsuzaki K, Itoh K, Ishiyama S, et al. IL-17 in synovial fluids from patients with rheumatoid arthritis is a potent stimulator of osteoclastogenesis. *The Journal of clinical investigation*. 1999; 103(9):1345–52. PMID: [10225978](#)

9. Schett G. Rheumatoid arthritis: inflammation and bone loss. *Wiener medizinische Wochenschrift*. 2006; 156(1–2):34–41. PMID: [16465612](#)
10. Xu S, Wang Y, Lu J, Xu J. Osteoprotegerin and RANKL in the pathogenesis of rheumatoid arthritis-induced osteoporosis. *Rheumatology international*. 2012; 32(11):3397–403. doi: [10.1007/s00296-011-2175-5](#) PMID: [22057136](#)
11. Gravallesse EM, Manning C, Tsay A, Naito A, Pan C, Amento E, et al. Synovial tissue in rheumatoid arthritis is a source of osteoclast differentiation factor. *Arthritis and rheumatism*. 2000; 43(2):250–8. PMID: [10693863](#)
12. Fonseca JE, Canhao H, Tavares NJ, Cruz M, Branco J, Queiroz MV. Persistent low grade synovitis without erosive progression in magnetic resonance imaging of rheumatoid arthritis patients treated with infliximab over 1 year. *Clinical rheumatology*. 2009; 28(10):1213–6. doi: [10.1007/s10067-009-1207-y](#) PMID: [19504146](#)
13. Joosten LA, Helsen MM, Saxne T, van De Loo FA, Heinegard D, van Den Berg WB. IL-1 alpha beta blockade prevents cartilage and bone destruction in murine type II collagen-induced arthritis, whereas TNF-alpha blockade only ameliorates joint inflammation. *Journal of immunology*. 1999; 163(9):5049–55.
14. Smolen JS, Han C, Bala M, Maini RN, Kalden JR, van der Heijde D, et al. Evidence of radiographic benefit of treatment with infliximab plus methotrexate in rheumatoid arthritis patients who had no clinical improvement: a detailed subanalysis of data from the anti-tumor necrosis factor trial in rheumatoid arthritis with concomitant therapy study. *Arthritis and rheumatism*. 2005; 52(4):1020–30. PMID: [15818697](#)
15. Singh JA, Furst DE, Bharat A, Curtis JR, Kavanaugh AF, Kremer JM, et al. 2012 update of the 2008 American College of Rheumatology recommendations for the use of disease-modifying antirheumatic drugs and biologic agents in the treatment of rheumatoid arthritis. *Arthritis care & research*. 2012; 64(5):625–39.
16. Vivar N, Van Vollenhoven RF. Advances in the treatment of rheumatoid arthritis. *F1000prime reports*. 2014; 6:31. doi: [10.12703/P6-31](#) PMID: [24860653](#)
17. Cascao R, Vidal B, Raquel H, Neves-Costa A, Figueiredo N, Gupta V, et al. Effective treatment of rat adjuvant-induced arthritis by celastrol. *Autoimmunity reviews*. 2012; 11(12):856–62. doi: [10.1016/j.autrev.2012.02.022](#) PMID: [22415021](#)
18. Cascao R, Moura RA, Perpetuo I, Canhao H, Vieira-Sousa E, Mourao AF, et al. Identification of a cytokine network sustaining neutrophil and Th17 activation in untreated early rheumatoid arthritis. *Arthritis research & therapy*. 2010; 12(5):R196.
19. Li H, Zhang YY, Tan HW, Jia YF, Li D. Therapeutic effect of tripterine on adjuvant arthritis in rats. *Journal of ethnopharmacology*. 2008; 118(3):479–84. doi: [10.1016/j.jep.2008.05.028](#) PMID: [18577440](#)
20. Venkatesha SH, Astry B, Nanjundaiah SM, Yu H, Moudgil KD. Suppression of autoimmune arthritis by Celastrol-derived Celastrol through modulation of pro-inflammatory chemokines. *Bioorganic & medicinal chemistry*. 2012; 20(17):5229–34.
21. Kusy S, Ghosn EE, Herzenberg LA, Contag CH. Development of B cells and erythrocytes is specifically impaired by the drug celastrol in mice. *PloS one*. 2012; 7(4):e35733. doi: [10.1371/journal.pone.0035733](#) PMID: [22545133](#)
22. Nanjundaiah SM, Venkatesha SH, Yu H, Tong L, Stains JP, Moudgil KD. Celastrol and its bioactive celastrol protect against bone damage in autoimmune arthritis by modulating osteoimmune cross-talk. *The Journal of biological chemistry*. 2012; 287(26):22216–26. doi: [10.1074/jbc.M112.356816](#) PMID: [22549786](#)
23. Gerlag DM, Haringman JJ, Smeets TJ, Zwinderman AH, Kraan MC, Laud PJ, et al. Effects of oral prednisolone on biomarkers in synovial tissue and clinical improvement in rheumatoid arthritis. *Arthritis and rheumatism*. 2004; 50(12):3783–91. PMID: [15593225](#)
24. Yanni G, Nabil M, Farahat MR, Poston RN, Panayi GS. Intramuscular gold decreases cytokine expression and macrophage numbers in the rheumatoid synovial membrane. *Annals of the rheumatic diseases*. 1994; 53(5):315–22. PMID: [8017985](#)
25. Smith MD, Kraan MC, Slavotinek J, Au V, Weedon H, Parker A, et al. Treatment-induced remission in rheumatoid arthritis patients is characterized by a reduction in macrophage content of synovial biopsies. *Rheumatology*. 2001; 40(4):367–74. PMID: [11312372](#)
26. Dolhain RJ, Tak PP, Dijkmans BA, De Kuiper P, Breedveld FC, Miltenburg AM. Methotrexate reduces inflammatory cell numbers, expression of monokines and of adhesion molecules in synovial tissue of patients with rheumatoid arthritis. *British journal of rheumatology*. 1998; 37(5):502–8. PMID: [9651076](#)
27. Kraan MC, Reece RJ, Barg EC, Smeets TJ, Farnell J, Rosenberg R, et al. Modulation of inflammation and metalloproteinase expression in synovial tissue by leflunomide and methotrexate in patients with active rheumatoid arthritis. Findings in a prospective, randomized, double-blind, parallel-design clinical

- trial in thirty-nine patients at two centers. *Arthritis and rheumatism*. 2000; 43(8):1820–30. PMID: [10943872](#)
28. Smeets TJ, Kraan MC, van Loon ME, Tak PP. Tumor necrosis factor alpha blockade reduces the synovial cell infiltrate early after initiation of treatment, but apparently not by induction of apoptosis in synovial tissue. *Arthritis and rheumatism*. 2003; 48(8):2155–62. PMID: [12905468](#)
 29. Taylor PC, Peters AM, Paleolog E, Chapman PT, Elliott MJ, McCloskey R, et al. Reduction of chemokine levels and leukocyte traffic to joints by tumor necrosis factor alpha blockade in patients with rheumatoid arthritis. *Arthritis and rheumatism*. 2000; 43(1):38–47. PMID: [10643698](#)
 30. Thurlings RM, Vos K, Wijbrandts CA, Zwinderman AH, Gerlag DM, Tak PP. Synovial tissue response to rituximab: mechanism of action and identification of biomarkers of response. *Annals of the rheumatic diseases*. 2008; 67(7):917–25. PMID: [17965121](#)
 31. Cunnane G, Madigan A, Murphy E, FitzGerald O, Bresnihan B. The effects of treatment with interleukin-1 receptor antagonist on the inflamed synovial membrane in rheumatoid arthritis. *Rheumatology*. 2001; 40(1):62–9. PMID: [11157143](#)
 32. Bresnihan B, Pontifex E, Thurlings RM, Vinkenoog M, El-Gabalawy H, Fearon U, et al. Synovial tissue sublining CD68 expression is a biomarker of therapeutic response in rheumatoid arthritis clinical trials: consistency across centers. *The Journal of rheumatology*. 2009; 36(8):1800–2. doi: [10.3899/jrheum.090348](#) PMID: [19671815](#)
 33. Haringman JJ, Gerlag DM, Smeets TJ, Baeten D, van den Bosch F, Bresnihan B, et al. A randomized controlled trial with an anti-CCL2 (anti-monocyte chemotactic protein 1) monoclonal antibody in patients with rheumatoid arthritis. *Arthritis and rheumatism*. 2006; 54(8):2387–92. PMID: [16869001](#)
 34. Wijbrandts CA, Vergunst CE, Haringman JJ, Gerlag DM, Smeets TJ, Tak PP. Absence of changes in the number of synovial sublining macrophages after ineffective treatment for rheumatoid arthritis: Implications for use of synovial sublining macrophages as a biomarker. *Arthritis and rheumatism*. 2007; 56(11):3869–71. PMID: [17968928](#)
 35. Haringman JJ, Gerlag DM, Zwinderman AH, Smeets TJ, Kraan MC, Baeten D, et al. Synovial tissue macrophages: a sensitive biomarker for response to treatment in patients with rheumatoid arthritis. *Annals of the rheumatic diseases*. 2005; 64(6):834–8. PMID: [15576415](#)
 36. LaBranche TP, Jesson MI, Radi ZA, Storer CE, Guzova JA, Bonar SL, et al. JAK inhibition with tofacitinib suppresses arthritic joint structural damage through decreased RANKL production. *Arthritis and rheumatism*. 2012; 64(11):3531–42. doi: [10.1002/art.34649](#) PMID: [22899318](#)
 37. Kim HY, Lee SW, Park SY, Baek SH, Lee CW, Hong KW, et al. Efficacy of concurrent administration of cilostazol and methotrexate in rheumatoid arthritis: pharmacologic and clinical significance. *Life sciences*. 2012; 91(7–8):250–7. doi: [10.1016/j.lfs.2012.07.003](#) PMID: [22820172](#)
 38. Ma Y, Wang X, Wu X, Wei X, Ma L, Zheng H, et al. (Z)-5-(4-methoxybenzylidene) thiazolidine-2, 4-dione ameliorates the adjuvant-induced arthritis via inhibiting the migration of macrophage and down-regulating the cytokine mRNA expression. *International immunopharmacology*. 2010; 10(11):1456–62. doi: [10.1016/j.intimp.2010.08.022](#) PMID: [20837171](#)
 39. Chen SY, Wu CL, Lai MD, Lin CC, Yo YT, Jou IM, et al. Amelioration of rat collagen-induced arthritis through CD4+ T cells apoptosis and synovial interleukin-17 reduction by indoleamine 2,3-dioxygenase gene therapy. *Human gene therapy*. 2011; 22(2):145–54. doi: [10.1089/hum.2009.217](#) PMID: [20825285](#)
 40. Le Goff B, Soltner E, Charrier C, Maugars Y, Redini F, Heymann D, et al. A combination of methotrexate and zoledronic acid prevents bone erosions and systemic bone mass loss in collagen induced arthritis. *Arthritis research & therapy*. 2009; 11(6):R185.
 41. Zhang J, Li CY, Xu MJ, Wu T, Chu JH, Liu SJ, et al. Oral bioavailability and gender-related pharmacokinetics of celastrol following administration of pure celastrol and its related tablets in rats. *Journal of ethnopharmacology*. 2012; 144(1):195–200. doi: [10.1016/j.jep.2012.09.005](#) PMID: [22982018](#)
 42. Stolina M, Bolon B, Middleton S, Dwyer D, Brown H, Duryea D, et al. The evolving systemic and local biomarker milieu at different stages of disease progression in rat adjuvant-induced arthritis. *J Clin Immunol*. 2009; 29(2):158–74. doi: [10.1007/s10875-008-9238-8](#) PMID: [18726678](#)
 43. da Silva JA, Fonseca JE, Graca L, Moita L, Carmo-Fonseca M. Reinnervation of post-arthritic joints in the rat. *Clinical and experimental rheumatology*. 1996; 14(1):43–51. PMID: [8697656](#)
 44. Tsubaki T, Arita N, Kawakami T, Shiratsuchi T, Yamamoto H, Takubo N, et al. Characterization of histopathology and gene-expression profiles of synovitis in early rheumatoid arthritis using targeted biopsy specimens. *Arthritis research & therapy*. 2005; 7(4):R825–36.
 45. Sims NA, Green JR, Glatt M, Schlicht S, Martin TJ, Gillespie MT, et al. Targeting osteoclasts with zoledronic acid prevents bone destruction in collagen-induced arthritis. *Arthritis and rheumatism*. 2004; 50(7):2338–46. PMID: [15248235](#)

46. Brauer R, Kittlick PD, Thoss K, Henzgen S. Different immunological mechanisms contribute to cartilage destruction in antigen-induced arthritis. *Experimental and toxicologic pathology: official journal of the Gesellschaft fur Toxikologische Pathologie*. 1994; 46(4–5):383–8.
47. Bendele AM, Chlipala ES, Scherrer J, Frazier J, Sennello G, Rich WJ, et al. Combination benefit of treatment with the cytokine inhibitors interleukin-1 receptor antagonist and PEGylated soluble tumor necrosis factor receptor type I in animal models of rheumatoid arthritis. *Arthritis and rheumatism*. 2000; 43(12):2648–59. PMID: [11145022](#)
48. Vidal B, Cascao R, Vale AC, Cavaleiro I, Vaz MF, Brito JA, et al. Arthritis induces early bone high turnover, structural degradation and mechanical weakness. *PloS one*. 2015; 10(1):e01117100. doi: [10.1371/journal.pone.01117100](#) PMID: [25617902](#)
49. Zhu X, Zhang J, Huo R, Lin J, Zhou Z, Sun Y, et al. Evaluation of the efficacy and safety of different Tripterygium preparations on collagen-induced arthritis in rats. *Journal of ethnopharmacology*. 2014; 158 Pt A:283–90. doi: [10.1016/j.jep.2014.10.021](#) PMID: [25456434](#)
50. Nawroth PP, Bank I, Handley D, Cassimeris J, Chess L, Stern D. Tumor necrosis factor/cachectin interacts with endothelial cell receptors to induce release of interleukin 1. *The Journal of experimental medicine*. 1986; 163(6):1363–75. PMID: [3011946](#)
51. Venkatesha SH, Yu H, Rajaiah R, Tong L, Moudgil KD. Celastrol-derived celastrol suppresses autoimmune arthritis by modulating antigen-induced cellular and humoral effector responses. *The Journal of biological chemistry*. 2011; 286(17):15138–46. doi: [10.1074/jbc.M111.226365](#) PMID: [21402700](#)
52. Astry B, Venkatesha SH, Laurence A, Christensen-Quick A, Garzino-Demo A, Frieman MB, et al. Celastrol, a Chinese herbal compound, controls autoimmune inflammation by altering the balance of pathogenic and regulatory T cells in the target organ. *Clinical immunology*. 2015; 157(2):228–38. doi: [10.1016/j.clim.2015.01.011](#) PMID: [25660987](#)
53. Idris AI, Krishnan M, Simic P, Landao-Bassonga E, Mollat P, Vukicevic S, et al. Small molecule inhibitors of I κ B kinase signaling inhibit osteoclast formation in vitro and prevent ovariectomy-induced bone loss in vivo. *FASEB journal: official publication of the Federation of American Societies for Experimental Biology*. 2010; 24(11):4545–55.
54. Gan K, Xu L, Feng X, Zhang Q, Wang F, Zhang M, et al. Celastrol attenuates bone erosion in collagen-Induced arthritis mice and inhibits osteoclast differentiation and function in RANKL-induced RAW264.7. *International immunopharmacology*. 2015; 24(2):239–46. doi: [10.1016/j.intimp.2014.12.012](#) PMID: [25529994](#)
55. Li G, Liu D, Zhang Y, Qian Y, Zhang H, Guo S, et al. Celastrol inhibits lipopolysaccharide-stimulated rheumatoid fibroblast-like synoviocyte invasion through suppression of TLR4/NF- κ B-mediated matrix metalloproteinase-9 expression. *PloS one*. 2013; 8(7):e68905. doi: [10.1371/journal.pone.0068905](#) PMID: [23861949](#)
56. Vieira-Sousa E, Gerlag DM, Tak PP. Synovial tissue response to treatment in rheumatoid arthritis. *The open rheumatology journal*. 2011; 5:115–22. doi: [10.2174/1874312901105010115](#) PMID: [22279510](#)
57. Fonseca JE, Edwards JC, Blades S, Goulding NJ. Macrophage subpopulations in rheumatoid synovium: reduced CD163 expression in CD4+ T lymphocyte-rich microenvironments. *Arthritis and rheumatism*. 2002; 46(5):1210–6. PMID: [12115225](#)
58. Li GQ, Zhang Y, Liu D, Qian YY, Zhang H, Guo SY, et al. Celastrol inhibits interleukin-17A-stimulated rheumatoid fibroblast-like synoviocyte migration and invasion through suppression of NF- κ B-mediated matrix metalloproteinase-9 expression. *International immunopharmacology*. 2012; 14(4):422–31. doi: [10.1016/j.intimp.2012.08.016](#) PMID: [22954486](#)
59. Suzuki M, Hashizume M, Yoshida H, Shiina M, Mihara M. IL-6 and IL-1 synergistically enhanced the production of MMPs from synovial cells by up-regulating IL-6 production and IL-1 receptor I expression. *Cytokine*. 2010; 51(2):178–83. doi: [10.1016/j.cyto.2010.03.017](#) PMID: [20403707](#)
60. Mihara M, Moriya Y, Kishimoto T, Ohsugi Y. Interleukin-6 (IL-6) induces the proliferation of synovial fibroblastic cells in the presence of soluble IL-6 receptor. *British journal of rheumatology*. 1995; 34(4):321–5. PMID: [7788145](#)
61. Romano M, Sironi M, Toniatti C, Polentarutti N, Fruscella P, Ghezzi P, et al. Role of IL-6 and its soluble receptor in induction of chemokines and leukocyte recruitment. *Immunity*. 1997; 6(3):315–25. PMID: [9075932](#)
62. Lee JH, Koo TH, Yoon H, Jung HS, Jin HZ, Lee K, et al. Inhibition of NF- κ B activation through targeting I κ B kinase by celastrol, a quinone methide triterpenoid. *Biochemical pharmacology*. 2006; 72(10):1311–21. PMID: [16984800](#)
63. Tas SW, Vervoordeldonk MJ, Hajji N, May MJ, Ghosh S, Tak PP. Local treatment with the selective I κ B kinase beta inhibitor NEMO-binding domain peptide ameliorates synovial inflammation. *Arthritis research & therapy*. 2006; 8(4):R86.

64. Vincenti MP, Coon CI, Brinckerhoff CE. Nuclear factor kappaB/p50 activates an element in the distal matrix metalloproteinase 1 promoter in interleukin-1beta-stimulated synovial fibroblasts. *Arthritis and rheumatism*. 1998; 41(11):1987–94. PMID: [9811054](#)
65. Yu H, Venkatesha SH, Moudgil KD. Microarray-based gene expression profiling reveals the mediators and pathways involved in the anti-arthritic activity of Celastrus-derived Celastrol. *International immunopharmacology*. 2012; 13(4):499–506. doi: [10.1016/j.intimp.2012.05.015](#) PMID: [22664142](#)

Arthritis Research & Therapy

Celastrol preserves bone structure and mechanics in arthritic rats

--Manuscript Draft--

Manuscript Number:					
Full Title:	Celastrol preserves bone structure and mechanics in arthritic rats				
Article Type:	Research article				
Section/Category:	Pharmacology and Therapeutics				
Funding Information:	<table border="1"><tr><td>Fundação para a Ciência e a Tecnologia (SFRH/BPD/92860/2013)</td><td>Ms. Rita Cascão</td></tr><tr><td>European Research Council (ERC-2014-CoG 647888-iPROTECTION)</td><td>Prof Luis F. Moita</td></tr></table>	Fundação para a Ciência e a Tecnologia (SFRH/BPD/92860/2013)	Ms. Rita Cascão	European Research Council (ERC-2014-CoG 647888-iPROTECTION)	Prof Luis F. Moita
Fundação para a Ciência e a Tecnologia (SFRH/BPD/92860/2013)	Ms. Rita Cascão				
European Research Council (ERC-2014-CoG 647888-iPROTECTION)	Prof Luis F. Moita				
Abstract:	<p>Background: Rheumatoid arthritis (RA) is characterized by chronic inflammation leading to articular bone and cartilage damage. Despite recent progress in RA management, adverse effects, lack of efficacy and economic barriers to treatment access still limit therapeutic success, which means that RA is currently an unremitting and debilitating disease. Therefore, safer and less expensive treatments that control inflammation and bone resorption are needed. We have previously shown that celastrol is a candidate for RA treatment based on its anti-inflammatory properties and ability to decrease synovial CD68 macrophages. Herein our goal was to evaluate the effect of celastrol in local and systemic bone loss. Methods: Celastrol was administered intraperitoneally at a dose of 1µg/g/day to female Wistar adjuvant-induced arthritis (AIA) rats. Rats were sacrificed after 22 days of disease progression and blood, femurs, tibias and paw samples were collected for the quantification of bone remodeling markers, 3-point bending test, micro-computed tomography analysis, and immunohistochemical evaluation. Results: We have observed that celastrol preserved articular structures and decreased the number of osteoclasts and osteoblasts present in arthritic joints. Moreover, celastrol reduced TRACP-5b, P1NP and CTX-II levels. Importantly, celastrol prevented bone loss and bone microarchitecture degradation, with an increase in trabecular bone volume fraction and endosteal bone quantity. Animals treated with celastrol also have less fragile bones, as depicted by an increase in maximum load and yield displacement. Conclusions: These results suggest that celastrol reduces both bone resorption and cartilage degradation, and preserves bone structure and mechanics.</p>				
Corresponding Author:	Rita Cascão, PhD Instituto de Medicina Molecular Lisbon, PORTUGAL				
Corresponding Author Secondary Information:					
Corresponding Author's Institution:	Instituto de Medicina Molecular				
Corresponding Author's Secondary Institution:					
First Author:	Rita Cascão, PhD				
First Author Secondary Information:					
Order of Authors:	Rita Cascão, PhD Bruno Vidal Mikko A. J. Finnilä Inês P. Lopes Simo Saarakkala Luis F. Moita João E. Fonseca				

Order of Authors Secondary Information:	
Opposed Reviewers:	

[Click here to view linked References](#)

Celastrol preserves bone structure and mechanics in arthritic rats

Rita Cascão^{1*}, Bruno Vidal^{1*}, Mikko A. J. Finnilä^{2,3}, Inês P. Lopes¹, Simo Saarakkala^{2,4,5},
Luis F. Moita^{6,a}, João E. Fonseca^{1,7,a}

¹ Instituto de Medicina Molecular, Faculdade de Medicina, Universidade de Lisboa, Lisbon, Portugal

² Research Unit of Medical Imaging, Physics and Technology, Faculty of Medicine, University of Oulu, Oulu, Finland

³ Department of Applied Physics, University of Eastern Finland, Kuopio, Finland

⁴ Medical Research Center Oulu, Oulu University Hospital and University of Oulu, Oulu, Finland

⁵ Department of Diagnostic Radiology, Oulu University Hospital, Oulu, Finland

⁶ Instituto Gulbenkian de Ciência, Oeiras, Portugal

⁷ Rheumatology Department, Centro Hospitalar de Lisboa Norte, EPE, Hospital de Santa Maria, Lisbon Academic Medical Centre, Lisbon, Portugal

* Contributed equally

^a Joint senior authors

E-mail address of all authors:

Rita Cascão - ritacacao@medicina.ulisboa.pt

Bruno Vidal - bvidal@medicina.ulisboa.pt

Mikko A. J. Finnilä - mikko.finnila@oulu.fi

Inês P. Lopes - ilopes@medicina.ulisboa.pt

Simo Saarakkala - simo.saarakkala@oulu.fi

26 Luis F. Moita - lmoita@igc.gulbenkian.pt

27 João E. Fonseca - jecfonseca@gmail.com

28

29 **Corresponding author:**

30 Full name – Rita Cascão

31 Address – Instituto de Medicina Molecular, Edifício Egas Moniz, Faculdade de Medicina da

32 Universidade de Lisboa, Av. Professor Egas Moniz, Lisboa, 1649-028, Portugal

33 E-mail – ritacascão@medicina.ulisboa.pt

34 Phone number – (+351) 217 999 411

35

36

37 **ABSTRACT**

38 **Background:** Rheumatoid arthritis (RA) is characterized by chronic inflammation leading to
39 articular bone and cartilage damage. Despite recent progress in RA management, adverse
40 effects, lack of efficacy and economic barriers to treatment access still limit therapeutic
41 success, which means that RA is currently an unremitting and debilitating disease. Therefore,
42 safer and less expensive treatments that control inflammation and bone resorption are needed.
43 We have previously shown that celastrol is a candidate for RA treatment based on its anti-
44 inflammatory properties and ability to decrease synovial CD68 macrophages. Herein our goal
45 was to evaluate the effect of celastrol in local and systemic bone loss. **Methods:** Celastrol was
46 administered intraperitoneally at a dose of 1µg/g/day to female Wistar adjuvant-induced
47 arthritis (AIA) rats. Rats were sacrificed after 22 days of disease progression and blood,
48 femurs, tibias and paw samples were collected for the quantification of bone remodeling
49 markers, 3-point bending test, micro-computed tomography analysis, and
50 immunohistochemical evaluation. **Results:** We have observed that celastrol preserved

1
2
3
4
5
6
7
8
9
10
11
12
13
14
15
16
17
18
19
20
21
22
23
24
25
26
27
28
29
30
31
32
33
34
35
36
37
38
39
40
41
42
43
44
45
46
47
48
49
50
51 articular structures and decreased the number of osteoclasts and osteoblasts present in arthritic
52 joints. Moreover, celastrol reduced TRACP-5b, P1NP and CTX-II levels. Importantly,
53 celastrol prevented bone loss and bone microarchitecture degradation, with an increase in
54 trabecular bone volume fraction and endosteal bone quantity. Animals treated with celastrol
55 also have less fragile bones, as depicted by an increase in maximum load and yield
56 displacement. **Conclusions:** These results suggest that celastrol reduces both bone resorption
57 and cartilage degradation, and preserves bone structure and mechanics.

58
59 **KEYWORDS:** Rheumatoid arthritis, Adjuvant-induced arthritis, Celastrol, Inflammation,
60 Bone loss

61 62 63 **BACKGROUND**

64 Rheumatoid arthritis (RA) is a chronic immune-mediated inflammatory disease with an
65 estimated worldwide prevalence of 1%. This disease has a great impact on both individuals
66 and society. RA patients are ten times more likely to be disabled, have three times more direct
67 healthcare costs and are also two times more likely to require hospitalization than healthy
68 individuals[1, 2]. RA is characterized by chronic edema and inflammation of the synovial
69 tissue that lines joints. As disease progresses, cartilage and bone are damaged leading to
70 articular destruction[3]. This periarticular and systemic bone loss leads to an increased risk of
71 fracture in RA patients[4, 5]. Bone loss in RA results from an imbalance between the
72 osteoblastic synthesis and osteoclastic degradation of bone, with bone resorption dominating
73 over bone formation leading to systemic osteopenia[6].

74 Over the past 2 decades, more effective therapies for RA have been developed, but they still
75 have issues related with safety and production costs. In addition, only around 30% of the

1
2
3
4
5
6
7
8
9
10
11
12
13
14
15
16
17
18
19
20
21
22
23
24
25
26
27
28
29
30
31
32
33
34
35
36
37
38
39
40
41
42
43
44
45
46
47
48
49
50
51
52
53
54
55
56
57
58
59
60
61
62
63
64
65

76 patients reach remission, leaving most of the individuals affected by a chronic unremitting
77 destructive disease, with the need for nonsteroidal anti-inflammatory drugs and
78 corticosteroids for symptoms control[7]. Moreover, current treatment approaches primarily
79 target inflammation with varying success in limiting the progression of bone damage[8].
80 Therefore, new therapies targeting both inflammatory processes and bone resorption, with a
81 good safety profile and low production costs are still an unmet medical need in the field of
82 RA.

83 We have previously reported increased levels of IL-1 β in very recent onset arthritis and in the
84 synovial fluid of established RA patients[9]. This may be explained by the activation of
85 caspase-1, responsible for the processing of pro-IL-1 β , which we have also observed to be
86 increased since early RA[10]. Through an *in vitro* drug screening using the THP-1
87 macrophagic cell line, we have identified compounds that decrease the production of IL-1 β
88 together with a reduction in another central pro-inflammatory cytokine of RA
89 physiopathology, TNF. Among them, celastrol was a promising therapeutic candidate for
90 arthritis, due to its ability to downregulate the production of IL-1 β and TNF, by inhibiting
91 both the activation of caspase-1 and NF-kB[11]. Celastrol is a pentacyclic-triterpene extracted
92 from a plant used in traditional Chinese medicine, the *Trypterigium wilfordii* Hook. *In vivo*,
93 we have recently described that celastrol has significant anti-inflammatory and anti-
94 proliferative properties, with a decrease in the overall synovial inflammatory cellularity and,
95 most importantly, in the number of sublining CD68 positive macrophages, a biomarker of
96 drug efficacy in RA[11, 12]. In this study we have now hypothesized that celastrol is able to
97 control, not only inflammation, but also focal and systemic bone resorption that occurs in
98 arthritis.

99 Our aim in the herein study was to evaluate the ability of celastrol to counteract bone loss in
100 the adjuvant-induced arthritis (AIA) rat model. The AIA rat model is the most widely used

101 animal model for the evaluation of experimental compounds for RA treatment[13, 14]. We
102 have recently documented that this is also an adequate model to study the impact of new
103 compounds on bone[15]. In this work, celastrol administration was introduced therapeutically
104 both at the early (preclinical stage) and late (clinical stage peak) phases of arthritis
105 development to more closely model the clinical practice, with a complete analysis of bone
106 quality.

107

108 **MATERIALS AND METHODS**

109 **Animals**

110 Eight-week-old female Wistar AIA rats weighing 230-250gr were purchased from Charles
111 River Laboratories International (Massachusetts, USA). AIA rats were maintained in specific
112 pathogen free (SPF) facilities, randomly housed per groups under standard laboratory
113 conditions (at 20-22°C under 10-hour light/14-hour dark), and given free access to food
114 (RM3, SDS diets, UK) and water (ultrapure). In addition, to minimize animal discomfort it
115 was used paper shavings as bedding material in Double Decker GR1800 cages (Techniplast,
116 UK) with 5 animals each. In accordance with Directive 2010/63/EU, all animal procedures
117 were approved by the institutional animal welfare body (ORBEA-iMM) and licensed by the
118 Portuguese competent authority (DGAV – Direcção Geral de Alimentação e Veterinária).
119 Human end-points were established and animals were sacrificed when presenting the
120 maximum inflammatory score (0-3)[16] in more than 2 paws or when presenting more than
121 20% of body weight loss.

122

123 **Celastrol treatment**

124 The dose of celastrol (1µg/g/day) used in this study was based on that used in our previous
125 study[11] and in other studies[17]. Also, we have already reported that this dose is effective in

126 suppressing synovial inflammation in the AIA rat model, with no evidence of drug-induced
127 toxicity[12]. Celastrol (Sigma, Missouri, USA) stock solution of 100mg/ml in DMSO was
128 dissolved in normal saline solution and injected intraperitoneally in the early treatment group
129 of AIA rats since the 4th day of disease induction (N=15) and in the late treatment group
130 since the 11th day of disease induction (N=15), and was maintained until day 22. Studies
131 using the AIA model are generally completed at this time point due to a plateau effect of
132 inflammatory manifestations. A group of healthy non-arthritis and arthritis untreated female
133 age-matched Wistar rats sacrificed at day 4 (baseline for the celastrol early-treated group, at
134 preclinical stage, N=5-13), day 11 (baseline for the celastrol late-treated group, at acute
135 clinical stage, N=5-17) and day 22 after disease induction (chronic clinical stage) were used
136 as controls in all experiments. The sample size in each group was calculated using free sample
137 size calculating G*Power version 3.1.9.2 software (Type of power analysis: a priori; α err
138 prob: 0.05; power (1- β err prob): 0.95; Effect size d: 1.526112; Actual power: 0.9576654). At
139 the preclinical AIA progression stage evidence of inflammation or bone erosions is still
140 lacking in the contralateral hind paw and fore paws. Hind paw swelling, inflammation and
141 joint erosions steadily progress during acute clinical stage and reach a plateau in the chronic
142 stage[18]. Rats were sacrificed by CO₂ narcosis and blood, femurs, tibias and paw samples
143 were collected.

144

145 **Immunohistochemical staining of cathepsin k and osteocalcin positive cells in hind paws**

146 Left hind paw samples collected at the time of sacrifice were fixed immediately in 10%
147 neutral buffered formalin solution and then decalcified in 10% formic acid. Samples were
148 next dehydrated and embedded in paraffin, serially sectioned at a thickness of 5 μ m using a
149 microtome, and mounted on microscope slides. Immunolocalization of osteoclasts and
150 osteoblasts was performed by staining with cathepsin k (osteoclast marker; mature osteoclast

151 enzyme. Biorbyt, Cambridge, UK) and osteocalcin (osteoblast marker; indicator of
152 osteoblastic activity. Abcam, Cambridge, UK) primary antibodies followed by EnVision+
153 (Dako, Glostrup, Denmark). Color was developed in solution containing diaminobenzadine-
154 tetrahydrochloride (DAB, Sigma, Missouri, USA), 0.5% H₂O₂ in phosphate-buffered saline
155 buffer (pH 7.6). Slides were counterstained with hematoxylin and mounted.
156 Immunohistochemical evaluation of rat joints was performed in a blinded fashion using a
157 semi-quantitative score of 0-3 (0 — 0-25% staining; 1 — 25-50% staining; 2 — 50-75%
158 staining; 3 — more than 75% staining)[19]. Slides were analyzed using a Leica DM2500
159 microscope (Leica Microsystems, Wetzlar, Germany).

160

161 **Serum biochemical measurement of bone and cartilage turnover markers**

162 Bone and cartilage turnover were analyzed by quantifying the levels of TRACP-5b (Tartrate-
163 resistant acid phosphatase 5b), P1NP (procollagen type 1 amino-terminal propeptide) and
164 CTX-II (C-terminal crosslinked telopeptide of type II collagen) in rat serum using ELISA
165 (Immunodiagnostic System, Boldon, UK). All of the commercial assays were performed
166 according to the manufacturers' instructions and standard curves were generated using
167 supplied reference concentrations. Samples were measured using a plate reader Infinite M200
168 (Tecan, Mannedorf, Switzerland).

169

170 **Micro-computed tomography (micro-CT) analysis**

171 Structural properties of the trabecular and cortical tibiae were determined with a high-
172 resolution micro-CT system (SkyScan 1272, Bruker micro-CT, Kontich, Belgium). Moist
173 bones were wrapped in parafilm and covered with dental wax to prevent drying and
174 movement during the scanning. X-ray tube voltage was set to 50kV and the beam was filtered
175 with 0.5mm Aluminum filter. Sample position and camera settings were tuned to provide

176 3.0 μ m isotropic pixel size and projection images were collected every 0.2°. Density
177 calibration was performed against hydroxyapatite phantoms with densities of 250mg/cm³ and
178 750mg/cm³. Image reconstruction was done with NRecon software (v1.6.9.8; Bruker micro-
179 CT, Kontich, Belgium) and appropriate corrections were applied to reduce beam hardening
180 and ring artifacts. Trabecular bone was manually segmented from cortical bone, and
181 trabecular bone parameters were analyzed over 1400 slices starting 200 slices distal from
182 growth plate. Cortical bone parameters were analyzed over 300 slices starting 1800 slices
183 distal from growth plate.

184 Analyses were performed in agreement with guidelines for assessment of bone microstructure
185 in rodents using micro-CT[20]. Trabecular bone morphology was analyzed by applying global
186 threshold and despeckling to provide binary image for 3D analyzes. Cortical bone ROI was
187 refined with ROI-shrink wrap operation, which also provided cortical bone shape for 2D
188 morphological analysis. This was followed by segmentation of blood vessels using adaptive
189 thresholding. Blood vessels (porosity) were analyzed using 3D morphological analyses.

191 **3-point bending biomechanical test**

192 In order to investigate bone strength after celastrol treatment, femurs were subjected to a 3-
193 point bending test in a universal testing machine (Instron 3366, Instron Corp., Massachusetts,
194 USA) with a load-cell of 500N. Femurs were placed horizontally anterior side upwards on a
195 support with span length of 5mm. The load was applied with a constant speed of 0.005mm/s
196 until a failure occurred. Stiffness was analyzed by fitting first-degree polynomial function to
197 the linear part of recorded load deformation data. The breaking point was defined when force
198 reached a maximum value and corresponding deformation and absorbed energy were
199 analyzed.

200

201 **Statistical analysis**

1
2 202 Statistical differences were determined with non-parametric Mann–Whitney tests using
3
4 203 GraphPad Prism (GraphPad, California, USA). Differences were considered statistically
5
6
7 204 significant for $p < 0.05$. Data are presented as median with interquartile range. The primary
8
9 205 outcome of this study was to prevent the structural and mechanical damage of bone induced
10
11 206 by inflammation, and the secondary outcome was to treat the structural and mechanical
12
13 207 deterioration of bone in a chronic phase of arthritis development in the AIA rat model.
14
15
16
17 208

18
19 209 **RESULTS**

20
21
22 210 **Celastrol decreases the number of osteoclasts and osteoblasts present in arthritic joints**

23
24 211 Previously, we have observed that celastrol administration significantly reduced disease
25
26 212 severity and suppressed joint bone erosions in arthritic rats, with no observed adverse
27
28 213 effects[12]. At baseline celastrol early-treated group had a mean inflammatory score of
29
30 214 1.5 ± 0.7 and celastrol late-treated group had a mean inflammatory score of 3.9 ± 2.0 , with no
31
32 215 differences in body weight comparing to untreated arthritic animals. Arthritic rats showed
33
34 216 enhanced numbers of osteoclasts (cathepsin k+ cells) in the hind paw ($p < 0.0001$ vs healthy
35
36 217 controls, Fig 1). Importantly, celastrol administration significantly lowered the number of
37
38 218 osteoclasts to levels similar to healthy controls ($p < 0.0001$ in both treatment groups vs arthritic
39
40 219 rats). Arthritic rats also showed increased numbers of osteoblasts (osteocalcin+ cells) in the
41
42 220 hind paw ($p < 0.0001$ vs healthy controls, Fig 1). Notably, celastrol administration significantly
43
44 221 reduced the number of osteoblasts ($p < 0.0001$ and $p = 0.0003$ in early and late-treated animals
45
46 222 vs arthritic rats, respectively).
47
48
49
50
51
52

53 223

54
55 224 **Celastrol reduces arthritis-induced bone resorption and cartilage degradation**
56
57
58
59
60
61
62
63
64
65

225 To further elucidate the protective effect of celastrol on inflammation-mediated articular joint
1
2 226 damage, bone and cartilage turnover markers were quantified in serum samples. The levels of
3
4
5 227 serum TRACP-5b, P1NP and CTX-II of healthy, arthritic and celastrol-treated rats are shown
6
7 228 in Fig 2. In the arthritic group, there was a marked increase of TRACP-5b after 4 days of
8
9
10 229 disease induction ($p=0.0267$ vs healthy controls and $p=0.0089$ vs arthritic rats after 22 days of
11
12 230 disease induction) with a gradual decrease throughout disease progression (Fig 2A), as also
13
14 231 previously described by Stolina et al[21, 22]. In addition, there was a significant increase in
15
16 232 serum P1NP ($p=0.0034$, Fig 2B) and CTX-II ($p=0.0082$, Fig 2C), as a consequence of the
17
18
19 233 high bone turnover and cartilage degradation. Importantly, both in celastrol early and late-
20
21
22 234 treated rats there was a significant reduction in TRACP-5b levels comparing with arthritic rats
23
24 235 ($p=0.0004$ and $p=0.0001$, respectively) and with treatment baselines ($p=0.0014$ vs arthritic
25
26 236 rats at day 4 and $p<0.0001$ vs arthritic rats at day 11, respectively), suggesting a decrease in
27
28
29 237 bone resorption. In addition, both treatment groups showed a significant drop in P1NP levels
30
31 238 ($p=0.0069$ in early-treated and $p=0.0135$ in late-treated rats vs arthritic animals). Finally, the
32
33
34 239 decrease in CTX-II ($p=0.0149$ in celastrol early-treated vs arthritic rats) revealed that
35
36 240 treatment is also effective in protecting cartilage integrity. Of note, although a strong
37
38
39 241 tendency towards a decrease in CTX-II was observed in celastrol late-treated rats, it did not
40
41 242 reach statistical significance. These results suggest that there is a reduction both in bone and
42
43
44 243 cartilage degradation in celastrol treated rats.

45
46 244

47 48 245 **Celastrol prevents bone loss and bone microarchitecture degradation in arthritis**

49
50
51 246 The effect of celastrol on inflammation-induced systemic bone loss was assessed by micro-
52
53 247 CT analysis of tibial bones (Fig 3). Representative reconstructions of micro-CT analysis of rat
54
55
56 248 tibiae are shown in Fig 3A. Arthritis progression led to significant reductions in trabecular
57
58 249 bone mass and in trabecular bone volume fraction and number ($p<0.0001$ vs healthy controls,
59
60

250 Fig 3B), and an increase in trabecular separation and porosity ($p < 0.0001$ vs healthy controls,
251 Fig 3B). Also the structural integrity declines with arthritis, as trabeculae have fewer
252 connections and have rather rod-like appearance, indicated by increased structure model
253 index. An 18-day course of therapy with celestrol, starting 4 days after disease induction,
254 preserved bone mass and integrity, with a significant increase in trabecular bone volume
255 fraction (+16.6%, $p = 0.02$) and number (+20.3%, $p = 0.0047$) as well as with a decrease in
256 trabecular separation (-12.9%, $p = 0.0023$) and porosity (-4.5%, $p = 0.0148$) in comparison to
257 arthritic rats. Importantly, celestrol early-treated rats also showed a significant reduction in
258 trabecular separation even when comparing with their baseline (-22.1%, $p = 0.0101$ vs arthritic
259 rats sacrificed at day 4 after disease induction). Celestrol treatment also preserved structural
260 integrity, as trabeculae have more connections and have less rod-like appearance ($p = 0.0462$
261 and $p = 0.0047$ in early-treated vs arthritic rats, respectively). Additionally, micro-CT analysis
262 revealed that trabecular thickness is reduced in arthritic rats ($p < 0.0001$ vs healthy controls),
263 but there was no effect after celestrol treatment. As depicted in Fig 3B, no effect in trabecular
264 bone microarchitecture was observed in celestrol late-treated group, except for a significant
265 reduction in trabecular separation (-10.6%, $p = 0.0325$ vs arthritis rats).

266 A similar pattern can be observed for cortical bone. Arthritis decreases cortical bone area (-
267 10.8%, $p < 0.0001$) and thickness (-11%, $p < 0.0001$) in arthritic tibias compared to healthy
268 controls. Although overall cortical porosity is similar between arthritic and healthy controls,
269 blood vessel channels are significantly wider in arthritic bones compared to controls
270 ($p = 0.0146$).

271 As shown in Fig 3C, both treatment approaches affect cortical bone by inhibiting bone
272 resorption as shown by significantly smaller endosteal volume (-14.5%, $p = 0.0026$ in early-
273 treated and -20.1%, $p = 0.0017$ in late-treated celestrol rats vs arthritic animals). Also both
274 groups have decreased cortical porosity (-18.2%, $p = 0.0161$ in early-treated and -30.1%,

1
2
3
4
5
6
7
8
9
10
11
12
13
14
15
16
17
18
19
20
21
22
23
24
25
26
27
28
29
30
31
32
33
34
35
36
37
38
39
40
41
42
43
44
45
46
47
48
49
50
51
52
53
54
55
56
57
58
59
60
61
62
63
64
65

275 p=0.0001 in late-treated rats) due to a decrease in the number (-17.1%, p=0.0211 in early-
276 treated and -29.7%, p=0.0004 in late-treated animals) and thickness (-3.1%, p=0.0425 in
277 early-treated and -4.8%, p=0.0026 in late-treated rats) of blood vessel channels and thus
278 increasing their separation (+7.9%, p=0.180 in early-treated and +14.6%, p=0.0037 in late-
279 treated group) compared to arthritic rats. Of note, both treatment groups significantly showed
280 an improvement in these cortical parameters when compared with their respective baselines
281 (p<0.05).

282 These data show that treatment with celestrol significantly prevented the marked
283 inflammation-induced bone loss and microarchitecture degradation of AIA rats as pointed out
284 by the improved trabecular and cortical parameters.

286 **Celestrol improves bone mechanical properties in arthritic rats**

287 Bone strength of rat femurs was evaluated using the 3-point bending test (Fig 4). There was a
288 significant reduction in the maximal load that arthritic femurs were able to resist before
289 breaking as compared to healthy controls (-13.6%, p=0.0017). Early administration of
290 celestrol restored bone strength and maximal breaking load was increased by 9.4%, when
291 comparing to arthritic group (p=0.0434, Fig 4A). Late celestrol administration was
292 insufficient to correct bone damage and these animals showed decreased maximal
293 deformation and capability to absorb energy, which were significantly reduced by -14.7%
294 (p=0.0298, Fig 4B) and -18.8% (p=0.0377, Fig 4C), respectively. Additionally, arthritic rats
295 have a reduction in the yield displacement (-28,3%, p=0.0192 in arthritic rats *vs* healthy
296 controls). In contrast, in celestrol early-treated rats there was an increase in the elastic
297 properties of bone with an augment in yield displacement (+20.7%, p=0.0498 in celestrol
298 early-treated *vs* arthritic rats), meaning that a higher elastic deformation of the femur was
299 arising before the first micro fractures occur (Fig 4D). In addition, mechanical results revealed

1
2 300 that there was a significant reduction in the load (Fig 4E) and elastic energy at yield point (Fig
3 301 4F) in arthritic rats comparing with healthy controls (p=0.0229 and p=0.0161, respectively),
4 302 only partially corrected in arthritic rats under celastrol treatment since the early phase of the
5 303 disease (+7.4% and +34.8% than arthritic rats, respectively). Celastrol early-treated rats also
6
7 304 showed a significant reduction in bone stiffness (Fig 4G) in comparison to arthritic rats and
8
9 305 celastrol late-treated rats (-7.5%, p=0.0177 and -17.8%, p=0.0016, respectively). However, no
10
11 306 difference was observed between healthy controls and arthritic rats in this mechanical
12
13 307 parameter.
14
15
16
17
18
19
20
21

22 308 **DISCUSSION**

23
24 309 In this study the AIA rat model was used to assess the bone protective properties of celastrol
25
26 310 *in vivo*. Here we demonstrated that celastrol treatment exerts a therapeutic effect on arthritic
27
28 311 joint damage, with an efficacy not only limited to anti-inflammatory properties[11, 12], but
29
30 312 also with a substantial inhibition of cartilage and focal bone destruction and reduction of
31
32 313 systemic bone degradation, translated by the preservation of its structure and strength.
33
34 314

35
36 315 In the present work, we have shown that celastrol decreases the number of joint tissue
37
38 316 osteoclasts and osteoblasts. Several cell populations residing in the inflamed synovial
39
40 317 membrane provide signals that stimulate osteoclast formation and facilitate bone resorption.

41
42 318 We have previously shown that celastrol significantly reduces the number of synovial B and T
43
44 319 cells as well as fibroblasts and macrophages[12]. Macrophages do not only mediate synovial
45
46 320 inflammation, but are also critical in osteoclast differentiation[23]. Most importantly, we have
47
48 321 previously shown that celastrol inhibits NF-kB activation *in vitro*[11]. NF-kB activation is
49
50 322 also crucial for osteoclast formation and function, and is upstream activated by the
51
52 323 engagement of RANKL with RANK. Recent *in vitro* findings showed that celastrol inhibits
53
54 324 the recruitment of TGF β -activated kinase (TAK)1, an upstream receptor-associated factor of
55
56
57
58
59
60
61
62
63
64
65

1 325 IκB kinase (IKK), to RANK and TNF receptors[24], inhibiting both RANKL-induced NF-κB
2 326 activation and the osteoblast-related ERK signaling[25]. Work from the Moudgil laboratory
3
4 327 has shown, *in vitro*, that celastrol reduces other osteoclastic mediators besides RANKL, such
5
6
7 328 as granulocyte-macrophage colony-stimulating factor (GM-CSF), insulin-like growth factor
8
9 329 (IGF) and osteopontin (OPN), suggesting a shift in bone remodeling in favor of an
10
11 330 antiosteoclastic activity[17]. Finally, also in line with our data, it has been reported in bone
12
13 331 metastasis and ovariectomy-induced bone loss models that celastrol reduces osteoclast
14
15 332 numbers and bone loss and preserves its trabecular architecture, together with an inhibitory
16
17 333 effect on osteoblasts viability and function[25, 26]. Likewise, the gold standard and first-line
18
19 334 drug in RA, methotrexate, also slows down articular damage in RA patients by inhibiting
20
21 335 osteoclastogenesis[27] together with a reduction in osteoblasts proliferation[28].

22 336 The reduction in osteoclast and osteoblast numbers is consistent with the reduction in serum
23
24 337 levels of TRACP-5b and P1NP observed in arthritic rats treated with celastrol, suggesting a
25
26 338 reduction in the accelerated bone turnover induced by arthritis.

27 339 We have also quantified serum CTX-II. This is a major component of articular cartilage[29]
28
29 340 with a significant correlation between serum levels and the severity of cartilage damage[30,
30
31 341 31]. Celastrol treatment reduced serum CTX-II concentration, suggesting a chondroprotective
32
33 342 effect, which was confirmed by histological observations. This protective effect on cartilage
34
35 343 could be explained by the inhibition of heat shock protein 90β and of NF-κB activation[32],
36
37 344 combined with the control of inflammation.

38 345 Trabecular bone microarchitecture is an important feature of bone quality[33]. Micro-CT
39
40 346 analysis revealed arthritis-induced reduction of trabecular bone volume fraction and
41
42 347 trabecular number as well as increase in trabecular separation and in the occurrence of rod-
43
44 348 like shape trabeculae. All these are associated with decreased strength of trabecular bone.
45
46 349 Notably, celastrol treatment improved all these trabecular bone parameters and mitigated bone
47
48
49
50
51
52
53
54
55
56
57
58
59
60
61
62
63
64
65

1
2
3
4
5
6
7
8
9
10
11
12
13
14
15
16
17
18
19
20
21
22
23
24
25
26
27
28
29
30
31
32
33
34
35
36
37
38
39
40
41
42
43
44
45
46
47
48
49
50
51
52
53
54
55
56
57
58
59
60
61
62
63
64
65

350 loss. Consistent with this, our results showed that celestrol administration prevented the loss
351 of bone mechanical compliance of femurs in arthritic rats by increasing maximum load and
352 yield displacement. In addition, celestrol treated arthritic animals also showed positive effects
353 on cortical bone morphology, which is a major factor defining the mechanical properties of
354 bone. In fact, celestrol-treated rats had decreased cortical porosity and increased endosteal
355 bone quantity. Overall, these results suggest that early celestrol treatment could prevent bone
356 fragility in RA patients.

357 Despite celestrol efficacy there are still some differences between treated and healthy
358 phenotypes, therefore it is reasonable to speculate that the extent of bone protection could be
359 even further improved by optimized doses of celestrol or by augmenting treatment duration,
360 which is not possible when using the AIA model.

361

362 **CONCLUSIONS**

363 To sum up, celestrol significantly halted cartilage and bone joint resorption and preserved
364 systemic bone structure and strength, and thus may serve as a useful therapeutic agent for the
365 treatment of inflammation-induced bone damage. Moreover, our study also suggests that an
366 early treatment initiation is crucial to effectively prevent bone destruction in RA patients.

367

368 **LIST OF ABBREVIATIONS**

369 RA - Rheumatoid arthritis

370 AIA - Adjuvant-induced arthritis

371 SPF - Specific pathogen free

372 DAB - Diaminobenzadine-tetrahydrochloride

373 TRACP-5b - Tartrate-resistant acid phosphatase 5b

374 P1NP - Procollagen type 1 amino-terminal propeptide

375 CTX-II - C-terminal crosslinked telopeptide of type II collagen
1
2 376 micro-CT - Micro-computed tomography
3
4 377 TAK-1 - TGF β -activated kinase
5
6
7 378 IKK - I κ B kinase
8
9 379 RANK - Receptor Activator of Nuclear Factor κ B
10
11 380 TNF - Tumor necrosis factor
12
13 381 NF- κ B - Nuclear factor kappa-light-chain-enhancer of activated B cells
14
15
16 382 ERK - Extracellular signal-regulated kinases
17
18 383 GM-CSF - Granulocyte-macrophage colony-stimulating factor
19
20
21 384 IGF - Insulin-like growth factor
22
23
24 385 OPN - osteopontin
25
26

386

387 **DECLARATIONS**

388 **Ethical approval**

389 All animal procedures were approved by the institutional animal welfare body (ORBEA-
390 iMM) and licensed by the Portuguese competent authority (DGAV – Direcção Geral de
391 Alimentação e Veterinária).

392

393 **Consent for publication**

394 Not applicable.

395

396 **Availability of data and material**

397 The datasets generated and analyzed during study are included in this published article. If
398 additional information is required, supplementary datasets can be available from the
399 corresponding author on a reasonable request.

400

1

2 401 **Competing interests**

3

4 402 The authors have declared that no competing interests exist.

5

6 403

7

8 404 **Funding**

9

10 405 RC was supported by a fellowship from Fundação para a Ciência e a Tecnologia (FCT,
11
12 SFRH/BPD/92860/2013). LFM is an FCT Investigator and receives financial support from the
13
14 European Research Council (ERC-2014-CoG 647888-iPROTECTION). This work was also
15
16 supported by a grant from Sociedade Portuguesa de Reumatologia. The funders had no role in
17
18 study design, data collection and analysis, decision to publish, or preparation of the
19
20 manuscript.
21
22 409
23
24 410

25

26 411

27

28 412 **Authors contributions**

29

30 413 Study design: RC, LFM and JEF. Study conduct: RC. Data collection: RC, BV, MAJF and
31
32 IPL. Data analysis: RC, BV and MAJF. Data interpretation: RC, BV and MAJF. Drafting
33
34 manuscript: RC and MAJF. Revising manuscript content: RC, BV, MAJF, IPL, SS, LFM and
35
36 JEF. Approving final version of manuscript: RC, BV, MAJF, IPL, SS, LFM and JEF. RC,
37
38 BV, MAJF, IPL, SS, LFM and JEF take responsibility for the integrity of the data analysis.
39
40
41 417

42

43 418

44

45 419 **Acknowledgment**

46

47 420 The authors would like to acknowledge the Histology and Comparative Pathology Laboratory
48
49 from Instituto de Medicina Molecular for technical assistance.
50
51 421

52

53 422

54

55 423 **REFERENCES**

56

57

58

59

60

61

62

63

64

- 424 1. Birnbaum HG, Barton M, Greenberg PE, *et al.* Direct and indirect costs of rheumatoid arthritis
1 425 to an employer. *J Occup Environ Med* 2000;42:588-96.
- 2 426 2. American College of Rheumatology Subcommittee on Rheumatoid Arthritis G. Guidelines for
3 427 the management of rheumatoid arthritis: 2002 Update. *Arthritis Rheum* 2002;46:328-46.
- 4 428 3. Noss EH, Brenner MB. The role and therapeutic implications of fibroblast-like synoviocytes in
5 429 inflammation and cartilage erosion in rheumatoid arthritis. *Immunol Rev* 2008;223:252-70.
- 7 430 4. Dequeker J, Geusens P. Osteoporosis and arthritis. *Ann Rheum Dis* 1990;49:276-80.
- 8 431 5. Schett G, Saag KG, Bijlsma JW. From bone biology to clinical outcome: state of the art and
9 432 future perspectives. *Ann Rheum Dis* 2010;69:1415-9.
- 10 433 6. Schett G, Gravallese E. Bone erosion in rheumatoid arthritis: mechanisms, diagnosis and
11 434 treatment. *Nat Rev Rheumatol* 2012;8:656-64.
- 13 435 7. Agarwal SK. Core management principles in rheumatoid arthritis to help guide managed care
14 436 professionals. *J Manag Care Pharm* 2011;17:S03-8.
- 15 437 8. Dimitroulas T, Nikas SN, Trontzas P, Kitas GD. Biologic therapies and systemic bone loss in
16 438 rheumatoid arthritis. *Autoimmun Rev* 2013;12:958-66.
- 17 439 9. Cascao R, Moura RA, Perpetuo I, *et al.* Identification of a cytokine network sustaining
19 440 neutrophil and Th17 activation in untreated early rheumatoid arthritis. *Arthritis Res Ther*
20 441 2010;12:R196.
- 21 442 10. Cascao R, Polido-Pereira J, Canhao H, *et al.* Caspase-1 is active since the early phase of
22 443 rheumatoid arthritis. *Clin Exp Rheumatol* 2012;30:144.
- 23 444 11. Cascao R, Vidal B, Raquel H, *et al.* Effective treatment of rat adjuvant-induced arthritis by
24 445 celastrol. *Autoimmun Rev* 2012;11:856-62.
- 26 446 12. Cascao R, Vidal B, Lopes IP, *et al.* Decrease of CD68 Synovial Macrophages in Celastrol
27 447 Treated Arthritic Rats. *PLoS One* 2015;10:e0142448.
- 28 448 13. Noguchi M, Kimoto A, Kobayashi S, *et al.* Effect of celecoxib, a cyclooxygenase-2 inhibitor, on
29 449 the pathophysiology of adjuvant arthritis in rat. *Eur J Pharmacol* 2005;513:229-35.
- 30 450 14. Toh K, Kukita T, Wu Z, *et al.* Possible involvement of MIP-1alpha in the recruitment of
32 451 osteoclast progenitors to the distal tibia in rats with adjuvant-induced arthritis. *Lab Invest*
33 452 2004;84:1092-102.
- 34 453 15. Vidal B, Cascao R, Vale AC, *et al.* Arthritis induces early bone high turnover, structural
35 454 degradation and mechanical weakness. *PLoS One* 2015;10:e0117100.
- 36 455 16. da Silva JA, Fonseca JE, Graca L, Moita L, Carmo-Fonseca M. Reinnervation of post-arthritic
37 456 joints in the rat. *Clin Exp Rheumatol* 1996;14:43-51.
- 39 457 17. Nanjundiah SM, Venkatesha SH, Yu H, *et al.* Celastrol and its bioactive celastrol protect
40 458 against bone damage in autoimmune arthritis by modulating osteoimmune cross-talk. *J Biol Chem*
41 459 2012;287:22216-26.
- 42 460 18. Stolina M, Bolon B, Middleton S, *et al.* The evolving systemic and local biomarker milieu at
43 461 different stages of disease progression in rat adjuvant-induced arthritis. *J Clin Immunol* 2009;29:158-
44 462 74.
- 46 463 19. Chen DL, Wang DS, Wu WJ, *et al.* Overexpression of paxillin induced by miR-137 suppression
47 464 promotes tumor progression and metastasis in colorectal cancer. *Carcinogenesis* 2013;34:803-11.
- 48 465 20. Boussein ML, Boyd SK, Christiansen BA, *et al.* Guidelines for assessment of bone
49 466 microstructure in rodents using micro-computed tomography. *J Bone Miner Res* 2010;25:1468-86.
- 51 467 21. Stolina M, Schett G, Dwyer D, *et al.* RANKL inhibition by osteoprotegerin prevents bone loss
52 468 without affecting local or systemic inflammation parameters in two rat arthritis models: comparison
53 469 with anti-TNFalpha or anti-IL-1 therapies. *Arthritis Res Ther* 2009;11:R187.
- 54 470 22. Stolina M, Adamu S, Ominsky M, *et al.* RANKL is a marker and mediator of local and systemic
55 471 bone loss in two rat models of inflammatory arthritis. *J Bone Miner Res* 2005;20:1756-65.
- 56 472 23. Firestein GS. Evolving concepts of rheumatoid arthritis. *Nature* 2003;423:356-61.

- 473 24. Sethi G, Ahn KS, Pandey MK, Aggarwal BB. Celastrol, a novel triterpene, potentiates TNF-
1 474 induced apoptosis and suppresses invasion of tumor cells by inhibiting NF-kappaB-regulated gene
2 475 products and TAK1-mediated NF-kappaB activation. *Blood* 2007;109:2727-35.
- 3 476 25. Idris AI, Krishnan M, Simic P, *et al.* Small molecule inhibitors of IkappaB kinase signaling
4 477 inhibit osteoclast formation in vitro and prevent ovariectomy-induced bone loss in vivo. *FASEB J*
5 478 2010;24:4545-55.
- 7 479 26. Idris AI, Libouban H, Nyangoga H, *et al.* Pharmacologic inhibitors of IkappaB kinase suppress
8 480 growth and migration of mammary carcinosarcoma cells in vitro and prevent osteolytic bone
9 481 metastasis in vivo. *Mol Cancer Ther* 2009;8:2339-47.
- 10 482 27. Kanagawa H, Masuyama R, Morita M, *et al.* Methotrexate inhibits osteoclastogenesis by
11 483 decreasing RANKL-induced calcium influx into osteoclast progenitors. *J Bone Miner Metab* 2015;
12 484 28. Annusek T, Kleinheinz J, Thomas S, Joos U, Wermker K. Short time administration of
13 485 antirheumatic drugs - methotrexate as a strong inhibitor of osteoblast's proliferation in vitro. *Head*
14 486 *Face Med* 2012;8:26.
- 16 487 29. Elsaid KA, Chichester CO. Review: Collagen markers in early arthritic diseases. *Clin Chim Acta*
17 488 2006;365:68-77.
- 19 489 30. Oestergaard S, Chouinard L, Doyle N, *et al.* The utility of measuring C-terminal telopeptides of
20 490 collagen type II (CTX-II) in serum and synovial fluid samples for estimation of articular cartilage status
21 491 in experimental models of destructive joint diseases. *Osteoarthritis Cartilage* 2006;14:670-9.
- 22 492 31. Oestergaard S, Chouinard L, Doyle N, *et al.* Early elevation in circulating levels of C-
23 493 telopeptides of type II collagen predicts structural damage in articular cartilage in the rodent model
24 494 of collagen-induced arthritis. *Arthritis Rheum* 2006;54:2886-90.
- 26 495 32. Ding QH, Cheng Y, Chen WP, Zhong HM, Wang XH. Celastrol, an inhibitor of heat shock
27 496 protein 90beta potently suppresses the expression of matrix metalloproteinases, inducible nitric
28 497 oxide synthase and cyclooxygenase-2 in primary human osteoarthritic chondrocytes. *Eur J Pharmacol*
29 498 2013;708:1-7.
- 30 499 33. Dempster DW. The contribution of trabecular architecture to cancellous bone quality. *J Bone*
32 500 *Miner Res* 2000;15:20-3.

33
34 501

35
36
37 502

38 39 503 **FIGURE LEGENDS**

40
41
42 504

43
44 505 **Fig 1 – Celastrol reduces the number of bone-related cells in arthritic joints.**

45
46 506 Representation of the immunohistochemical evaluation performed in paw sections at day 22
47 507 after celastrol treatment. Magnifications of 200×. Bar: 100 μm (A). Cathepsin k positive cells
48
49 508 and osteocalcin positive cells were identified in arthritic joints by immunohistochemistry of
50
51 509 paw sections (B). Immunohistochemical analysis was performed using a semi-quantitative
52
53 510 score. Notice that celastrol treatment significantly reduced both types of cells. Paw samples
54
55 511 were collected at the time of sacrifice. Data are expressed as median score with interquartile
56
57
58
59
60
61
62
63
64
65

1
2
3
4
5
6
7
8
9
10
11
12
13
14
15
16
17
18
19
20
21
22
23
24
25
26
27
28
29
30
31
32
33
34
35
36
37
38
39
40
41
42
43
44
45
46
47
48
49
50
51
52
53
54
55
56
57
58
59
60
61
62
63
64
65

512 range. Differences were considered statistically significant for p-values<0.05, according to the
513 Mann–Whitney tests. H – Healthy, A – Arthritic, E – Celestrol early-treated, L – Celestrol
514 late-treated. Healthy N=16, Arthritic N=10, Celestrol early-treated N=15 and Celestrol late-
515 treated N=15.

516
Fig 2 – Celestrol diminishes bone and cartilage turnover markers. TRACP-5b (A), P1NP
(B) and CTX-II (C) levels were quantified in rat serum samples collected at the time of
sacrifice. Celestrol is able to significantly reduce the levels of TRACP-5b, P1NP and CTX-II
in comparison with untreated arthritic rats. Data are expressed as median with interquartile
range. Differences were considered statistically significant for p-values<0.05, according to the
Mann–Whitney tests. H – Healthy, A – Arthritic, E – Celestrol early-treated, L – Celestrol
late-treated. Healthy N=13, Arthritic N=18, Celestrol early-treated N=15 and Celestrol late-
treated N=15.

Fig 3 – Celestrol preserves bone microarchitecture in arthritis. Inflammation-induced
bone loss and bone microarchitecture degradation, and the protective effect of celestrol are
illustrated in representative micro-CT reconstructions (A). Trabecular (B) and cortical (C)
bone indices were quantified from micro-CT reconstructions. Notice that tibiae from the
celestrol early-treated group have improved trabecular and cortical parameters comparing
with arthritic rats. Tibias were collected at the time of sacrifice. Data are expressed as median
with interquartile range. Differences were considered statistically significant for p-
values<0.05, according to the Mann–Whitney tests. H – Healthy, A – Arthritic, E – Celestrol
early-treated, L – Celestrol late-treated. Healthy N=30, Arthritic N=30, Celestrol early-treated
N=15 and Celestrol late-treated N=15.

537 **Fig 4 - Celestrol ameliorates bone mechanical properties in arthritic rats.** Maximal load

538 (A), Maximal deformation (B), Total absorbed energy (C), Yield displacement (D), Yield

539 load (E), Elastic energy (F) and Stiffness (G) parameters were obtained by 3-point bending.

540 Celestrol early-treated rats have higher levels of yield point displacement and maximum load

541 comparing with untreated arthritic rats. Femurs were collected after 22 days of disease

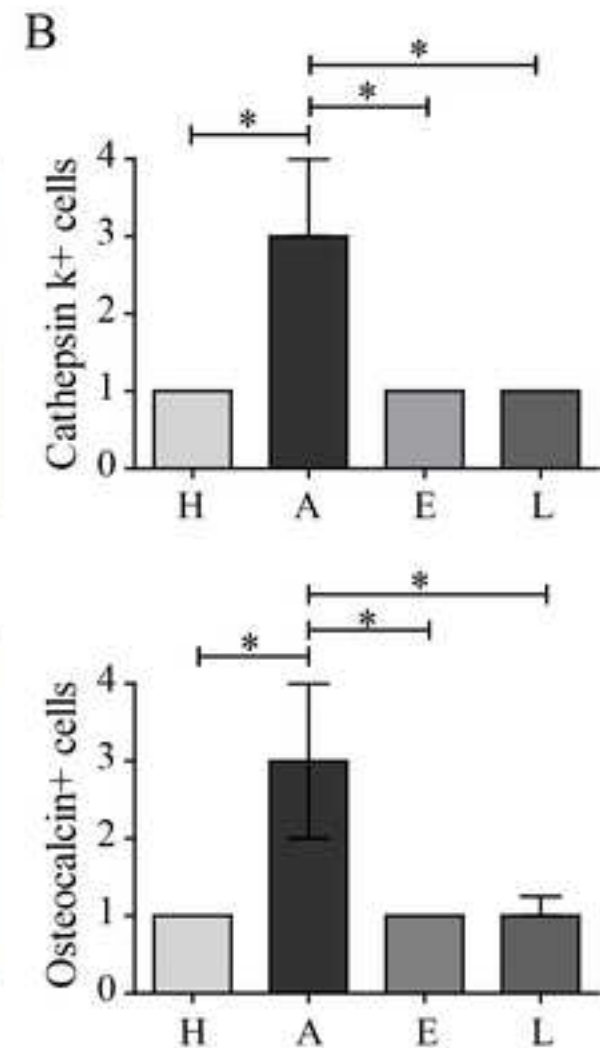
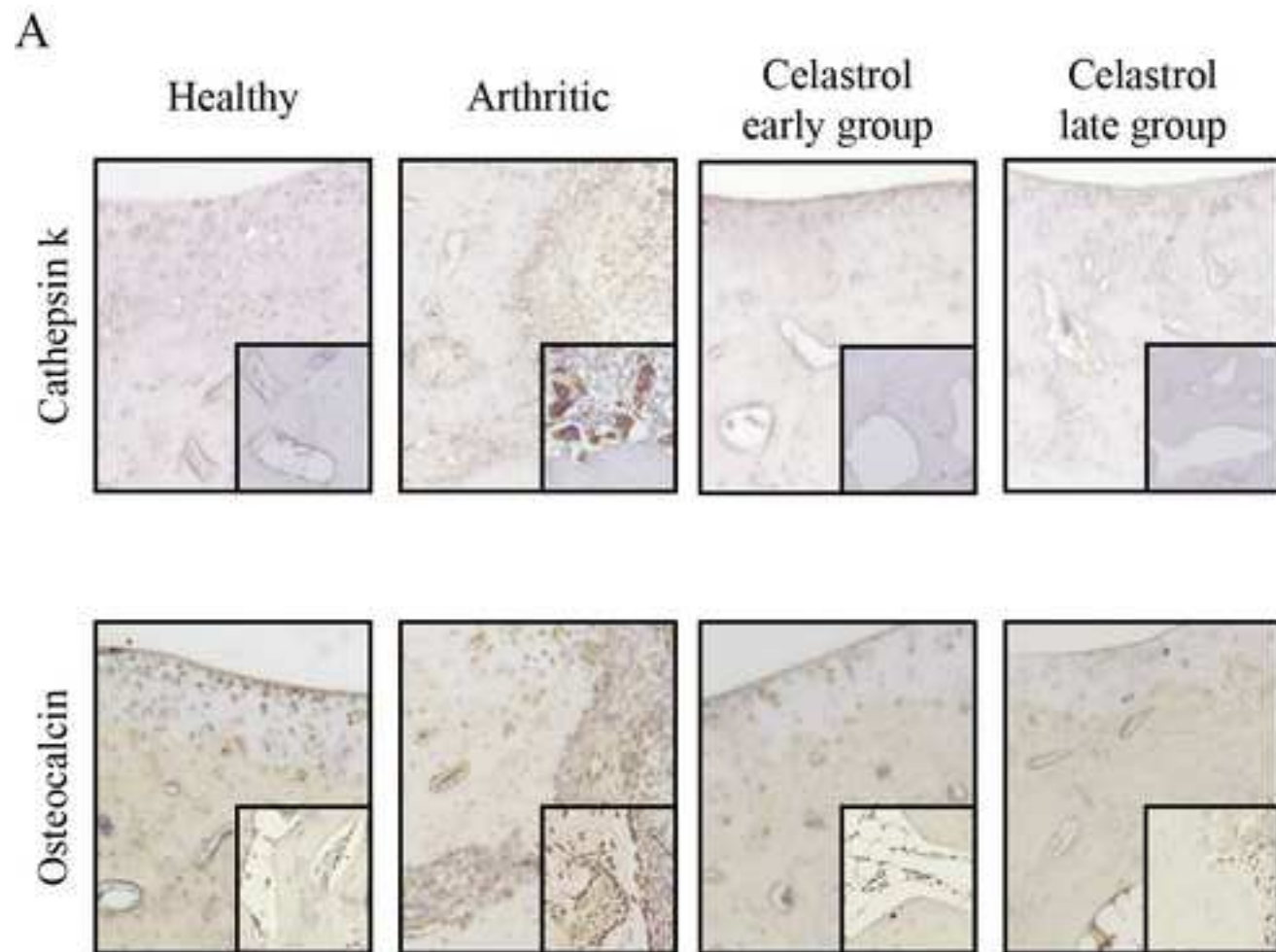
542 induction. Data are expressed as median with interquartile range. Differences were considered

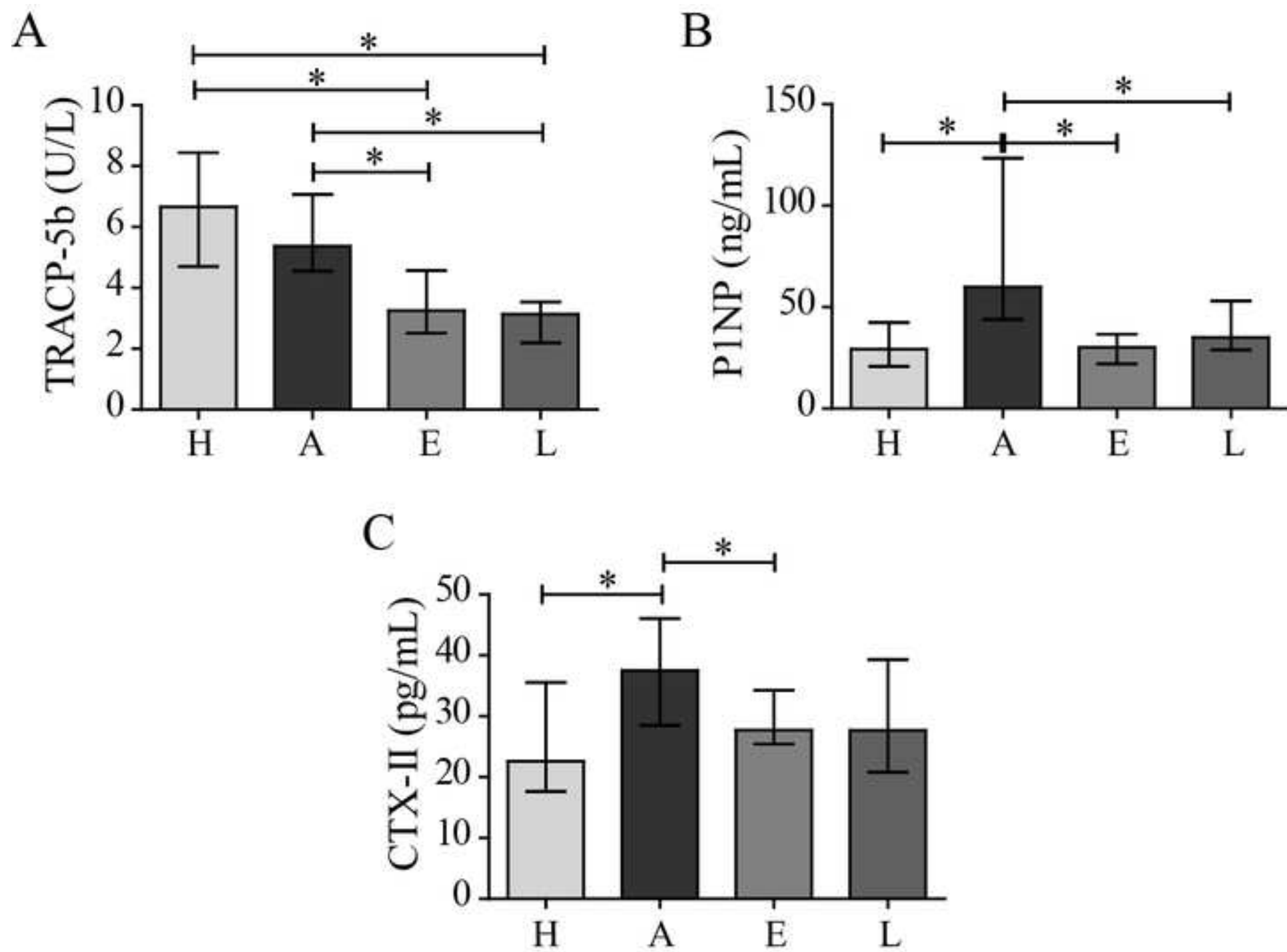
543 statistically significant for p-values<0.05, according to the Mann–Whitney tests. H – Healthy,

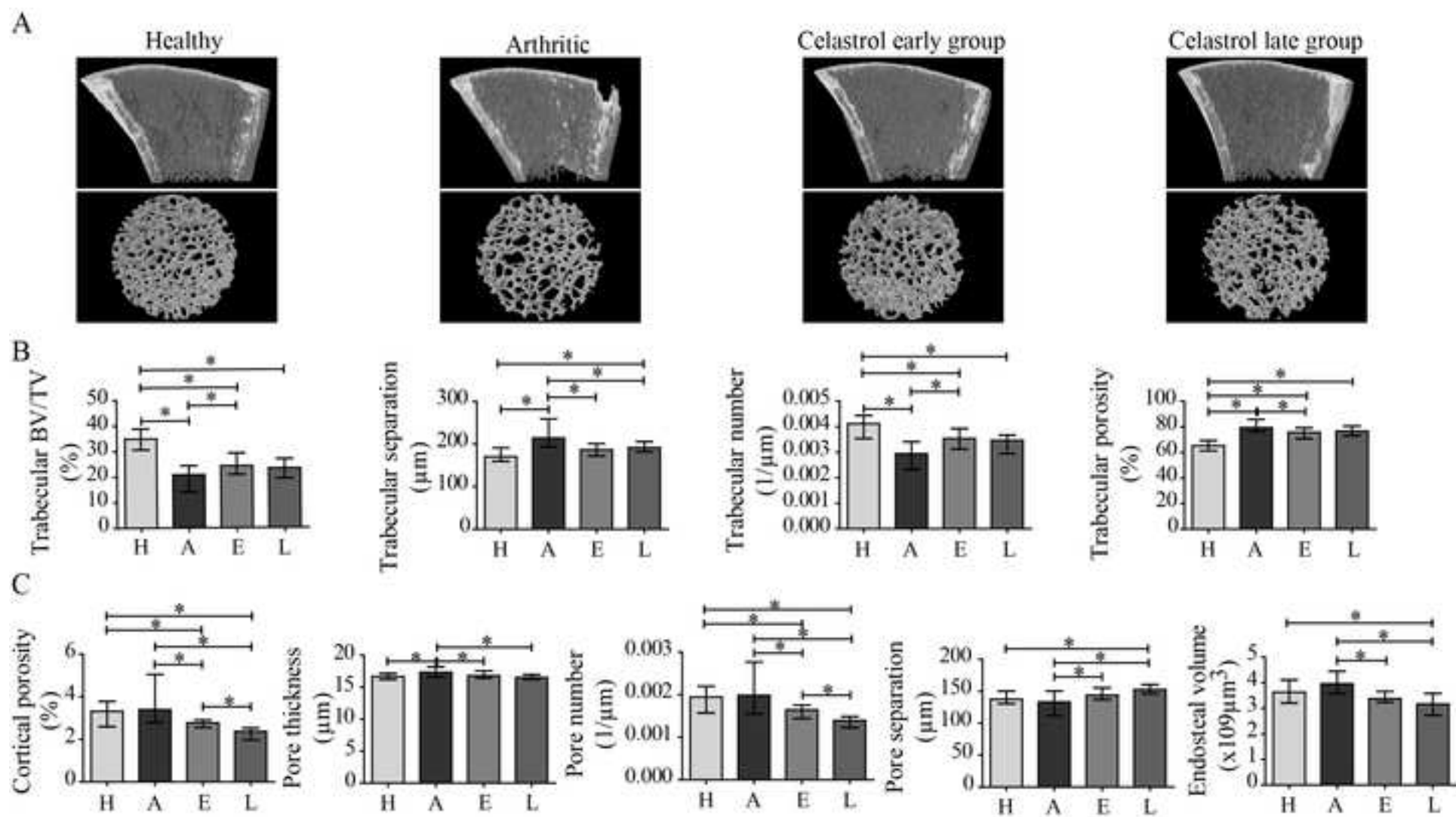
544 A – Arthritic, E – Celestrol early-treated, L – Celestrol late-treated. Healthy N=13, Arthritic

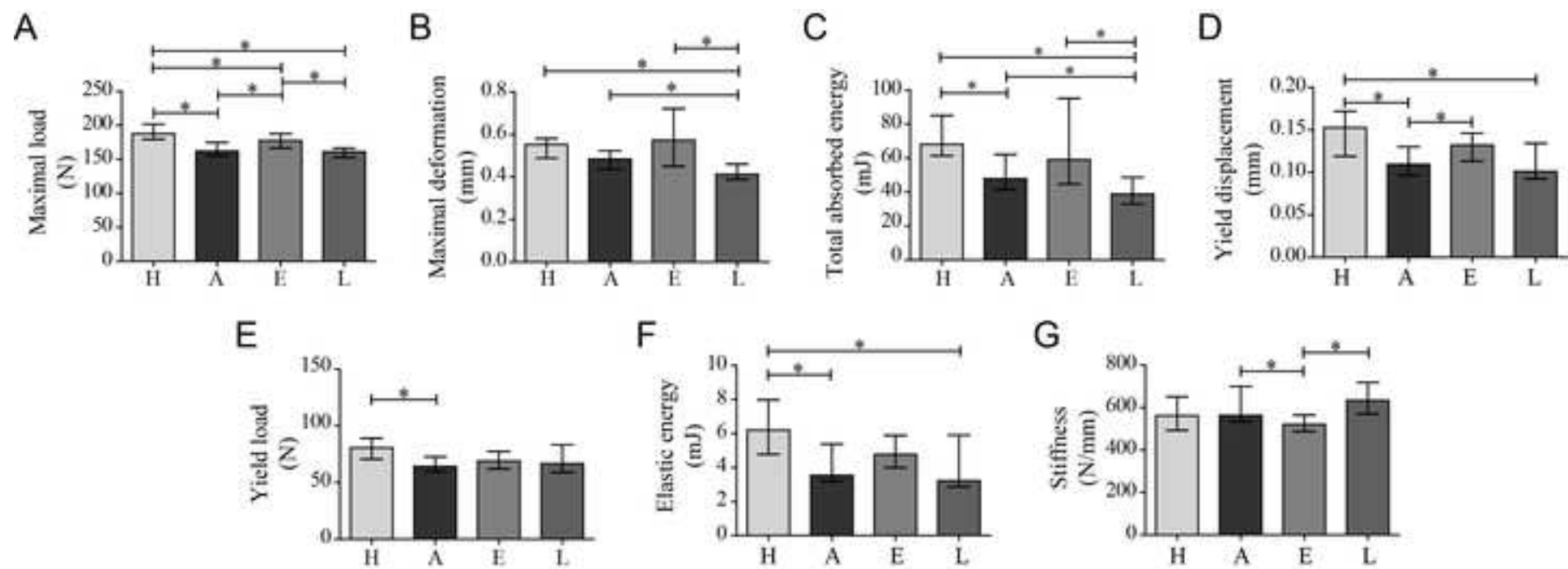
545 N=10, Celestrol early-treated N=15 and Celestrol late-treated N=15

546










Effects of tofacitinib in early arthritis bone loss

Journal:	<i>Rheumatology</i>
Manuscript ID	RHE-16-1635
Manuscript Type:	Original Article (includes systematic reviews)
Date Submitted by the Author:	07-Oct-2016
Complete List of Authors:	<p>Vidal, Bruno; Instituto de Medicina Molecular, Faculdade de Medicina, Universidade de Lisboa, Rheumatology Research Unit Cascão, Rita; Instituto de Medicina Molecular, Faculdade de Medicina, Universidade de Lisboa, Rheumatology Research Unit Finnilä, Mikko; Research Unit of Medical Imaging, Physics and Technology, Faculty of Medicine, University of Oulu, Oulu, Finland, Physics and Technology; Department of Applied Physics, University of Eastern Finland, Kuopio, Finland , Department of Applied Physics Lopes, Inês; Instituto de Medicina Molecular, Faculdade de Medicina, Universidade de Lisboa, Rheumatology Research Unit Saarakkala, Simo; Institute of Biomedicine University of Oulu, Department of Medical Technology; Research Unit of Medical Imaging, Physics and Technology, Faculty of Medicine, University of Oulu, Oulu, Finland, Physics and Technology Canhão, Helena; CEDOC, NOVA Medical School, NOVA University, Lisbon, Portugal, EpiDoc Fonseca, João Eurico; Instituto de Medicina Molecular, Faculdade de Medicina, Universidade de Lisboa, Rheumatology Research Unit; Hospital de Santa Maria, Centro Hospitalar Lisboa Norte, EPE, Lisbon Academic Medical Centre, Rheumatology Department Zioupos, Peter; Cranfield Forensic Institute, Cranfield University, DA of the UK, Biomechanics Labs</p>
Keywords Please select a minimum FIVE keywords from the list provided. These keywords will be used to select reviewers for this manuscript. The keywords in the main text of your paper do not need to match these words.:	Rheumatoid arthritis < RHEUMATIC DISEASES, Bone < TISSUES, Inflammation < BASIC & CLINICAL SCIENCES, DMARDs < THERAPIES, Animal models < BASIC & CLINICAL SCIENCES
<div style="text-align: center;">  </div>	

1
2
3
4
5
6
7
8
9
10
11
12
13
14
15
16
17
18
19
20
21
22
23
24
25
26
27
28
29
30
31
32
33
34
35
36
37
38
39
40
41
42
43
44
45
46
47
48
49
50
51
52
53
54
55
56
57
58
59
60

For Peer Review

Effects of tofacitinib in early arthritis bone loss

Bruno Vidal¹, Rita Cascão¹, Mikko Finnilä^{2,3}, Inês Lopes¹, Simo Saarakkala^{2,4},
Peter Zioupos⁵, Helena Canhão⁶, João Fonseca^{1,7}

1 Instituto de Medicina Molecular, Faculdade de Medicina, Universidade de Lisboa, Lisbon, Portugal; 2
Research Unit of Medical Imaging, Physics and Technology, Faculty of Medicine, University of Oulu,
Oulu, Finland; 3 Department of Applied Physics, University of Eastern Finland, Kuopio, Finland; 4
Medical Research Center, University of Oulu, Oulu, Finland; 5 Biomechanics Labs, Cranfield Forensic
Institute, Cranfield University, DA of the UK; ; 6 EpiDoC Unit, CEDOC, NOVA Medical School, NOVA
University, Lisbon, Portugal; 7 Rheumatology Department, Centro Hospitalar de Lisboa Norte, EPE,
Hospital de Santa Maria, Lisbon Academic Medical Centre, Lisbon, Portugal

Corresponding author: Bruno Vidal

Instituto de Medicina Molecular, Faculdade de Medicina da Universidade de
Lisboa

Av. Professor Egas Moniz 1649-028 Lisboa, Portugal

T +(351) 217 999 411

Email: vidal.bmc@gmail.com

ABSTRACT

Rheumatoid arthritis (RA) causes immune mediated local and systemic bone damage. **Objectives** - The main goal of this work was to analyze, how treatment intervention with tofacitinib prevents the early disturbances on bone structure and mechanics in adjuvant induced arthritis rat model. This is the first study to access the impact of tofacitinib on the systemic bone effects of inflammation. **Methods** - Fifty Wistar adjuvant-induced arthritis (AIA) rats were randomly housed in experimental groups, as follows: non-arthritic healthy group (N=20), arthritic non-treated (N=20) and 10 animals under tofacitinib treatment. Rats were monitored during 22 days after disease induction for the inflammatory score, ankle perimeter and body weight. Healthy non-arthritic rats were used as controls for comparison. After 22 days of disease progression rats were sacrificed and bone samples were collected for histology, micro-CT, 3-point bending and nanoindentation analysis. Blood samples were also collected for bone turnover markers and systemic cytokine quantification. **Results** - At tissue level, measured by nanoindentation, tofacitinib increased bone cortical and trabecular hardness. However, micro-CT and 3-point bending tests revealed that tofacitinib did not revert the effects of arthritis on cortical and trabecular bone structure and on mechanical properties. **Conclusion** - Possible reasons for these observations might be related with the mechanism of action of tofacitinib, which leads to direct interactions with bone metabolism, and/or with kinetics of its bone effects that might need longer exposure.

KEYWORDS: Rheumatoid arthritis, DMARD, bone, animal model, inflammation

INTRODUCTION

Rheumatoid arthritis (RA) is a chronic immune-mediated inflammatory disease, which affects around 1% of the world-population.(1) It causes joint and systemic inflammation that is reflected in local and systemic bone damage.(2) In fact, as RA progresses there is marked bone destruction, with radiological evidence of bone erosion within 2 years of disease onset.(3) In addition, osteoporosis is a common finding in patients with RA.(4) This is responsible for increased rates of vertebral and hip fractures in these patients.(5, 6) RA is associated with an increased expression of the receptor activator of nuclear factor kappa-B ligand (RANKL) and low levels of its antagonist, osteoprotegerin (OPG).(7) RANKL is a crucial activator of osteoclastogenesis.(8) In addition, RA serum and synovial fluid present an inflammatory cytokine profile, including interleukin (IL) 1 β , IL6, IL17 and tumour necrosis factor (TNF), which further favors osteoclast differentiation and activation since the early phase of the disease.(9-11) Evidence suggests that bone remodeling imbalance in RA contribute not only to local bone erosions but also to the development of systemic osteoporosis.(12)

We have previously found in the adjuvant-induced arthritis (AIA) rat model that 22 days of inflammatory disease progression directly led to the degradation of bone biomechanical properties, namely stiffness, ductility and bone strength, which was paralleled by a high collagen bone turnover.(13)

Tofacitinib is a selective inhibitor of janus kinase 1 (JAK1) and janus kinase 3 (JAK 3), thus interfering with the dimerization of signal transducer and activator of transcription (STAT) molecules, blocking the activation of gene transcription that is dependent on the JAK-STAT signaling pathway.(14-16)

1
2
3 The main goal of this work was to analyze, if treatment intervention with
4 tofacitinib in the AIA rat model prevents the early disturbances on bone
5 structure and strength induced by inflammation.
6
7
8
9

10 11 12 **METHODS**

13 14 15 16 17 **Animal experimental design**

18
19 Fifty 8 week-old female Wistar AIA Han rats weighing approximately 200-
20 220gr were housed in European type II standard filter top cages (Tecniplast,
21 Buguggiate, Italy) and transferred into the SPF animal facility at the Instituto
22 de Medicina Molecular, Faculdade de Medicina, Universidade de Lisboa,
23 under a 14h light/10h dark light cycle, acclimatized to T= 20-22°C and RH=
24 50-60%. They were given access to autoclaved rodent breeder chow (Special
25 Diet Service, RM3) and triple filtered water. AIA rats were purchased from
26 Charles River laboratories international (Barcelona, Spain) and they were
27 delivered at Instituto de Medicina Molecular after three days of disease
28 induction.
29
30
31
32
33
34
35
36
37
38
39
40
41

42 Upon arrival, animals were randomly housed in groups, individually identified
43 and cages were labelled according to the experimental groups, as follows:
44 non-arthritic healthy group (N=20), arthritic treated with tofacitinib
45 (10mg/kg/day orally) (N=10) and arthritic non-treated (N=20). Tofacitinib
46 administration was started 4 days after disease induction, when animals
47 already presented clinical signs of arthritis. The inflammatory score, ankle
48 perimeter and body weight were measured during the period of treatment.
49
50
51
52
53
54
55
56
57
58
59
60 Inflammatory signs were evaluated by counting the score of each joint in a

1
2
3 scale of 0 – 3 (0 – absence; 1 – erythema; 2 – erythema and swelling; 3 –
4 deformities and functional impairment). The total score of each animal was
5 defined as the sum of the partial scores of each affected joint. Rats were
6 sacrificed 22 days post disease induction and blood, paws and bone samples
7 were collected. All experiments were approved by the Animal User and
8 Ethical Committees at the Instituto de Medicina Molecular (Lisbon University),
9 according to the Portuguese law and the European recommendations.
10
11
12
13
14
15
16
17
18
19
20

21 **Histological evaluation of hind paws**

22
23 Left hind paw samples collected at the time of sacrifice were fixed
24 immediately in 10% neutral buffered formalin solution and then decalcified in
25 10% formic acid. Samples were then dehydrated and embedded in paraffin,
26 serially sectioned at a thickness of 5 μ m. Sections were stained with
27 hematoxylin and eosin for histopathological evaluation of structural changes
28 and cellular infiltration. This evaluation was performed in a blind fashion using
29 5 semi-quantitative scores:
30
31
32
33
34
35
36
37
38
39
40
41

- 42 • Sublining layer infiltration score (0—none to diffuse infiltration; 1—lymphoid
43 cell aggregate; 2—lymphoid follicles; 3—lymphoid follicles with germinal
44 center formation);
45
46
47
- 48 • Lining layer cell number score (0—fewer than three layers; 1—three to four
49 layers; 2—five to six layers; 3—more than six layers);
50
51
52
- 53 • Bone erosion score (0—no erosions; 1—minimal; 2—mild; 3—moderate; 4—
54 severe);
55
56
57
58
59
60

- Cartilage surface (0 –normal; 1 – irregular; 2 – clefts; 3 – clefts to bone);
- Global severity score (0—no signs of inflammation; 1—mild; 2—moderate; 3—severe).(17)

Images were acquired using a Leica DM2500 (Leica Microsystems, Wetzlar, Germany) microscope equipped with a colour camera.

Bone remodeling markers quantification

Serum samples were collected at sacrifice and stored at -80°C. Bone remodeling markers, CTX-I and P1NP, were quantified by Serum Rat Laps ELISA assay (Immunodiagnostic Systems Ltd, Boldon, UK).

Proinflammatory cytokines IL-1 β , IL-6 (Boster Bio, California, USA), IL-17, OPG, RANKL (Sunred Biological Technology, Shanghai, China) and TNF (RayBiotech, Georgia, USA) were quantified in serum samples using specific rat ELISA kits. Both kits were used following strictly provider's recommendations.

For all biomarkers standard curves were generated by using reference biomarker concentrations supplied by the manufacturers. Samples were analyzed using a plate reader Infinite M200 (Tecan, Mannedorf, Switzerland).

Micro-computed tomography (micro-CT) analysis

Structural properties of the trabecular and cortical tibiae were determined with a high-resolution micro-CT system (SkyScan 1272, Bruker microCT, Kontich, Belgium). Moist bones were wrapped in parafilm and covered with dental wax

1
2
3 to prevent drying and movement during the scanning. X-ray tube was set to
4
5 50kV and beam was filtered with 0.5mm Aluminum filter. Sample position and
6
7 camera settings were tuned to provide 3.0 μ m isotropic pixel size and
8
9 projection images were collected every 0.2°. Tissue mineral density values
10
11 were calibrated against hydroxyapatite phantoms with densities of
12
13 250mg/cm³ and 750mg/cm³. Reconstructions were done with NRecon (v
14
15 1.6.9.8; Bruker microCT, Kontich, Belgium) where appropriate corrections to
16
17 reduce beam hardening and ring artifacts were applied. Bone was segmented
18
19 in slices of 3 μ m thickness. After 200 slices from growth plate, we selected and
20
21 analyzed 1400 slices of trabecular bone. For cortical bone, 300 slices (1800
22
23 slices from growth plate) were analyzed.
24
25

26
27 Analyses were performed in agreement with guidelines for assessment of
28
29 bone microstructure in rodents using micro-computed
30
31 tomography.(18) Trabecular bone morphology was analyzed by applying
32
33 global threshold and despeckle to provide binary image for 3D analyzes. For
34
35 cortical bone ROI was refined with ROI-shrink wrap operation. This was
36
37 followed by segmentation of blood vessels using adaptive thresholding. Blood
38
39 vessels and porosity were analyzed using 3D morphological analyses.
40
41
42
43
44

45 **Bone mechanical tests**

46
47 Femurs were subjected to a 3-point bending test using a universal materials
48
49 testing machine (Instron 3366, Instron Corp., Massachusetts, USA). Femurs
50
51 were placed horizontally anterior side upwards on a support with span length
52
53 of 5mm. The load was applied with a constant speed of 0.005mm/s until
54
55 failure occurred. Stiffness was analyzed by fitting first-degree polynomial
56
57
58
59
60

1
2
3 function to the linear part of recorded load deformation data. A displacement
4
5 of $0.15\mu\text{m}$ between fitted slope and measured curve was used as criteria for
6
7 yield point, whereas the breaking point was defined as set where force
8
9 reached maximal value. Force, deformation and absorbed energy were
10
11 defined at both yield and at the breaking point.
12
13

14 15 16 17 **Nanoindentation**

18
19 Nanoindentation was performed using a CSM-Nano Hardness Tester System
20
21 (CSM Instruments SA; Switzerland; Indentation v.3.83) equipped with a
22
23 Berkovich based pyramid diamond tip. After micro-CT, 0.5mm of top tibia was
24
25 cut and proximal part was embedded to low viscosity epoxy resin (EpoThin,
26
27 Buehler, Knorrung Oy Ab, Helsinki, Finland). Slow speed diamond saw was
28
29 used to remove 10% of bone length. The sample surface was polished using
30
31 silicon carbide sandpaper with a decreasing grid size (800, 1200, 2400 and
32
33 4800) and finished with cloth with containing $0.05\ \mu\text{m}$ γ -alumina particles.
34
35 Indentation protocol was adopted from previous work(19) and on average 8
36
37 indentations were done on both cortical and trabecular bone with a quasi-
38
39 static (CSM called 'advanced') loading protocol. All indentations were
40
41 performed under an optical microscope to achieve the precise location of
42
43 indentations at the center of the targeted area in the tissue.(20)
44
45
46

47
48 In the 'advanced' protocol, a trapezoidal loading waveform was applied with a
49
50 loading/unloading rate of 20mN/min and with an intermediate load-hold-phase
51
52 lasting 30s hold at a maximum load 10 mN. The hardness (H_{IT}), indentation
53
54 modulus (E_{IT}), indentation creep (C_{IT}) and elastic part of indentation work (η_{IT})
55
56 were measured by using the Oliver and Pharr (1992) method (21).
57
58
59
60

1
2
3 Histological images of rat tibiae from diaphyseal cortical region were acquired
4
5 during the nanoindentation technique, using a CSM instruments (Switzerland)
6
7 microscope equipped with a color camera.
8

9
10 A histologic score was applied in order to evaluate the lamellar structures of
11
12 bone tissue. This evaluation was performed in a blind fashion using a semi-
13
14 quantitative score:
15

- 16 • Lamellar bone structure: (1- predominantly parallel-lamella; 2 -
17 concentric and parallel-lamellae in the same proportion; 3 -
18 predominantly concentric lamella).
19
20
21
22

23 The ratio of osteocyte lacuna area / total tissue area was also evaluated at
24
25 x200 magnification in order to analyse the percentage of total tissue area
26
27 occupied by osteocyte lacunae. The method of acquisition and analysis used
28
29 was the same applied for the evaluation of bone volume / tissue volume in
30
31 histomorphometry technique (13). All variables were expressed and
32
33 calculated according to the recommendations of the American Society for
34
35 Bone and Mineral Research (22), using a morphometric program (Image J
36
37 1.46R with plugin Bone J).
38
39
40
41
42
43

44 **Statistical analysis**

45
46 Statistical differences were determined with Mann–Whitney tests using
47
48 GraphPad Prism (GraphPad, California, USA). Correlation analysis was
49
50 performed with the Spearman test. Differences were considered statistically
51
52 significant for $p < 0.05$.
53
54
55
56
57
58
59
60

RESULTS

Tofacitinib effectively reduced inflammation in the AIA rat model of arthritis

Results showed that 10mg/kg/day of tofacitinib effectively controlled and abrogated disease development in comparison with untreated arthritic rats (fig.1A). Moreover, untreated arthritic animals sharply increased the ankle perimeter throughout disease progression (fig.1B). Rats under tofacitinib treatment presented an ankle perimeter similar to healthy controls.

Tofacitinib abrogated local joint inflammation and local bone and cartilage damage in AIA rats

To evaluate the effect of tofacitinib treatment in the preservation of joint structure and periarticular bone, paw sections stained with haematoxylin and eosin were performed (illustrative images can be observed in Fig 2A). The histological evaluation using 5 semi-quantitative scores is depicted in Fig 2 (B-F).

Sublining layer infiltration (B) and the number of lining layer cells (C) were lower in the tofacitinib group when compared with the untreated arthritic group at the end of the study ($p < 0.0001$). Tofacitinib was also effective in preventing joint bone erosions (D) and cartilage damage (E) ($p < 0.0001$ and $p = 0.0001$ tofacitinib group vs. arthritic rats, respectively).

1
2
3 Thus, these data reveals that tofacitinib was able to significantly diminish
4 inflammation and local bone damage (Fig. 2F, $p < 0.0001$ tofacitinib group vs.
5 arthritic rats).
6
7
8
9

10 11 12 **Tofacitinib reduced bone turnover**

13
14 We have observed that both CTX-I (Fig. 3A) and P1NP (Fig. 3B) were
15 significantly increased in the arthritic group in comparison with the healthy
16 control animals ($p < 0.0001$ and $p = 0.0015$, respectively), revealing an
17 increase of bone turnover in the arthritic group. The tofacitinib group showed
18 decreased values for CTX-I ($p = 0.0002$) and P1NP ($p = 0.0018$) when
19 compared with the arthritic group, suggesting a decreased bone turnover
20 (Fig.3).
21
22
23
24
25
26
27
28
29

30 RANKL levels were decreased in the serum of tofacitinib-treated rats in
31 comparison with healthy control and untreated arthritic rats ($p = 0.0083$ and $p =$
32 0.0141 , respectively), as observed in Fig 3C. OPG levels were also reduced
33 in tofacitinib group in comparison with healthy control and untreated arthritic
34 rats ($p = 0.0031$ and $p = 0.0002$, respectively)(Fig. 3D). No differences were
35 observed in RANKL/OPG ratio between tofacitinib and arthritic untreated
36 group. The tofacitinib group showed an increased RANKL/OPG ratio when
37 compared to healthy control group ($p = 0.0370$ Fig. 3E).
38
39
40
41
42
43
44
45
46
47

48 We have also quantified the circulating concentration of IL-1 β , IL-6 and TNF,
49 but no differences were found when comparing arthritic rats with animals
50 treated with tofacitinib (Fig. 3F, 3G and 3H). However, there was a slight
51 tendency for IL-6 to be diminished in the tofacitinib group when compared
52 with untreated arthritic animals.
53
54
55
56
57
58
59
60

1
2
3 Tofacitinib administration significantly reduced the levels of IL-17 detected in
4
5 peripheral blood, ($p < 0.0001$, tofacitinib group vs. untreated arthritic rats after
6
7 22 days of disease induction) (Fig. 3I).
8
9

10 11 12 **Micro-CT**

13
14 The effect of tofacitinib on inflammation-induced bone loss was assessed by
15
16 micro-CT of cortical (Fig 4 A-C) and trabecular (Fig 4 D - I) bone tibia. Arthritic
17
18 rats showed a reduction in cross-sectional area (A) and thickness (B) and
19
20 tofacitinib treatment did not restore these cortical changes ($p < 0.0001$ vs
21
22 healthy controls, respectively). These bone changes affected the ability of
23
24 bone's torsion as showed by decreased values of polar moment of inertia (C)
25
26 in arthritic and tofacitinib group ($p = 0.0059$ and $p = 0.0197$ vs healthy controls,
27
28 respectively). Trabecular bone also presented dramatic deterioration with
29
30 arthritis as evidenced by a reduced trabecular bone volume fraction (D)
31
32 ($p = 0.0007$ and $p < 0.0001$ vs healthy controls, respectively), thickness (E) and
33
34 number (F) ($p < 0.0001$ vs healthy controls) and also by an increased
35
36 trabecular separation (G) ($p < 0.0001$ in arthritic group and $p = 0.0002$ in
37
38 tofacitinib group vs healthy controls) and porosity (H) ($p < 0.0001$ vs healthy
39
40 controls). Furthermore, structure model index (I) showed declined values in
41
42 arthritic and tofacitinib group ($p < 0.0001$ vs healthy controls, respectively)
43
44 indicating that trabeculae shape was rather rod-like compared to plate-like
45
46 shape in healthy controls.
47
48
49
50

51
52 Tofacitinib could not rescue trabecular bone integrity and trabecular bone
53
54 properties in treated rats (Fig.4J).
55
56
57
58
59
60

Three-point bending

Tissue-level mechanical properties of rat femurs were evaluated using 3-point bending mechanical test at the end of the experiment. As shown in Fig. 5, arthritic rats revealed decreased mechanical properties at yield point, namely displacement ($p=0.0192$ vs healthy controls, Fig 5A), strength ($p=0.0229$ vs healthy control, Fig 5B) and pre yield energy (elastic energy) ($p=0.0161$ vs healthy controls, Fig 5C). These results showed that arthritic bones started to accumulate micro fractures with smaller deformations and lower loads, leading to a decreased energy absorption capability at yield point. Tofacitinib treated rats showed a significant decreased displacement ($p=0.0039$ vs healthy controls, Fig 5D) and elastic properties ($p=0.0443$ vs healthy controls, Fig 5E) at fracture point, meaning that there was a lower deformation (related to decreased elastic properties) during the plastic phase, before the total fracture of bone. Results also demonstrated that arthritic and tofacitinib rats had decreased maximum load ($p= 0.0017$ vs healthy controls, Fig 5F). Finally, arthritic rats and the tofacitinib treated group showed a significant decrease in toughness ($p=0.0143$ and $p=0.0048$ vs healthy controls, respectively, Fig 5G), demonstrating that arthritic and tofacitinib-treated bone could absorb less energy before fracturing.

Altogether, mechanical data revealed that arthritic and tofacitinib groups had significantly lower mechanical properties as compared to healthy controls, meaning that tofacitinib was unable to abrogate the structural deterioration during the time frame of treatment observed in this animal model.

Tofacitinib increased bone hardness

Nanoindentation was performed in order to assess the quality at tissue matrix level and this technique can be used at the level of a single trabecula or within a confined submicron area of the cortical bone tissue.

Nano-mechanical tests revealed that arthritic rats had decreased hardness in cortical (Fig. 6A) and trabecular bone (Fig. 6B) ($p= 0.0010$ and $p= 0.0080$ in arthritic rats vs healthy controls, respectively). In contrast, rats treated with tofacitinib showed restored hardness in cortical bone (Fig. 6A) and increased hardness in trabecular (Fig. 6B) bone ($p=0.0003$ and $p=0.0012$ vs untreated arthritic rats, respectively). No differences were observed in the other parameters analysed.

Topographic images gathered during nanoindentation allowed the characterization of bone histologic features from healthy animals, arthritic untreated animals and tofacitinib treated animals after 22 days of disease induction.

Concentric lamellas were identified in secondary osteons (SO) and more frequently observed in arthritic animals (Fig.6 F) than in healthy controls ($p= 0.0022$) and tofacitinib treated animals ($p= 0.0043$) (Fig. 6C). On the contrary, healthy animals (Fig. 6 E) and tofacitinib treated animals (Fig. 6 G) presented more parallel-lamellae (PL) structures than concentric lamellas.

In addition, arthritic animals showed an increased area occupied by osteocyte lacunae in the total tissue when compared to healthy animals and tofacitinib treated animals (Fig. 6D) ($p=0.0067$, $p=0.0011$, respectively).

DISCUSSION

In this study, we used the AIA rat model to evaluate the efficacy of tofacitinib to treat inflammation as well as inflammation-induced bone damage. Tofacitinib showed significantly reduced arthritis manifestations, synovial tissue inflammation and bone erosions, which was associated with lower serum RANKL and OPG levels. These results are in line with previous observations. (23)

The effects of tofacitinib on pro-inflammatory cytokines production were assessed through serum quantification of IL-1 β , IL-6, IL-17 and TNF. Our study depicted decreased levels of IL-17 in AIA rats under tofacitinib treatment in comparison with untreated arthritic animals. In addition, we have observed a tendency towards a decrease in serum IL-6 concentration in tofacitinib treated rats. These observations are expected by tofacitinib inhibition of the JAK and STAT3 pathways.(15, 24-26) Tofacitinib did not affect circulating levels of TNF or IL-1 β comparing with untreated arthritic rats, but this might be related to the relatively low circulating levels of these cytokines in this animal model.(23)

Biochemical markers of bone turnover were quantified in order to evaluate the impact of tofacitinib on bone metabolism. A reduced bone turnover was shown in tofacitinib treated animals, as depicted by decreased CTX-I and P1NP levels.

At tissue level, measured by nanoindentation, tofacitinib increased bone cortical and trabecular hardness. On the contrary, arthritic animals showed decreased values of hardness after 22 days post disease induction. We also

1
2
3 observed at day 11 and 22 post arthritis induction concentric lamellas in
4
5 secondary osteons (SO) microstructures resulting from high bone
6
7 remodelling, as previously described (13, 27, 28). Dall'Ara et al. suggested
8
9 that larger numbers of this younger, less mineralised and less hard structures,
10
11 could be related to reduced hardness of bone tissue identified by
12
13 nanoindentation. On the contrary, healthy and tofacitinib treated animals
14
15 presented more parallel-lamellae (PL) structures than concentric lamellas in
16
17 SO structures and this PL structures are 10% more harder than the former,
18
19 representing the mature bone structure (and normal bone remodelling)(28). In
20
21 addition, arthritic animals had an increased area occupied by osteocyte
22
23 lacunae in total tissue. Tofacitinib treated animals, on the contrary, had a
24
25 normal number of osteocytes lacunae and of the lacunae area per tissue
26
27 volume. Osteocytes are responsible for the maintenance of the bone
28
29 homeostasis, regulating the behaviour of osteoblasts and osteoclasts by
30
31 communicating through gap junctions (29). Although no previous data is
32
33 available in the context of arthritis some studies revealed that osteocytes from
34
35 osteoarthritis patients have an irregular morphology, with limited ability to
36
37 reply to mechanical stimuli, leading to significant changes in the structure and
38
39 mineral density (30). Despite being still unclear, this apparent change of
40
41 osteocyte morphology in arthritic bone might contribute to the
42
43 nanomechanical changes observed in this context.
44
45
46
47
48
49
50
51
52
53

54 Micro-CT and 3-point bending tests revealed that tofacitinib did not revert the
55
56 effects of arthritis on cortical and trabecular bone structure and mechanical
57
58
59
60

1
2
3 properties. There are several possible explanations for these observations.
4
5 Using this same animal model we were able to revert the structural and
6
7 mechanical damage induced by arthritis using an experimental
8
9 compound.(17) However, the kinetics of the effects of tofacitinib might be
10
11 different, needing more exposure time to have an impact on bone quality. The
12
13 effect at a tissue level might be an early sign of its delayed impact on bone. Of
14
15 interest, an increase in hardness is associated with a decrease in the relative
16
17 ratio of elastic-to-plastic behaviour of the tissue and thus it is unclear if it
18
19 represents ultimately a true improvement in mechanical properties. Another
20
21 explanation might be related with the mechanism of action. Tofacitinib targets
22
23 JAK1 and 3, downregulating STAT 1 and 3 of the JAK-STAT signaling
24
25 pathway,(15, 16, 23) and these intracellular molecules have complex
26
27 interactions with bone. JAK1 is expressed in bone cells and is involved in
28
29 bone formation. The depletion of JAK1 promotes bone growth delays,
30
31 suggesting that JAK1 is critical for skeletal development. On the other hand,
32
33 STAT1 inhibits Runx2 transcription in osteoblasts, the master transcription
34
35 factor of osteoblast differentiation. Thus, STAT1 is an inhibitor of
36
37 differentiation of osteoblasts and the inactivation of STAT1 leads to an
38
39 osteopetrotic bone phenotype.(31) Consistent with the higher bone mass in
40
41 STAT1-deficient mice, inactivation of STAT1 can accelerate fracture
42
43 repair.(32) These data suggest that STAT1 negatively regulates bone
44
45 formation in vivo.(33) On the contrary, JAK-STAT3 signal transduction
46
47 pathway promotes osteoblast differentiation (33). Inactivation of STAT3 in
48
49 osteoblasts leads to lower bone mass due to inhibition of bone formation. In
50
51 humans, STAT3 mutations reduce bone mass and increase incidence of
52
53
54
55
56
57
58
59
60

1
2
3 minimal trauma fractures. Clinical studies indicate that STAT3 mutations
4
5 increase osteoclast number and bone resorption, and are associated with
6
7 recurrent fractures.
8

9
10 It is conceivable that these types of molecular interactions with bone have an
11
12 overall effect that might not be totally compensated by the benefits on bone
13
14 obtained by the control of inflammation. To fully clarify these open questions it
15
16 will be relevant to test several doses of tofacitinib in longer duration arthritis
17
18 models and in healthy animals.
19

20 21 22 23 24 25 26 27 28 **KEY MESSAGES**

- 29
30 • Tofacitinib was able to control and suppress inflammatory activity in an AIA
31
32 rat model of arthritis.
33
- 34
35 • Tofacitinib wasn't able to revert structural and mechanical bone changes
36
37 promoted by inflammation.
38
- 39
40 • JAK-STAT pathway inhibition downregulates several targets which may not
41
42 be totally beneficial for bone homeostasis.
43
44
45
46
47
48
49

50 51 **COMPETING INTERESTS**

52
53 The authors have declared that no competing interests exist.
54
55
56
57
58
59
60

FUNDING

This work was supported by Aspire 2013 prize from Pfizer. The funders had no role in study design, data collection and analysis, decision to publish, or preparation of the manuscript.

For Peer Review

REFERENCES

1. Alamanos Y, Drosos AA. Epidemiology of adult rheumatoid arthritis. *Autoimmun Rev.* 2005 Mar;4(3):130-6. PubMed PMID: 15823498.
2. Yelin E, Callahan LF. The economic cost and social and psychological impact of musculoskeletal conditions. National Arthritis Data Work Groups. *Arthritis and rheumatism.* 1995 Oct;38(10):1351-62. PubMed PMID: 7575685.
3. Lin YY, Jean YH, Lee HP, Chen WF, Sun YM, Su JH, et al. A soft coral-derived compound, 11-epi-sinulariolide acetate suppresses inflammatory response and bone destruction in adjuvant-induced arthritis. *PLoS One.* 2013;8(5):e62926. PubMed PMID: 23675440. Pubmed Central PMCID: 3652811.
4. Haugeberg G, Orstavik RE, Uhlig T, Falch JA, Halse JI, Kvien TK. Bone loss in patients with rheumatoid arthritis: results from a population-based cohort of 366 patients followed up for two years. *Arthritis and rheumatism.* 2002 Jul;46(7):1720-8. PubMed PMID: 12124854.
5. Marshall D, Johnell O, Wedel H. Meta-analysis of how well measures of bone mineral density predict occurrence of osteoporotic fractures. *BMJ.* 1996 May 18;312(7041):1254-9. PubMed PMID: 8634613. Pubmed Central PMCID: 2351094.
6. Eric-Jan JA K. Bone mass in rheumatoid arthritis. *CLINICAL AND EXPERIMENTAL RHEUMATOLOGY.* 2000.
7. Fonseca JE, Cortez-Dias N, Francisco A, Sobral M, Canhao H, Resende C, et al. Inflammatory cell infiltrate and RANKL/OPG expression in rheumatoid synovium: comparison with other inflammatory arthropathies and correlation with outcome. *Clin Exp Rheumatol.* 2005 Mar-Apr;23(2):185-92. PubMed PMID: 15895888.
8. Boyle WJ, Simonet WS, Lacey DL. Osteoclast differentiation and activation. *Nature.* 2003 May 15;423(6937):337-42. PubMed PMID: 12748652.
9. Moura RA, Cascao R, Perpetuo I, Canhao H, Vieira-Sousa E, Mourao AF, et al. Cytokine pattern in very early rheumatoid arthritis favours B-cell activation and survival. *Rheumatology (Oxford).* 2011 Feb;50(2):278-82. PubMed PMID: 21047805.
10. Cascao R, Moura RA, Perpetuo I, Canhao H, Vieira-Sousa E, Mourao AF, et al. Identification of a cytokine network sustaining neutrophil and Th17 activation in untreated early rheumatoid arthritis. *Arthritis research & therapy.* 2010;12(5):R196. PubMed PMID: 20961415. Pubmed Central PMCID: 2991033.
11. Caetano-Lopes J, Canhao H, Fonseca JE. Osteoimmunology--the hidden immune regulation of bone. *Autoimmunity reviews.* 2009 Jan;8(3):250-5. PubMed PMID: 18722561.
12. Caetano-Lopes J, Rodrigues A, Lopes A, Vale AC, Pitts-Kiefer MA, Vidal B, et al. Rheumatoid arthritis bone fragility is associated with upregulation of IL17 and DKK1 gene expression. *Clin Rev Allergy Immunol.* 2014 Aug;47(1):38-45. PubMed PMID: 23546988.
13. Vidal B, Cascao R, Vale AC, Cavaleiro I, Vaz MF, Brito JA, et al. Arthritis induces early bone high turnover, structural degradation and mechanical weakness. *PloS one.* 2015;10(1):e0117100. PubMed PMID: 25617902. Pubmed Central PMCID: 4305284.
14. Tofacitinib. *Drugs R D.* 2010;10(4):271-84. PubMed PMID: 21171673. Pubmed Central PMCID: 3585773.
15. Meyer DM, Jesson MI, Li X, Elrick MM, Funckes-Shippy CL, Warner JD, et al. Anti-inflammatory activity and neutrophil reductions mediated by the JAK1/JAK3 inhibitor, CP-690,550, in rat adjuvant-induced arthritis. *Journal of inflammation.* 2010;7:41. PubMed PMID: 20701804. Pubmed Central PMCID: 2928212.
16. Maeshima K, Yamaoka K, Kubo S, Nakano K, Iwata S, Saito K, et al. The JAK inhibitor tofacitinib regulates synovitis through inhibition of interferon-gamma and interleukin-17

1
2
3 production by human CD4+ T cells. *Arthritis and rheumatism*. 2012 Jun;64(6):1790-8.
4 PubMed PMID: 22147632.

5 17. Cascao R, Vidal B, Raquel H, Neves-Costa A, Figueiredo N, Gupta V, et al. Effective
6 treatment of rat adjuvant-induced arthritis by celestrol. *Autoimmun Rev*. 2012
7 Oct;11(12):856-62. PubMed PMID: 22415021. Pubmed Central PMCID: 3582326.

8 18. Bouxsein ML, Boyd SK, Christiansen BA, Guldborg RE, Jepsen KJ, Muller R. Guidelines
9 for assessment of bone microstructure in rodents using micro-computed tomography.
10 *Journal of bone and mineral research : the official journal of the American Society for Bone
11 and Mineral Research*. 2010 Jul;25(7):1468-86. PubMed PMID: 20533309.

12 19. Herlin M, Finnilla MA, Zioupos P, Aula A, Risteli J, Miettinen HM, et al. New insights
13 to the role of aryl hydrocarbon receptor in bone phenotype and in dioxin-induced
14 modulation of bone microarchitecture and material properties. *Toxicology and applied
15 pharmacology*. 2013 Nov 15;273(1):219-26. PubMed PMID: 24035824.

16 20. Zhang R, Gong H, Zhu D, Ma R, Fang J, Fan Y. Multi-level femoral morphology and
17 mechanical properties of rats of different ages. *Bone*. 2015 Jul;76:76-87. PubMed PMID:
18 25857690.

19 21. W.C. Oliver GMP. An improved technique for determining hardness and elastic
20 modulus using load and displacement sensing indentation experiments1992.

21 22. Parfitt AM, Drezner MK, Glorieux FH, Kanis JA, Malluche H, Meunier PJ, et al. Bone
22 histomorphometry: standardization of nomenclature, symbols, and units. Report of the
23 ASBMR Histomorphometry Nomenclature Committee. *Journal of bone and mineral research
24 : the official journal of the American Society for Bone and Mineral Research*. 1987
25 Dec;2(6):595-610. PubMed PMID: 3455637.

26 23. LaBranche TP, Jesson MI, Radi ZA, Storer CE, Guzova JA, Bonar SL, et al. JAK
27 inhibition with tofacitinib suppresses arthritic joint structural damage through decreased
28 RANKL production. *Arthritis and rheumatism*. 2012 Nov;64(11):3531-42. PubMed PMID:
29 22899318.

30 24. Milici AJ, Kudlacz EM, Audoly L, Zwillich S, Changelian P. Cartilage preservation by
31 inhibition of Janus kinase 3 in two rodent models of rheumatoid arthritis. *Arthritis research
32 & therapy*. 2008;10(1):R14. PubMed PMID: 18234077. Pubmed Central PMCID: 2374467.

33 25. Tanaka Y, Maeshima K, Yamaoka K. In vitro and in vivo analysis of a JAK inhibitor in
34 rheumatoid arthritis. *Annals of the rheumatic diseases*. 2012 Apr;71 Suppl 2:i70-4. PubMed
35 PMID: 22460142.

36 26. Tanaka Y, Yamaoka K. JAK inhibitor tofacitinib for treating rheumatoid arthritis: from
37 basic to clinical. *Modern rheumatology / the Japan Rheumatism Association*. 2013
38 May;23(3):415-24. PubMed PMID: 23212593.

39 27. Bailey AJ, Mansell JP, Sims TJ, Banse X. Biochemical and mechanical properties of
40 subchondral bone in osteoarthritis. *Biorheology*. 2004;41(3-4):349-58. PubMed PMID:
41 15299267.

42 28. Dall'Ara E, Ohman C, Baleani M, Viceconti M. Reduced tissue hardness of trabecular
43 bone is associated with severe osteoarthritis. *Journal of biomechanics*. 2011 May
44 17;44(8):1593-8. PubMed PMID: 21496822.

45 29. Taylor AF, Saunders MM, Shingle DL, Cimbala JM, Zhou Z, Donahue HJ. Mechanically
46 stimulated osteocytes regulate osteoblastic activity via gap junctions. *American journal of
47 physiology Cell physiology*. 2007 Jan;292(1):C545-52. PubMed PMID: 16885390.

48 30. Jaiprakash A, Prasadam I, Feng JQ, Liu Y, Crawford R, Xiao Y. Phenotypic
49 characterization of osteoarthritic osteocytes from the sclerotic zones: a possible pathological
50 role in subchondral bone sclerosis. *International journal of biological sciences*.
51 2012;8(3):406-17. PubMed PMID: 22419886. Pubmed Central PMCID: 3303142.

52 31. Kim S, Koga T, Isobe M, Kern BE, Yokochi T, Chin YE, et al. Stat1 functions as a
53 cytoplasmic attenuator of Runx2 in the transcriptional program of osteoblast differentiation.
54
55
56
57
58
59
60

1
2
3
4
5
6
7
8
9
10
11
12
13
14
15
16
17
18
19
20
21
22
23
24
25
26
27
28
29
30
31
32
33
34
35
36
37
38
39
40
41
42
43
44
45
46
47
48
49
50
51
52
53
54
55
56
57
58
59
60

Genes Dev. 2003 Aug 15;17(16):1979-91. PubMed PMID: 12923053. Pubmed Central PMCID: 196253.

32. Tajima K, Takaishi H, Takito J, Tohmonda T, Yoda M, Ota N, et al. Inhibition of STAT1 accelerates bone fracture healing. J Orthop Res. 2010 Jul;28(7):937-41. PubMed PMID: 20063384.

33. Zhou Y, Tan L, Que Q, Li H, Cai L, Cao L, et al. Study of association between HLA-DR4 and DR53 and autoantibody detection in rheumatoid arthritis. Journal of immunoassay & immunochemistry. 2013;34(2):126-33. PubMed PMID: 23537298.

For Peer Review

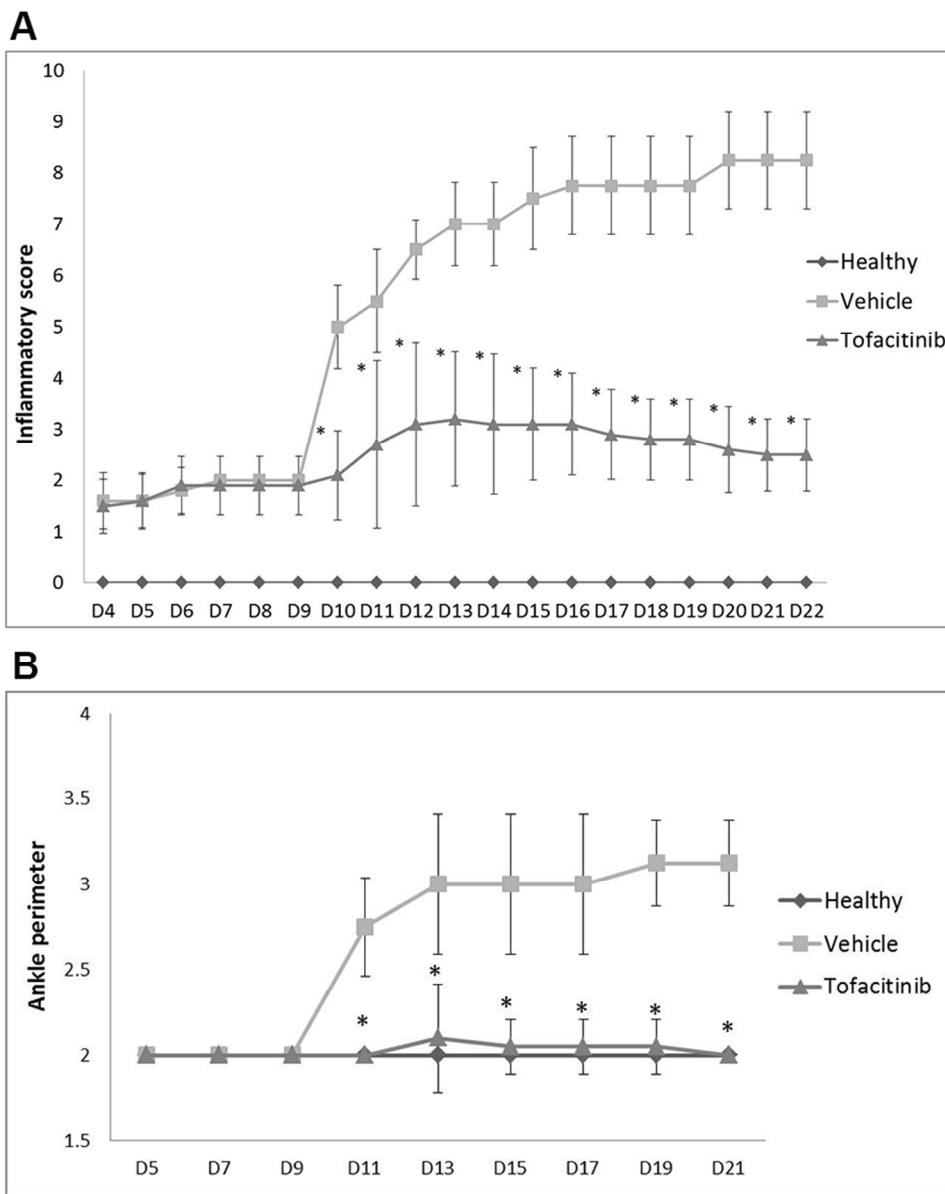


Figure 1 - Inflammatory score and ankle perimeter. (A) Inflammatory score - Tofacitinib group was compared with the vehicle group (arthritic). Results showed statistical differences throughout time since day 10 $p= 0.0071$ up to day 22 $p= 0.0058$. (B) Ankle perimeter. Tofacitinib group was compared with the vehicle group (arthritic). Results showed statistical differences throughout time since day 11 $p= 0.0057$ up to day 22 $p= 0.0056$. Statistical differences were determined with non-parametric Mann Whitney test using GraphPad Prism (GraphPad, California, USA). Differences were considered statistically significant for p values ≤ 0.05 . Healthy $N=20$, Arthritic $N=20$, Tofacitinib $N=10$.
Rats under tofacitinib treatme
317x394mm (300 x 300 DPI)

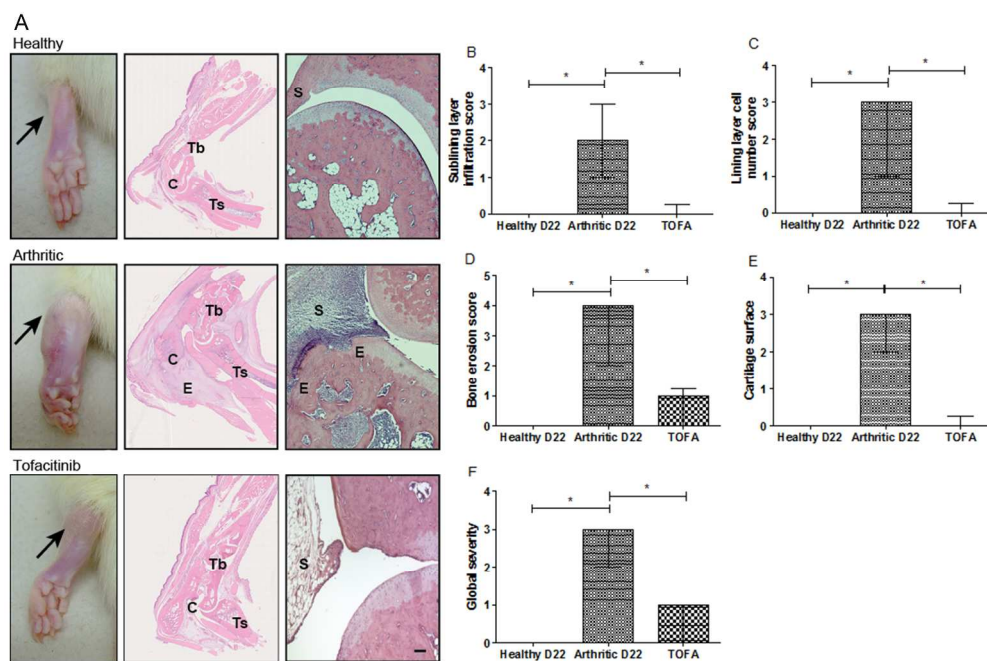


Figure 2 – (A) Histological images of joints after tofacitinib treatment. These patterns are merely illustrative of the type of histological features observed. Black arrow indicates the absence/presence of ankle swelling in rat hind paws. C–calcaneus, E–edema or erosion, S–synovia, Tb–tibia, Ts–tarso. Magnification of 50X. Bar: 100 μ m. Tofacitinib suppressed inflammation and tissue damage locally in the joints of AIA rats. A semi-quantitative evaluation of histological sections was performed. Notice that tofacitinib inhibited cellular infiltration (B), completely reversed the number of lining layer cells to the normal values (C) and prevented bone erosion occurrence (D), allowing for a normal cartilage (E) and joint structure, comparable to healthy rats (F). Data are expressed as median with interquartile range. Differences were considered statistically significant for p-values<0.05, according to Mann Whitney test. Healthy N=20, Arthritic N=20, Tofacitinib N=10.

structure and periarticular bo
418x281mm (300 x 300 DPI)

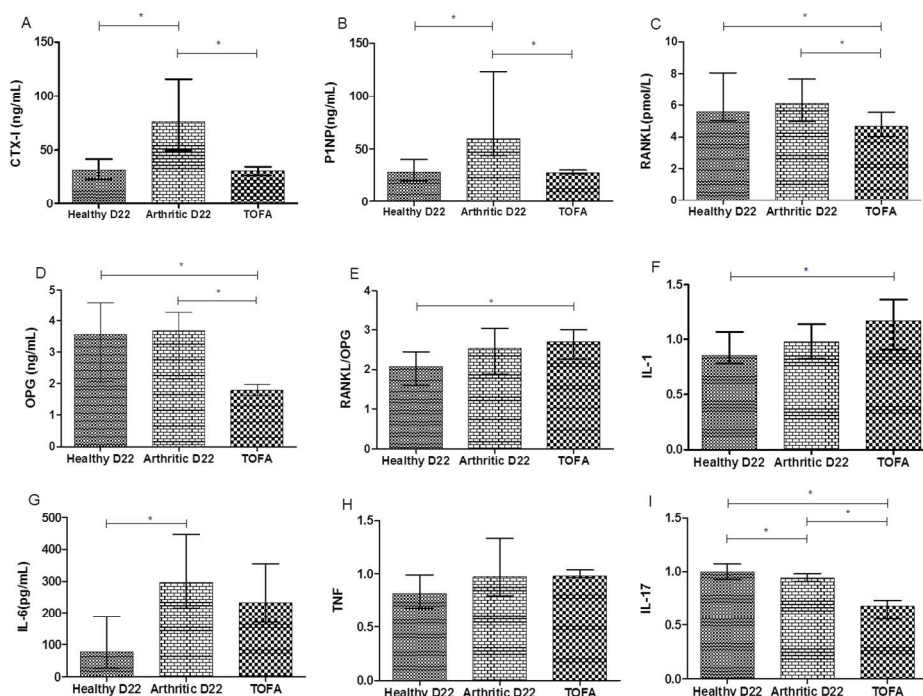


Image 3 - Bone turnover markers and systemic cytokines quantifications. Serum samples collected at day 22 (sacrifice) were analyzed by ELISA technique. Bone resorption marker, CTX-I (A) and bone formation marker, P1NP (B) were increased in arthritic rats ($p < 0.0001$ and $p = 0.0015$, respectively). Tofacitinib group showed decreased values for CTX-I ($p = 0.0002$) and P1NP ($p = 0.0018$). RANKL (C) and OPG (D) were diminished in tofacitinib treated rats ($p = 0.0002$ and $p = 0.0141$, respectively). RANKL/OPG ratio (E) showed higher values when compared to healthy group ($p = 0.0370$). Tofacitinib, in this animal model, did not affect circulating levels of IL-1 β (F) and TNF (H). Results have also demonstrated a significant decrease in the serum quantification of IL-17 (I) ($p < 0.0001$) and a tendency towards a decrease of IL-6 (G). IL-1, TNF and IL-17 were normalized. Differences were considered statistically significant for p -values < 0.05 , according to the Mann Whitney tests. Healthy N=20, Arthritic N=20, Tofacitinib N=10.

Tofacitinib administration sig
260x189mm (300 x 300 DPI)

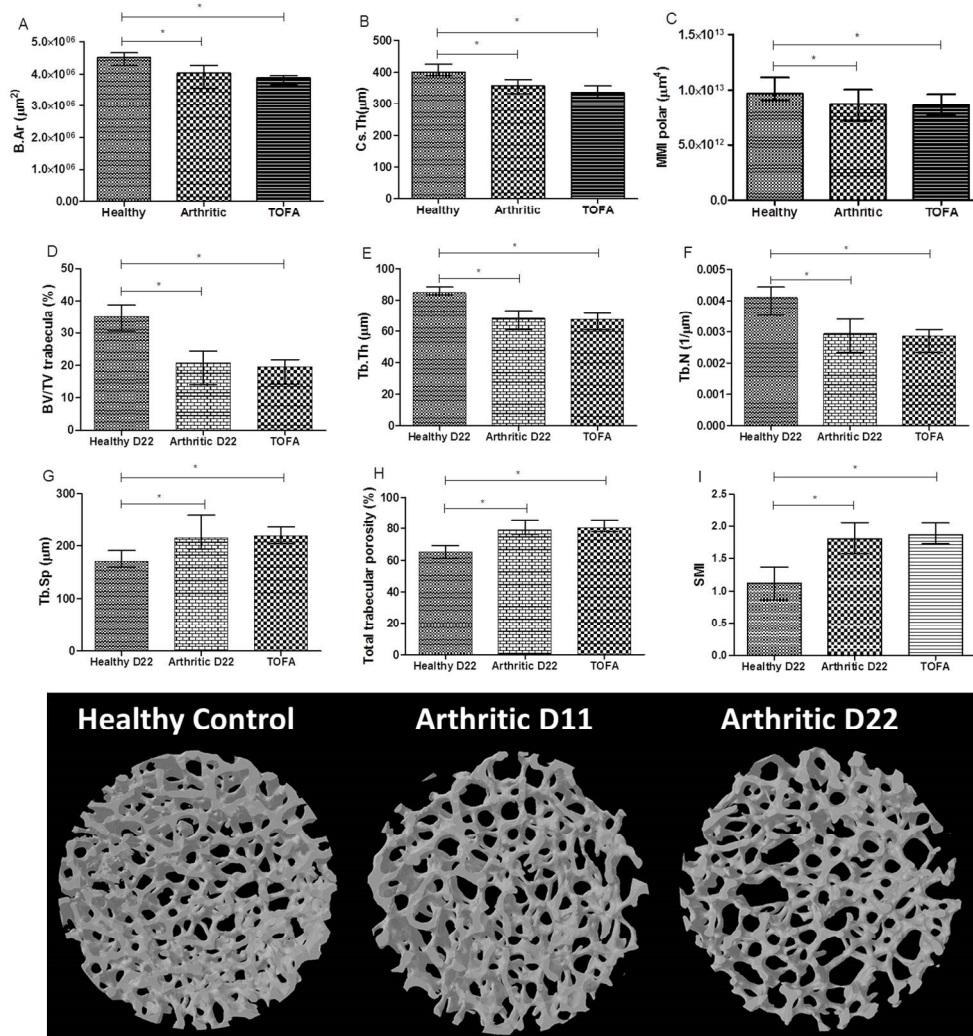


Image 4 – Micro-computed tomography (micro-CT) analysis of tibiae rat sample.

The arthritic and tofacitinib groups showed decreased values for cortical crosssectional bone area (A), thickness (B) and polar moment of inertia (C) when compared to healthy controls. Trabecular bone also showed lower values of ratio bone volume/tissue volume (D), trabecular thickness (E) and number (F) in comparison with healthy controls. Arthritic and tofacitinib rats demonstrated higher values of trabecular separation (G) and porosity (H) when compared to healthy controls. Structural model index showed decreased values in arthritic and tofacitinib rats in comparison to healthy rats. MicroCT images from healthy, arthritic untreated and tofacitinib tibiae rats (J). Images acquired with SkyScan 1272, Bruker microCT, Kontich, Belgium. Differences were considered statistically significant for p -values < 0.05 , according to the Mann-Whitney tests. Healthy N=20, Arthritic N=20, Tofacitinib N=10.

The effect of tofacitinib on i
253x263mm (300 x 300 DPI)

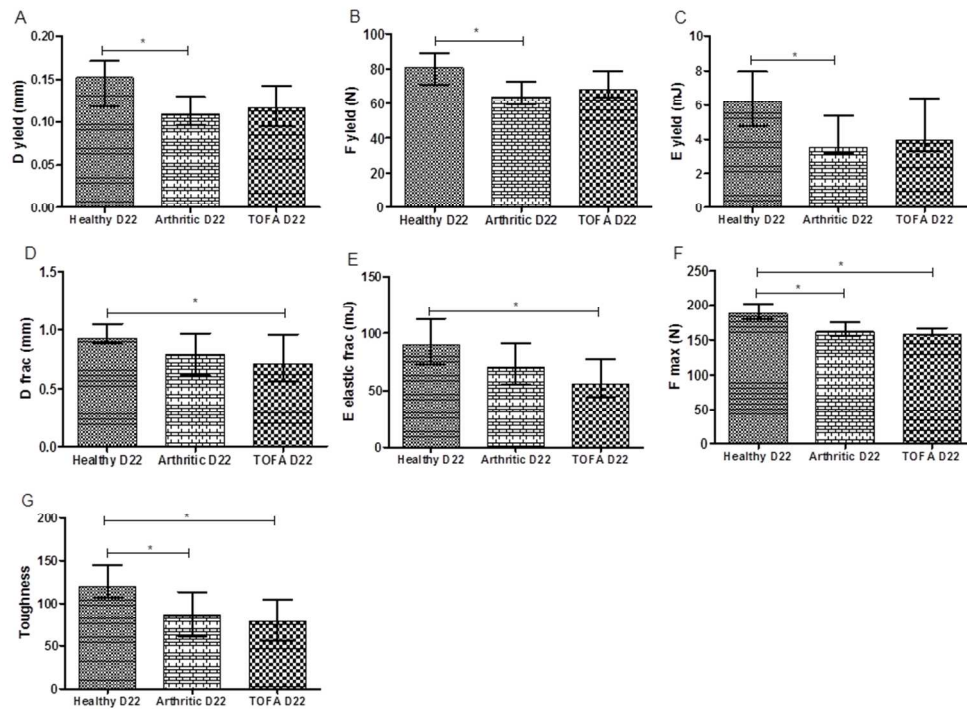


Image 5 – Bone mechanical properties assessed by three-point bending tests in rat femur at 22 days post disease induction. Results showed that arthritic rats have decreased properties at yield point, related to displacement (A), strength (B) and pre yield energy (elastic energy) (C). Tofacitinib treated rats had a significant decrease in displacement (D) and elastic properties (E) at fracture point. Arthritic and tofacitinib treated bones required a lower maximum load (F) to fracture and a decreased toughness (G) was observed. Differences were considered statistically significant for p-values < 0.05, according to the Mann-Whitney tests.

Healthy N=20, Arthritic N=20, Tofacitinib N=10.

Altogether, mechanical data re
253x183mm (300 x 300 DPI)

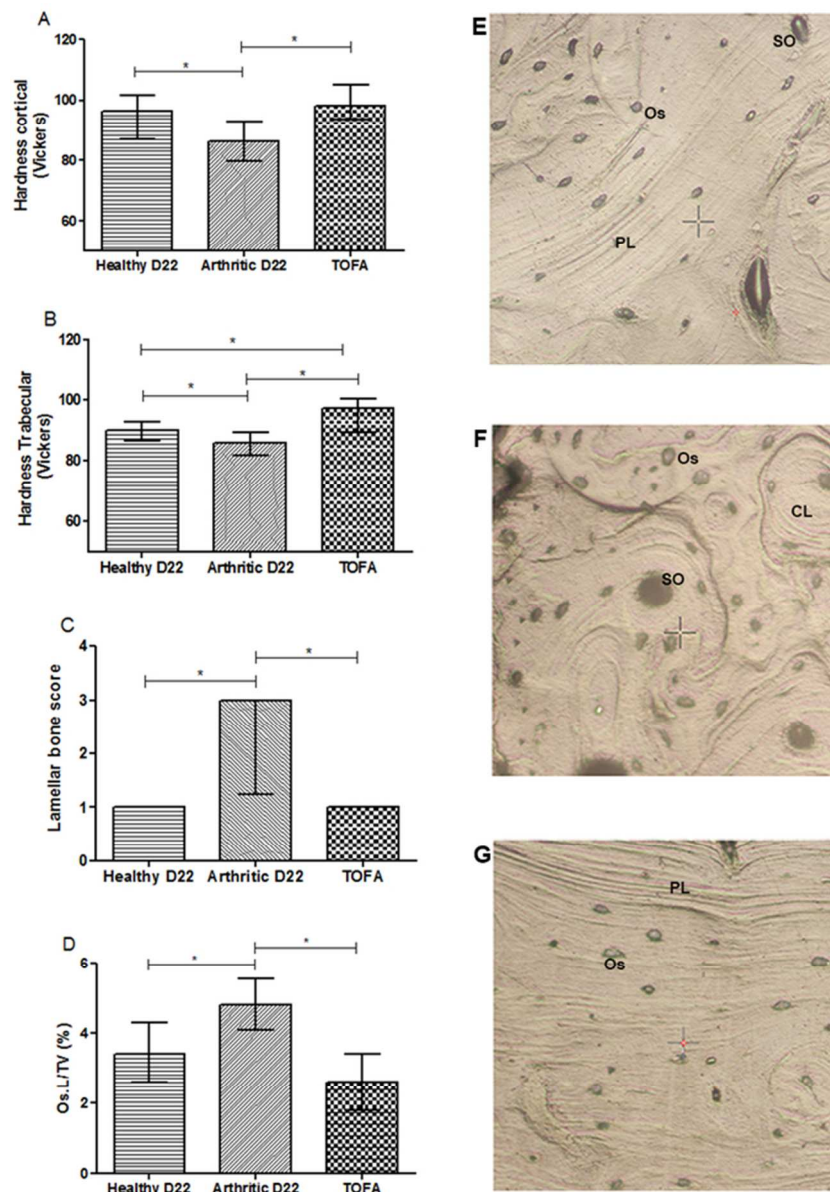


Image 6 – Bone mechanical properties assessed by nanoindentation in rat femur at 22 days post disease induction and respective topographic images from the indentation tissue area. Nano-mechanical tests revealed a decreased cortical (A) and trabecular (B) hardness in arthritic group at day 22 when compared to healthy rats. Of notice, rats treated with tofacitinib showed increased hardness in cortical (A) and trabecular (B) bone in comparison with untreated arthritic rats. Results demonstrated that the number of concentric lamellae (C) and ratio of area occupied by osteocyte lacunae in the total tissue (D) were higher when compared to healthy controls and tofacitinib treated groups at day 22.

Images are merely illustrative of the type of histological features observed. Concentric lamellae were identified in secondary osteons (SO), characteristic from arthritic animals (F). On the contrary, parallel-lamellae (PL) were identified in healthy controls (E) and tofacitinib treated groups (G). Os – Osteocytes, SO – Secondary osteons, PL – Parallel-lamellae, CL – Concentric lamellas. Magnification 20X. Differences were considered statistically significant for p -values < 0.05 , according to the Mann-Whitney tests. Healthy N=20, Arthritic N=20, Tofacitinib N=10.

In addition, arthritic animals
58x82mm (300 x 300 DPI)

For Peer Review

1
2
3
4
5
6
7
8
9
10
11
12
13
14
15
16
17
18
19
20
21
22
23
24
25
26
27
28
29
30
31
32
33
34
35
36
37
38
39
40
41
42
43
44
45
46
47
48
49
50
51
52
53
54
55
56
57
58
59
60